ORNL-3320
UC-4 – Chemistry
TID-4500 (17th ed., Rev.)

CHEMISTRY DIVISION
ANNUAL PROGRESS REPORT
FOR PERIOD ENDING JUNE 20, 1962

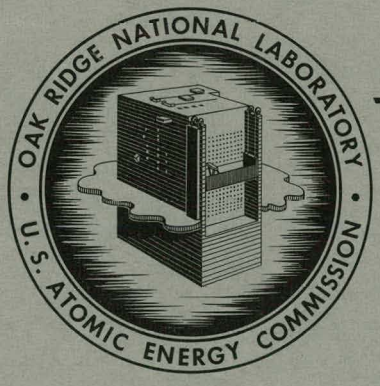

OAK RIDGE NATIONAL LABORATORY
operated by
UNION CARBIDE CORPORATION
for the
U.S. ATOMIC ENERGY COMMISSION

DISCLAIMER

Printed in USA. Price $2.75. Available from the
Office of Technical Services
U. S. Department of Commerce
Washington 25, D. C.

ORNL-3320
UC-4 – Chemistry
TID-4500 (17th ed., Rev.)

Contract No. W-7405-eng-26

CHEMISTRY DIVISION ANNUAL PROGRESS REPORT

for Period Ending June 20, 1962

E. H. Taylor, Director
M. A. Bredig, Associate Director

DATE ISSUED

DEC 11 1962

OAK RIDGE NATIONAL LABORATORY
Oak Ridge, Tennessee
operated by
UNION CARBIDE CORPORATION
for the
U. S. ATOMIC ENERGY COMMISSION

THIS PAGE

WAS INTENTIONALLY

LEFT BLANK

Summary

1. NUCLEAR CHEMISTRY

Values of 920 ± 90 and 48 ± 5 barns were measured for the resonance integral and (mean) thermal cross section of Pa^{233}, with a cadmium-filter technique. On the assumption that Pa^{233} obeys the $1/v$ law for cadmium-absorbable neutrons, a 2200-m/sec cross section of 46 ± 5 barns was obtained. A comparison of measurements made with cadmium and gadolinium filters indicated that no large resonances exist in the thermal-to-cutoff energy ranges.

With cadmium-filter techniques and irradiating samples of bismuth containing Bi^{210}, the thermal cross section and resonance integral to form the 2.16-min Bi^{211} (AcC) were found to be 0.054 and 0.20 barn respectively.

Effective energy cutoffs were calculated on an IBM 7090 computer for cadmium, gadolinium, samarium, and boron filters as functions of the ratio of Maxwellian to epithermal (assumed to be $1/E$) flux, the lower energy limit of the $1/E$ flux, the energy corresponding to the Maxwellian most probable (modal) velocity, the filter thickness, and the height/diameter ratio (of cylindrical filters). The filters were spherical (which on the assumptions made is equivalent to a beam flux case), cylindrical, and slab. By the use of two or three different filters (cadmium and gadolinium and perhaps samarium), it should be possible to detect resonances in the thermal-to-cutoff energy regions, in addition to measuring resonance integrals and thermal cross sections of unknown nuclides. The calculated cutoff varied by at most 2% as the lower limit of the $1/E$ flux was varied between 3 and 6 times the Maxwellian temperature.

Values of 97 ± 10 and 255 ± 25 barns were found for the activation thermal cross section and resonance integral of Sm^{150} respectively. These values are of interest because Sm^{150} is the nuclide of lowest cross section in the sequence starting with Pm^{147}; this sequence, via successive neutron capture, results in Gd^{156}. Samarium-150 can effectively interrupt the chain of neutron losses at mass 150 in a high-flux reactor.

By measuring the specific activity of the 2.615-Mev gamma ray in a reactor-irradiated and calutron-enriched sample of bismuth and by measuring the Bi^{208} content mass-spectrographically, a half-life of $(5.61 \pm 0.15) \times 10^5$ years was found for Bi^{208}.

By irradiating samples of pure Ce^{140} with neutrons and measuring, with both mass spectrograph and neutron activation analyses, the Ce^{142} produced as the result of double neutron capture, a value of 30 ± 3 barns was obtained for the effective neutron cross section of Ce^{141} in a reactor with a ratio of thermal flux to resonance flux of 12.4.

Values of 0.59 and 0.48 barn, respectively, were obtained for the thermal-neutron cross section and resonance integral of Ce^{140}.

The beta and gamma radiations of 2.7-hr Pm^{150} were investigated by using single- and multicrystal scintillation spectrometers. A decay scheme is proposed which involves excited states in Sm^{150} at 0.333, 0.743, 1.18, 1.66, 1.96, 2.07, 2.41, and 3.08 Mev, together with tentative assignments at 1.77, 1.90, 2.86, and 2.91 Mev.

A study of the decay properties of Cs^{132} disclosed energy levels in Xe^{132} at 669, 1300, 1808, and 1988 kev and levels in Ba^{132} at 464 and 1034 kev. From angular correlation measurements, spins are assigned for all of these states. A comparison of these levels with those predicted by various nuclear models is made.

Recent experiments extended the information on fission-product yields and half-lives in the mass-99 decay chain; in particular, the existence of a new isomer of Nb^{99} ($T_{1/2}$ = 10 sec) was established.

A comprehensive literature survey and evaluation of U^{233} fission-yield data led to the selection of a set of preferred fission-product yield values for the thermal-neutron-induced fission of U^{233}.

The level structures of Ge^{71}, Ge^{73}, Ge^{75} and Ge^{77} were studied with the (d,p) reaction. The energy spectra of proton groups leading to excited levels up to approximately 1 Mev were obtained through the use of a silicon surface-barrier detector. The Q values corresponding to newly observed levels were determined.

Some of the properties of lithium-drifted silicon diodes were studied. Measurements with these diodes were used in an investigation of the Ce^{135} decay scheme.

2. ISOLATION AND CHEMICAL PROPERTIES OF SYNTHETIC ELEMENTS

The preparation and properties of a number of rhenium species in aqueous or organic solution which may be prepared from pentavalent and hexavalent rhenium in 18 *M* H_2SO_4 are described. All the species have the common property of exhibiting very intense absorption bands in the visible region.

Nonaqueous acidimetric titrations of H_2ReCl_6 and H_2SO_4 suggested that the second ionization constant for the rhenium compound is significantly larger than that for H_2SO_4.

Measurements of the near-infrared absorption spectrum of pertechnetate ion revealed a characteristic strong absorption band at 906 cm^{-1}.

3. CHEMICAL SEPARATION OF ISOTOPES

Ion exchange of alkali metal ions has been studied in systems involving ion exchange resins equilibrated with nonaqueous solutions. Diffusion and selectivity coefficients were determined.

Vapor pressure measurements were made of various mixtures of BF_3 and ethyl sulfide. Single-stage isotopic equilibrium constants were determined for the exchange of boron between BF_3 and $BF_3 \cdot (CH_3)_2O$ at 22, 4, and −8°C.

Nitrite and nitrate ions were shown to exchange nitrogen atoms in acid solutions. The rate is pH dependent.

The salt $K_6[(NC)_5CoOOCo(CN)_5]$ in solution does not exchange its peroxygen bridge with O_2.

Preoperational testing of the water distillation cascade of the Oxygen-17 Plant was completed during fiscal year 1962. The unit was placed "on stream" during June. The cascade is expected to attain steady-state operation during the latter part of 1963.

The single-stage separation factor for carbon and oxygen isotopes between carbon dioxide and dimethyl carbamic acid was measured.

Separation factors per mass unit for the system, aqueous metal hydroxide–metal amalgam, at 25°C were 1.0023 for sodium and 1.00017 for rubidium. With sodium, the light isotope concentrates in the amalgam; with rubidium, the heavy isotopes concentrate in the amalgam. A rubidium-cesium separation factor larger than 2 was obtained for the same system.

A nuclear magnetic resonance study of rates of exchange, activation energies, and equilibrium constants for mixtures of BF_3 with two donor solvents was begun.

Dielectric-constant measurements on diethylammonium diethylcarbamate indicate the material is salt-like in the molten state, but undissociated in organic solvents.

Mass spectroscopic investigations of metastable ions produced in the isotopic nitrous oxides by electron impact were published. Infrared and Raman spectral studies of isotopic molecules were continued. Observations of the spectra of $BF_3 \cdot (CH_3)_2O$ and its B^{10}-, B^{11}-, and D-substituted analogs were completed and published. The isotopic equilibrium constant between BF_3 and $BF_3 \cdot (CH_3)_2O$ was calculated from the spectral data and compared with experimental observations. A computer program for using isotopic data in calculating force constants was refined and used to calculate vibrational frequencies for $N_2^{14}O_4$ and $N_2^{15}O_4$, which agree closely with observed values.

4. RADIATION CHEMISTRY

In the electron bombardment studies of mixtures of $(C_2N_2 + H_2)$ and $(C_2H_2 + N_2)$, a common ion at mass 27 was shown by appearance-potential

techniques to be HCN^+ and not $C_2H_3^+$. Other common masses were not identified as to specific ions. This study of the (C_2H_2 + N_2) mixture is in agreement with early alpha radiolysis studies of the same mixture in that only small amounts (not more than 10%) of nitrogenated products are produced.

The gaseous and liquid products resulting from the alpha radiolysis of ethylene were analyzed. The results show that hydrocarbons with an even number of carbon atoms predominate and that the straight-chain hydrocarbons predominate over the branched compounds. Infrared spectra show the major unsaturated products to be RCH=CHR′. Molecular weight and iodine number determinations on the liquid polymer show an average of 16 carbons per molecule and one double bond per 10 carbons.

The catalytic activity and activation energy of germanium for H_2-D_2 exchange and its catalytic activity for formic acid dehydrogenation varied significantly with the Fermi level as the latter was altered by doping with *n*- and *p*-type impurities.

Colors produced on irradiation of certain polynuclear aromatic compounds adsorbed on silica gel were used as evidence for ionic intermediates in the radiolysis. Further experiments on the enhancement by radiation of the H_2-D_2 exchange activity of silica gel make it even less likely that the mechanism is the removal of a poison by radiolysis.

The photolysis of hydrogen peroxide was studied in the presence of dissolved hydrogen and oxygen. The ratio of rate constants, $k_{H_2+OH}/k_{H_2O_2+OH}$ = 0.93, is the same as that previously reported for the radiolysis of water. This indicates that the hydroxyl radical produced in the radiolysis of water has the same chemical structure as OH produced by the photodecomposition of hydrogen peroxide. Presumably, the H_2O^+ initially produced in the radiolysis of water is rapidly converted to OH. The above ratio is insensitive to hydrogen ion concentration. However, HSO_4^- and OH^- react with OH to form, presumably, HSO_4 and O^-, respectively. The ratios of rate constants $k_{H_2+OH}/k_{HSO_4^-+OH}/k_{OH^-+OH}$ = 1.0/0.005/8.0. The ratio of rate constants $k_{H+H_2O_2}/k_{H+O_2}$ = 2.2×10^{-3}, where the hydrogen atom is that produced by reaction of H_2 with the OH from the photodecomposition of H_2O_2. The corresponding ratio for reaction with the hydrogen atom produced in the radiolysis of water is 0.6. This and other evidence indicates that the hydrogen atom produced by reaction of H_2 with OH is a true hydrogen atom, and that the "hydrogen atom" produced in the radiolysis of water is some form of hydrated electron.

An important parameter in the diffusion-kinetics model of water radiolysis is linear energy transfer, LET. Yields were measured for the oxidation of ferrous sulfate and for the reduction of ceric sulfate both with and without added thallous ion, by protons of various energies in the range 11 to 23 Mev. From these measurements, derived yields of intermediates G_H, G_{OH}, G_{H_2}, $G_{H_2O_2}$, and G_{-H_2O} were evaluated. The measurements extend the range previously covered (to 10 Mev at Argonne and Brookhaven National Laboratories) into the lower LET range. Methods were devised for accurately measuring both the proton energy and the proton beam current.

The Co^{60} gamma irradiation of aqueous H_2SO_4 solutions produces the free radicals, H, OH, HSO_4, and HSO_3 and the molecular products H_2, H_2O_2, $H_2S_2O_8$, H_2SO_5, and SO_2. The 100-ev yield of each of these intermediates as a function of H_2SO_4 concentration is presented graphically. The hydrogen atom reacts with both oxygen molecules and H_3O^+ ions. The ratio of rate constants $k_{(H+O_2)}/k_{(H+H_3O^+)}$ has been calculated from the the ferrous–sulfuric acid system to be 700,000 (±6%).

When Ce^{4+}–0.8 *N* H_2SO_4–$NaNO_3$ solutions are irradiated with Co^{60} gamma rays, the $G(Ce^{3+})$ increases with increasing $NaNO_3$ concentration. Mass spectrographic analyses of molecular oxygen in the H_2O^{18}-$NaNO_3$ system are correlated with the ionic spectrophotometric analyses of Ce^{4+} in the Ce^{4+}–0.8 *N* H_2SO_4–$NaNO_3$ system to explain the enhanced $G(Ce^{3+})$. The measured $G(Ce^{3+})$ is deduced to be a composite of the following: (1) the $G(Ce^{3+})$ measured in the absence of $NaNO_3$, (2) the stoichiometrically equivalent $G(Ce^{3+})$ resulting from the suppression of $G(H_2)$, (3) a direct-action effect on nitrate ion which is directly proportional to nitrate ion concentration, and (4) a possible scavenging reaction of nitrate ion.

The investigation of radiolysis by transferred energy was continued with a study of the decomposition of nitrite ions dispersed in potassium

bromide. It was found that the nitrite ion is so distributed in the matrix as to decompose simultaneously by two first-order processes. The initial rates of both processes vary in a regular manner with the initial concentration of nitrite ion. This is qualitatively explained by considering each unirradiated mixture of potassium nitrite and potassium bromide to have a different structure varying regularly with concentration.

Discontinuities were found in turbidity-concentration curves measured on pressed disks of dispersions of large ions in potassium bromide. It is believed that this behavior may be compared to that of "colloidal electrolytes" in liquid solutions.

By means of low-temperature cells and absorption spectrophotometry, the formation of ozone in liquid oxygen and oxygen-nitrogen mixtures was observed *in situ* at 77°K by alternate gamma irradiation and ultraviolet absorption measurement. Extensive energy transfer and enhanced ozone yields were found in the O_2-N_2 system. In a solution only 0.050% O_2, the yield of ozone is equal to 32% of that from pure oxygen. In pure oxygen at 77°K, $G(O_3) = 12.5$ molecules/100 ev.

The two cobalt sources of the Radiation Chemistry Group were reloaded with 2900 and 280 curies; the maximum dose rates are about 2×10^{18} and 2×10^{17} ev g^{-1} min^{-1} respectively. The cobalt is distributed to provide a uniform dose rate (within ±2%) over a 3-in. length along the vertical axis.

Measurements of the decompositions of the alkali-metal bromates by nuclear reactor radiations as a function of exposure dose at ambient temperatures showed that the gross radiolytic stability sequence was the same as that observed previously with Co^{60} gamma rays. In some instances, however, the relative stabilities differed, and these differences could be attributed to the production of internal radiation sources by thermal-neutron capture in the alkali-metal cation or by the formation of high-LET recoil fragments, as in the fission of Li^6. The separate decompositions by thermal neutrons, fast neutrons, and reactor gamma rays were estimated from experiments performed in a thermal column, with thick lithium or metal shielding, and with thick bismuth metal shielding, respectively. Evidence was obtained for the stepwise radiolytic decomposition of the BrO_3^- ion.

5. ORGANIC CHEMISTRY

The differential method developed at this Laboratory for studying small isotope effects – particularly the secondary effects of C^{14} and deuterium – was extended to include several isotope-position isomers of acetophenone, phenyl *t*-butyl ketone, and propiophenone. In general, substitution of deuterium in the aliphatic side chains of these ketones increases the reaction rate, the only exception being propiophenone-ω-d_3. Carbon-14 in the carbonyl groups of all ketones studied decreases the reaction rate by 5.0%, whereas in adjacent positions it causes a small rate increase.

A study was made of the nuclear magnetic resonance spectrum of erythro-2-amino-1-phenylpropanol hydrochloride. The population of the various conformations was estimated from the appropriate spin-spin coupling constant. The data were used to predict the product ratio upon deamination of the compound, and the validity of the prediction was confirmed from experimental evidence.

The compound (−)-*exo*-norbornyl amine was prepared in the optically pure form and subjected to deamination. The retention of optical activity in the product, *exo*-norbornyl acetate, was evidence that the reaction intermediate was not a nonclassical cyclic ion.

A nuclear magnetic resonance study of the *syn*- and *anti*-stereoisomers of *iso*-butyrophenone-2,4-dinitrophenylhydrazone was started. The *syn-anti* chemical shifts for both α- and β-protons were in the same direction. The two isomers do not exist in equilibrium in solution, because of the rotational isomerization about the C=N bond. The reaction between sodium nitrate and tributyl phosphate (TBP) was further studied with differential-thermal-analysis techniques. The first reaction (exothermic, 79 cal per g of TBP) was partially quenched by an endothermic reaction of sodium nitrate. The return to a net exothermic reaction was finally quenched by the fusion of sodium nitrate.

Organic thiophosphorus compounds form complexes with silver and mercuric cations that can be used for solvent extraction. Electronic distributions are important in that more stable complexes are formed with neutral thiophosphorus compounds that have more electron-releasing groups attached to the phosphorus. The cor-

responding monobasic thiophosphoric acids form complexes with silver that are soluble in and show association between molecules in benzene.

6. CHEMISTRY OF AQUEOUS SYSTEMS

The solubilities of Ag_2SO_4 were measured in KNO_3-K_2SO_4, K_2SO_4-$MgSO_4$ and K_2SO_4-H_2SO_4 aqueous mixtures in the range 90° to 175°C. Two different types of expressions were tried for representing the logarithm of the solubility product vs ionic strength: (1) a single-parameter Debye-Hückel equation and (2) a Debye-Hückel expression with fixed parameter plus a linear term with an adjustable parameter. The adjustable Debye-Hückel parameter in expression (1) was very nearly temperature independent, while the adjustable linear parameter in (2) varied quadratically with temperature in all mixed-electrolyte media.

A generalized least-squares technique can be used to calculate equilibrium constants in solvent extraction equilibria by minimizing the difference between observed and calculated distribution ratios. The method was successfully applied to the extraction of uranyl nitrate and nitric acid by TBP dissolved in an inert diluent.

The optical absorption of hydrolyzed U(VI) in 1 *M* chloride solutions was correlated with a hydrolysis scheme based on acidity and ultracentrifugation measurements, involving as principle species $(UO_2)_2(OH)_2^{2+}$, $(UO_2)_3(OH)_4^{2+}$, and $(UO_2)_3(OH)_5^{+}$. Ultracentrifugation of Bi(III) perchlorate solutions as a function of concentration and degree of hydrolysis indicates that estimates of equilibrium quotients and their temperature coefficients for polymeric reactions may be possible by comparing experimental equilibrium refractive index patterns with those computed on the basis of an assumed model. Equilibrium ultracentrifugations of hydrolyzed Pb(II) solutions in general confirm the scheme postulated on the basis of emf measurements carried out elsewhere.

The $NbOF_5^{2-}$ ion and the NbF_6^{-} ion were identified in 0% to 50% HF solutions by comparing the Raman spectra of the solutions with the spectra of crystalline $CsNbF_6$, K_2NbF_7, and $K_2NbOF_5 \cdot H_2O$. The NbF_7^{2-} ion was not found in the solutions.

A new spectrophotometer cell assembly was constructed for high-temperature aqueous spectrophotometric studies. In both sample and reference cells, temperature and pressure are precisely controlled, and liquid-gas equilibration is provided for.

Preliminary study indicates that the $DClO_4$-D_2O-H_2O system is a usable solvent for spectrophotometry of inorganic ions at least to 1 / $DClO_4$, to 250°C, and over the wavelength range 0.33 to 1.8 μ.

The applicability of the mass law to ion exchange equilibria with concentrated aqueous salt solutions was demonstrated with a liquid anion exchanger. Equilibria involving concentrated hydrochloric acid solutions with both liquid and resinous anion exchangers, however, could not be rationalized because of the invasion of these exchangers by this electrolyte. An attractive explanation for this invasion and the associated large nonideality of the resultant organic phase was that hydrogen dichloride ions, HCl_2^{-}, were being formed at the exchange sites. Infrared absorption, vapor pressure and other measurements have appeared to give support to the explanation.

Systematic measurements of the osmotic and activity coefficients at 25°C for a wide variety of quaternary ammonium halides in aqueous solutions as a function of concentration have continued. The degree of interaction between a given halide ion and the quaternary ammonium cation depended on the structure of the latter. For example, substitution of a benzyl for a methyl group greatly increased the anion binding of the resulting quaternary ammonium cation.

Calorimetric measurements of the heat of exchange of bromide for chloride ion with high-molecular-weight linear anionic polyelectrolyte gave values in reasonable agreement with previously observed heats for the same reaction with cross-linked anion exchangers.

Heat of solution and dilution measurements were completed on *p*-ethylbenzene sulfonic acid (the "model" compound for Dowex 50) and on the lithium, sodium, potassium, and cesium salts of the acid. The heat content–concentration dependency observed with these compounds was notable in that the initial slopes were larger than for any other common alkali-metal salt of the 1:1 type.

The extraction of microquantities of Fe(III) from concentrated hydrochloric and perchloric acid solutions by a strong acid liquid cation exchanger and by a lightly cross-linked Dowex 50 have been

compared. In all four cases a marked increase in the extraction of iron above acid concentrations of 3 to 4 *M* was observed.

A systematic study is in progress of the ion exchange properties of essentially all metallic elements with the objective of developing a general ion exchange separations scheme. Anion and cation exchange methods are being explored in HCl, HNO_3, $HClO_4$, H_2SO_4, and HF solutions and various mixtures of these acids. High-ionic-strength media are being stressed. Approximately six major ion exchange groups, which are expected to form the basis of a generalized scheme, have been evaluated.

The cation exchange behavior of U(VI) was studied in mixtures of $HClO_4$, HNO_3, HCl, and H_2SO_4 solutions at high ionic strength. The presence of small amounts of chloride affects the adsorbability of U(VI) greatly. Some of the unique features of the adsorbability of U(VI) at high ionic strength can be utilized for a number of novel separations techniques.

A large number of vanadates were found to have interesting cation exchange properties. Zirconium antimonate was found to be a cation exchanger with relatively unique selectivities.

7. ELECTROCHEMICAL KINETICS AND ITS APPLICATION TO CORROSION

By use of tracer techniques, a study was made on the kinetics of ion exchange between the passive surface of iron or stainless steel and an aqueous solution. The results can be interpreted mathematically by assumption of a linear variation in the heat of activation with the extent of exchange.

It has been shown that hydrogen penetration into the metal is an important factor in determining the electrochemical behavior of iron in acid media. This conclusion results from quantitative analyses of cathodic polarization transients on cylindrical electrodes, and from observations of the effects of hydrogen diffusion through an iron membrane electrode on the rates of the reactions occurring at the metal-solution interface.

An investigation of the dissolution of zirconium in aqueous solutions containing HF is underway. Pulse methods are being used to obtain dissolution rates and kinetic parameters. The studies on passive zirconium are being continued, with the application of current pulses in an effort to calculate film thicknesses from the capacities due to the thin film present on the electrode surface.

A model of the passive state on iron, developed on the basis of certain concepts of semiconductor theory and electrochemical kinetics, is discussed in relation to experimental observations. The model predicts correctly the observed potential independence of corrosion rate in the passive region as well as the proper pH dependence of the corrosion rate. The assumption of a hole-catalyzed corrosion reaction accounts for the existence of the transpassive state and for the observed pH dependence of corrosion rate in this region. The existence of a limiting potential analogous to the Flade potential follows directly from the model.

Measurements of the electrode potential and the differential capacity of the electrical double layer on electrolytic iron in Cl^-, Br^-, I^-, and SO_4^{2-} solutions show that specific adsorption plays an important role in the mechanism of corrosion inhibition by halide ions. Electrode potentials and differential capacities were measured as a function of time, acidity, and anion concentration. For the case of inhibition by iodide ions, the data support an electrochemical desorption mechanism proposed previously for the explanation of transient and steady-state polarization characteristics of iron in iodide solutions.

8. NONAQUEOUS SYSTEMS AT HIGH TEMPERATURE

The electrical conductivity of rare-earth metal solutions in their molten triiodides was found to reflect the stability of Nd^{2+} and the instability or nonexistence of La^{2+} and Ce^{2+}, as first indicated by phase diagrams, with Pr^{2+} exhibiting intermediate stability. The entropies of fusion of the trihalides were determined calorimetrically and yielded, in conjunction with the phase diagrams, a cryoscopic number $n \approx 3$ for the dissolution of the metals in the trihalides, corresponding either to the reaction $M + 2M^{3+} \rightarrow 3M^{2+}$, as for Nd and, partially, Pr, or to the ionization $M \rightarrow M^{3+} + 3e^-$, as for La and Ce, and, partially, Pr.

Large differences in the electronic conductance of pairs of systems such as K-KX and La-LaX_3, involving salts of different stoichiometry, are explained by the assumption that the electronic

conductance is proportional not only to the concentration of mobile electrons but also to the concentration of the metal ions between which the electrons are being exchanged.

The suggestion that electron exchange between Nd^{2+} and Nd^{3+} contributes to the conductance in molten NdX_3-NdX_2 mixtures was supported by measurements on molten $NdCl_3$-$SrCl_2$ and NdI_3-SrI_2 mixtures, in which a similar exchange is not possible.

The decrease in the rate of increase in electrical conductance with increasing metal concentration in the alkaline earth systems $CaBr_2$-Ca, CaI_2-Ca, and $SrBr_2$-Sr is attributed, as in $CaCl_2$-Ca, to the pairing of the mobile electrons, which are present in dilute solution, to form M_2^{2+} ions.

The alleged existence, in molten $CdCl_2$-KCl mixtures, of a minimum in electrical conductance at the composition $KCl:CdCl_2 = 1:1$, attributed to the formation of $CdCl_3^-$ ions, was ruled out by measurements at 460°, 500°, and 570°C. The data are in agreement with higher-temperature data of the literature and with the assumption of $CdCl_4^{2-}$ rather than $CdCl_3^-$ ions. An analysis of emf measurements by Russian investigators leads to the same result.

Heat capacities over limited temperature ranges and heats of fusion were determined by means of a drop calorimeter for a number of rare-earth and alkaline-earth halides. $SrBr_2$ and $BaCl_2$ undergo phase changes just below their melting points with fairly large heats of transition. Their high-temperature forms are believed to have the fluorite type of structure characterized, as in CaF_2 and $SrCl_2$, by an unusually low entropy of fusion, probably because a high degree of disorder occurs in that structure at elevated temperatures.

9. CHEMICAL PHYSICS

The laboratories for paramagnetic resonance work were enlarged, and new spectrometers for studies at 9000 and 23,000 Mc were assembled and put into operation. Progress was made in the design of a new cavity for extending work to liquid-helium temperature.

The single crystal paramagnetic resonance parameters of NO_2 in irradiated $NaNO_2$ and in irradiated KNO_3 were found to differ significantly. The differences are satisfactorily explained if NO_2 in KNO_3 is undergoing rapid reorientations between two mirror-related sites in a nitrate ion vacancy. Study of KNO_3 doped with nitrogen-labeled NO_2^- showed that NO_2 is produced from NO_2^- by irradiation at 77°K. Studies of the production of NO_2 suggest that NO_2^- is not produced in pure KNO_3 at 77°K but is produced after the irradiated salt is warmed.

A paramagnetic resonance study of irradiated single crystals of hydrogen peroxide has been reactivated. Conditions for forming three distinct spectra by ultraviolet irradiations have now been found.

A paramagnetic species exhibiting chlorine hyperfine structure and believed to be ClO_2 has been studied in gamma-irradiated $KClO_3$. Machine computations were made in an attempt to fit the data to a spin Hamiltonian which included the quadrupole interaction. If $Ba(ClO_3)_2 \cdot H_2O$ is irradiated at 77°K and then warmed to room temperature, a species with a similar spectrum is formed.

The crystal structure of chloral hydrate was determined to high precision by three-dimensional neutron diffraction methods. Complete details of the molecular structure and hydrogen bonding have been elucidated.

Neutron diffraction measurements on NaCl, KCl, and RbCl single crystals have (1) demonstrated the consistency and precision of intensity measurements with the Oak Ridge automatic neutron diffractometer, (2) refined the values for the nuclear scattering amplitudes of the metals relative to Cl, and (3) yielded precise values of the thermal-displacement parameters in these crystals.

X-ray diffraction studies of structure in molten alkali halides and aqueous solutions are continuing. Work on liquid water and on aqueous $Pb(OH)ClO_4$ is nearing completion. The data for water are consistent with a model based on the ordinary ice structure, with "interstitial" water molecules filling approximately half the ice structure cavities. The $Pb(OH)ClO_4$ data were interpreted in terms of a model containing a tetrahedral arrangement of lead atoms, each lead atom having three other lead atom neighbors at a distance of about 3.83 A.

A program has been prepared to plot contours of a two-dimensional density function using the California Computer Products model 570 magnetic tape plotter.

An experimental computer program has been prepared which will postulate crystal structures

when given the unit cell size, symmetry, and number of molecules per cell.

Several computer programs for crystallographic calculations were rewritten in FORTRAN language in order to permit their use on different machines and to facilitate any modifications which may become necessary.

Low-temperature heat capacity measurements on a third preparation of K_2ReBr_6 agree poorly with previous measurements. This places a large uncertainty upon the calculated entropy; the revised value is $S°(298.16°K) = 108.0 \pm 1.5$ cal deg^{-1} $mole^{-1}$.

The heat of mixing in the molten-salt system LiF-KF was measured with the Bunsen ice calorimeter as a function of composition. The system exhibits energetic asymmetry and has a maximum heat of solution of about 1200 cal/mole.

In a mass spectrometric study of both the catalytic decomposition of ammonia on platinum and its radiolytic decomposition by 90-ev electrons, the NH_4^+ ion was the most abundant transient species observed.

The two-stage mass spectrometer was developed into a highly sensitive and reliable instrument for the accurate determination of isotopic abundance ratios.

Studies on electron shake-off and molecular fragmentation as the result of nuclear decay were reported in the Physics Division Annual Progress Report, ORNL-3268.

In preliminary experiments with crossed molecular beams of D and H_2 it was possible to observe part of the angular distribution of the product HD. If the results can be taken at their face value, they present an ambiguity concerning the distribution of the energy between various internal modes.

In the same apparatus, a surprising specularity was observed in the reflection of D_2 and helium beams from a polycrystalline platinum foil.

The differential surface-ionization detector for alkali metals and their compounds was revised to eliminate previous difficulties caused by scattering from supporting members of the gage. A fast surface-ionization detector with electron multiplier was constructed and found to be satisfactory for use with phase-sensitive detection. A velocity selector was also built and tested.

Contents

1. Nuclear Chemistry

REACTOR NEUTRON CROSS SECTIONS

Thermal Cross Section and Resonance Integral of Pa^{233}

Joseph Halperin R. E. Druschel
R. W. Stoughton A. E. Cameron[1]
R. L. Walker[1]

Eastwood and Werner[2] reported 39 ± 5 and 930 ± 135 barns for the 2200-m/sec cross section σ_0 and resonance integral I (including the $1/v$ "tail") of Pa^{233}. Since effective cross section measurements of Pa^{233} in the LITR and a graphite reactor indicated higher values[3] than those computed from the results of Eastwood and Werner, it appeared that there might be a low-lying resonance in the region 0.1 to 0.5 ev which might explain the discrepancy. In order to check this possibility and to redetermine the Pa^{233} thermal cross section and resonance integral, reaction rates for Pa^{233} neutron capture were measured inside and outside both gadolinium and cadmium filters by measuring the U^{234}/U^{233} ratios in the beta decay products.

Bare and filtered samples of ThO_2 were irradiated in the ORR at thermal fluxes of about 10^{14} $n/(cm^2\,sec)$ for periods of 3 to 5 days. The cadmium filters were 40 mils thick, which involves an effective cutoff of 0.55 ev; the gadolinium filters contained 80 mg/cm^2 of Gd, which results in an effective cutoff of 0.2 ev. Dilute alloys of cobalt (0.151% Co) and aluminum were put with the samples as flux monitors. Flux computations were based on values of 37 and 75 barns for the cobalt σ_0 and I respectively. In general the procedures and conventions used have been described previously.[3]

After the irradiations the samples were left to cool for about two weeks; subsequently the uranium fractions (several micrograms each) were separated from the mixture by anion exchange. The U^{234}/U^{233} ratios were determined mass-spectrographically with a 12-in. 2-stage mass spectrometer using thermal ionization and electron multiplier detectors.

The ratio U^{234}/U^{233} obtained in a bare irradiation at constant flux is given by

$$N_{24}/N_{23} = \phi_{th}(\sigma_{eff})_{13}\, t\, f(t,T)\,, \qquad (1)$$

where

$$f(t,T) = \frac{1}{\lambda_{13}t}\,\frac{1-(1-e^{-\lambda_{13}t}/\lambda_{13}t)}{1-(1-e^{-\lambda_{13}t}/\lambda_{13}t)e^{-\lambda_{13}T}}\,.$$

In the above equations t is the irradiation time, T is the cooling time, ϕ_{th} is the thermal flux, and the subscript 13 refers to Pa_{233}. Equation (1) holds for the filtered irradiation if ϕ_{th} and σ_{eff} are replaced by ϕ_r (the epithermal flux per lethargy unit) and I respectively. Although a second-order reaction is involved, the equation assumes the usual form of $(\sigma_{th}/I)_{13} = (\phi_r/\phi_{th})(C.R. - 1)$, where $C.R.$ is the ratio of the bare to the filtered ratios (U^{234}/U^{233}).

Data from these irradiations are summarized in Table 1.1, where the reported cross sections have been corrected for capture by U^{233} during irradiation. The mean thermal cross section from the cadmium-filtered irradiations is 48 ± 5 barns. The corresponding 2200-m/sec cross section σ_0 is 46 ± 5 barns, on the assumption that Pa^{233} obeys the $1/v$ law in the thermal and cutoff regions. The mean thermal and 2200-m/sec cross sections obtained with the gadolinium filter were both about

[1]Analytical Chemistry Division.

[2]T. A. Eastwood and R. D. Werner, *Can. J. Phys.* **38**, 751 (1960).

[3]R. W. Stoughton and Joseph Halperin, *Nucl. Sci. Eng.* **6**, 100 (1959).

Table 1.1. Irradiation Data for Pa^{233} Cross Section Measurement

Filter Material	ϕ_{th} [$n/(cm^2\ sec)$]	ϕ_{th}/ϕ_r	Irradiation Time (sec)	Cooling Time (sec)	$f(t,T)$	N_{24}/N_{23}	σ_{eff}[a] (barns)	I[a] (barns)	σ_{th}[a] (barns)	σ_{2200} (g = 1) (barns)
	$\times 10^{14}$		$\times 10^{5}$	$\times 10^{6}$		$\times 10^{-2}$				
Cd	1.83_0	10.81	4.46_7	1.28	1.34_2	1.515[b]	135	924	49.5	47.6
						0.942[c]				
Cd	1.24_9	10.63	2.35	1.33	1.43	0.550[b]	130	915	46.4	44.6
						0.351[c]				
Gd	1.27_3	11.96	2.59_2	1.20	1.54	0.5653[b]	110	796	43.0	42.6
						0.340[c]				

[a]Corrected.
[b]Bare.
[c]Filtered.

43 ± 5 barns. Since the values obtained with the two different filters are probably in agreement within the precision of the method, there must not be any large resonance between thermal energies and the cadmium cutoff (0.55 ev).

The resonance integrals (including the $1/v$ portion) measured with cadmium and gadolinium filters were 920 ± 90 and 800 ± 80 barns, respectively. While these two values agree within the overall estimated errors, the disagreement is definitely outside the experimental precision. The lower value in the case of the gadolinium filter is consistent with the fact that some of the gadolinium and Pa^{233} resonances overlap.[4]

The values of 46 ± 5 and 920 ± 90 barns reported here for the 2200-m/sec cross section and resonance integral for cadmium filters compare favorably with the 39 ± 5 and 930 ± 135 barns reported by Eastwood and Werner.

[4]F. B. Simpson and R. P. Schuman, "Cross Section Measurements on Radioactive Samples," pp 85–91 in *Proc. Symp. Neutron Time-of-Flight Methods, Saclay, 1961*, ed. by J. Spaepen, European Atomic Energy Community (EURATOM), Brussels, 1961; see *Neutron Cross Sections*, BNL-325 2d ed. (July 1, 1958) for gadolinium resonances.

Activation Cross Section of the 2.6×10^6 yr Bi^{210}

Joseph Halperin J. H. Oliver

The thermal cross section and resonance integral for the reaction

$$Bi^{210} \xrightarrow{(n,\gamma)} Bi^{211}\ (AcC)$$
$$\alpha \searrow\ 2.6 \times 10^6\ yr \qquad \alpha \searrow\ 2.16\ min$$

were measured using a cadmium-filter technique.

Samples from two batches of bismuth containing Bi^{210} produced in reactor irradiations were used. Batch *A* contained 8.0 ppm Bi^{210}; batch *B*, of different irradiation history and calutron-concentrated,[5] contained 0.268% Bi^{210}. The bismuth samples were mounted on 7-mil polyethylene film and placed in polyethylene "rabbits." They were then irradiated in the pneumatic tube of the ORR with and without cadmium filters. In general it was possible to retrieve the sample and transfer it to a 2π proportional alpha counter in times ranging from 30 sec to 2 min. Only the 2.16-min

[5]We are indebted to J. R. Huizenga of the Argonne National Laboratory for the use of this material.

period of Bi^{211} (AcC) was observed over the length of time (about 15 min) that the decay was followed. Irradiated blanks gave no evidence for contributing to the background by beta and gamma "pile up." After a period of hours to days, Po^{210} alphas could be observed as they were formed from the beta decay of the 5.0-day Bi^{210} (RaE).

The Bi^{210} was assayed[6] by measurement of the alpha decay rate in weighed samples of either vacuum-evaporated bismuth metal or a $BiONO_3$ solution precipitated under vacuum with NH_3 vapor. The spectrum was examined with a Frisch chamber and a multichannel analyzer and found to be sufficiently thin that self-absorption losses were negligible.

The neutron flux was measured with a manganese monitor in an aluminum alloy containing 0.087% Mn. The computation was based upon the values of $\sigma_{2200} = 13.2$ and $I = 13.1$ barns for forming 2.58-hr Mn^{56}.

The data are summarized in Table 1.2. An average effective cross section of 0.063 barns for a flux ratio $\phi_{th}/\phi_r \approx 25$ was observed. The thermal cross section ϕ_{th} was found to be 0.054 barn and the resonance integral I was 0.20 barn. These values are considered uncertain to ±10%.

Effective Cutoff Energies for Cadmium, Gadolinium, Samarium, and Boron Filters

R. W. Stoughton Joseph Halperin

Previous calculations of effective neutron cutoff energies for cylindrical and spherical filters of cadmium or boron have been extended to include gadolinium and samarium filters and slab-shaped filters by using a new program written for the IBM 7090 computer.[7] The model assumed a point $1/v$

[6] We are indebted to C. R. Baldock and L. E. Idom for checking the assays by mass analysis. They were found to be consistent with the radiochemical measurements.

[7] *Chem. Div. Ann. Progr. Rept. June 20, 1961*, ORNL-3176, p 2; also see ORNL TM-236 for more details and numerical results of the calculations.

Table 1.2. Irradiation Data for the Reaction $Bi^{210}(n,\gamma)Bi^{211}$

Sample No.	Sample Weight (μg)	Bi^{210} Weight (μg)	Fluxes[a] ϕ_{th} [n/(cm^2 sec)]	Fluxes[a] ϕ_r [n/(cm^2 sec)]	Irradiation Time (sec)	N^{211} chain / N^{210}	σ_{eff} (barn)	σ_{th} (barn)	I (barn)
		$\times 10^{-3}$	$\times 10^{13}$	$\times 10^{13}$		$\times 10^{-10}$			
Bare[b]									
1	414	3.21	5.81		240	6.7_6	0.062	0.053	
					240	6.5_6	0.060	0.051	
					240	6.8_4	0.063	0.054	
2		114	6.23		20	7.5_9	0.065	0.056	
					20	7.3_4	0.063	0.054	
Filtered									
3	1616	12.9		0.251	20	0.96_1			0.19
4		78.0		0.273	20	1.00			0.19_6
5		123.5		0.273	20	0.70_2			0.21

[a] Samples 1 and 3 were irradiated in the same geometry; samples 2, 4, and 5 in another. Flux ratios should be compared for samples irradiated in the same geometry.

[b] Samples reirradiated (e.g., the three sets of values for sample No. 1 are for three irradiations of that sample).

detector inside the filter and a Maxwellian plus a $1/E$ epithermal flux, both isotropic with respect to the detector. The parameters varied were the Maxwellian temperature T_m (where $E_m = kT_m$), the ratio r of Maxwellian flux to $1/E$ flux per lethargy unit, the lower limit μ of the $1/E$ flux, the filter thickness l_o, and, in the case of cylindrical filters, the height/diameter ratio.

Also calculated were differential reaction rates vs energy and the fraction *FRACT* of total reactions occurring below the cutoff, both of which give a measure of the filter efficiency. The effective cutoff was defined in terms of the cutoff of a perfect filter (infinitely sharp) which gave the same reaction rate, for the filtered sample, as the filter actually used.

In the cases of cadmium and gadolinium the cross sections were set equal to Breit-Wigner expressions for the resonances at 0.178 and 0.03 ev, respectively. In the case of samarium the resonance most pertinent to its properties as a filter is that at 0.0976 ev. However, because of other relatively near higher-energy resonances, particularly that at 0.88 ev, the cross section does not continue to decrease as $E^{-5/2}$ above 0.0976 ev, and the 0.88-ev resonance causes a perturbation on the filter properties. The cross section of samarium for most calculations was set equal to a single Breit-Wigner expression (one level: $E_r = 0.0976$ ev) plus a $1/v$ term; for comparative purposes some calculations were conducted in which the cross section was set equal to the sum of two Breit-Wigner expressions (two level: $E_r = 0.0976$ and 0.88 ev) plus a $1/v$ term. The boron cross section was set equal to a $1/v$ term normalized to 755 barns at 0.0253 ev.

Cutoffs and Filter Efficiencies. – Effective cutoffs and *FRACT*'s are shown for the various filter materials for a typical set of conditions in Figs. 1.1 and 1.2. As expected, boron is the poorest filter. Of the others, cadmium shows the lowest values of *FRACT* (i.e., the most efficient filter) and the highest cutoffs, for reasonable thicknesses. The effect on the cutoff E_c of taking into account the resonance at 0.88 ev in samarium is seen in Fig. 1.1.

Recently Hickman and Leng[8] published a similar calculation of effective cutoffs for cadmium, gadolinium, and samarium in which they considered only the beam flux and isotropic flux cases. On the assumptions made, these should be the same as the spherical and slab filters, respectively, of the current work. The agreement in all cases, except for samarium with isotropic flux (slab filter), was good – within about 5% in E_c. Since the cross-section parameters and certain aspects of the calculational procedures were not identical in the two calculations, the agreement is probably as good as should be expected. In the case of a samarium slab, the current E_c results were higher by a maximum of about 20% than those of Hickman and Leng. This discrepancy may result largely from the fact that Hickman and Leng did not include a $1/v$ term (as did the current calculations). The inclusion of a $1/v$ term should increase the calculated values of E_c; the increase should be greater in the slab than in the sphere, because of the greater effective thickness of the filter (for given actual thickness). Thus the discrepancy is at least in the expected direction.

Hickman and Leng[8] also varied the thickness of the $1/v$ detector from essentially infinite thinness to near opacity, and found a maximum variation of

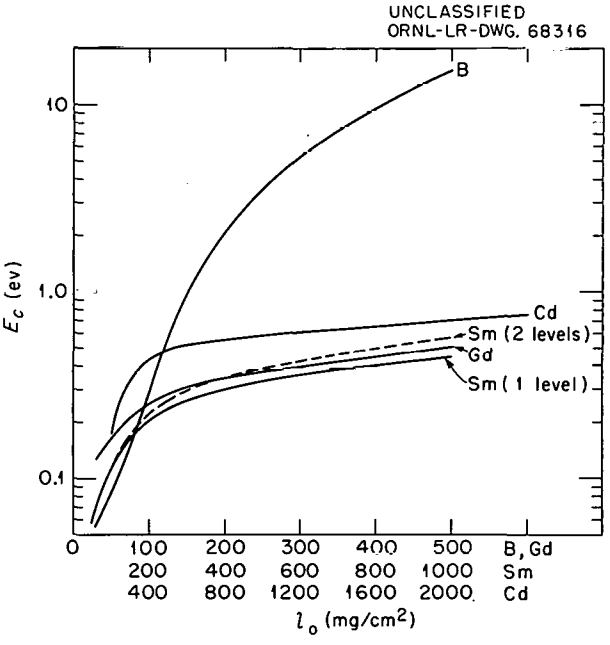

Fig. 1.1. Comparative Values of Effective Cutoffs for B, Cd, Gd, and Sm Cylindrical Filters (H/D = 2, $E_m = 0.0253$ ev, $\mu = 5$, $r = 10$).

[8] G. D. Hickman and W. B. Leng, *Nucl. Sci. Eng.* **12**, 523 (1962).

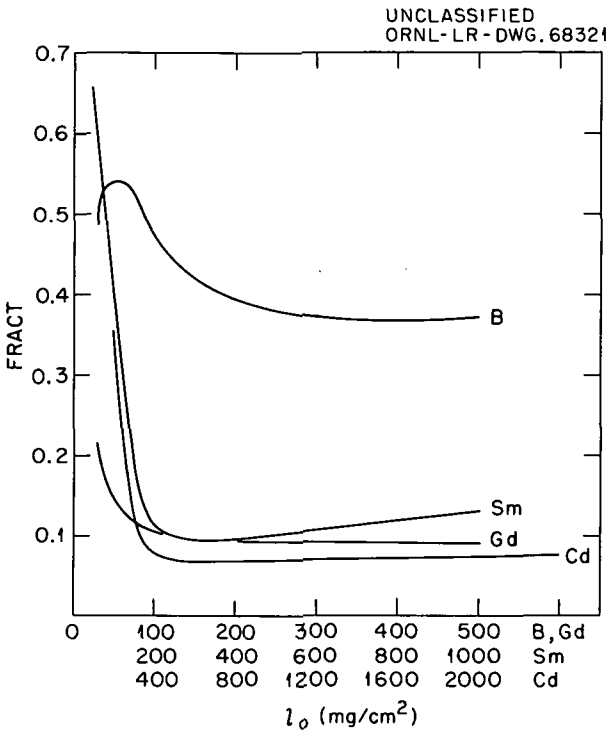

Fig. 1.2. Comparative Values of FRACT (Fraction of Reactions Below Cutoff) for B, Cd, Gd, and Sm Cylindrical Filters (H/D = 2, E_m = 0.0253 ev, μ = 5, r = 10).

only about 10% in E_c. Thus the effect is relatively small, and a correction could be made if necessary for thick detectors.

Filter Thickness and Efficiency. – From a study of the differential rates vs energy and filter thickness an appraisal can be made of the desired thicknesses of the filters. For example, for cadmium at a thickness of 10 mils (E_m = 0.0253 ev, r = 10), some 40% of the reactions result from Maxwellian neutrons below the cutoffs; at 30 mils or thicker, only 7% of the reactions result from neutrons below the cutoff, and these are near the cutoff rather than near the Maxwellian maximum (E_m). For gadolinium, samarium, and boron, reactions resulting from neutrons near the Maxwellian maximum become relatively unimportant at thicknesses above about 100, 500, and 300 mg/cm^2, respectively (although of course boron is a poor filter at all thicknesses).

In the case of gadolinium, its resonance at 0.03 ev is only slightly above the value of E_m even at low values of the latter (around 0.025 ev). The low value of the resonance is desirable in providing a cutoff near the lower limit of the $1/E$ flux (some 5 E_m). However, it is undesirable in that the lower the cutoff the more Maxwellian neutrons are transmitted by the filter.

Variation in the Lower Limit μ of the $1/E$ Flux. – Westcott[9] has reported that experimental measurements in thermal reactors indicate that the $1/E$ flux goes to zero at some 3 to 6 times the energy E_m corresponding to the Maxwellian most probable velocity, and he discusses four different continuous expressions which go rapidly to zero with decreasing energy.

In the calculations reported here, variation between μ = 3 and μ = 5 for reasonable thicknesses of filters showed only a 1% change in E_c for cadmium and only about 2% for the others. In going to μ = 10 and still using reasonable thicknesses, variations of 10% in E_c were observed. Hickman and Leng[8] found only a 1% variation in E_c in going from μ = 4 to μ = 6. Hence it does not appear to be important to know the exact lower limit of the $1/E$ flux or to have a continuous function for its termination. A sharp termination at μ = 5 should be satisfactory.

Additional Conclusions. – Cadmium with a thickness of 30 or (preferably) 40 mils is perhaps the most useful all-around filter, with gadolinium a reasonably good second choice. Cylindrical filters are probably best for in-pile work.

By the use of cadmium and gadolinium (and perhaps samarium too) with their different cutoffs, it should be possible to detect resonances in the thermal-to-cutoff regions in an unknown sample.

Thermal Neutron Cross Section and Resonance Integral of Sm^{150}

Joseph Halperin R. E. Druschel
C. R. Baldock

A number of fission products of relatively high cross section occur in the rare earth region. Their cross sections are of particular interest in the problem of reactor poisoning. In the sequence of nuclides starting with Pm^{147}, successive neutron

[9] C. H. Westcott, *Effective Cross Section Values for Well-Moderated Thermal Reactor Spectra* (3d ed. corrected) CRRP-960 (Nov. 1, 1960); also earlier editions: CRRP-662 (1956); addendum to CRRP-680; CRRP-787 (1958).

capture in a high-flux reactor finally results in Gd^{156}. Therefore one atom of fission product poison can result in the loss of a number of neutrons, thus multiplying the poisoning effect. The cross section of Sm^{150} has been measured and found to be sufficiently low to effectively interrupt these sequences which start at masses 147 and 149, thus limiting reactor poison losses.

Several samples of samarium oxide enriched in Sm^{150} to 96.3% were irradiated in the ORR with a cadmium ratio technique.[10] The irradiation tube contained a sample in a cadmium capsule at each end and an unfiltered sample in the middle; thus three samarium samples were irradiated simultaneously. A cobalt monitor in the form of a cobalt-aluminum alloy (0.15% Co) was placed on each side of each samarium sample. Following the irradiation the samples were examined in a two-stage 12-in. mass spectrometer using a thermal ionization source and electron multiplier detectors. Ratios of Sm^{151}/Sm^{150} were measured.[11]

Three runs were made (see Table 1.3), from about 40 to 95 hr in duration, on submilligram quantities of Sm_2O_3. The flux measurements were based on cobalt cross sections of $\sigma_{2200} = 37$ barns and $I = \int_{0.54\,ev} \sigma\, dE/E = 75$ barns. The specific activities of the cobalt monitors were compared with 4π beta-gamma coincidence measurements. The samples in run B apparently stuck at a point short of the normal high-flux position in the hydraulic tube. This is evident from the flux measurement of about 2×10^{12} $n/(cm^2\ sec)$, which is almost 100-fold less than its normal value, and is further attested to by the lower mass ratio measurements. The smaller value of both the effective cross section σ_{eff} and the resonance integral I is attributed to the larger uncertainty in the mass measurements at the level of 7 ppm, and these values were not included in the final average.

Due to the large cross section of Sm^{151}, it was necessary to take into account its burnup in the cross section computation. The computation was based on $\sigma_{2200} = 16{,}080$ barns, $I = 3450$ barns, and $g(0.033\ ev) = 0.85$ as given by Westcott.[12] The samples were sufficiently thin so that no self-shadowing took place in the Sm^{151}.

The cross section conventions used have been described previously.[10] The thermal flux ϕ_{th} is taken as the Maxwellian component of the flux spectrum, and ϕ_r is the epithermal flux per unit ln E. The effective cross section is taken as the reaction rate divided by the thermal flux. The thermal cross section σ_{th} is the subcadmium reaction rate divided by thermal flux; that is,

$$\sigma_{th} = g\sigma_0 + \frac{\phi_r}{\phi_{th}} \int_{5E_m}^{0.54\,ev} \sigma\, dE/E\ .$$

[10] R. W. Stoughton and Joseph Halperin, *Nucl. Sci. Eng.* **6**, 100 (1959).

[11] The authors are indebted to L. E. Idom for his aid in making these measurements.

[12] C. H. Westcott, *Effective Cross Section Values for Well-Moderated Thermal Reactor Spectra* (3d ed. corrected) CRRP-960 (Nov. 1, 1960).

Table 1.3. Irradiation Data for Sm^{150} Cross Section Measurement

Run No.	Sample Weight (μg of Sm_2O_3) No. 2 (Bare)	No. 1 (Cd Filtered)	No. 3 (Cd Filtered)	Irradiation Time at 30 Mw (hr)	ϕ_{th} $[n/(cm^2\ sec)]$	ϕ_{th}/ϕ_r	Sm^{151}/Sm^{150} No. 2 (Bare)	No. 1 (Cd Filtered)	No. 3 (Cd Filtered)	σ_{eff} (barns)	σ_{th} (barns)	I (barns)
					$\times 10^{14}$		$\times 10^{-5}$	$\times 10^{-5}$	$\times 10^{-5}$			
A	688	726	673	95.4	1.46	10.6_5	446	115	117	124	$100._5$	248
B	690	702	702	85.4	0.0205	16.8_3	6.7	0.66	0.81	107	$95._1$	196
C	652	638	645	41.5	1.56	11.7_4	230	51.0	52.6	116	93.8	261
										Av	97	255

An average effective cross section of about 120 barns for Sm^{150} was observed in these irradiations for a ratio of thermal to resonance flux of about 11. An average thermal cross section of 97 barns and a resonance integral of 255 barns were measured. These values are considered uncertain to ±10%.

Half-Life of Bi^{208}

Joseph Halperin R. W. Stoughton
R. E. Druschel C. R. Baldock

Bi^{208} has been found by Millar *et al.*[13] to decay by orbital electron capture to the 2.615-Mev level in Pb^{208} so that all decay transitions involve emission of this gamma ray. A reactor-irradiated sample[14] of bismuth was sufficiently enriched in Bi^{208} by a calutron separation[15] to enable a mass spectrographic analysis. From measurement of the specific activity of the 2.615-Mev gamma ray in this sample, the half-life of this nuclide was estimated to be $(5.61 \pm 0.15) \times 10^5$ years.

The bismuth sample had a history of a one-year irradiation in the MTR. The Bi^{208} is formed in the reactor through the reaction $Bi^{209}(n,2n)Bi^{208}$ by neutrons in the fission spectrum of energy greater than about 8 Mev. Consequently it would be formed in low yield; in fact an effective cross section based on the thermal flux of ~3 mb was observed, assuming a 20-mb cross section for the formation of the 2.6×10^6 year Bi^{210}.

The concentrated sample was found[16] to contain 184 ± 4 ppm of Bi^{208}, compared with the 25 ± 5 ppm in the pile-irradiated sample. A measurement of the 2.615-Mev gamma ray in 100.8 mg of the concentrated sample in the form of Bi_2O_3 yielded a specific activity of $(1.39 \pm .03) \times 10^3$ dis/min of Bi^{208} per mg of bismuth. Calibration of the $2\frac{1}{2} \times 2\frac{1}{2}$ in. NaI crystal used was carried out using the 2.754-Mev photopeak of Na^{24}, which in turn was calibrated by the 4π beta-gamma coincidence technique. A correction of 2.5% was applied for the difference in photopeak efficiency of the 2.754- and 2.615-Mev gamma rays.

Effective Capture Cross Section of Ce^{141} for Thermal Neutrons

P. M. Lantz

Although Ce^{141} is formed in high yield (6.3%) in U^{235} fission, a literature search revealed no measurement of its neutron capture cross section. In this work the effective capture cross section of Ce^{141} was determined by irradiating samples of Ce^{140} containing about 9 ppm Ce^{142} in the MTR for periods of 113 and 222 days. The Ce^{142} formed by two successive neutron captures was determined both by activation and by mass analysis.

The irradiations were carried out in the L-45 position of the MTR, where the thermal flux is 3.43×10^{14} neutrons cm^{-2} sec^{-1}. The average ratio of thermal flux to resonance flux per ln E interval was about 12. This is based on a cadmium ratio of 7.25 for a 600-Mwd cycle at a 40-Mw power level. The samples were monitored with cobalt in a Co-Al alloy (0.15% Co^{59}). The values of 36.7 (ref 17) and 75 (ref 18) barns for the thermal cross section σ_0 and resonance integral I_0 of cobalt and the value of 0.0253 for the peak E_m in the Maxwellian neutron spectrum were used in the determination of the flux ratio ϕ_{th}/ϕ_r.

Mass spectrographic analysis[19] of the Ce^{140} irradiated 113 days showed an increase to 35.5 ppm at the 142 mass position and the sample irradiated 222 days showed 187 ppm (both relative to Ce^{140}). After the tetravalent cerium had been exhaustively purified by extraction with di(2-ethylhexyl) phosphoric acid in *n*-heptane, the abundance at the 142 mass position had dropped to 32 ppm and 116 ppm, respectively, indicating that a secondary process such as neutron capture by Pr^{141}, the daughter of 32.5-day Ce^{141}, had contributed mass 142.

---

[13] C. H. Millar, T. A. Eastwood, and C. J. Roy, *Can. J. Phys.* **37**, 1126 (1959).

[14] The authors are indebted to J. R. Huizenga of Argonne National Laboratory for making this reactor sample available.

[15] The authors are grateful to L. O. Love and numerous associates for their generous aid in making this separation.

[16] The authors wish to thank L. E. Idom for his help in the mass measurements.

[17] D. J. Hughes and R. B. Schwartz, *Neutron Cross Sections*, BNL-325, 2d ed. (July 1, 1958).

[18] F. J. Johnston, Joseph Halperin, and R. W. Stoughton, *J. Nucl. Energy: Pt A*, **11**, 90–100 (1959).

[19] Performed by C. R. Baldock and L. E. Idom.

The Ce^{142} content in the purified Ce^{140} sample was confirmed by neutron activation, by irradiating in the LITR with natural cerium monitors. The 3-min Ce^{143} produced by (n,γ) reaction on Ce^{142} was determined by following the decay of the separated 13.8-day Pr^{143} daughter for several half-lives with a 4π beta counter and extrapolating back to the time of removal from the reactor. This analysis showed that the Ce^{142} contents of the initial Ce^{140} and of the Ce^{140} irradiated 113 days in the MTR were 12 and 34 ppm, respectively.

The data necessary for the determination of the effective neutron capture cross section of Ce^{141} were programmed[20] for the IBM 7090 computer. In developing the program, the radiation time represented reactor operation time at full power (40 Mw). Consideration was also given to the beta decay of Ce^{141} during reactor shutdown. In this determination a 32.5-day half-life for Ce^{141} and a 0.59-barn thermal neutron capture cross section[21] for Ce^{140} were used. Since no information could be found on the resonance absorption integral for Ce^{140}, several measurements were made in the LITR using pure Ce^{140} and are reported separately. The value of 0.48 barn for the resonance integral[21] of Ce^{140} was used in the determination of the 0.63-barn effective neutron capture cross section σ_{eff} for Ce^{140} in the MTR. An effective cross section of 30 ± 3 barns was found for Ce^{141}.

Since mass analysis of the Ce^{140} irradiated 222 days showed a reduction of 71 ppm at the 142 mass position after the Ce(IV) purification, a check was made to determine whether the difference was consistent with the published values. On the assumption that the 71-ppm difference at the 142 mass position was due to the reaction

$$Pr^{141} \xrightarrow{(n,\gamma)} Pr^{142} \xrightarrow{\beta^-} Nd^{142}$$

in the MTR, the effective cross section for Pr^{141} would be 11.1 barns. The effective cross section for Pr^{141} in the MTR determined from the values $\phi_{th}/\phi_r = 12.4$, $\sigma_{th} = 10.8$ barns,[22] and $I_0 = 11.3$ barns[23] would be 11.7 ± 0.4 barns by the formula[24]

$$\sigma_{eff} = \sigma_{th} + \frac{\phi_r}{\phi_{th}} I_0 .$$

[20] By R. W. Stoughton.

[21] Reported in the section, "Thermal Neutron Absorption Cross Section and Resonance Integral of Ce^{140}," (this chapter).

Thermal Neutron Absorption Cross Section and Resonance Integral of Ce^{140}

P. M. Lantz

Since a value for the I_0 of Ce^{140} was unavailable, yet essential for the determination of the σ_{eff} of Ce^{141}, and a pure source of Ce^{140} was available, both the ϕ_{th} and the I_0 of Ce^{140} were measured. Several samples of $Ce^{140}O_2$, the same source material used in the Ce^{141} cross section measurement, were irradiated in the LITR with cobalt and gold monitors, both with and without (40 mil) cadmium filters. The Ce^{141} produced was determined by 4π beta-gamma coincidence counting. Values of $\sigma_{th} = 0.59$ barn and $I_0 = 0.48$ barn were measured. The conventions used in these determinations have been discussed by Stoughton and Halperin.[25] This thermal cross section may be compared with a value of 0.31 ± .07 barn measured by Katcoff *et al.*[26]

FISSION STUDIES AND CHARACTERIZATION OF LOW-ENERGY PROPERTIES OF NUCLEI

Decay of Pm^{150}[27]

N. B. Gove[28] G. D. O'Kelley

The preliminary investigation[29] of radiations from 2.7-hr Pm^{150} has been extended with the aid of additional single-crystal and coincidence scintillation spectrometry experiments.

Gamma-ray spectra taken with a 3 × 3 in. NaI scintillation spectrometer disclosed gamma rays with energies in Mev (and relative intensities)

[22] D. J. Hughes, B. A. Magurno, and M. K. Brussel, *Neutron Cross Sections*, BNL-325, 2d ed., suppl 1 (Jan. 1, 1960).

[23] J. D. Garrison and B. W. Roos, *Nucl. Sci. Eng.* **12**, 115 (1962).

[24] R. W. Stoughton and Joseph Halperin, *Nucl. Sci. Eng.* **6**, 100 (1959).

[25] R. W. Stoughton and Joseph Halperin, *Nucl. Sci. Eng.* **6**, 100–118 (1959).

[26] *Neutron Cross Sections*, BNL-325, 2d ed. (1958).

[27] Abstract published in *Bull. Am. Phys. Soc.* **7**, 352 (1962).

[28] Nuclear Data Project, National Academy of Sciences.

[29] N. B. Gove and G. D. O'Kelley, *Chem. Div. Ann. Progr. Rept. June 20, 1960*, ORNL-2983, p 4.

of 0.333 (100), 0.407 (10), 0.59 (5), 0.72 (11), 0.84 (30), 0.88 (12), 1.02 (4), 1.18 (32), 1.23 (7), 1.330 (31), 1.625 (2.6), 1.75 (14), 1.96 (3.5), 2.07 (1.7), 2.2 (0.8), 2.41 (0.35), 2.53 (1.3), 2.75 (0.4), 2.91 (0.5), and 3.08 (0.16). Gamma-ray spectra were recorded in coincidence with the gamma-ray peaks at 0.333, 0.407, 0.85, 1.18, 1.23, 1.33, and 1.75 Mev. Three gamma-beta coincidence experiments were performed, in which gamma-ray spectra were recorded in coincidence with beta rays of energy greater than 1.1, 1.4, and 1.8 Mev.

Fermi analyses of beta-ray spectra recorded with an anthracene scintillation spectrometer yielded beta components at 3.16 ± 0.08 Mev, 2.28 ± 0.08 Mev, and lower energies. Additional information was obtained on the energies of the beta groups and their places in the decay scheme by a series of beta-gamma coincidence experiments, in which beta-ray spectra were measured in coincidence with peaks at 0.333, 0.407, 0.84, 1.18, 1.33, and 1.75 Mev in the gamma-ray spectrum. The single-crystal and coincidence results identified the following beta groups with energies in Mev (and intensities) of 1.4 (8%), 1.8 (19%), 2.28 (36%), 2.77 (weak), and 3.16 (16%). The remaining beta-ray intensity is associated with unresolved beta groups which decay to some of the higher energy levels.

The decay scheme shown in Fig. 1.3 is consistent with most of the information available from this investigation. The levels in Sm^{150} at 0.333, 0.743, 1.18, 1.66, 1.96, 2.07, 2.41, and 3.08 Mev were established by means of the coincidence data. The remaining level assignments must be considered only tentative at present. Several of the low-lying levels in Sm^{150} seen in this investigation correspond to levels observed in Eu^{150} decay[30], in the Sm^{149} neutron-capture gamma-ray spectrum,[31] and in nuclear reactions.[32]

The disintegration energy for Pm^{150} is 3.50 ± 0.08 Mev, which is about 1.5 Mev lower than the previously published value.[33] The present energy is in accord with the systematics of Way and Wood.[34]

Decay of Cs^{132}

R. L. Robinson[35] N. R. Johnson
E. Eichler

A previous investigation[36] of 2.3-hr I^{132} by this group established many of the properties for nine low-lying levels in Xe^{132}. Since a study of Cs^{132} would be expected to disclose additional information about levels of Xe^{132}, an investigation of its gamma rays was undertaken. This type of information provides a test of the numerous nuclear models that have been proposed to explain the properties of low-lying levels of even-even, medium-weight nuclei. It should also prove useful in the future development of these models.

The Cs^{132} sources used in this study were prepared with the ORNL 86-in. cyclotron by means of the nuclear reaction Cs^{133} $(p,pn)Cs^{132}$. Gamma-ray spectra were measured with 3 × 3 in. NaI crystals; the singles intensities are shown in Table 1.4. From the rate of decay of the intense 669-kev gamma ray, the half-life of Cs^{132} was computed to be 6.54 ± 0.03 days.

Coincidence measurements were made with the single-channel analyzer gating on the 464-, 509-, 669-, 1139-, and 1319-kev gamma rays. In Table 1.4 we show, for each designated transition, the intensity of the gamma ray(s) in coincidence with the gating gamma ray of interest. The coincidence intensities have been corrected for contributions from Compton scattering caused by entrance of higher-energy gamma rays through the single-channel window and for the angular correlation, when known, between the coincident gamma rays.

Energy levels and transitions of Xe^{132} and Ba^{132} compatible with the results of Table 1.4 are illustrated in Fig. 1.4*b*. Levels of Xe^{132} with

---

[30]B. Harmatz, T. H. Handley, and J. W. Mihelich, *Phys. Rev.* **123**, 1781 (1961).

[31]R. K. Smither, *Bull. Am. Phys. Soc.* **7**, 316 (1962).

[32]R. A. Kenefick and R. K. Sheline, Paper D2 presented at the Meeting of the Southeastern Section of the American Physical Society, Florida State University, April 5–7, 1962; abstract to be published in the Bulletin of the American Physical Society.

[33]V. K. Fischer and E. A. Remler, *Bull. Am. Phys. Soc.* **3**, 63 (1958).

[34]Katharine Way and Marion Wood, *Phys. Rev.* **94**, 119 (1954).

[35]Physics Division.

[36]R. L. Robinson, E. Eichler, and N. R. Johnson, *Phys. Rev.* **122**, 1863 (1961); *Chem. Div. Ann. Progr. Rept. June 20, 1960*, ORNL-2983, p 3.

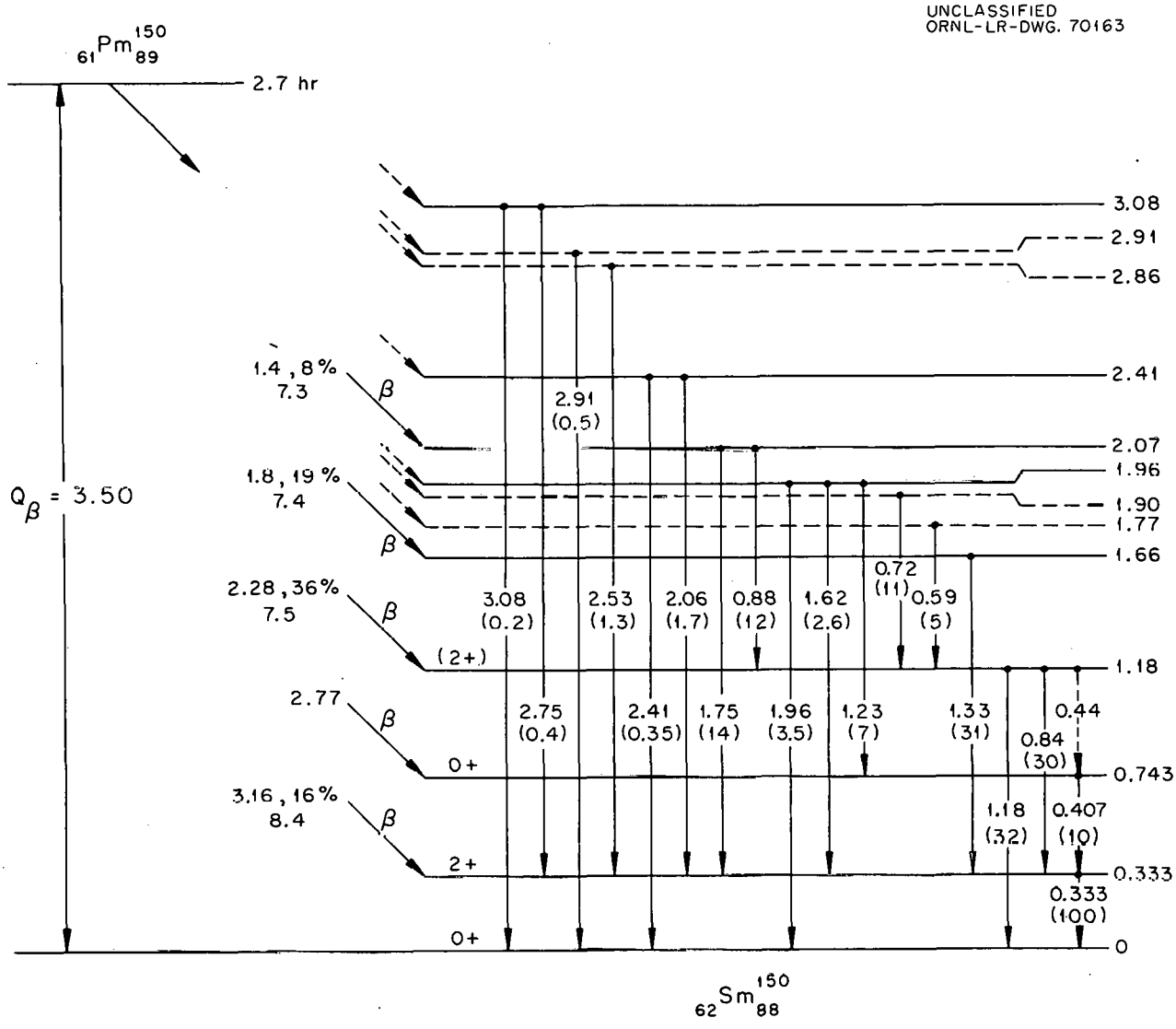

Fig. 1.3. Decay Scheme Proposed for Pm^{150}. The pair of numbers shown for each gamma ray gives its energy in Mev and its relative intensity. The numbers shown for each beta-ray transition give the energy in Mev, the intensity, and the log *ft* value.

energies less than 2.0 Mev and populated by I^{132} have been included in Fig. 1.4*a* for comparison. The numbers shown with each gamma ray designate the energy and relative intensity, whereas those shown for the decay by electron capture, positron emission, and beta-ray emission give the relative intensity and log *ft* value. These log *ft* values are based on an energy separation of 1.48 Mev between Cs^{132} and the 0.669-Mev level of Xe^{132}. This energy difference was calculated[37] from the ratio of decay by electron capture to that by positron emission.

The coincidence experiments showed that the 464- and 1035-kev gamma rays were not associated with Xe^{132} levels, and yet their half-lives link them with the decay of Cs^{132}. They are therefore assigned as transitions in Ba^{132}. The energy of the 464-kev transition is consistent with the value of 470 ± 7 kev reported by Fagg[38] for a Coulomb-

[37]Eugene Feenberg and George Trigg, *Revs. Mod. Phys.* **22**, 399 (1950).

[38]L. W. Fagg, *Phys. Rev.* **109**, 100 (1958).

Table 1.4. Cesium-132 Gamma-Ray Energies and Relative Intensities

The intensities are normalized to a value of 1000 for the 669-kev gamma ray in the singles spectrum

E_γ (kev)	Singles Spectrum Intensities	Intensities in Spectra in Coincidence with Gating Gamma Rays of Indicated Energies				
		464 kev	509 kev[a]	669 kev	1139 kev	1319 kev
464 ± 5	21 ± 5					
509 ± 7	17 ± 4			18 ± 4	<0.1	0.31 ± 0.16[b]
569 ± 6		2.7 ± 0.8				
631 ± 8			5.6 ± 1.9	8.5 ± 1.8		
669 ± 4	1000 ± 30		16 ± 5		4.8 ± 0.8	4.6 ± 1.5
1035 ± 12	1.6 ± 0.3					
1139 ± 11	5.2 ± 0.5			5.0 ± 0.6		
1304 ± 20			0.58 ± 0.20			
1319 ± 10	6.5 ± 0.6			6.6 ± 0.7		
2000 ± 30	0.53 ± 0.06					

[a] The intensities are for the spectrum taken with $\theta = 90°$.

[b] This gamma ray is believed to result from coincidences with the 1304-kev gamma ray.

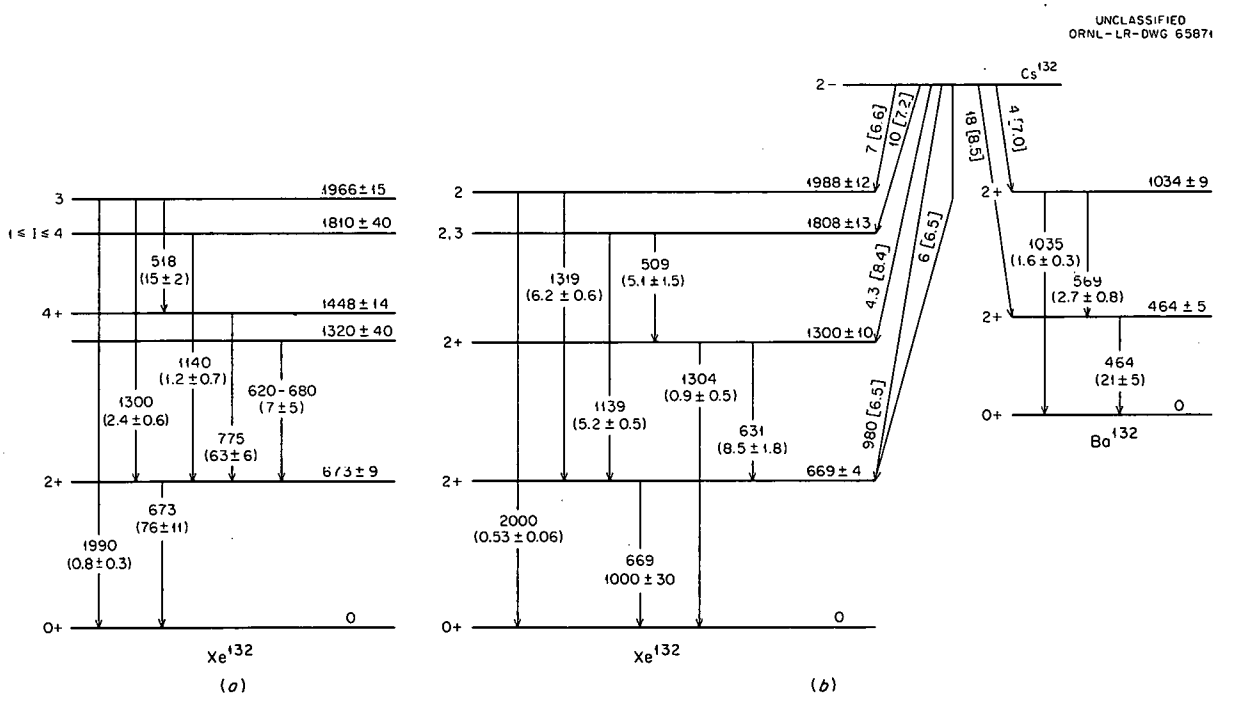

Fig. 1.4. (*a*) Transitions and Energy Levels of Xe^{132} Below 2.0 Mev in the Decay of I^{132} as Previously Reported (ref 36); (*b*) Transitions and Energy Levels of Xe^{132} and Ba^{132} in the Decay of Cs^{132}. The pair of numbers with each gamma ray gives its energy in kev and its relative intensity. Those pairs of numbers shown for decay by electron capture, beta-ray emission, and positron emission give the relative intensities and log *ft* values.

excited 2^+ level of Ba^{132}. Coincidences between this gamma ray and a weak 569-kev transition establish a second level in Ba^{132} at 1034 kev. Additional evidence for this latter level is provided by the 1035-kev gamma ray.

Gamma-gamma angular correlations were measured for each gamma ray coincident with the 669- and 464-kev transitions. Data were taken every 10° between 90° and 180° and were fitted by the method of least squares to the equation $W(\theta) = 1 + A_2P_2(\cos\theta) + A_4P_4(\cos\theta)$ on an IBM 7090 computer. These measurements led to the spins assigned for the 1300-, 1808-, and 1988-kev levels in Xe^{132} and for the 1034-kev state in Ba^{132}.

Although in Fig. 1.4 the energies of the (1988 ± 12)-kev level populated by Cs^{132} and the (1966 ± 15)-kev level populated by I^{132} are in reasonable agreement, their spins and the branching ratios of gamma rays from them are different. Therefore, it is concluded that they are not the same level.

We have previously compared the levels of Xe^{132} populated by I^{132} with levels predicted by various nuclear models.[36] This comparison, which is reproduced in Fig. 1.5, includes the information about the 1300-, 1808-, and 1988-kev levels obtained from the present study of Cs^{132}. As pointed out before, the second 2^+ and the first 4^+ levels can be explained by all models[39–44] except that of Davydov and Filippov.[41] However, none of the models can account for all four levels between 1.8 and 2.1 Mev. It is possible that a low-lying 0^+ level as predicted by several of the models does exist. Neither Cs^{132} nor I^{132} would be expected to populate a level of this spin with sufficient intensity to be observed.

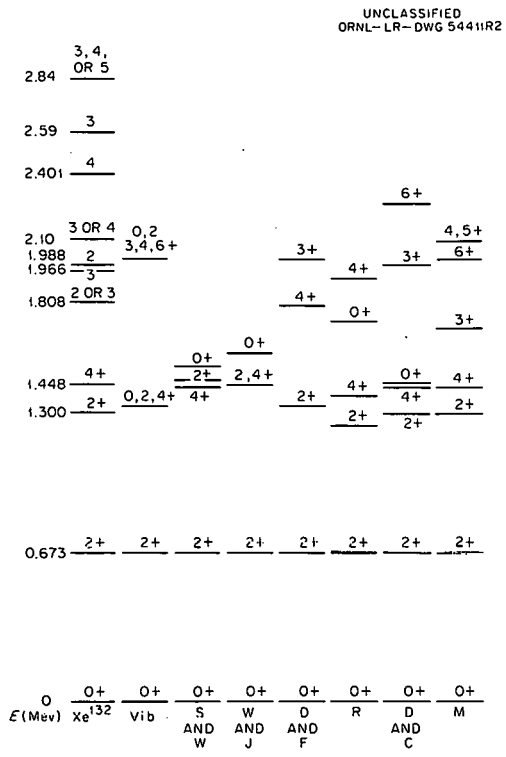

Fig. 1.5. Comparison of the Xe^{132} Levels with Levels Predicted by the Pure Vibrational Model (Vib) and by Nuclear Models of the Following Investigators: Scharff-Goldhaber and Weneser (S and W), Wilets and Jean (W and J), Davydov and Filippov (D and F), Raz (R), Davydov and Chaban (D and C), and Mallmann (M). These models are discussed in refs 39–44. The parameters which were used are given in ref 36.

Yields and Half-Lives in the Mass-99 Fission-Product Chain

D. E. Troutner[45] R. L. Ferguson
G. D. O'Kelley

Experiments described previously[46] have given some evidence for the existence of unreported isomers of Zr^{99} and/or Nb^{99}. Additional experiments have now been performed in which zirconium was rapidly separated from both niobium and

[39]Gertrude Scharff-Goldhaber and J. Weneser, *Phys. Rev.* **98**, 212 (1955).

[40]Lawrence Wilets and Maurice Jean, *Phys. Rev.* **102**, 788 (1956).

[41]A. S. Davydov and G. F. Filippov, *Nucl. Phys.* **8**, 237 (1958).

[42]B. J. Raz, *Phys. Rev.* **114**, 1116 (1959).

[43]A. S. Davydov and A. A. Chaban, *Nucl. Phys.* **20**, 499 (1960).

[44]C. A. Mallmann, *Nucl. Phys.* **24**, 535 (1961).

[45]ORINS Research Participant, 1960 and 1961. Permanent address: University of Missouri, Columbia.

[46]D. E. Troutner and R. L. Ferguson, *Chem. Div. Ann. Progr. Rept. June 20, 1961*, ORNL-3176, p 6.

molybdenum, following brief thermal-neutron irradiations of U^{235} solutions. The zirconium was separated by coprecipitation with $Fe(OH)_3$ in an NH_4OH-H_2O_2 medium. The results of these experiments are shown in Fig. 1.6, with data from the earlier work, in which a zirconium-niobium fraction was separated from molybdenum.

It is apparent that the upper curve of Fig. 1.6 (labeled Zr + Nb) represents primarily the decay of niobium precursors of Mo^{99}, since the lower curve ("Zr only") is at all times <5% of the Zr + Nb curve. The 140-sec half-life obtained for the longer-lived niobium component is in good agreement with the published value[47] for Nb^{99}. The 10-sec activity is due to a previously-unknown isomer of Nb^{99}, which has been found to decay directly to Mo^{99} in at least 65% of its disintegrations. Attempts to observe gamma radiation from this isomer in rapidly separated niobium fission products were inconclusive, because of the relatively long time (~60 sec) between irradiation and counting and because of the very complex spectra of the short-lived niobium fission products. The ordinate intercept of the upper curve gives the total fractional cumulative yield of both Nb^{99} isomers (0.94 ± 0.11), which is consistent with the predicted[48] value (~0.99). Unfortunately, this result is not accurate enough to test the postulated preference for a 50-42 proton division in uranium fission.[49]

The 75-sec half-life obtained from the "Zr only" data of Fig. 1.6 does not agree with the published value[47] (35 sec) for the half-life of Zr^{99}, and the fractional cumulative yield (0.019), given by the ordinate intercept of the curve, is in disagreement with the predicted[48] yield (~0.80). In addition, control experiments with Nb^{95} tracer showed that at least 2% of the niobium was carried by zirconium–iron hydroxide precipitate. Therefore, since it is probable that the Mo^{99} observed in the zirconium fraction was due to Nb^{99} contamination, the data from these experiments provide no evidence for a 35-sec zirconium precursor of Mo^{99}. If it is assumed that the predicted yield is correct (i.e., assume ordinate intercept ≈ 0.80), then the upper limit of the Zr^{99} half-life is 1.6 sec, as calculated from the minimum amount of Mo^{99} observed at the earliest separation time (9 sec). However, the Mo^{99} activities determined for separation times of 13, 24, and 27 sec were equal, within experimental error, to that found at 9 sec, indicating that only a small part of the observed Mo^{99} could be due to

[47] C. J. Orth and R. K. Smith, *J. Inorg. Nucl. Chem.* **15**, 4 (1960).

[48] A. C. Wahl *et al.*, *Phys Rev.* **126**, 1112–27 (1962).

[49] A. C. Wahl, *J. Inorg. Nucl. Chem.* **6**, 263 (1958).

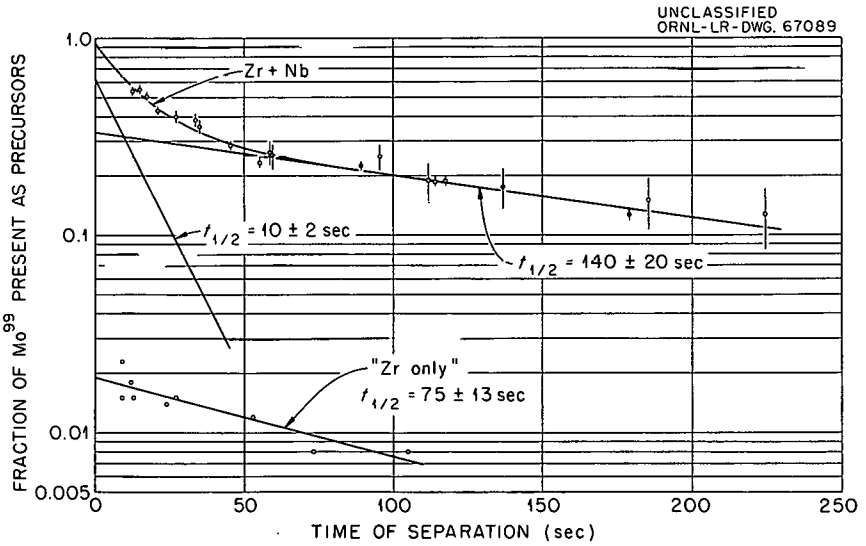

Fig. 1.6. Fraction of the Mass-99 Fission-Product Chain Present as Nb^{99} at Various Separation Times Following Irradiation.

decay of a short-lived Zr^{99}. Therefore, the half-life of Zr^{99} may be much less than 1.6 sec.

Survey and Evaluation of U^{233} Fission-Yield Data

R. L. Ferguson G. D. O'Kelley

A comprehensive literature survey has been made to ascertain the status of data on U^{233} fission-product yields. The various experimental determinations were evaluated, and the most recent mass-spectrometric results were used as a basis for deriving a set of preferred yields. These results were compared with values reported in two other recent compilations,[50,51] and, for yields > 1%, the three groups of values agreed with an average deviation of <5%. A report[52] has been prepared which outlines the procedure used in obtaining these selected yields and includes a tabulation of all published U^{233} thermal-neutron-induced fission yields, an extensive list of references, and some recommendations concerning additional experimental work.

Level Structures of Ge^{71}, Ge^{73}, Ge^{75}, and Ge^{77} from the (d,p) Reaction

R. J. Silva E. Eichler

Separated isotopes of germanium were bombarded with 5.2-Mev deuterons from the ORNL 5.5-Mev Van de Graaff accelerator. The energy spectra of proton groups leading to excited levels in Ge^{71}, Ge^{73}, Ge^{75}, and Ge^{77} up to approximately 1 Mev were obtained through the use of a silicon surface-barrier detector. For the highest-energy proton group from Ge^{71}, Ge^{73}, Ge^{75}, and Ge^{77}, Q values of 5.140 ± 0.050, 4.429 ± 0.050, 4.200 ± 0.050, and 3.554 ± 0.050 Mev, respectively, were determined. The first three of these values are in agreement with published Q values for ground-state transitions.[53] Within the measured resolution of the system (30–35 kev fwhm), proton groups corresponding to all previously known levels were observed, with the exceptions of the 139-kev level in Ge^{75} and the ground state in Ge^{77}. These two levels have assigned spins of $\frac{7}{2}^+$. They are probably multiparticle states arising from coupling of an odd number of $g_{9/2}$ neutrons to give a resultant spin of $\frac{7}{2}$. One would then not expect transitions to these levels, as d,p stripping would be shell-model forbidden. The Q values for proton groups leading to newly observed levels were: for Ge^{71}, 4.625, 4.071 Mev; for Ge^{73}, 3.939, 3.789, 3.550, 3.417 Mev; for Ge^{75}, 4.158 (?), 4.005, 3.959, 3.894, 3.627, 3.535, 3.335 Mev; for Ge^{77}, 3.484, 3.218, 3.092, 2.844, 2.709, 2.494 Mev. The relative error between the Q values for a given isotope is ±10 kev. A typical spectrum is shown in Fig. 1.7.

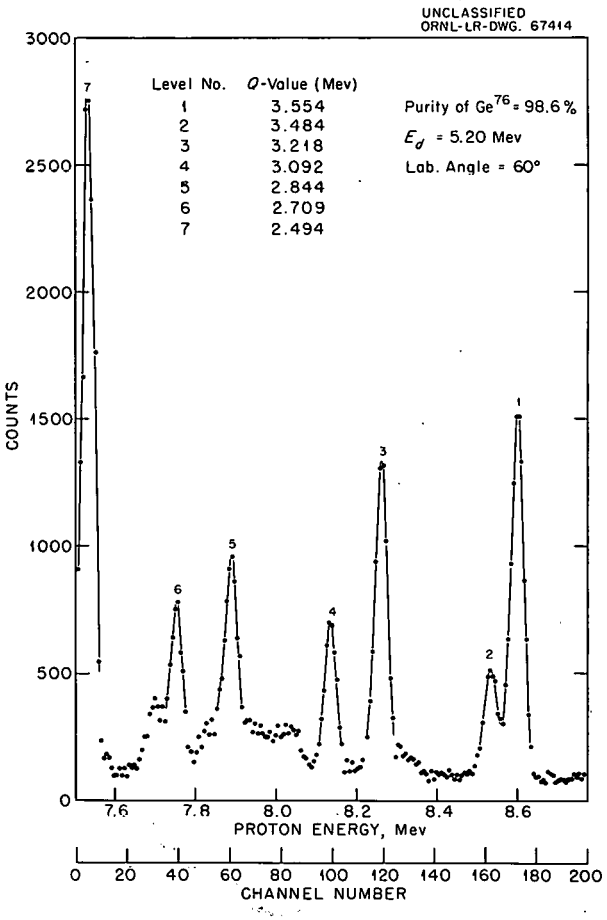

Fig. 1.7. Proton Energy Spectrum from the $Ge^{76}(d,p)Ge^{77}$ Reaction.

[50] S. Katcoff, *Nucleonics* 18(11), 201 (1960).

[51] W. H. Walker, *Yields and Effective Cross Sections of Fission Products and Pseudo-Fission-Products*, CRRP-913 (March 1960).

[52] R. L. Ferguson and G. D. O'Kelley, *A Survey and Evaluation of U^{233} Fission Yield Data*, ORNL CF-62-3-71, to be published as ORNL-3305.

[53] L. A. Koenig, J. H. E. Mattauch, and A. H. Wapstra, *Nuclear Data Tables, 1960*, Part 2, National Academy of Sciences – National Research Council, Washington, 1961.

NUCLEAR SPECTROSCOPY

Semiconductor Detector Measurements of Ce^{135} Radiations

A. R. Brosi B. H. Ketelle
E. Sakai[54]

The emphasis in this work has been on the application of semiconductor detector measurements to decay-scheme studies. The detectors used were lithium-drifted, silicon diodes made in the Instrumentation and Controls Division; in general, they had a resolution (full width at half maximum) of about 8 kev for the Cs^{137} *K*-conversion electrons.

Monoenergetic electrons were focused on semiconductor detectors with an electrostatic or a thin-magnetic-lens spectrometer. The pulse-height distributions obtained with lithium-drifted diodes showed that electrons with energies up to about 700 kev were counted with constant efficiency. Although some high-energy electrons lost their full energy by scattering within the detector, the most probable energy loss in the detector was approximately 700 kev. Because of scattering, these detectors could be used for electron energy measurements up to about 2 Mev, but intensity measurements required calibration in the energy region above 700 kev. In the case of electrons with energies below 700 kev, the pulse-height distributions had a peak with a relatively flat region on the low-pulse-height side, which resulted from backscattering with partial loss of energy in the detector. The counting rate per channel in the flat region was about 1% of the counting rate per channel at the peak.

In the work on Ce^{135}, Ce_2O_3 with the isotopic composition 30% Ce^{136}, 0.7% Ce^{138}, 65.2% Ce^{140}, and 4.1% Ce^{142} was bombarded with 22-Mev protons in the ORNL 86-in. cyclotron. The initial products were largely 22-min Pr^{135} and 4.5-hr Pr^{139}. These decayed to 18-hr Ce^{135} and 140-day Ce^{139}. The Ce^{135} was separated after decay of the 22-min Pr^{135} parent by solvent extraction of tetravalent cerium from trivalent praseodymium and lanthanum. The chief impurities, 140-day Ce^{139} and 20-hr La^{135}, did not interfere with most measurements until after the Ce^{135} had decayed through several half-lives.

A semiconductor detector was used to measure the conversion-electron spectrum of Ce^{135}. Because of the high resolution, many more lines were present than were found in the scintillation counter gamma-ray spectrum. In those cases where the gamma rays were resolved, conversion coefficients were computed. In some cases there was ambiguity as to whether a line was due to *K*- or *L*-shell conversion. It was possible to resolve the uncertainty by the use of photoelectron spectra obtained with gold or lead radiators, which gave photoelectron peaks with 25 to 50% poorer resolution than the conversion-electron peaks. In spite of the resolution loss caused by use of relatively thick radiators, the semiconductor detector with a radiator gave much better resolution of gamma rays than a scintillation detector.

Coincidence measurements were made using a semiconductor detector for conversion electrons and a scintillation counter for gamma rays. Gamma-gamma coincidences were also measured using two scintillation detectors.

On the basis of an incomplete analysis of the data, a tentative decay scheme has levels at 0.266, 0.300, 0.486, 0.609, 0.786, 0.872, 0.970, 1.14, 1.46, and 1.76 Mev. It is hoped that a more complete analysis of the data will lead to a more detailed energy-level scheme and permit the assignment of spins and parities to some of the levels.

[54]Guest from Japan Atomic Energy Research Institute.

2. Isolation and Chemical Properties of Synthetic Elements

CHEMISTRY OF TECHNETIUM

Rhenium Species Derived from Rhenium(V) and Rhenium(VI) in Concentrated Sulfuric Acid

R. H. Busey

This paper briefly describes a spectrophotometric study of a number of rhenium species in aqueous or organic solution which may be prepared from Re(V) and Re(VI) in 18 *M* H_2SO_4. The preparation and properties of, and equilibria between, the penta- and hexavalent species in 18 *M* H_2SO_4 have been described.[1] This work has been preliminary to a similar study to be made on oxidation states of technetium above Tc(IV).

Hexavalent Rhenium Chloride Complexes. – Observation of the spectra of solutions obtained by the controlled addition of Cl^- (HCl or NaCl) to a solution containing the maximum concentration of hexavalent rhenium in 18 *M* H_2SO_4 revealed the existence of at least three Re(VI) chloride species. The first readily recognized species, with a strong absorption band at 5300 A, developed to a maximum at a Cl/Re ratio of 5 to 6. Before this species fully developed, a second, with an absorption band at 4200 A, began to form at Cl/Re > 5. At Cl/Re > 25, a third species began to develop, with an absorption band at 4360 A. This third species was apparently fully developed at Cl/Re ~ 75, giving a molar absorbancy of 3900 at 4360 A. (Some chloride complexes containing less Cl^- than the species with an absorption band at 5300 A probably exist, as shown by a shift in the wavelength of the maximum absorption as Cl/Re was increased from 1 to 4.) The spectra demonstrated that each of the above complexes readily dissociates into the next lower chloride-containing complex.

The highest chloride-containing complex, with an absorption maximum at 4360 A in 18 *M* H_2SO_4, is readily extracted into CCl_4 or $CHCl_3$, in which the species shows an intense, sharp absorption band at 4400 A with a molar absorbancy of 4500. The spectrum in CCl_4 is given in Fig. 2.1. The stability of the complex in the organic solvent is shown by the fact that it, and it alone, is extracted from a solution of Re(VI) in sulfuric acid containing insufficient Cl^- to form the highest chloride-containing species (i.e., containing only the 5300- or 4200-A-absorbing species).

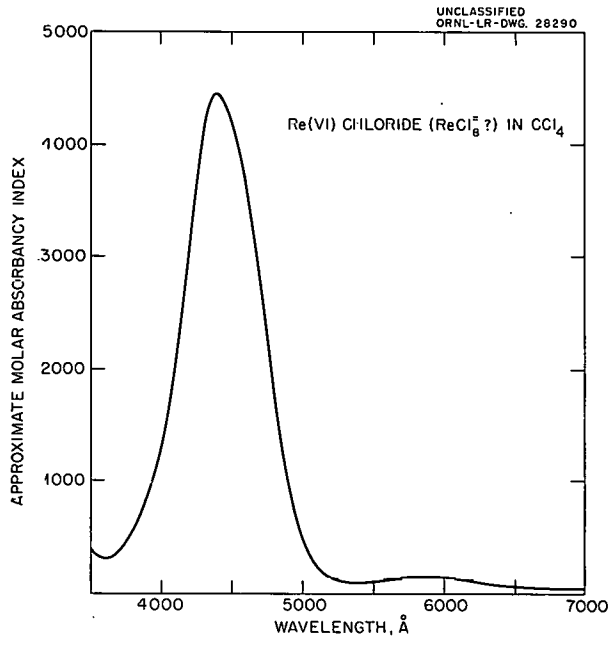

Fig. 2.1. Absorption Spectrum of Hexavalent Rhenium Chloride Complex in Carbon Tetrachloride.

[1] R. H. Busey, *Chem. Div. Ann. Progr. Rept. June 20, 1961*, ORNL-3176, p 14.

Analysis of the spectrophotometric observations of the $SnSO_4$ reduction of Re(VII) in 18 *M* H_2SO_4 in the presence of excess HCl (Cl/Re ~ 75) revealed that the Re(VII) is reduced to Re(VI) (highest chloride complex), which in turn is reduced to Re(IV). This is in contrast to the same reduction in absence of Cl^- (ref 1). The presence of excess Cl^- causes the sapphire blue Re(V) to disproportionate into the Re(VI) chloride complex and Re(IV): $[Re(VI)\cdot xCl][Re(IV)]/[Re(V)]^2 = 5.6 \pm 3$.

Hexavalent Rhenium Bromide Complexes. – Three bromide species of Re(VI) in 18 *M* H_2SO_4 were detectable, but only the highest bromide-containing complex could be characterized. The spectrum in 18 *M* H_2SO_4 gave two absorption bands, at 6475 and 5525 A with molar absorbancies of approximately 4500 and 4200, respectively. Analogous to the highest chloride complex, the bromide complex is extractable from the sulfuric acid solution with CCl_4, $CHCl_3$, or n-C_6H_{14}, giving an intense blue solution; the species corresponding to lower bromide contents do not extract. The spectrum for CCl_4 is given in Fig. 2.2. Unlike the chloride complex, the Re(VI) bromide complex in 18 *M* H_2SO_4 was formed slowly, the rate of formation from Re(V) being first-order with respect to HBr, with an apparent bimolecular rate constant of 4.9 liters $mole^{-1}$ min^{-1}. A study of the effect of Br^- on the disproportionation of Re(V) was not possible in this case, because Br^- causes reduction of Re(VII) in 18 *M* H_2SO_4.

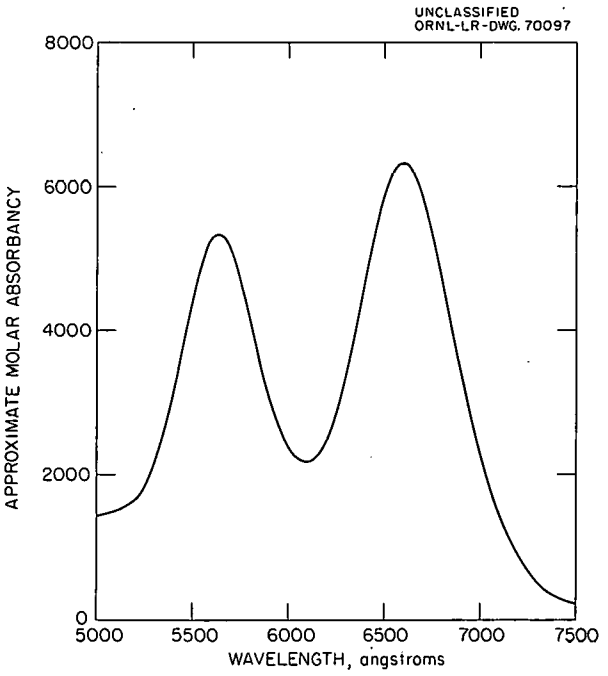

Fig. 2.2. Absorption Spectrum of Hexavalent Rhenium Bromide Complex in Carbon Tetrachloride.

Violet and Amber Species. – Wehner and Hindman[2] observed a violet species and an amber species of rhenium in 6 *M* H_2SO_4. The amber species was obtained by H_2S reduction of the violet species; coulometric measurements gave 0.5 as the oxidation state difference between the two species. They were unable to obtain reproducible results for the apparent oxidation state of the violet species by $Ce(SO_4)_2$ titration, a fact which they attributed to a reducing impurity in the solutions. From other observations, however, they tentatively concluded that the amber species is Re(V) and the violet species a mixed Re(V)·Re(VI) species.

In this research, the violet species has been prepared from sapphire blue Re(V) (ref 1) in 18 *M* H_2SO_4 by dilution to 6 *M* H_2SO_4 and allowing the resulting suspension to oxidize in air. The violet species so produced was usually contaminated with some other rhenium species, as evidenced by excess absorption on each side of the 5450-A absorption band (Fig. 2.3). The solution was freed of this contaminating species by further dilution to 3 *M* H_2SO_4 and allowing the solution to stand overnight protected from atmospheric oxygen. Concentrated H_2SO_4 was then added to stabilize (toward oxidation by air) the violet species in 6 *M* H_2SO_4. Approximately 10% of the rhenium was converted to the violet species; the remainder was oxidized to ReO_4^-, which was removed by precipitation as Re_2S_7 with H_2S. The H_2S reduced the violet species to the amber species, as previously observed.[2] The amber species is extremely sensitive to air oxidation to the violet one, after the solution is freed of H_2S by argon or nitrogen purging.

The spectra of the two species are given in Fig. 2.3. The molar absorbancy was determined spectrophotometrically by oxidation of an aliquot of the violet species to ReO_4^- with 1 *M* $HClO_4$. Spectrophotometric titrations with $Ce(SO_4)_2$ gave 5.54 ± 0.10 as the apparent oxidation state of the violet species, based on the linear portion of the

[2]Philip Wehner and J. C. Hindman, *J. Am. Chem. Soc.* **75**, 2873 (1953).

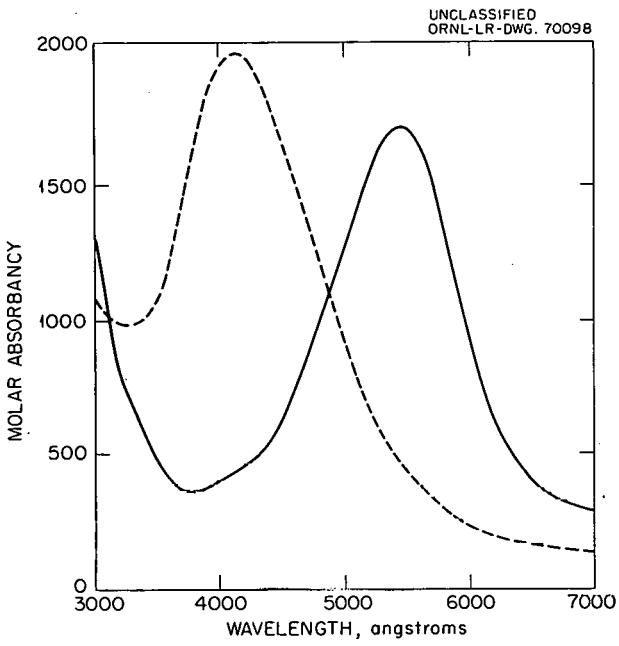

Fig. 2.3. Absorption Spectrum of Violet (Solid Curve) and Amber (Broken Curve) Species of Rhenium in 6 *M* H_2SO_4.

curve of absorbancy at 5450 A vs the $Ce(SO_4)_2$ added; the last 20 to 35% of the $Ce(SO_4)_2$ required to oxidize the violet species gave a concave upward curve. Based on the total $Ce(SO_4)_2$ titer, the apparent oxidation state was 5.29 ± 0.10. Evidence presented later indicates that the solutions of the violet species were contaminated with excess Re(V). The above result and the 0.5 difference[2] in oxidation states between the violet and the amber species lead to the conclusion that the amber species is Re(V).

These results are in agreement with the tentative conclusion of Wehner and Hindman[2] that the violet is an Re(V)·Re(VI) dimer and that the amber is Re(V). There are serious discrepancies, however. They give 2320 for the molar absorbancy of the violet species at 5450 A and 2740 for the amber species at 4150 A (values obtained from Fig. 3 of ref 2). The values obtained in this research are 1720 and 1990, respectively. The absorption band at 5450 A (Fig. 2.3) is considerably sharper than that given by Wehner and Hindman; for the ratio of peak absorption to valley absorption they give 2.9, vs 4.5 ± 0.2 observed in this research. A difference in behavior was observed when solutions of the violet species were diluted in 10 to 11 *M* HCl; they state that their violet solutions appeared to be stable in 10 *M* HCl, whereas our violet solutions were not.

Dilution of the amber species in 11 *M* HCl ultimately gave a pure Re(V) chloride species with an absorption band at 2410 A, as previously observed.[2] The process is not a simple reaction of amber Re(V) giving Re(V) chloride. Approximately 30 min after mixing, the spectrum of the solution shows an absorption band at 5450 A, presumably due to the presence of the violet species. (The solution was protected by argon from oxidation by air.) Within 2 hr, the 5450-A band was replaced by a band at 4080 A. After three weeks, the 4080-A band decreased to 5% of its original value, and the spectrum of the solution was that of pure Re(V) chloride species. During the course of the disappearance of the 4080-A species, the ultraviolet spectrum of the solution was observed to be that of Re(V) chloride and showed essentially no change, indicating that the ultraviolet spectrum of the 4080-A species must be very similar to that of the Re(V) chloride species.

Dilution of the violet species in 11 *M* HCl was similarly complicated but ultimately gave a solution whose spectrum indicated the presence of Re(V) chloride and ReO_4^-, a result which is consistent with the hypothesis:

$$\underset{\text{violet}}{\text{Re(V)·Re(VI)}} \xrightarrow[\text{HCl}]{11\ M} 1.5\ \text{Re(V) chloride} + 0.5\ ReO_4^- .$$

Both the $Ce(SO_4)_2$ titrations and the dilutions in 11 *M* HCl showed that the solutions of the violet species so far prepared were contaminated with varying amounts of excess Re(V).

An alternative method was devised for determining the apparent oxidation state of the violet species, based on the extraction with CCl_4 of the Re(VI) chloride complex (Fig. 2.1) from a concentrated H_2SO_4-HCl solution of the violet species. No reaction with HCl or extraction occurred until Re(VII) in the form of $KReO_4$ was added to the acid phase. The observed ratio of moles of Re(VI) chloride produced per mole of rhenium in the violet species was 1.5 ± 0.1, which gives the reaction

$$\underset{\text{violet}}{\text{Re(V)·Re(VI)}} + \text{Re(VII)} \xrightarrow[\text{HCl}]{H_2SO_4} 3\text{Re(VI)}\cdot x\text{Cl} .$$

It is readily seen that a ratio of 2.0 would signify an apparent oxidation state of 5, etc.

The violet species in 1 *M* H_2SO_4 (protected by argon from air oxidation) was extracted by 0.1 *N* tri-*n*-octylamine in toluene. The spectrum of the species was essentially the same in both phases. These two observations demonstrate that the violet species is anionic.

Wine-Red Species. – Solutions of Re(V) and Re(VI) in 18 *M* H_2SO_4 are not stable indefinitely; after a few months to a year, a black or blue-black solid usually precipitates, forms a colloidal suspension, or plates out on the sides of the flask holding the solution. Suspension of this solid in 6 *M* H_2SO_4 and oxidation with O_2 usually results in the formation of a wine-red solution. In contrast, suspension of freshly precipitated Re(V), made by dilution with H_2O of Re(V) or Re(VI) in 18 *M* H_2SO_4,[1] in 6 *M* H_2SO_4 and oxidation with O_2 produced the violet species described above. Presumably an aging process is required before the precipitated solid yields the wine-red solution.

The majority of the solutions of the wine-red species used for study were prepared from a colloidal suspension of rhenium in 18 *M* H_2SO_4 with an apparent oxidation state of 5.9. This colloidal Re(VI) was approximately four years old. The wine-red species was prepared by dilution with H_2O of the colloidal Re(VI) solution to 7–8 *M* H_2SO_4 and passing O_2 into the solution for a few days to a week. The wine-red species produced was usually contaminated with a species having appreciable absorption in the region of 6500 A; this was eliminated by further dilution to 5 *M* H_2SO_4 and exposure to air overnight. Sufficient 18 *M* H_2SO_4 was then added to stabilize the wine-red species in 6 *M* H_2SO_4.

Approximately 20% of the rhenium was converted to the wine-red species; the remainder was oxidized to ReO_4^-, which was separated by precipitation as Re_2S_7 by H_2S. The wine-red species is not reduced by the H_2S. The spectrum of the wine-red species is given in Fig. 2.4.

Spectrophotometric titrations with $Ce(SO_4)_2$ established the apparent oxidation state as 5.2 ± 0.1. The molar absorbancy was determined spectrophotometrically by dilution of an aliquot of the species to approximately 1 *M* H_2SO_4, at which acid concentration the species is readily oxidized by air to ReO_4^-. The method for determining the apparent oxidation state by CCl_4 extraction of Re(VI) chloride complex from a concentrated H_2SO_4-HCl solution of the wine-red species confirmed the oxidation state determined by $Ce(SO_4)_2$ titration. As in the case of the violet species, no reaction with HCl or extraction occurred until Re(VII) was added to the acid phase. The behaviors of both the violet and wine-red species in this respect are in contrast to the behavior of the sapphire blue Re(V).

Tri-*n*-octylamine in toluene extracted the wine-red species from a 1 *M* H_2SO_4 solution with no change in the spectrum, demonstrating that the species is anionic.

The behavior of the wine-red species in 11 *M* HCl is very complex. Whereas dilution of the violet species in 11 *M* HCl ultimately gave Re(V) chloride and ReO_4^-, and the amber species gave Re(V) chloride, the wine-red species in 11 *M* HCl produced a solution whose spectrum showed, in addition to Re(V) chloride, the presence of a species (or a mixture of species) which was apparently stable indefinitely. Dilution of the wine-red species in 11 *M* HCl with H_3PO_2 present produced, on heating, a species (or a mixture of species) of Re(IV) with two intense (molar absorbancy ~3000) absorption bands in the visible

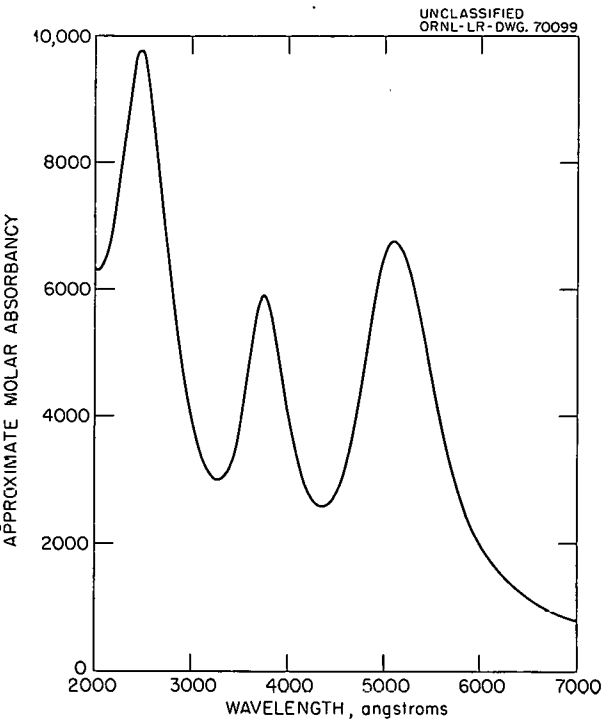

Fig. 2.4. Absorption Spectrum of Wine-Red Species of Rhenium in 6 *M* H_2SO_4.

region. This Re(IV) species must be the same type of complex as the amber, violet, wine-red, and Re(VI) chloride and bromide species, all of which have in common very intense absorption bands in the visible region.

Acid Strength of H_2ReCl_6

Q. V. Larson Siegfried Lindenbaum
G. E. Boyd

Aqueous and nonaqueous titrations of H_2SO_4 and H_2ReCl_6 were performed to obtain an estimate of the acid strength of H_2ReCl_6.

Curves of the potential of the glass-calomel electrode pair as a function of titrant delivered were produced with an automatic recording titrator. Titrant was delivered with a syringe buret for which 1.000 ml gave a full-scale reading. All samples were diluted to 10 ml before titrating.

For the aqueous titration 0.1 *N* NaOH was used as the titrant. Nonaqueous titrations were performed in ethylene glycol,[3] and the titrant was 0.1 *N* piperidine in ethylene glycol. This system was chosen because it best resolved the two breaks in the titration curve of H_2SO_4. The presence of water (5%)[3] considerably decreased the slope of the first break in the titration of H_2SO_4. The water concentration was therefore kept to a minimum (less than 1%) in all the nonaqueous titrations.

Sulfuric acid solutions in ethylene glycol were prepared by adding concentrated H_2SO_4 to ethylene glycol by means of a micropipet.

The hexachlororhenic acid, H_2ReCl_6, was prepared by dissolving K_2ReCl_6 in a slurry of Dowex 50-X10 in the hydrogen-ion form. The solution and resin were poured onto a column of the same resin, and the column rinsed with sufficient water to give a 0.05 *N* solution of H_2ReCl_6. This procedure minimized the hydrolysis of $ReCl_6^{2-}$, since the solution was at a low pH at all times.

For the nonaqueous titrations, samples of H_2ReCl_6 were pipeted into the titration cell and evaporated at room temperature *in vacuo* nearly to dryness. Ten milliliters of ethylene glycol was added and the solution titrated with 0.1 *N* piperidine in ethylene glycol.

[3]N. M. Das and Debabrata Mukherjee, *Anal. Chem.* 31, 233 (1959).

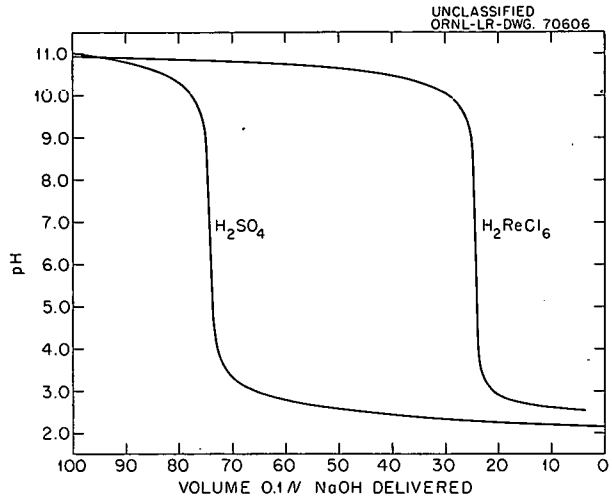

Fig. 2.5. Titration of H_2SO_4 and H_2ReCl_6 in Aqueous Solution.

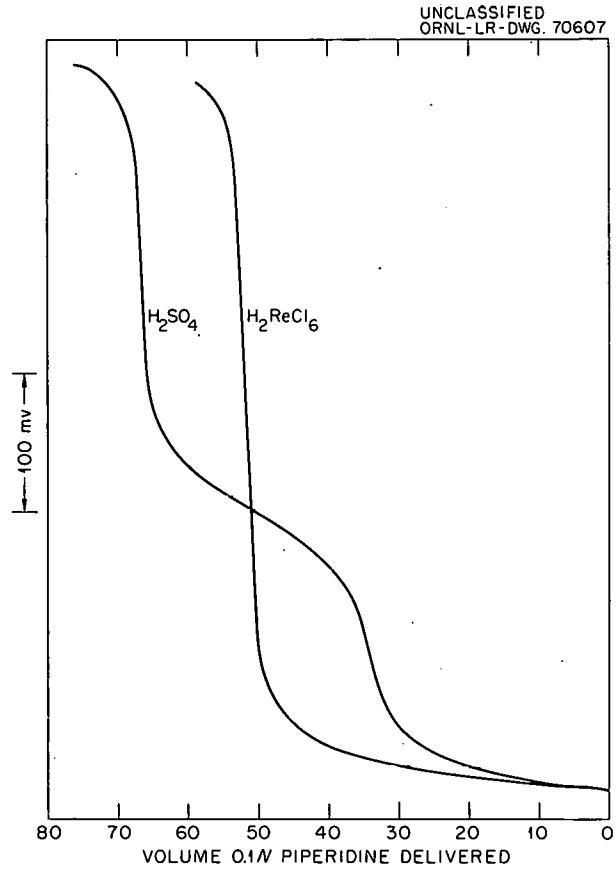

Fig. 2.6. Titration of H_2SO_4 and H_2ReCl_6 in Ethylene Glycol.

Titration curves for H_2SO_4 and H_2ReCl_6 in water are shown in Fig. 2.5. Typical strong-acid titration curves were obtained, with no apparent differentiation between the first and second ionization.

The nonaqueous titration curves (Fig. 2.6) show two distinct breaks for the sulfuric acid titration, but only one for H_2ReCl_6. Apparently, therefore, the second ionization for H_2ReCl_6 is considerably greater than that for H_2SO_4 ($pK_2 = 2.0$).

Measurement of the Near-Infrared Absorption Spectrum of Pertechnetate Ion

C. A. Horton[4] Q. V. Larson G. E. Boyd

The near-infrared absorption spectrum of pertechnetate ion was determined (Fig. 2.7) with the KBr-pellet technique, wherein milligram quantities of crystalline $KTcO_4$ were mixed with spectrograde KBr. A characteristic, strong absorption band at 906 cm^{-1} was found which corresponded in its general shape to that observed with $KReO_4$ at 915 cm^{-1}. A Beckman model IR-7 was used for the measurements in the range from 2.5 to 16 μ.

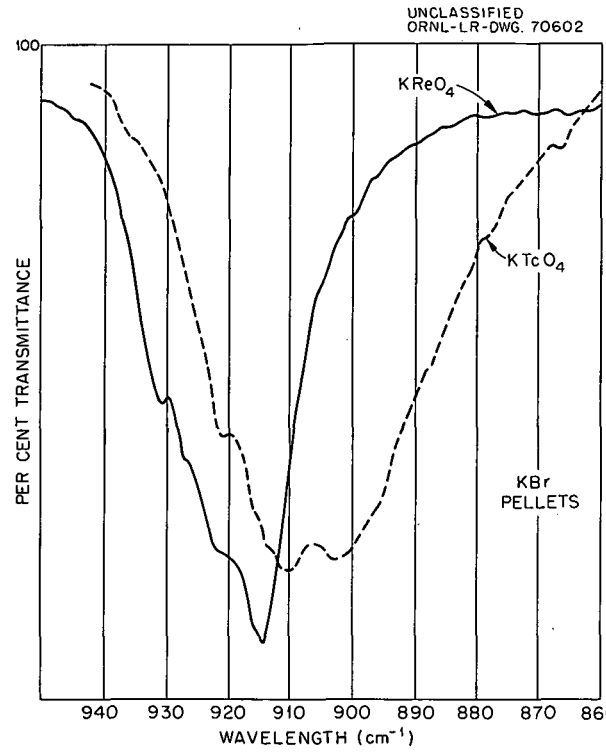

Fig. 2.7. Near-Infrared Absorption Spectra of $KTcO_4$ and $KReO_4$.

[4]Analytical Chemistry Division.

3. Chemical Separation of Isotopes

Ion Exchange Studies in Nonaqueous Solvents

D. A. Lee

Selectivities and diffusion coefficients were determined for exchange of some alkali-metal ions between cation exchange resins and nonaqueous salt solutions. A new ion exchange resin, Amberlite 200, was studied. It enables relatively rapid exchange in nonaqueous systems. Cesium-134 was used as the tracer in these experiments. Generally, the diffusion coefficients were smaller and the selectivities higher in nonaqueous systems than in aqueous systems.

An experiment was performed using Amberlite 200 in an aqueous system to compare this resin with Dowex 50. The effective diffusion coefficient for the exchanging cations (Cs^+ and K^+) was 3.4×10^{-7} cm^2/sec, and the selectivity coefficient K_K^{Cs} was 1.27. These results compare favorably with those given for alkali-metal ions on Dowex 50 in an aqueous system.[1]

[1]G. E. Boyd and B. A. Soldano, *J. Am. Chem. Soc.* **75**, 6091 (1954); G. E. Myers and G. E. Boyd, *J. Phys. Chem.* **60**, 521 (1956).

A series of experiments was made in amides; 0.1 *N* KSCN solutions in formamide, dimethylformamide, and dimethylacetamide were equilibrated with K^+-form Amberlite 200 containing Cs^{134} tracer. The results are given in Table 3.1. *N*-Methylacetamide was also tried, but the exchange was so slow that no data were obtained. In the same system, using propylene carbonate as the solvent, the diffusion coefficient was 8.53×10^{-9} cm^2/sec and K_K^{Cs} was 0.76.

Several experiments performed with Dowex 50 resins in ethylenediamine (EDA) solutions are summarized in Table 3.2.

Table 3.1. Ion Exchange Diffusion and Selectivity Coefficients in Amides

Solvent	D_i (cm^2/sec)	K_K^{Cs}
Formamide	2.03×10^{-8}	1.09
Dimethylformamide	2.02×10^{-8}	5.45
Dimethylacetamide	2.05×10^{-8}	7.21

Table 3.2. Ion Exchange Diffusion and Selectivity Coefficients in Ethylenediamine

System	D_i (cm^2/sec)	K_M^{Cs}
Dowex 50-X1-K^+-Cs* vs 0.16 *N* KSCN-EDA	1.15×10^{-9}	0.97
Dowex 50-X1-Na^+-Cs* vs 0.16 *N* NaBr-EDA	2.63×10^{-8}	5.04
Dowex 50-X1-Cs^+-Cs* vs 0.16 *N* CsSCN-EDA	1.31×10^{-9}	
Dowex 50-X1-Cs^+-Cs* vs 0.16 *N* NaBr-EDA	3.99×10^{-9}	3.25
Dowex 50-X8-K^+-Cs* vs 0.15 *N* KSCN-EDA	3.37×10^{-10}	3.93
Dowex 50-X16-K^+-Cs* vs 0.16 *N* KSCN-EDA	9.81×10^{-11}	7.63

The effect of the amount of water in the resin was studied in the system K^+-Amberlite 200-Cs^{134} vs 0.02 *N* KSCN in CH_3OH. The resin, the KSCN, and the CH_3OH were rigorously dried. Increasing amounts of water were added to separate portions of the resin which were then equilibrated with the methanol solution. The results are given in Table 3.3. The diffusion coefficient is seen to decrease rapidly with increasing water concentration in the resin, up to 1 molecule per resin site (Fig. 3.1). This effect appears to be related to changes in charge density of the sulfonic group and to steric effects. Further studies are in progress.

Table 3.3. Effect of Water in the Resin on Diffusion and Selectivity Coefficients

H_2O in CH_3OH Phase at Equilibrium (mg/ml)	D_i (cm^2/sec)	K_K^{Cs}
	$\times 10^{-7}$	
0.17	3.07	2.69
0.45	2.10	2.55
0.74	1.66	2.56
1.45	1.52	2.47
5.26	1.41	2.26

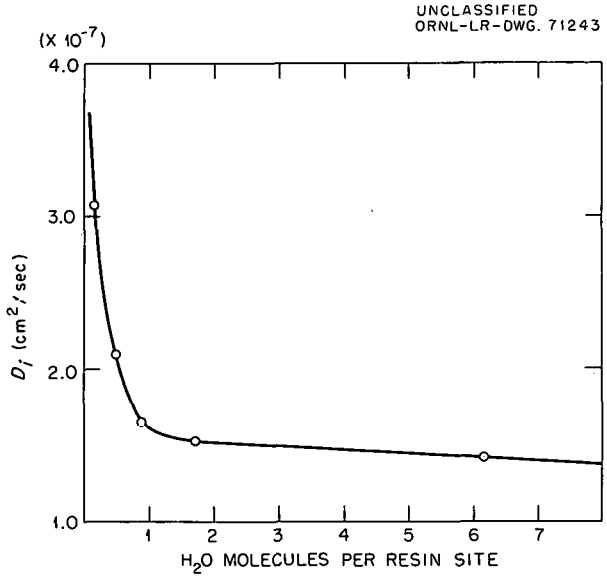

Fig. 3.1. Effect of H_2O in the Resin on the Diffusion Coefficient for K^+-Amberlite 200-Cs^{134} vs 0.02 *N* KSCN in CH_3OH.

Isotopic Chemistry of Boron

A. A. Palko

The systematic study of BF_3-organic complexes has continued. Characterization of the $(C_2H_5)_2S$-BF_3 system was completed. The procedures and methods used were reported previously.[2] Lack of consistency of earlier data made it necessary to repeat many of the vapor pressure–composition determinations. These corrected data may be expressed by the least-squares equation and constants shown in Table 3.4.

Table 3.4. Vapor Pressure–Temperature Constants for the System $(C_2H_5)_2S + BF_3 \rightleftharpoons (C_2H_5)_2S \cdot BF_3$

Moles of BF_3 per Mole of $(C_2H_5)_2S$	Constants for the Equation $\log p = a - b/T$	
	a	*b*
0.230	9.173	2160
0.530	10.400	2490
0.804	11.369	2700
0.881	12.006	2840
0.896	11.126	2580
0.941	12.069	2790
0.972	11.833	2680
1.000	9.989	2100

Single-stage isotopic equilibrium constants have been determined at −8, 4, and 22°C for the exchange

$$(CH_3)_2O \cdot B^{11}F_3\,(l) + B^{10}F_3\,(g) \rightleftharpoons B^{11}F_3\,(g) + (CH_3)_2O \cdot B^{10}F_3\,(l).$$

These data are shown in Table 3.5; they may be expressed by the least-squares equation $\log \alpha = (7.769/T) - 0.0141$.

[2] A. A. Palko, *Chem. Div. Ann. Progr. Rept. June 20, 1961*, ORNL-3176, p 18.

Table 3.5. Single-Stage Isotopic Equilibrium Constants for the $(CH_3)_2O$-BF_3 System

+22°C	+4°C	−8°C
1.0293	1.0373	1.0330
1.0207	1.0384	1.0343
1.0338	1.0328	1.0426
1.0348	1.0328	1.0345
1.0329		1.0339
1.0253	1.0305	1.0328
	1.0338	1.0346
1.0263	1.0285	
1.0259	1.0321	1.0403
	1.0297	1.0397
1.0315		1.0387
1.0245	1.0286	
1.0250		1.0325
1.0264		
1.0340		1.0382
1.0313		1.0333
		1.0367
av 1.029 ± 0.003	av 1.033 ± 0.002	av 1.036 ± 0.002

Nitrogen Exchange Between Nitrite and Nitrate

L. L. Brown

A study was made of the rate of exchange of nitrogen between NO_2^- and NO_3^- in aqueous solution, as a function of pH. This exchange does not take place in neutral or basic solutions. The reaction was studied with labeled nitric acid (12.6% N^{15}) and normal sodium nitrite at 0°C. The acidity of the exchange solution was adjusted by adding NaOH. Samples were taken at intervals and quenched with caustic. The nitrite portion was separated by precipitation as $AgNO_2$ and analyzed for N^{15}.

The data in Table 3.6 clearly indicate that exchange will take place in slightly acid solution (such as *I*), but only at high acid concentration is the rate appreciable.

Oxygen Exchange Study of a Peroxygen Bridge

L. L. Brown

The separation factor between oxygen and oxygenated solid cobalt di(salicylal)ethylenediimine was reported earlier.[3] A recent paper by Haim and Wilmarth[4] described a water-soluble cobalt complex with a peroxygen bridge similar to that in the solid complex previously examined. Such a complex, when equilibrated with molecular oxygen, should provide a mechanism for fractionating the isotopes of oxygen if exchange of oxygen occurs at a reasonable rate between the isotopic species.

To determine whether such exchange occurs, an aqueous solution of $K_6[(NC)_5CoOOCo(CN)_5]$ was equilibrated with O_2 enriched in O^{18} to 1.248%. The potassium salt was prepared according to Haim; it assayed: K, 34.2; Co, 19.2; CN, 37.7% (calculated: K, 32.2; Co, 18.1; CN, 35.5%). Samples of the gas phase taken at 46, 52, and 92 hr averaged 1.187 ± 0.006% O^{18}. Complete exchange of oxygen in the system would have resulted in 0.846% O^{18} in both the salt and the gas (ignoring an isotope effect). Thus, exchange of oxygen does not occur under the conditions of the experiment. (The slight decrease in O^{18} content of the gas phase was attributed to an impurity in the salt; it does not represent exchange with O_2^{2-} as it is time independent.)

Oxygen-17 Enrichment

A. H. Narten

Preoperational testing of the water distillation cascade was completed during fiscal year 1962. The unit was placed "on stream" during June. Barring mechanical failures, the cascade is expected to reach steady-state operation during the summer or fall of 1963. Projections of the cascade's separative capacity, based on transient isotopic gradients, are favorable; they predict that design performance will be attained.

[3] L. L. Brown and J. S. Drury, *J. Chem. Phys.* 33, 1889–90 (1960).

[4] A. Haim and W. K. Wilmarth, *J. Am. Chem. Soc.* 83, 509–16 (1961).

Table 3.6. Nitrogen Exchange Between NO_2^- (0.38% N^{15}) and NO_3^- (12.6% N^{15})

Run No.	Composition (moles per liter)				Time (hr)	N^{15} in NO_2^-	
	NO_3^-	NO_2^-	OH^-	$H^{+(a)}$		Found	100% Exchange
I	0.96	1.00	1.00	1.00	118	0.51	5.97
II	0.88	1.00	0.75	1.00	5.5	0.47	5.46
III	0.88	1.00	0	1.00	5	2.83	5.46
IV	1.32	1.00	0	1.50	4	6.57	6.78
					24	6.68	6.78

[a] Partly as sulfate, partly as nitrate.

Isotopic Fractionation Between Carbon Dioxide and Dimethyl Carbamic Acid

A. C. Rutenberg

The single-stage carbon and oxygen isotopic fractionation factors were measured for the exchange reaction

$$C^{13}O^{16}O^{16} + (CH_3)_2NC^{12}O^{18}O^{16}H \rightleftharpoons C^{12}O^{18}O^{16} + (CH_3)_2NC^{13}O^{16}O^{16}H .$$

The reaction was studied as an aid to interpreting isotopic fractionation data for alkyl ammonium carbamates.

The dimethyl carbamic acid was prepared by reacting CO_2 with dimethylamine in benzene and was used in solution. Forty milliliters of 4.6 *M* $(CH_3)_2NCOOH$ in benzene was equilibrated with ~200 cc of CO_2 gas at about 1 atm. Two experiments at 23.5°C were similar except that the time allowed for exchange was increased from 9 hr in the first to 92 hr in the second, to ensure attainment of equilibrium. The CO_2 was liberated from the liquid phase with H_3PO_4; it was sampled directly from the gas phase. The CO_2 samples were sublimed several times at dry-ice temperature before mass-spectrometer analysis. The analysis showed no significant impurities. The observed separation factors and average deviations were:

$$(O^{18}/O^{16})(g)/(O^{18}/O^{16})(l) = 1.006 \pm 0.001 ,$$

$$(C^{12}/C^{13})(g)/(C^{12}/C^{13})(l) = 1.006 \pm 0.000 .$$

Separation of Alkali-Metal and of Alkaline-Earth Isotopes

Donald Zucker

The single-stage separation factor for Na^{22} and Na^{23} in the system, aqueous NaOH–Na amalgam, was 1.0023 ± 0.0016 (95% confidence interval) at 25°C, with the light isotope concentrating in the amalgam phase. The radioactive Na^{22} (half-life, 2.6 years) was assayed by counting gamma rays with a scintillation counter. Na^{23} was determined by converting the sample to NaCl and titrating Cl^-. Quartz, Vycor, and polyethylene containers were used to reduce contamination with normal sodium and other metals.

The separation factor for rubidium isotopes in a similar system was determined by mass-spectrometric analysis of Rb^{85} and Rb^{87} after eight stages of separation, and by counting 0.525- and 1.08-Mev gammas from Rb^{83} and Rb^{86} after nine stages. The weighted average of the two results was 1.00017 ± 0.00007 (95% confidence interval) per mass unit, with the heavy isotopes concentrating in the amalgam phase.

In the rubidium experiment, it was found that cesium, present as an impurity, was very strongly concentrated in the amalgam phase, with an Rb-Cs separation factor larger than 2. The application of this technique to the preparation of rubidium-free cesium is being investigated more fully.

NMR Study of BF_3 Addition Compounds

A. C. Rutenberg

A kinetic study of the reactions

$$XBF_3 + Y = X + YBF_3 ,$$

where X is $(C_2H_5)_2O$, and Y is $(CH_3)_2O$, $(CH_2)_4O$, $C_6H_5OCH_3$, or $(C_2H_5)_2S$, was begun, using nuclear magnetic resonance (NMR) techniques. Rates of exchange for pairs of donor solvents were studied over the range +45 to −75°C, or over as much of this range as the physical properties of each system permits. Preliminary data indicated that the geometric mean of the average lifetime for a BF_3 stay on sites X and Y, τ, was about 3×10^{-5} sec at 25°C for the methyl ether or ethyl sulfide systems, and about an order of magnitude longer for the anisole or tetrahydrofuran systems. The τ values were dependent on composition, and the values quoted are representative of systems containing comparable amounts of XBF_3 and YBF_3 and an $(X + Y)/BF_3$ mole ratio of about 2.

The activation energies for the BF_3 exchanges are about 11, 12, 14, and 15 kcal/mole for the methyl ether, tetrahydrofuran, anisole, and ethyl sulfide systems, respectively.

The methyl ether system was the only one of the four which had an equilibrium constant within the range 10^{-2} to 10^2 and, therefore, measurable by the techniques employed. The equilibrium constant for the reaction

$$(C_2H_5)_2O{\cdot}BF_3 + (CH_3)_2O \rightleftharpoons (CH_3)_2O{\cdot}BF_3 + (C_2H_5)_2O$$

was about 2 at −50°C; it exhibited a complex temperature and concentration dependence. A detailed study of the effects of changes in composition on the rates and equilibrium constants is in progress.

The BF_3-organic mixtures used in this study were prepared by A. A. Palko.

Structure of Alkylammonium Carbamates

A. C. Rutenberg

The nuclear magnetic resonance (NMR) study[5] of alkylammonium carbamates was discontinued after low-temperature experiments in several solvents indicated that the rates of exchange of the hydrogen atoms of interest were still so rapid that only average positions, which were compatible with more than one structure, were observed.

The infrared spectra of these compounds gave evidence for both covalent and ionic species. The presence of contaminants, such as alkyl carbamic acids which would not interfere with the NMR spectra unless present in large quantities, complicated the infrared spectra.

Dielectric-constant measurements were made on diethylammonium diethylcarbamate using the equipment of W. J. McDowell[6] of the Chemical Technology Division. The carbamate had a molar composition of 1.95 amine/CO_2 and melted at ~30°C. The molten carbamate at 31°C indicated a very large apparent dielectric constant. The cell resembled an electrolytic capacitor with a very high capacitance, well outside the range of the equipment.

A 0.12 *M* solution of diethylammonium diethylcarbamate in cyclohexane at 24°C gave a dielectric constant of 2.034, compared with 2.019 for the pure solvent. An 18 wt % (0.85 *M*) solution of the diethylammonium diethylcarbamate in benzene at 24°C gave a dielectric constant of 2.80, compared with 2.28 for the pure solvent. The data indicate that this carbamate is salt-like in the molten state, and probably exists as ion pairs when dissolved in nonpolar solvents. The present data are, however, not extensive enough to eliminate the existence of covalent structures, such as tetraethylurea hydrate, in nonpolar solvents.

Spectroscopic Investigations of Isotopic Molecules

G. M. Begun W. H. Fletcher[7]

Infrared and Raman studies of isotopic molecules were made to provide information for the calculation of isotopic equilibrium constants. These investigations were also concerned with the potential fields in molecules and ions and the use of isotopic substitution to study these properties.

---

[5] A. C. Rutenberg, *Chem. Div. Ann. Progr. Rept. June 20, 1961*, ORNL-3176, p 23.

[6] W. J. McDowell and K. A. Allen, *J. Phys. Chem.* 63, 747 (1959).

[7] Consultant from Chemistry Department, University of Tennessee, Knoxville.

Such studies of $BF_3 \cdot (CH_3)_2O$ and $BF_3 \cdot (CD_3)_2O$ substituted with B^{10} and B^{11} were completed and published.[8] The experimental determination of the boron-isotope shifts in the $BF_3 \cdot (CH_3)_2O$ molecule made possible the first theoretical treatment of the isotope separation system BF_3-$BF_3 \cdot (CH_3)_2O$. The distillation of $BF_3 \cdot (CH_3)_2O$ as a means of separation of boron isotopes was first proposed in 1944 at Columbia University.[9] It was quickly recognized that the isotopic fractionation in this system was due primarily to the exchange reaction between the liquid complex and gaseous BF_3. The concentration of B^{11} in the BF_3 phase, however, is contrary to expectation and has not been previously explained theoretically. Using the isotopic-shift data shown in Table 3.7, with similar data for BF_3, isotopic partition function ratios and equilibrium constants for the exchange reaction

$$B^{10}F_3(g) + B^{11}F_3 \cdot (CH_3)_2O(l) \rightleftharpoons B^{11}F_3(g) + B^{10}F_3 \cdot (CH_3)_2O(l)$$

were calculated at several temperatures.

The calculated equilibrium constants are compared with experimental values measured by mass-spectrometric analyses of equilibrated samples in Table 3.8. The experimental results are reported separately by A. A. Palko ("Isotopic Chemistry of Boron," this chapter).

If all the uncertainties are considered, the agreement between the experimental and calculated equilibrium constants is quite good.

Physically, the picture of the concentration of $B^{10}F_3$ in the addition complex, contrary to expectation, can be seen to be due to a weakening of the B–F bonds upon complex formation. In the planar BF_3 molecule, the B–F distance is 1.295 A, and the B–F symmetric and antisymmetric stretches in $B^{11}F_3$ occur at 888 and 1453.9 cm^{-1}, respectively. In $BF_3 \cdot O(CH_3)_2$ the BF_3 changes from planar to pyramidal form. The boron and oxygen are now tetrahedrally bonded with a lone pair of electrons occupying the fourth orbital of the oxygen atom. The B–F bond distance is increased to 1.43 A, and the B–F symmetric and antisymmetric stretches for $B^{11}F_3 \cdot O(CH_3)_2$ are found at 805 cm^{-1} and at 1216 and 1177 cm^{-1}, respectively. (The antisymmetric frequency, a doubly degenerate one, is split into two by the destruction of the molecular symmetry in the complex.) Thus the change in BF_3 from planar to tetrahedral results in an increase in the B–F distance and a weakening of the B–F force constant. This effect is so marked that it overbalances the formation of the B–O bond, which has the opposite effect upon the partition function ratio. Thus the B^{11} concentrates in the BF_3 and the B^{10} in the $BF_3 \cdot (CH_3)_2O$.

Table 3.7. Vibrational Frequencies of $BF_3 \cdot O(CH_3)_2$ that Shift upon Boron-Isotope Substitution

Frequency (cm^{-1})		Assignment	
B^{10}	B^{11}		
506	505	ν_{13}, ν_{29}	BF_3 deformation
672	661	ν_{12}	B–O stretch
810	805	ν_{11}	B–F stretch (sym.)
925	918	ν_{10}	C–O stretch (sym.)
1225	1177	ν_7	B–F stretch (antisym.)
1259	1216	ν_{25}	B–F stretch (antisym.)

The computer program for the evaluation of force constants which describe molecular force fields was continued. The general program for computing the force constants for molecules containing up to 15 atoms has been corrected and refined. A Urey-Bradley treatment of N_2O_4 yielded a set of 13 constants, which reproduced the spectral data for $N_2^{14}O_4$ and $N_2^{15}O_4$ quite well. The observed and calculated frequencies are shown in Table 3.9. Further studies, with other types of potential functions, are being made to enable comparisons with similar nitrogen and oxygen compounds.

During the year the mass spectroscopic investigations of the isotopic nitrous oxides (N^{15}-substituted) were completed and published.[10]

[8] G. M. Begun, W. H. Fletcher, and A. A. Palko, "Infrared and Raman Spectra of the Boron Trifluoride–Dimethyl Ether Complex," *Spectrochim. Acta* **18**, 655–65 (1962).

[9] M. Kilpatrick *et al.*, *Separation of Boron Isotopes* (ed. by G. M. Murphy), TID-5227 (1952).

[10] G. M. Begun and Lawrence Landau, *J. Chem. Phys.* **35**, 547–51 (1961); **36**, 1083–84 (1962).

Table 3.8. Equilibrium Constants for Boron Isotope Exchange

T (°K)	$\frac{Q(B^{11}F_3)}{Q(B^{10}F_3)}$	$\frac{Q[B^{11}F_3 \cdot O(CH_3)_2]}{Q[B^{10}F_3 \cdot O(CH_3)_2]}$	α[a]	
			Calculated	Observed
250	1.310	1.256	1.043	1.041[b]
265.16	1.283	1.233	1.040	1.036
277.16	1.264	1.217	1.038	1.033
295.16	1.239	1.196	1.036	1.029
325	1.205	1.167	1.032	1.024[b]
350	1.182	1.148	1.030	
373.16	1.164	1.132	1.028	
400	1.146	1.118	1.025	

[a] The equilibrium constant $\alpha = \frac{[B^{10}F_3 \cdot O(CH_3)_2](l)/[B^{11}F_3 \cdot O(CH_3)_2](l)}{[B^{10}F_3](g)/[B^{11}F_3](g)}$.

[b] Estimated graphically.

Table 3.9. Observed and Calculated Fundamental Frequencies for N_2O_4 (cm^{-1})

Assignment	$N_2{}^{14}O_4$		$N_2{}^{15}O_4$	
	Observed[a]	Calculated	Observed[a]	Calculated
ν_1	1380	1379.4	1360	1360.6
ν_2	808	808.6	797	796.5
ν_3	266	265.8	264	264.3
ν_4		(Inactive)		(Inactive)
ν_5	1712	1713.8	1672	1670.3
ν_6	482	481.2	478	478.8
ν_7	429	429.5	420	419.5
ν_8	672	672.6	654	653.5
ν_9	1748	1746.9	1707	1707.8
ν_{10}	381	380.7	380	380.3
ν_{11}	1262	1262.9	1251	1250.2
ν_{12}	750	749.5	739	739.5

[a] G. M. Begun and W. H. Fletcher, *J. Mol. Spectr.* **4**, 388–97 (1960).

Isotopic Mass Spectroscopy

Lawrence Landau

The 60° copper tube of the Nuclide Analysis Associates RMS-1 ratio mass spectrometer[10,11] was replaced with an Inconel tube. The elimination of copper from the system should reduce error caused by memory for certain samples, particularly SO_2 and BF_3. The new tube also provides a gold-wire vacuum seal and an improved design for differential pumping.

Analyses of BF_3 were made by peak-height analysis for the B^{10}/B^{11} ratio at mass positions 10 and 11. The BF_3 samples compared were from gas and liquid phases of BF_3 in contact with $(CH_3)_2O$ and with $(C_2H_5)_3N$ at several temperatures.

Analyses of CO_2, N_2, O_2, and CO were made by direct ratio analysis of 46/44 and 45/44 for the CO_2 samples, 29/28 for the N_2, 34/32 for the O_2, and 30/28 for the CO. The CO_2 was from samples of CO_2 in contact with a variety of amine carbamates, the N_2 converted from NO in equilibrium with NO_2^- or NO_3^-, the O_2 from exchange experiments between $K_6[(CN)_5CoOOCo(CN)_5]$ and O_2 enriched in O^{18}, and the CO from acetaldehyde in equilibrium with paraldehyde.

Samples of $(C_2H_5)_3B$ were analyzed by the peak heights of mass positions 10 and 11; the compound appeared to give quite acceptable results. Duplicate analyses of the samples showed the 10/11 ratio to be 0.248 ± 0.002 (95% confidence interval). This compound shows very little memory in the mass spectrometer, and may prove to be very useful for the determination of B^{10}/B^{11} ratios.

---

[11] Lawrence Landau, *Chem. Div. Ann. Progr. Rept. June 20, 1960*, ORNL-2983, p 24.

4. Radiation Chemistry

Electron-Bombardment Studies of the Gaseous Mixtures ($C_2N_2 + H_2$) and ($C_2H_2 + N_2$) in a Mass Spectrometer

P. S. Rudolph C. E. Melton S. C. Lind

In the alpha radiolysis of an equimolecular mixture of ($C_2N_2 + H_2$) it was observed[1] that the ratio $-\Delta P_{C_2N_2}/-\Delta P_{H_2}$ remained constant at about 1.5 to complete depletion of the 536 mm (partial pressure) of C_2N_2. A dark solid (with a reddish cast) was formed, which from material balance had an empirical formula of $C_6N_6H_4$. In a complementary experiment[2] a mixture of approximately ($2C_2H_2 + 1N_2$) was irradiated, and very little nitrogenated products were observed. Of the initial 358 mm of N_2, final analysis showed a deficiency of only 29 mm. Upon heating the solid product from the ($2C_2H_2 + 1N_2$) irradiation, 16 mm of condensable (in liquid air) gas was evolved which had the properties of HCN. Further, the yellow solid had a darker hue than the polymer from pure C_2H_2, indicating possible traces of a nitrogenated product admixed with the acetylene polymer.

An exploratory experiment in our research mass spectrometer[3,4] at a total pressure of 50 μ in the ionization chamber indicated that at least one ion, HCN^+, is formed by ion-molecule reactions in equimolar mixtures of both systems ($C_2N_2 + H_2$) and ($C_2H_2 + N_2$). Appearance-potential techniques[5] show that mass 27 cannot be attributed to $C_2H_3^+$. Numerous other masses common to both systems were detected but were not identified. For example, mass 54 could be $C_3NH_4^+$, $C_2N_2H_2^+$, and/or CN_3^+, and mass 80 could be $C_2N_4^+$, $C_3N_3H_2^+$, and/or $C_4N_2H_4^+$. In a previous mass spectrometric study of C_2N_2 (ref 6), ions of varying proportions of C to N were observed, including $(CN)_{10}^+$. In the alpha-particle mass spectrometric studies of C_2H_2 (ref 7), nine ions each of whose percentage abundance exceeded 0.5% were observed, from $C_2H_2^+$ to $C_6H_5^+$. This complexity of ions in the individual gases made it advisable to limit this study of the mixtures to mass 27, which was known to be HCN^+. The approximate rate constants k (cc molecule^{-1} sec^{-1}) for the reactions producing HCN^+ are given below (the probable reactions were determined by appearance-potential technique):

Equimolecular Mixture	Probable Reaction	$k \times 10^{10}$
$C_2N_2 + H_2$	$CN^+ + H_2 \rightarrow HCN^+ + H$	6
$C_2H_2 + N_2$	$N_2^+ + C_2H_2 \rightarrow HCN^+ + (HCN)?$	3

In the present study of the $C_2H_2 + N_2$ mixture, over 80% of N_2^+ ions react by ion-molecule reactions (principally charge transfer to C_2H_2), which do not yield nitrogenated products. Hence, on the basis of ion-molecule reactions one would expect a maximum of 5 to 10% of the final products of this mixture to contain nitrogen. This is in agreement with early alpha-particle radiolysis[2] of $C_2H_2 + N_2$ quoted previously.

[1] S. C. Lind, D. C. Bardwell, and J. H. Perry, *J. Am. Chem. Soc.* **48**, 1556 (1926).

[2] S. C. Lind and D. C. Bardwell, *J. Am. Chem. Soc.* **48**, 1575 (1926).

[3] G. F. Wells and C. E. Melton, *Rev. Sci. Instr.* **26**, 1065 (1957).

[4] C. E. Melton, *J. Chem. Phys.* **35**, 1751 (1961).

[5] C. E. Melton, *J. Chem. Phys.* **33**, 647 (1960).

[6] C. E. Melton and P. S. Rudolph, *J. Chem. Phys.* **33**, 1594 (1960).

[7] P. S. Rudolph and C. E. Melton, *J. Phys. Chem.* **63**, 916 (1959).

Alpha Radiolysis of Ethylene

P. S. Rudolph W. H. Baldwin

The current literature contains many references to the radiolysis of ethylene. A few authors have analyzed the gaseous products. Yang[8] reports five gaseous products. Lampe[9] reports 12, which account for only about a third of the C_2H_4 consumed. The only reference[10] to the composition of the polymer reports six gaseous products and a liquid consisting of C_6H_{14}, C_6H_{12}, C_8H_{18}, C_8H_{16}, and possibly aromatics containing more than two rings. Yang[8] used gamma irradiation, and the other workers[9,10] used fast electrons.

In a previous report[11] on the alpha radiolysis of C_2H_4, insufficient polymer was produced for study (only 4×10^{-4} mole of C_2H_4 was irradiated). Hence, the authors initiated a series of alpha irradiations of C_2H_4 wherein about 0.1 mole of C_2H_4 could be irradiated, thereby producing a reasonable amount of polymer.

In this series of irradiations 3-liter flasks were used. A well was blown into the bottom of each so that the polymer, which first forms as a liquid, could drain into the well. Here it would be subjected to considerably less radiation than if it remained on the wall of the sphere.

The flasks were filled with reagent C_2H_4 to about 1 atm, and about 165 mc of radon was introduced. The volume of the vessel, the initial pressure of C_2H_4, and the charge of radon were accurately determined. The irradiations were continued until the radon had decayed to less than 1 μc. The total residual gas pressures were determined, and samples of this gas were analyzed by gas chromatography.[12] The results of the two runs thus far analyzed and other pertinent data are reported in Table 4.1.

Attempts were made to calculate G values for the appearance of products and the disappearance of C_2H_4 on the basis of energy absorbed in large spheres.[13] These calculated values varied by about 20%. However, both values were approximately twice the value calculated for a small sphere.[11] The ratio of surface to volume was 7 times as large in the small sphere. A possible explanation is termination of reaction at the wall, which is consistent with the smaller yield in the small sphere. However, the authors intend to check into the dosimetry more carefully before reporting G values for the large spheres.

The liquid polymer from these alpha radiolyses of ethylene is a mixture of hydrocarbons. From the molecular weight that was determined cryoscopically, 222 (in benzene) and 231 (in dicyclopentadiene), the average size is 16 carbons. The iodine number (Hanus iodine monobromide) corresponds, on the average, to one double bond for each 10 carbon atoms.

The infrared spectrum contains strong absorption bands at 3.4 to 3.6, 6.85, and 7.30 μ that are assigned to carbon-hydrogen vibrations and one at 13.9 μ that is assigned to an uninterrupted chain of methylene groups at least four carbons long. Unsaturation is confirmed by a band at 10.2 μ (*trans*-vinylene, RCH=CHR′) that accounts for over half of the unsaturation. Smaller contributions to the unsaturation are due to vinyl ($RCH=CH_2$, 11.0 μ) and to vinylidene groups ($RR'C=CH_2$, 11.2 μ). The distribution of unsaturation is in reasonable agreement with the findings of Chang, Yang, and Wagner[14] that the dimer from electron or gamma radiolysis of hexene-1 consisted of olefins that were 57% *trans*-vinylene, 27% vinyl, and 3% vinylidene groups. These results are in contrast with the distribution of the olefins in high-molecular-weight polyethylene polymerized catalytically (60% vinylidene, 20% *trans*-vinylene, and 20% vinyl), reported by Rugg, Smith, Wartman, and Bacon.[15]

Air oxidation of the liquid polymer (11 days at room temperature) was accompanied by a change in odor and changes in the infrared absorption spectrum. A new broad band appeared at 2.9 μ, due to the presence of hydrogen-bonded hydroxyl

[8] K. Yang and P. J. Mauno, *J. Phys. Chem.* **63**, 752 (1959).

[9] F. W. Lampe, *Radiation Res.* **10**, 691 (1959).

[10] B. M. Mikhailov, V. G. Kiselev, and V. S. Bogdanov, *Izv. Akad. Nauk SSSR., Otd. Khim. Nauk* **1958**(5), 545.

[11] P. S. Rudolph and W. H. Baldwin, *Chem. Div. Ann. Progr. Rept. June 20, 1961*, ORNL-3176, p 36.

[12] Gas analyses made by A. D. Horton of the Analytical Chemistry Division.

[13] G. Glockler and G. B. Heisig, *J. Phys. Chem.* **36**, 769 (1932); C. R. Maxwell, V. P. Henri, and D. C. Peterson, *J. Chem. Phys.* **18**, 179, 207 (1950).

[14] P. C. Chang, N. C. Yang, and C. D. Wagner, *J. Am. Chem. Soc.* **81**, 2060 (1959).

[15] F. M. Rugg, J. J. Smith, and J. H. Wartman, *J. Polymer Sci.* **11**, 1 (1953); F. M. Rugg, J. J. Smith, and R. C. Bacon, *J. Polymer Sci.* **13**, 535 (1954).

Table 4.1. Analyses of Gaseous Products of the Alpha Radiolysis of C_2H_4[a]

	Run II	Run III
Vol of reaction vessel:	3143 cc	3064 cc
Initial amount of C_2H_4:	741 mm at 24°C (3.58 g)	752 mm at 23°C (3.49 g)
Initial charge of Rn:	173 mc	156 mc
Final gas pressure:	619 mm at 23°C (estimated)	641 mm at 23.5°C

Product	Run II		Run III	
	Concentration (vol %)	Weight (mg)	Concentration (vol %)	Weight (mg)
H_2	1.3	3.0	0.90	2.0
CH_4	0.10	2.0	0.04	1.0
C_2H_2	95.5[b]	2860	0.69	19
C_2H_4			90.4	2680
C_2H_6	0.26	8.0	0.23	7.0
C_3H_8	0.09[c]	4.0	0.15[c]	7.0
i-C_4H_{10}	0.05	3.0	0.05	3.0
n-C_4H_{10}	0.44	27	0.45	28
cis-Butene-2	0.04	2.0	0.01	1.0
trans-Butene-2			0.005	0.3
Unknown C_5 hydrocarbon	<0.01	~0.8		
i-C_5H_{12}	0.01	0.8	0.002	0.1
n-C_5H_{12}	0.04	3.1	0.05	4.0
2,2-Dimethyl-butane	0.01	1.0	0.002	0.2
Unknown C_6 hydrocarbon			0.002	~0.2
2,3-Dimethyl-butane, 2-methyl-pentane	0.01	1.0	0.003	0.3
3-Methyl-pentane	0.02	2.0	0.01	1.0
n-C_6H_{14}	0.21	19	0.27	25
Unknown C_7 hydrocarbon	0.01	1.0	0.02	~2.0
n-C_7H_{16}	0.01	1.0	0.02	2.0
Unknown C_8 hydrocarbon	0.03	4.0	0.03	~4.0
n-C_8H_{18}			0.02	2.0
Unknown C_9 hydrocarbon			0.04	5.0
Liquid		500		435
Total	98.1	3440	93.4	3230

[a] See ref 12.

[b] With columns used for this analysis, C_2H_2 and C_2H_4 would not be separated.

[c] With columns used for this analysis, C_3H_6 and C_3H_8 would not be separated.

groups (alcohols or carboxylic acids), and a strong absorption band appeared at 6 μ, due to the presence of carbonyl groups (in the form of aldehydes, ketones, or acids). The relative intensities of the absorption bands due to olefins were little changed. The results are in agreement with the products that have been reported for the auto-oxidation of olefins.[16]

The composition of the liquid polymer was investigated by gas chromatography, with and without *n*-heptane added as an internal standard. The operating conditions of the chromatograph (150°C) limited the analysis; hydrocarbons above *n*-decane were not detectable, and the column did not separate olefins from saturated hydrocarbons of the same carbon chain. The results are shown in Table 4.2.

Table 4.2. Analysis of Liquid Products of the Alpha Radiolysis of C_2H_4, Run II

Product	Percent by Weight of Product in Liquid Phase	Weight of Product (mg)
n-Hexane, *n*-hexene	0.5	2.5
n-Heptane, *n*-heptene	0.2	1.0
Unknown C_8 hydrocarbon	1.3	6.5
n-Octane, *n*-octene	3.4	17.0
Unknown C_9/C_{10} hydrocarbon	<0.1	<0.5
Unknown C_9/C_{10} hydrocarbon	0.2	1.0
Unknown C_9/C_{10} hydrocarbon	1.2	6.0
Unknown C_9/C_{10} hydrocarbon	1.6	8.0
n-Decane, *n*-decene	3.9	19.5
Greater than C_{10} hydrocarbon[a]	87.6	438

[a]Not detected by the gas chromatograph at 150°C.

A study of the gaseous and liquid products reported in Tables 4.1 and 4.2, respectively, shows (1) that the even-numbered (carbon atoms) compounds predominate over the odd-numbered compounds and (2) that the straight-chain hydrocarbons predominate over the branched-chain products. The infrared spectrum is not in disagreement with this observation, as the RCH=CHR′ structure is far more abundant than the $RR'C=CH_2$ structure. Since the structure of R and R′ is not known, further inferences cannot be made at this time.

Yang[8] found that of the four hydrocarbon products observed, only C_2H_6 was formed by a free-radical mechanism. Lampe[9] found that the *G* of C_3H_8 and n-C_5H_{12} decreased by factors of 3 and 2, respectively, as the C_2H_4 pressure was increased from 75 to 150 mm.

The above observations and our results would indicate (1) that the majority of the products result from consecutive ion-molecule reactions, (2) that the ion-complexes formed are stabilized by collisions so that bond rupture is minimized, and (3) that wall effect may be important in the alpha radiolysis of C_2H_4.

Catalytic Reactions on Semiconductors[17]

G. E. Moore E. H. Taylor H. A. Smith[18]

Hydrogen-deuterium exchange and the decomposition of formic acid were studied from 100 to 400°C over samples of germanium doped with 10^{16} to 10^{20} atoms of *n*- and *p*-type impurities per cubic centimeter. Over these wide ranges of electronic chemical potential (Fermi level) and temperature, the rate and activation energy of the exchange reaction vary definitely with the Fermi level. A minimum in the activation-energy–Fermi-level curve suggests a mechanism in which one step is rate limiting on the *n*-type and a different step on the *p*-type side of the intrinsic composition. Of the two paths for formic acid decomposition, only dehydrogenation seems to be markedly affected by doping.

[16]J. L. Bolland, *Quart. Rev. (London)* **3**, 1 (1949).

[17]Abstract of paper accepted by the *Journal of Physical Chemistry.*

[18]Consultant from the University of Tennessee, Knoxville.

Radiation Effects on Surface Reactivity of Silica Gel

H. W. Kohn

The transfer of gamma-ray energy from high-surface-area materials such as silica gel to materials adsorbed on their surfaces has been studied by reactions such as pentane radiolysis,[19] cumene decomposition,[20] and deuterium exchange with methane and with hydrogen.[21] The study of intermediates involved in such reactions is being continued here by examining the reactions of several polynuclear aromatic compounds adsorbed on silica gel and then irradiated. The colored products were compared with the colored products produced by adsorption of the same compounds on silica-alumina but without irradiation.

The color reactions of these compounds were studied by the following procedure. First, samples were prepared in pairs by vaporizing 100 to 200 mg of organic adsorbate onto 10 g of silica gel or silica-alumina previously degassed at 520°C. In all cases, the compound adsorbed on the silica-alumina became colored, the colors varying from pale yellow for benzene to dark blue-gray for triphenylene, whereas the silica-gel-adsorbed compounds remained nearly colorless. Then, the silica-gel-plus-organic-adsorbate samples were irradiated for 1 hr in a 600-curie Co^{60} gamma source (about 2×10^5 r). The irradiations were carried out at −78°C in order to increase the stability of the colored intermediates. Of the 17 compounds so examined, 10 showed good color correlations; that is, the color of the organic compound irradiated on silica gel was similar to that obtained by simply adsorbing the same compound on silica-alumina. Since silica-alumina is known to produce predominantly carbonium ions,[22] the color comparisons indicate that most of the radiation-produced intermediates are ionic.

Five of these colored compounds were sufficiently stable that their reflection spectra could be obtained. The general shape of each reflectance-vs-wavelength curve depended only on the organic compound, whether adsorbed on silica-alumina or adsorbed on silica gel and then irradiated, although the actual positions of the reflectance maxima or minima shifted in some cases when the adsorbent was changed, sometimes by hundreds of angstroms. The intermediates are apparently identical on irradiated silica gel and unirradiated silica-alumina when anthracene and triphenyl methane are the adsorbates, but for diphenylethylene, naphthalene, and *p*-quaterphenyl there is only a qualitative similarity.

Experiments designed to determine the reactions of some of these intermediates with hydrogen or oxygen have been started. Reaction vessels containing 10 g of silica gel, previously degassed at 520°C, 1 millimole of organic adsorbate, and about 0.1 atm of O_2 or H_2, and fitted with a small mercury manometer, were irradiated in a 2900-curie Co^{60} source. The reaction was followed between irradiations by measuring gas pressure. Within experimental uncertainty, no radiation-induced reaction of hydrogen with any of the organic compounds tested so far was observed, but considerable reaction with oxygen was noted. Results to date for adsorbates on silica gel are summarized below; the G values, $G(-O_2)$, are calculated on the basis of the number of oxygen molecules which disappear per 100 ev of radiation energy absorbed by the silica gel:

Compound	G Value
Naphthalene	3.3
Biphenyl	1.6
Phenanthrene	1.8
Anthracene	28.4 (initial) 17.4 (final)
Toluene	3.6

The following observations show that we are actually studying a radiation-induced reaction of the organic material with oxygen, caused by the absorption and transfer of energy by the silica gel. Very little oxygen is adsorbed by the silica gel alone. [The most radiation-sensitive compound (anthracene), when dispersed on *fine sand* and irradiated in oxygen, does not form color or absorb oxygen.] The colors formed in the absence of oxygen are not observed when oxygen is present; instead, the organic compounds turn dark brown (except for those with toluene on them), probably

[19] J. M. Caffrey, Jr., and A. O. Allen, *J. Phys. Chem.* **62**, 38 (1958).

[20] R. R. Hentz, *J. Phys. Chem.* **65**, 1470 (1961).

[21] H. W. Kohn, *J. Phys. Chem.* **66**, 11 (1962).

[22] W. K. Hall, *J. Catalysis* **1**, 53 (1962).

indicative of a mixture of organic oxidation products. Finally, the energy absorbed by the organic molecules is so small that, if decomposition were attributed to this energy, the *G* values would be much too high, in the hundreds.

There is some postirradiation reaction of anthracene and toluene with oxygen, which indicates that irradiation can produce active sites in the silica gel which can catalyze the reaction of these compounds with oxygen. The silica-alumina-catalyzed (unirradiated) reaction of anthracene with oxygen at room temperature has been previously reported,[23] and this observation is consistent with the production of the oxidative catalytic properties in silica gel by irradiation. Such a postirradiation effect was not noted with the other compounds examined; it may be present but too slow to be noticeable within the usual time of the experiments.

We have completed experiments that relate hydrogen-deuterium exchange rates on irradiated and unirradiated silica gel to the aluminum impurity and the water content of the gel. After initial degassing at 500°C, the catalytic activity of the gel was proportional to its aluminum content, and the increase in catalytic activity produced by irradiation depended similarly upon aluminum content. Continued dehydration of the gel by heating under vacuum generally resulted in gels that were more active catalytically; however, the proportionality to aluminum content did not always persist through such treatment.

It had been supposed that the enhanced activity of silica gel was due to the removal of adsorbed water by the radiation. However, further evidence on poison removal by radiation makes this less likely as a mechanism for the radiation enhancement of its catalytic activity. On the one hand, the removal of small amounts of adsorbed hydrogen by a Tesla-coil discharge was accompanied by a decrease rather than an increase in catalytic activity. On the other hand, a high-temperature evacuation following a gamma irradiation resulted in a decrease in catalytic activity, although the evacuation should have removed some poison. Clearly, the decrease of catalytic activity caused by annealing of radiation-produced defects was more important than any enhancement by poison removal. Furthermore, the increased activity obtained by very-high-temperature evacuation could well result from crystallization, because quartz, cristobalite, and vitreous silica are all more active than the gel, even when degassed at 900°C (rate constants are 10^{-3} to 10^{-4} min^{-1} m^{-2} for these silicas compared with 1 to 6 $\times$ 10^{-6} for silica gel).

Photolysis of Dilute Hydrogen Peroxide Solution in the Presence of Dissolved Hydrogen and Oxygen: Evidence Relating to the Nature of the Hydroxyl Radical and the Hydrogen Atom Produced in the Radiolysis of Water

C. J. Hochanadel

Chemical measurements indicate radiation-induced decomposition of liquid water to OH radicals and H atoms or their chemical equivalents. Some studies suggest more than one form of each, but their actual identity and molecular constitution is not known. It is also not known whether only one form of each is produced in the initial processes of the radiation-induced decomposition of water. For example, very recent results of Czapski and Allen[24] indicate that only one form of hydrogen atom is produced initially, while other results suggest that about 20% of a second form is produced initially. It is conceivable that hydroxyl radicals may react either as OH, H_2O^+, or O^-, and hydrogen atoms as H, H_2^+, or e^-_{aq}. The three species in each case could be regarded as neutral, acidic, and basic forms, respectively. They could be distinguished by the nature and rates of reaction with various solutes.

Evidence regarding a postulated intermediate can be obtained by comparing the chemical behavior of the species produced in radiolysis with the species produced by methods which allow more certain identification. Most evidence indicates that photolysis of hydrogen peroxide proceeds via initial dissociation to two OH radicals. This system, therefore, offers a simple means of studying reactions of OH radicals uncontaminated by other initially produced species.

The kinetics of the photolysis of hydrogen peroxide was studied in the presence of dissolved

[23] R. M. Roberts, C. Barter, and H. Stone, *J. Phys. Chem.* **63**, 2077 (1959).

[24] G. Czapski and A. O. Allen, *J. Phys. Chem.* **66**, 262 (1962).

hydrogen and oxygen. This allowed comparison of the properties of the hydroxyl radical produced by the photolysis of hydrogen peroxide, and of the hydrogen atom produced by the reaction of H_2 with this hydroxyl radical, with the corresponding properties, previously determined, of the species produced in the radiolysis of water. The comparison was made by accurate evaluation of relative rate constants for the reaction of H_2O_2 and H_2 with the hydroxyl radicals, and for the reaction of H_2O_2 and O_2 with the hydrogen atoms produced in the two systems. The effect of pH on these ratios was also investigated. This study has been completed and will be published in the Fricke Commemorative issue of *Radiation Research* (September 1962). A summary follows.

At sufficiently low concentration of hydrogen peroxide and/or sufficiently high light intensity, the photolysis of hydrogen peroxide is a non-chain reaction, with an overall limiting quantum yield for peroxide removal of unity. Added hydrogen increases the quantum yield, probably by competing with peroxide for hydroxyl radicals to form hydrogen atoms which react with peroxide to reform hydroxyl radicals, etc. The ratio of rate constants, $k_{H_2+OH}/k_{H_2O_2+OH} = 0.93$, is the same as that reported previously for the radiolysis of water.[25] This indicates that the hydroxyl radical produced in the radiolysis of water has the same chemical structure as OH produced by the photodecomposition of hydrogen peroxide. Even though H_2O^+ may be produced initially in the radiolysis of water, presumably it is rapidly ($<10^{-13}$ sec) converted to OH ($H_2O^+ + H_2O \rightarrow H_3O^+ + OH$) before appreciable reaction with solutes occurs. Studies in perchloric acid solution showed the above ratio of rate constants to be independent of hydrogen ion concentration, at least in the range up to 0.4 *M*. However, both sulfuric acid and hydroxide ion diminish the effect of hydrogen (and of hydrogen plus oxygen) on the decomposition of peroxide. This can be interpreted most simply as the reaction of HSO_4^- or of OH^- with OH to give species (presumably HSO_4 and O^-) which do not react with H_2. On this assumption the relative rate constants were evaluated as:

$$k_{H_2+OH}/k_{HSO_4^-+OH}/k_{OH^-+OH} = 1.0/0.005/8.0 .$$

[25]C. J. Hochanadel, *J. Phys. Chem.* **56**, 587 (1952).

The addition of oxygen along with hydrogen lowers the quantum yield, with ϕ decreasing as the concentration ratios $(H_2)/(H_2O_2)$ and $(O_2)/(H_2O_2)$ increase. Oxygen competes with peroxide for the hydrogen atoms, thereby inhibiting the reaction. The ratio of rate constants in photolysis, $k_{H+H_2O_2}/k_{H+O_2} = 2.2 \times 10^{-3}$, is much lower than that reported for radiolysis, 0.6. Therefore, the hydrogen atom produced by the reaction of H_2 with OH does not have the same chemical structure as the hydrogen atom produced directly in the radiolysis of water. The above ratio of rate constants was not influenced by hydrogen ion concentration, at least in the range up to 0.4 *M*. On the other hand, Czapski and Allen[24] showed that O_2, H_2O_2, and H_3O^+ compete for the hydrogen atom produced in the radiolysis of water in the ratio 1.0/0.54/1.0. This and other evidence indicates that the "hydrogen atom" produced in the radiolysis of water is some form of hydrated electron e^-_{aq}. This is converted to a true hydrogen atom H by reaction with hydrogen ion. The hydrogen atom produced by the reaction of H_2 with OH is also a true hydrogen atom. Other evidence (see, for example, "Radiation Chemistry of Sulfuric Acid Solutions," this chapter) indicates that still a third form may be produced at very high acidity. The three forms and their relationships can be summarized as follows:

$$e^-_{aq} \xrightarrow{H^+ \text{ (or } H_3O^+)} H \xrightarrow{H^+} H_2^+ .$$

Radiation Chemistry Studies of Water as Related to the Initial Linear Energy Transfer of 10–23 Mev Protons

G. L. Kochanny, Jr.[26] C. D. Goodman[28]
Andrew Timnick[27] C. J. Hochanadel

The radiolysis of water is best interpreted on the basis of the expanding-spur (or expanding-

[26]Ph.D. candidate at Michigan State University. Research carried out at ORNL under an ORINS Fellowship.

[27]Department of Chemistry, Michigan State University.

[28]Electronuclear Division, ORNL.

track) model developed by Magee and co-workers.[29,30] Calculations of the spatial and temporal distribution of free-radical intermediates are based on an assumed distribution of primary species (i.e., distribution of initial spur sizes, concentration of species in a spur, spacing of spurs, etc.), diffusion coefficients of the radicals, and rate constants for all pertinent radical-radical and radical-solute reactions. Several measurable quantities which aid in formulating and testing the model are the yields of radical and "molecular" products as a function of LET (linear energy transfer or energy loss per unit track length) of the radiation, solute (scavenger) concentration, dose rate, isotopic content, and temperature.

The effect of LET (in the range 0.2 to 0.4 ev/A) on yields for several reactions was studied by using protons of various energies in the range 23 to 11 Mev. The solutes employed quantitatively scavenge the intermediates produced by the decomposition of the water and allow evaluation of the 100-ev yields G_H, G_{OH}, G_{H_2}, $G_{H_2O_2}$, and G_{-H_2O}. The yield for the oxidation of ferrous sulfate decreased from 12.8 for 23-Mev protons to 11.3 for 11-Mev protons. The yield for the reduction of ceric sulfate remained constant at 2.95 over this range of proton energies, while the yield for the reduction of ceric sulfate in the presence of thallous ion decreased from 6.78 for 23-Mev protons to 6.01 for 11-Mev protons.

The derived molecular yields, G_{H_2} and $G_{H_2O_2}$, were essentially constant at 0.38 and 0.93 respectively over this range of LET, while G_H decreased from 3.00 to 2.66 and G_{OH} decreased from 1.90 to 1.52 as the LET increased from 0.2 to 0.4. The net yield of water decomposition, G_{-H_2O}, decreased from 3.77 to 3.38 over this range of LET. Both the measured and derived yields extrapolate smoothly to the values reported for particles of LET >0.4 ev/A.[31,32] The results are in semiquantitative agreement with the diffusion-kinetics model.[30,31]

[29]A. H. Samuel and J. L. Magee, *J. Chem. Phys.* **21**, 1080 (1953).

[30]A. K. Ganguly and J. L. Magee, *J. Chem. Phys.* **25**, 129 (1956).

[31]A. R. Anderson and E. J. Hart, *Radiation Res.* **14**, 689 (1961).

[32]R. H. Schuler and A. O. Allen, *J. Am. Chem. Soc.* **79**, 1565 (1957).

The study entailed accurate measurements of proton energy and proton beam current, for which methods were devised. The beam current was monitored by counting the protons scattered at 90° by a very thin nickel foil through which the beam passed. The proton beam transmitted by the foil entered either a Faraday cup for calibration or the sample to be irradiated. The primary energy of the protons was determined by adding a known amount of aluminum absorber to reduce the energy to approximately 6 Mev and then determining the residual energy from the amount of ferrous sulfate oxidized and the known yield vs energy in this range. The measured value of 23.0 ± 0.1 Mev agreed within 1% with that determined by the Nuclear Physics Group.[33] In this method the energy is degraded by aluminum absorbers until the response of a silicon surface-barrier counter is the same as that produced by alpha particles of known energy.

Radiation Chemistry of Sulfuric Acid Solutions

J. W. Boyle

Ferrous ion dissolved in air-saturated 0.4 *M* H_2SO_4 has been used for years as a chemical dosimeter to determine the amount of energy deposited in solution by ionizing radiations. As the ferrous dosimeter has been extensively studied, the product yields (molecules oxidized or reduced per 100 ev of absorbed energy) and reaction mechanisms are well established for this system. With this knowledge as a foundation, a thorough Co^{60} radiation study was made on ferrous–sulfuric acid solutions as the acid concentration was increased from 0.4 *M* to 18 *M*.

One of the radiolysis products in the ferrous–sulfuric acid system is hydrogen, which appears to be produced by two processes. In one process hydrogen is formed in regions of high energy deposition (spurs) by the combination of two hydrogen atoms (molecular H_2 yield). In the second process, taking place in the bulk of the solution, competition for hydrogen atoms by dissolved oxygen and the hydronium ions is indicated. Hydrogen atoms presumably form the complexed HO_2 and H_4O^+, which react with ferrous ions.

[33]Personal communication, J. B. Ball and C. B. Fulmer, Electronuclear Division (1962).

The hydrogen atom reaction with an oxygen molecule results in the reduction of the oxygen molecule and the oxidation of three ferrous ions. The reaction of the hydrogen atom with a hydronium ion causes the oxidation of one ferrous ion and the formation of one molecule of hydrogen.

The rates of production of HO_2 and H_4O^+ are given by

$$d(HO_2)/d(\text{dose}) = G(HO_2) = k_{(H+O_2)}(H)(O_2) \qquad (1)$$

and

$$d(H_4O^+)/d(\text{dose}) = G(H_4O^+) = k_{(H+H_3O^+)}(H)(H_3O^+) \qquad (2)$$

respectively. $G(HO_2)$ and $G(H_4O^+)$ are obtained respectively from the $-O_2$ yield and the H_2 yield. The O_2 and H_3O^+ concentrations are obtained by chemical analysis. If Eq. (1) is divided by Eq. (2), the ratio of rate constants $k_{(H+O_2)}/k_{(H+H_3O^+)}$ can be evaluated. This ratio was found to be 700,000 (±6%) between 1 *M* and 17 *M* acid.

Other products besides hydrogen are ferric ion, sulfur dioxide, and reduced oxygen. Their yields were measured and are shown in Fig. 4.1. These results together with the results from the ceric–sulfuric acid system[34] were used to calculate the radical and molecular product yields in aqueous sulfuric acid solutions as a function of sulfuric acid concentration. The radical intermediates believed to be present are H, OH, HSO_4 (or SO_4^-), and HSO_3 (or SO_3^-). The molecular products, postulated to be formed from the combination of the above-mentioned radicals, are H_2, H_2O_2, $H_2S_2O_8$, H_2SO_5, and SO_2. Sulfur dioxide is produced from the decomposition of dithionic acid ($H_2S_2O_6$) and sulfurous acid. Yields of the radical and molecular products are given in Fig. 4.2.

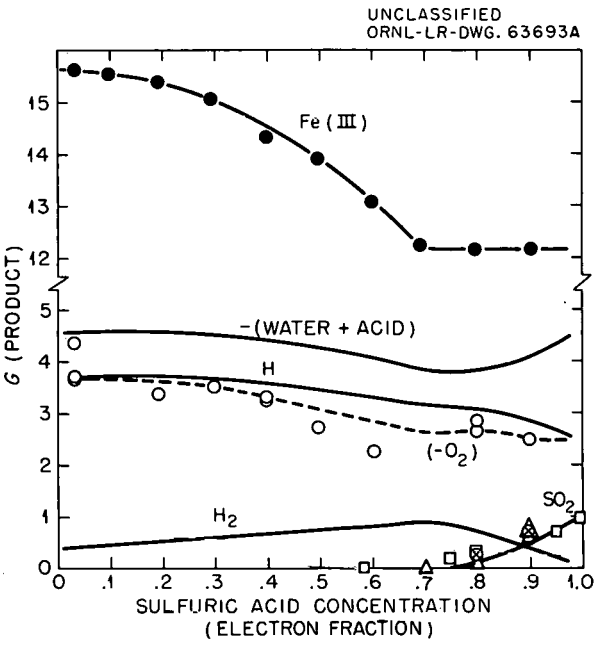

Fig. 4.1. Product Yields as a Function of Sulfuric Acid Concentration for the Gamma Irradiation of Ferrous Sulfate Solutions. Sources of the SO_2 yields: ⊗, J.W.B. [from Fe(II)–aqueous H_2SO_4]; Δ, J.W.B. [from Ce(IV)–aqueous H_2SO_4]; □, C.J.H., J.A.G., and T.J.S. [from aqueous H_2SO_4].

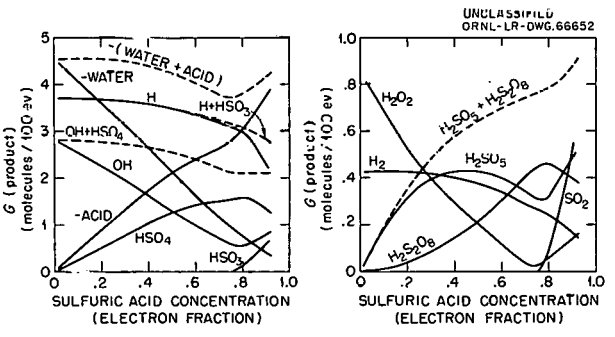

Fig. 4.2. Calculated Radical (at Left) and Molecular Product (at Right) Yields as a Function of Sulfuric Acid Concentration for Dilute Solutions of Ce(IV) and Fe(II).

Radiolysis of Aqueous Nitrate Solutions

H. A. Mahlman

Investigation of the Co^{60} gamma radiolysis of aqueous nitrate solutions, specifically concentrated aqueous $NaNO_3$ solutions, was continued. When water is irradiated it decomposes into hydrogen atoms and hydroxyl radicals. As these radicals diffuse from their site of origin, like radicals may react to form the detected molecular

[34] J. W. Boyle, *Chem. Div. Ann. Progr. Rept. June 20, 1961*, ORNL-3176, p 33.

products H_2 and H_2O_2, while the reaction of unlike radicals regenerates water.

When concentrated aqueous $NaNO_3$ solutions are irradiated, product yields in excess of those predicted from the radical yields are observed. These excess product yields have been descriptively termed "direct-action yields"[35] and imply a direct interaction of the incident radiation with the dissolved solute.

Ce^{4+}–0.8 *N* H_2SO_4–$NaNO_3$ System. – The radiation-induced reduction of Ce^{4+} in the Ce^{4+}–0.8 *N* H_2SO_4–$NaNO_3$ system offers a convenient method to demonstrate and investigate the direct-action effect. In the absence of $NaNO_3$ the ceric reduction has been shown to be

$$G(Ce^{3+}) = 2G_{H_2O_2} + G_H - G_{OH} + 2(0.45 - G_{H_2}) \quad (1)$$

(refs 36 and 37), where G represents the number of product molecules produced per 100 ev of absorbed energy. In Fig. 4.3, curve *A* represents the observed $G(Ce^{3+})$ as a function of the $NaNO_3$ concentration in the Ce^{4+}–0.8 *N* H_2SO_4–$NaNO_3$ system. There are several delineable contributions to the observed $G(Ce^{3+})$, such as (*a*) the ceric reduction by the radiolysis products from water as given by Eq. (1), (*b*) the suppression of the $G(H_2)$ by nitrate ions and the subsequent reduction of Ce^{4+} ions, and (*c*) the direct-action effects. The $G(Ce^{3+})$ associated with the water radiolysis products are assumed to be constant over the same $NaNO_3$ concentration range over which the G_{OH} remains constant,[38,39] as illustrated by curve *C* in Fig. 4.3. The observed $G(H_2)$ were determined in the Ce^{4+}–0.8 *N* H_2SO_4–$NaNO_3$ system and were found to agree with the decreased $G(H_2)$ observed in aqueous $NaNO_3$ solutions, pH 4–5.[40] The reduction of nitrate ions by hydrogen atoms that normally form molecular hydrogen caused a decrease in the observed $G(H_2)$, and a stoichiometric increase in the $G(Ce^{3+})$.

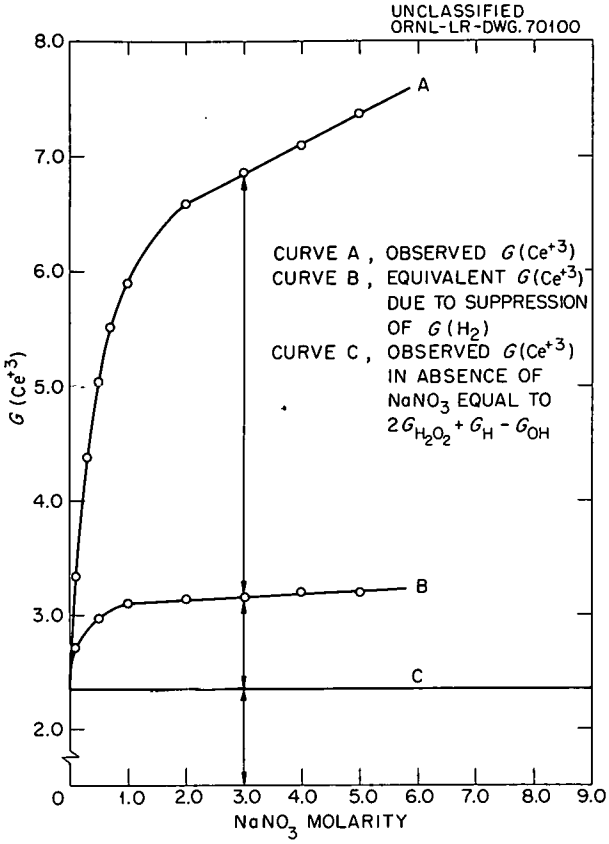

Fig. 4.3. $G(Ce^{3+})$ **in** Ce^{4+}–0.8 *N* H_2SO_4–$NaNO_3$ **System.**

The extent of this reaction is represented by the difference between curves *B* and *C*. Thus we have isolated the enhanced $G(Ce^{3+})$ as the difference between curves *A* and *B* in Fig. 4.3, more clearly presented as curve *D* of Fig. 4.4. Extrapolation of the linear portion of curve *D* (from 2.0 *M* and greater) to zero $NaNO_3$ concentration enables us to separate two contributions to the enhanced $G(Ce^{3+})$, one of which is directly proportional to $NaNO_3$ concentration.

H_2O^{18}-$NaNO_3$ System. – The use of O^{18}-labeled water enabled studies to be made of the origin of the molecular oxygen formed by the Co^{60} gamma irradiation of aqueous $NaNO_3$ solutions, pH = 4–5. Mass spectrographic analysis of the oxygen indicated that in $NaNO_3$ solutions less than 2.0 *M* the molecular oxygen was formed either by the decomposition of water or by some participation of water and nitrate ions. This process reached a maximum, while a second process, the formation

[35] T. J. Sworski, *J. Am. Chem. Soc.* **77**, 4689 (1955).

[36] A. O. Allen, *Radiation Res.* **1**, 87 (1954).

[37] H. A. Mahlman, *J. Am. Chem. Soc.* **81**, 3203 (1959).

[38] T. J. Sworski, *Radiation Res.* **4**, 483 (1956).

[39] H. A. Mahlman, *J. Phys. Chem.* **64**, 1598 (1960).

[40] H. A. Mahlman, *J. Chem. Phys.* **27**, 1434 (1957).

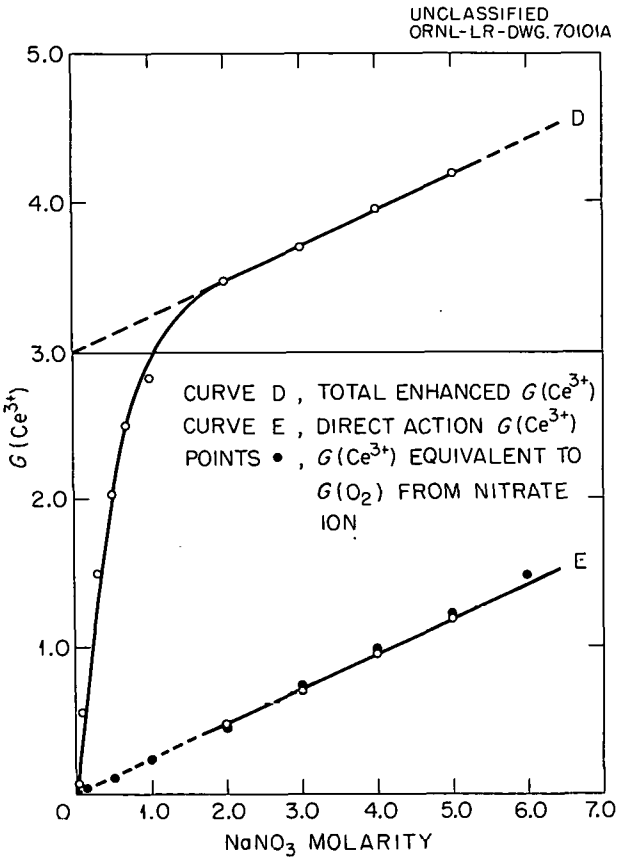

Fig. 4.4. Enhanced Cerous Yields.

of molecular oxygen from nitrate ions, steadily increased with increasing $NaNO_3$ concentration. This direct proportionality suggests a direct action on the nitrate ion by the radiation:

$$NO_3^- \rightsquigarrow NO_2^- + \tfrac{1}{2}O_2 \,. \qquad (2)$$

A comparison between the molecular oxygen formed from the nitrate ions and the linearly dependent portion of the enhanced $G(Ce^{3+})$ observed in the Ce^{4+}–0.8 *N* H_2SO_4–$NaNO_3$ system is also presented in Fig. 4.4. A direct comparison was accomplished by using the stoichiometric cerous ion equivalent of the oxygen yield according to Eq. (2), where each molecule of oxygen that is formed produces two nitrite ions, each of which reduces two ceric ions. The quantitative agreement of the cerous spectrophotometric data (curve *E*) with the mass spectrographic oxygen data (solid circles) supports the hypothesis of direct action in concentrated aqueous $NaNO_3$ solutions that is directly proportional to concentration.

An additional process may involve the participation of water and nitrate ions in the formation of molecular oxygen. This process occurs at $NaNO_3$ concentrations less than 2.0 *M* and is the cause of the rapid initial increase in $G(Ce^{3+})$ in the Ce^{4+}–0.8 *N* H_2SO_4–$NaNO_3$ system. This process is difficult to explain. We may, however, delineate criteria for the mechanism and then postulate a possible mechanism: The OH-radical yield must remain constant,[37,38] and the increase in $G(Ce^{3+})$ must be essentially equal to the OH-radical yield as shown by the extrapolated intercept of curve *D* of Fig. 4.4. Moreover, the isotopic composition of the O_2 formed indicates some scrambling of oxygen atoms from the H_2O and NO_3^-. A mechanism meeting these criteria may be merely scavenging of H_2O^+ by nitrate ion prior to the formation of hydroxyl radicals.

Radiolysis by Transferred Energy of Nitrite Ion in a Potassium Bromide Matrix

A. R. Jones

The investigation of radiolysis by transferred energy was continued.[41,42] The decomposition of nitrite ion dispersed in potassium bromide was studied as a function of the total energy absorbed by the dispersion for several initial concentrations of the reactant. It was found that the nitrite ion apparently disappears by two concurrent first-order processes. A typical plot of log *C* vs the cumulative dose is presented in Fig. 4.5*a*. The early portion of the curve is shown in expanded scale in Fig. 4.5*b*. Table 4.3 contains the first-order constants for the faster and slower reactions for each initial concentration, C_0 of NO_2^- investigated. Also shown in this table are the initial *G* values (G_0) for these reactions and their sums; each sum represents the total initial rate of disappearance of NO_2^- for each 100 ev of energy absorbed by that whole system. The number of ions decomposed by the faster reaction for each C_0 is included.

[41] *Chem. Div. Ann. Progr. Rept. June 20, 1960*, ORNL-2983, p 27.

[42] *Chem. Div. Ann. Progr. Rept. June 20, 1961*, ORNL-3176, p 28.

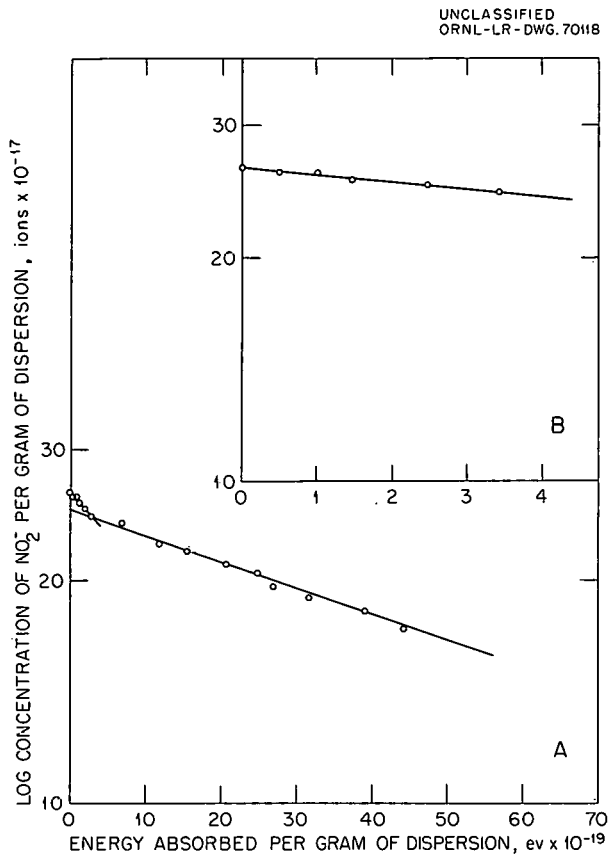

Fig. 4.5. The Disappearance of NO_2^- During Radiolysis. $C_0 = 26.32 \times 10^{17}$ NO_2^- ions per g of KBr.

The initial yields of both the faster and the slower reactions vary with the initial concentration of nitrate ion. The variation is a regular one, although no simple relation is yet evident (Fig. 4.6). It may be qualitatively explained by considering each unirradiated mixture of potassium nitrite and potassium bromide as a structurally different system. That is, although the faster reaction in each case probably represents the decomposition of isolated nitrite ions – those which have replaced bromide ions in the KBr lattice – there is present in each mixture a different concentration of some other active species which can compete with the NO_2^- for the available energy. Such species could be the dislocations, vacancies, etc., the concentrations of which are characteristic of the perfection of the lattice, and would depend on the strains inherent in incorporating the foreign nitrite ion.

Apparent Solubility of Some Substances in Potassium Bromide

A. R. Jones

Plots of the turbidity at 4000 A vs the concentrations of KNO_3 and KNO_2 dispersed in pressed KBr disks showed discontinuities which appeared to correspond to the respective solubilities of

Table 4.3. The Decomposition of NO_2^- Dispersed in KBr

	System					
	1	2	3	4	5	6
Initial concentration (C_0), ions $\times 10^{-17}$ per g of KBr	1.06	2.63	5.57	8.61	13.16	26.32
First-order constant for faster reaction, $ev^{-1} \times 10^{-21}$		2.32	2.21	1.98	1.61	1.25
First-order constant for slower reaction, $ev^{-1} \times 10^{-21}$	2.58	2.98	1.74	1.59	1.27	0.81
G_0 for disappearance of NO_2^- by faster reaction		0.061	0.123	0.170	0.212	0.330
G_0 for disappearance of NO_2^- by slower reaction	0.027	0.078	0.097	0.137	0.167	0.212
Total G_0 for disappearance		0.14	0.22	0.31	0.38	0.54
Total ions decomposed by faster reaction $\times 10^{-17}$ per g of KBr		0.42	0.65	0.81	1.00	1.42

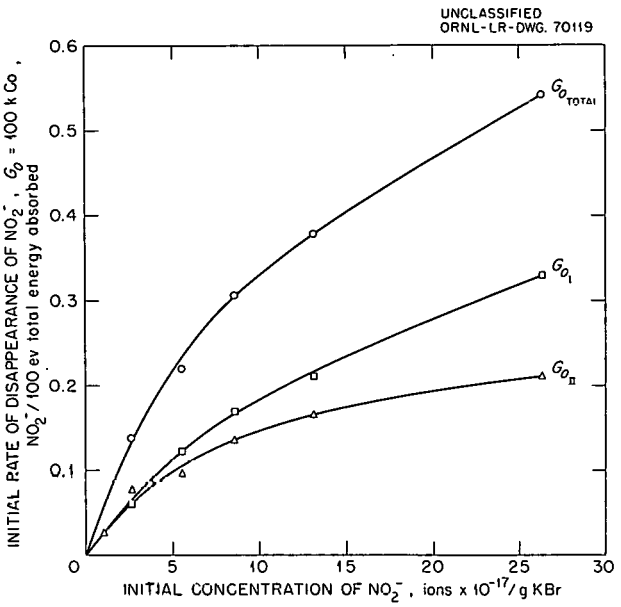

Fig. 4.6. The Variation of the Initial Rate of Disappearance of NO_2^- Dispersed in KBr with the Initial Concentration of NO_2^-.

Table 4.4. Concentration Required for the Appearance of Turbidity

Substance	No. of Ions or Molecules per gram of KBr	
	3000 A	5000 A
	$\times 10^{17}$	$\times 10^{17}$
BrO_3^-	420	480
CH_3COO^-	47	95
$C_6H_6O_2$ (hydroquinone)	21	42
$C_{14}H_{10}$ (anthracene)	17	15
$(C_6H_5)_3C^+$	9	14
$C_{20}H_{10}O_5^{2-}$ (fluorescein)	3	3

NO_3^- and NO_2^- in KBr.[43] In order to determine whether such discontinuities would appear when the dispersed ion became too large to be incorporated into the KBr lattice, and thus to confirm or deny the correspondence of the discontinuity with the solubility, a series of similar experiments was made for ions of increasing volume. The concentrations at the points of discontinuity (for two wavelengths) are listed in Table 4.4.

Listed also in the table are similar results for the neutral molecules hydroquinone and anthracene. The former was deposited from aqueous solution in the same fashion as the ions; the latter was deposited from acetone solution, in which KBr has more limited solubility.

Below a certain characteristic concentration, all these substances gave suspensions showing no greater turbidity than that shown by disks pressed from pure KBr. The concentration at which turbidity appears decreases as the volume of the dispersed substance increases.

It seems unlikely that the bulky, and even nonionic, substances are incorporated into the lattice, replacing bromide ions, as was proposed for the NO_3^- and NO_2^- cases. Instead, it is now believed that the behavior may be compared to that of "colloidal electrolytes" in liquid solutions. Such solutions show similar turbidity behavior at a concentration which coincides with that at which the thermodynamic properties of the solutions become nonideal.

This is interpreted to mean that, although there is undoubtedly some solubility of small ions such as NO_3^- and NO_2^- in the lattice itself, the remainder of the KNO_3 and KNO_2 and all the bulkier ions and neutral molecules exist in these mixtures as adsorbed or occluded aggregates ranging upward in size from individual ions or molecules. In a liquid system an equilibrium is attained for which the concentration of aggregates is low until the critical micelle concentration is reached. In the present system, however, the solid mixture is formed at continually changing concentration, and there may be larger numbers of 2, 3, 4, ...-unit aggregates than would be present at equilibrium in a liquid solution.

[43] *Chem. Div. Ann. Progr. Rept. June 20, 1961*, ORNL-3176, p 31 (Fig. 4.3 and the preceding paragraph).

Radiolysis of Liquid Oxygen and Oxygen-Nitrogen Mixtures

J. F. Riley

As previously indicated,[44] there has been very little study[45-48] of the radiolysis of liquid oxygen, despite a basic interest in the electron affinity of oxygen and its possible consequences.[49] Further, Pshezhetsky's limited report[45,46] of an ozone yield, $G(O_3)$ = 15 molecules per 100 ev, representing an extremely efficient (22%) energy conversion, was not confirmed by subsequent workers.[47,48]

Our experimental method of alternate gamma irradiation and ultraviolet absorption measurement allows the *in situ* observation of ozone formation. Because ozone is a much stronger ultraviolet absorber than oxygen, we are able to determine ozone concentrations by measurement of the absorption in the region from 2500 to 3000 A. Ozone concentrations as low as 0.4 ppm are readily determined with a precision of ±5%.

At any particular wavelength in the above spectral region, the change in absorbance with dose was a linear function for doses as high as 2×10^{18} ev/g. Incremental changes in absorbance were measured for dose increments of 2.2×10^{17} ev/g. The ratio of ozone yield from each O_2-N_2 mixture to that from pure oxygen was determined from the ratio of the slopes of the straight lines, absorbance vs dose, with allowance for the density differences.

From the change in absorbance with dose and a knowledge of the absorption coefficients for ozone, the ozone yield $G(O_3)$ was calculated. The absorption coefficients are known for gaseous ozone,[50,51] but several tests of internal consistency support their application to ozone in liquid oxygen and oxygen-nitrogen mixtures.

Ozone yields in the gamma radiolysis of liquid oxygen and oxygen-nitrogen mixtures are presented in Table 4.5. The values in the column labeled "$G(O_3)$, Mixture/$G(O_3)$, Pure O_2" show the extensive energy transfer occurring in the system. When the electron fraction of oxygen is 0.115 (mole fraction = 0.102), the yield of ozone is still 65% of that from pure oxygen. Even more striking is the behavior of the solution which is only 0.050% O_2 (mole fraction = 0.00050); the yield of ozone is equal to 32% of that from pure oxygen.

In our first design of low-temperature cells, liquid-nitrogen coolant was present in the optical path. Even when the liquid nitrogen contained only small amounts of oxygen (<500 ppm), energy transfer resulted in ozone formation, which would be included in the spectrophotometric assay. The results shown in Table 4.5 were obtained in our latest-design cell, which excludes all coolant from the optical path.

Table 4.5. Summary of Ozone Yields in the Radiolysis of Liquid Oxygen and Oxygen-Nitrogen Mixtures at 77°K

Mole Fraction O_2	$\frac{G(O_3), \text{ Mixture}}{G(O_3), \text{ Pure } O_2}$	$G(O_3)^a$
1	1	12.5
0.102	0.657 ± 0.006	8.2
0.0124	0.461 ± 0.007	5.8
0.0011	0.356 ± 0.005	4.5
0.00050	0.317 ± 0.003	4.0
0.102[b]	0.650 ± 0.007	8.1
1[c]	1.037 ± 0.003	13.0

[a] $G(O_3)$ is the number of molecules of ozone produced per 100 ev of energy absorbed by the solution.

[b] Repetition of an experiment to illustrate the precision.

[c] Radiolysis of liquid oxygen at its boiling point (90°K), for comparison with results for oxygen at 77°K.

[44] *Chem. Div. Ann. Progr. Rept. June 20, 1961*, ORNL-3176, p 33.

[45] S. Ya. Pshezhetsky *et al.*, *Collection of Papers on Radiation Chemistry*, p 133, Academy of Sciences, USSR, 1955.

[46] S. Ya. Pshezhetsky and M. T. Dmitriev, *Usp. Khim.* **26** (part 7), 725 (1957).

[47] J. F. Kircher *et al.*, *Radiation Res.* **13**, 452 (1960).

[48] D. W. Brown and L. A. Wall, *J. Phys. Chem.* **65**, 915 (1961).

[49] J. L. Magee and M. Burton, *J. Am. Chem. Soc.* **73**, 523 (1951).

[50] E. C. Y. Inn and Y. Tanaka, *J. Opt. Soc. Am.* **43**, 870 (1953).

[51] A. G. Hearn, *Proc. Phys. Soc. (London)* **78**, 932 (1961).

Figure 4.7*a* shows the ratios of ozone yields from oxygen-nitrogen mixtures to that from pure oxygen. The abscissa is the logarithm of the mole fraction of oxygen. The lower curve is the ratio of yields expected on the basis of electron fractions and *no* energy transfer. The upper curve passes through the experimental points.

To illustrate how the enhancement of ozone yield is changing with composition, Fig. 4.7*b* presents the difference between the curves of Fig. 4.7*a*, that is, the difference between the experimental ratio of yields and the ratio predicted on the assumption of no energy transfer. The maximum enhancement in the ratio of ozone yields occurs for a solution with a mole fraction of oxygen of about 0.1. It may be noteworthy that at this composition each nitrogen molecule has, on the average, one oxygen molecule in its nearest neighbor shell.[52]

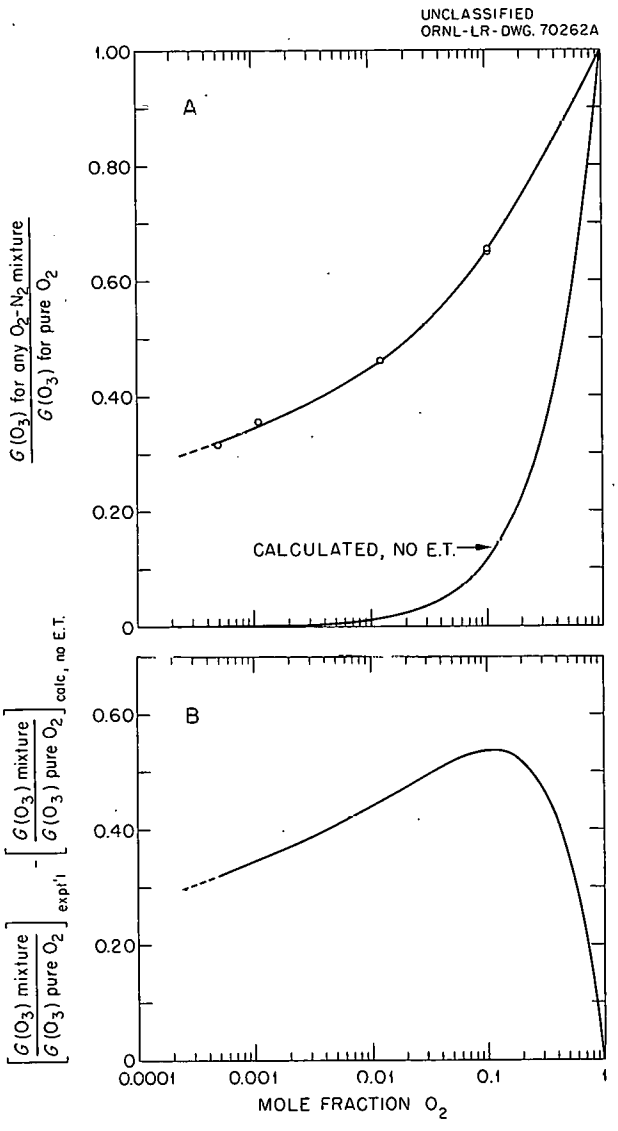

Fig. 4.7. (*a*) Ratio of Ozone Yields from O_2-N_2 Mixtures to the Yield from Pure Oxygen, 77°K; (*b*) Difference Between Experimental Curve and Curve Calculated on Basis of No Energy Transfer.

The *G* value for ozone formation in liquid oxygen at 77°K, as shown in the table, is twice as large as that reported by Brown or Kircher. Brown's yields were determined by titration and dilatometry after irradiation to 10^{21} ev/g, which is 10^4 times our first dose increment. Brown's results for oxygen mixtures indicate extensive energy transfer but do not extend below a mole fraction of oxygen of 0.25.

A mechanism to account for the observed yields is under consideration. Charge transfer from N_2^+ to O_2 is known to occur in gas-phase systems and should play a principal role in the mechanism. A coupling of charge transfer, electron capture by oxygen, and ionic recombination may describe what we have called "energy transfer."

The formation of ozone is an endothermic process, and in oxygen radiolysis it represents an efficient conversion of energy (radiation to chemical). In pure oxygen, $G(O_3) = 12.5$ shows an energy conversion efficiency of 19%; in 0.05% O_2, the energy conversion efficiency is 6%.

Reloading of Cobalt Sources

J. F. Riley C. J. Hochanadel

The Radiation Chemistry Group has two cobalt sources, both of which were reloaded to provide higher dose rates. The sources are housed in lead shields, the design of which was described previously.[53] One source was reloaded with 2900 curies of Co^{60}, and the other with 280 curies. The capsules containing the cobalt are of a new design. They consist of six stainless steel tubes which contain the cobalt, and they stand in a stainless steel rack in the form of a hollow cylinder with an external diameter of 2.375 in. and

[52] D. G. Henshaw, *Phys. Rev.* 119, 22 (1960).

[53] J. A. Ghormley and C. J. Hochanadel, *Rev. Sci. Instr.* 22, 473 (1951).

an internal diameter of 1.445 in. The capsule for the larger source is 11 in. tall, with the cobalt occupying the bottom 4.1 in. of the tubes. The cobalt was distributed to provide a uniform dose rate (within ±2%) over a 3-in. length along the vertical axis. The maximum dose rate in the center of the large source, as established by ferrous sulfate dosimetry, was 2.05×10^{18} ev g^{-1} min^{-1} on June 5, 1962.

The capsule for the smaller source is 7 in. tall, with the cobalt occupying the bottom 4.2 in. Again, the cobalt is distributed in such a way as to provide a uniform dose rate over a 3-in. length along the vertical axis. The maximum dose rate in the center of this source was 2.08×10^{17} ev g^{-1} min^{-1} on August 10, 1962.

Radiolysis of Crystalline Alkali-Metal Bromates by Neutron Reactor Radiations

G. E. Boyd Q. V. Larson

Nuclear reactor radiations were employed to effect the radiolysis of the alkali-metal bromates to decompositions of approximately 3 mole % (Fig. 4.8). The sequence of increasing radiolytic stability for the salts was the same as that observed previously with Co^{60} gamma rays, although in some instances their relative stabilities differed significantly. These differences could be attributed to the production of internal radiation sources by thermal-neutron capture in the cations and to the presence of low-energy components in the gamma-ray spectrum of the reactor. Irradiations

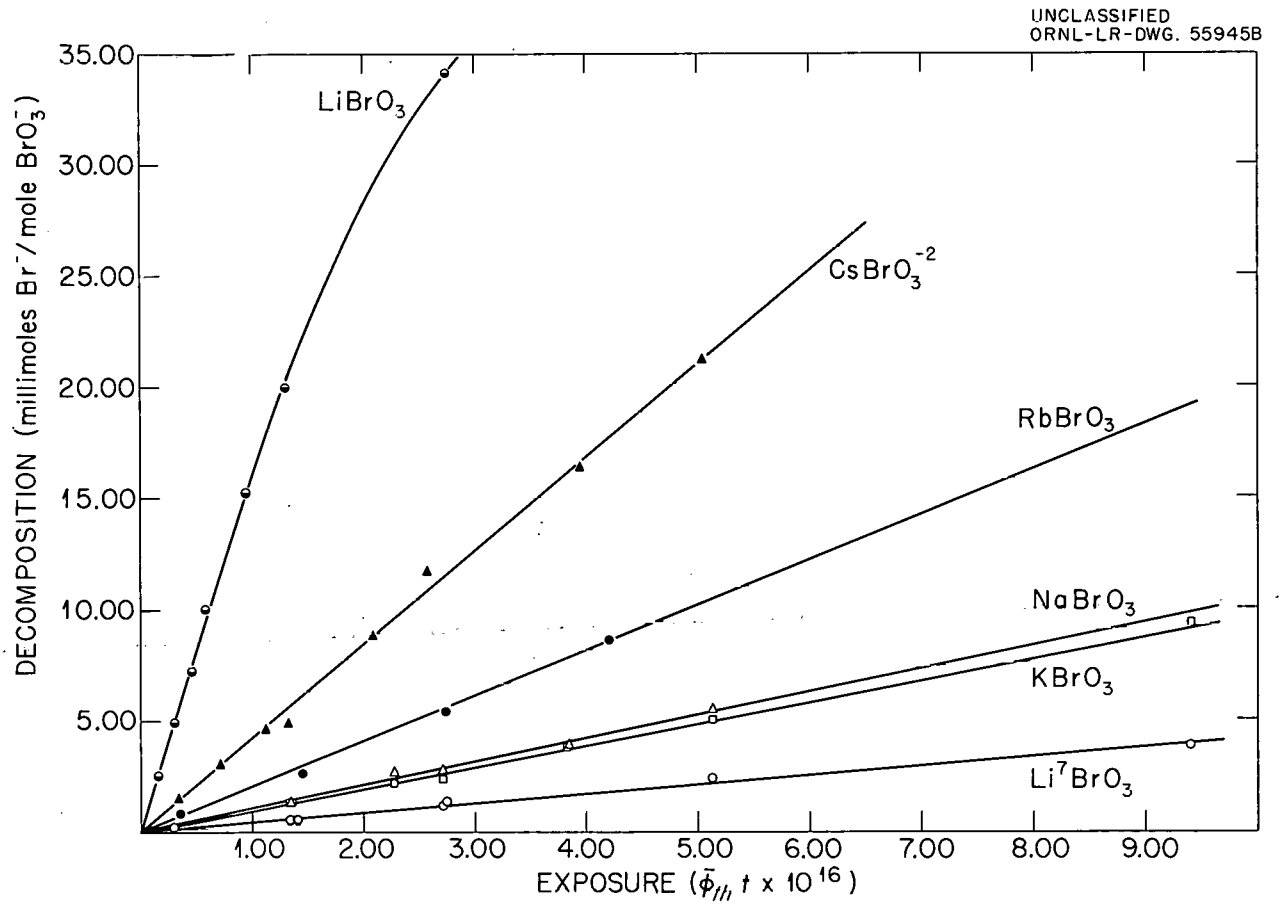

Fig. 4.8. Radiolysis of Alkali Bromates by Neutron Reactor Radiations.

in pure, gamma-ray-free thermal-neutron fluxes, behind thick lithium metal shielding, and behind thick bismuth metal shielding were employed to estimate the specific decompositions caused by thermal neutrons, fast neutrons, and gamma rays, respectively.

The formation of bromine oxidation states intermediate between bromate and bromide was observed. The radiolytic production of oxidizing fragments was dependent on the cation and became nonlinear with increasing exposure (Fig. 4.9); their "average oxidation number" appeared to decrease with the time of bombardment.

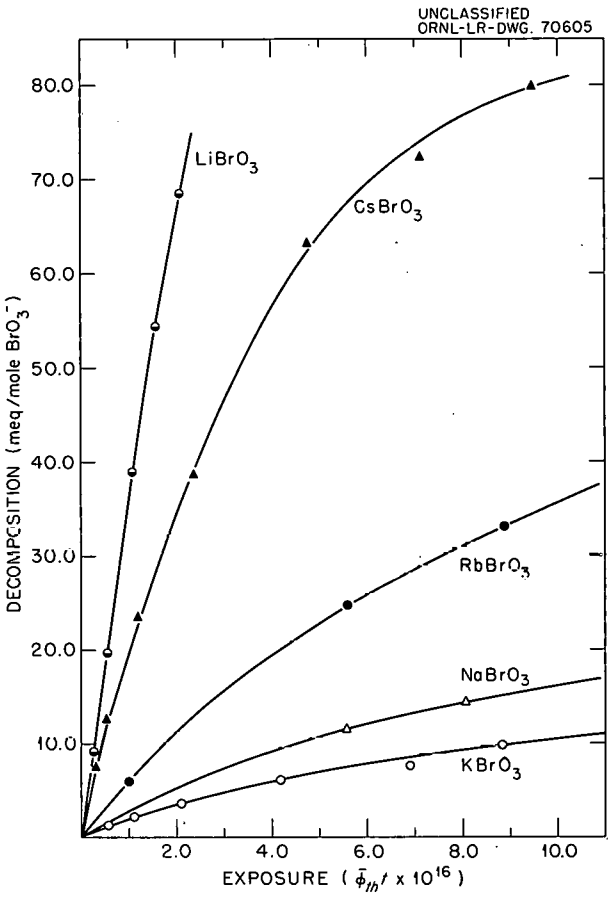

Fig. 4.9. Production of Oxidizing Fragments in the Decomposition of Alkali-Metal Bromates by Nuclear Reactor Radiations.

5. Organic Chemistry

Determination of Carbon-14 and Deuterium Isotope Effects by the Differential Method

V. F. Raaen T. K. Dunham[1]
C. J. Collins

The differential method[2] developed at this Laboratory for studying small isotope effects – particularly secondary effects of C^{14} and deuterium – was extended to include several isotope-position isomers of acetophenone, phenyl *t*-butyl ketone and propiophenone. The techniques employed were similar to those previously[2] described.

In determining the rate acceleration or deceleration caused by the substitution of deuterium for hydrogen, known mixtures of deuterated and undeuterated species were prepared, one of which was always labeled with C^{14}, and the rate of change of C^{14} content as a function of fraction of reaction was determined. The method requires that the isotope effects caused by the C^{14} itself be known, and these were determined in separate experiments. All reactants for study were purified on a preparative vapor-phase chromatograph.[3] The C^{14}-labeled materials were synthesized by standard methods.

The data for each run were fitted to Eq. (1) below by means of a nonlinear least-squares code.[4]

$$A = A_0 \frac{k^*}{k}(1 - f)^{[(k^*/k) - 1]}, \qquad (1)$$

where

A = molar radioactivity of each small sample at fraction f of reaction,
A_0 = molar radioactivity of reactant at $f = 0$,
k^*/k = ratio of specific rate constants for reaction of labeled and unlabeled molecules, respectively.

All experimental results, including those[2] reported before, are given in Table 5.1. In order to obtain the isotope effect values (k_D/k_H) due only to the substitution of deuterium for hydrogen, appropriate ratios from the third column of Table 5.1 were used. Thus, the isotope effect in the derivatization of trideuteroacetophenone can be calculated by two completely separate and independent methods, the results being identical within ±2 times the estimated error:

$$\frac{k_D}{k_H} = \frac{0.949 \pm 0.002}{0.847 \pm 0.003} = 1.119 \pm 0.005$$

(from runs 1 and 5, Table 5.1)

$$= \frac{1.0085 \pm 0.0004}{0.915 \pm 0.002} = 1.104 \pm 0.002$$

(from runs 2 and 6, Table 5.1).

[1] Undergraduate trainee from Austin College, summer 1961.

[2] *Chem. Div. Ann. Progr. Rept.* (*a*) for June 20, 1960, ORNL-2983, p 36, (*b*) for June 20, 1961, ORNL-3176, p 41; (*c*) V. F. Raaen, A. K. Tsiomis and C. J. Collins, *J. Am. Chem. Soc.* **82**, *5502 (1960).*

[3] A Burrell Kromo-Tog model K-1, fitted with a ½-in. column packed with Apiezon-L supported on Kromat F-13, was used.

[4] We are indebted to M. H. Lietzke of this Laboratory for writing the code for use with the IBM 7090 computer. Equation (1) is the exponential form of the equation derived by A. M. Downes, *Australian J. Sci. Research* **5A**, 521 (1952). See also C. J. Collins and M. H. Lietzke, *J. Am. Chem. Soc.* **81**, 5379 (1959). A least-squares fit to Downes' linear equation gave identical results with those reported in Table 4.1. The error (σ) in k^*/k was obtained as follows:

$$\sigma = \sqrt{\frac{\Sigma r^2}{n - 2} b_{11}}$$

where Σr^2 = sum of squares of the residuals of fit;
n = number of data points;
b_{11} = 1,1-element of the matrix $(X^T X)^{-1}$, where X = the matrix of the partial derivatives with respect to the parameters.

Table 5.1. Experimentally Determined Values of the Isotope Effect in Conversion of Ketones to Their 2,4-Dinitrophenylhydrazones

Run No.	Mixture	k^*/k (ref *a*)
1	PhC^*OCH_3 [b]	0.949 ±0.002
2	$PhCOC^*H_3$ [b,c]	1.0085 ±0.0004
3	PhC^*OCH_3 [b]	1.0038 ±0.0003
4	PhC^*OCD_3 [b]	0.941 ±0.001
5	PhC^*OCH_3:$PhCOCD_3$	0.847 ±0.003
6	$PhCOC^*H_3$:$PhCOCD_3$	0.915 ±0.002
7	$PhC^*OC(CH_3)_2CH_3$ [b]	0.951 ±0.001
8	$PhCO^*C(CH_3)_2CH_3$ [b]	1.0041 ±0.0007 [d] 1.0020 ±0.0009 [d] 1.0027 ±0.0005 [d]
9	$PhCOC(C^*H_3)(CD_3)_2$:$PhCOC(CH_3)_2CH_3$	1.046 ±0.0015
10	$PhC^*OCH_2CH_3$ [b]	0.943 ±0.002
11	$PhC^*OCD_2CH_3$ [b]	0.943 ±0.004
12	$PhC^*OCD_2CH_3$:$PhCOCH_2CH_3$	1.060 ±0.001
13	$PhCOCH_2C^*D_3$ [e]:$PhCOCH_2CH_3$	0.9952 ±0.0006

[a] Ratio of specific rate constants for C^{14}-labeled (k^*) and unlabeled (k) species. These values are corrected for the mole fraction of each species present. All reactions were carried out under conditions of proven irreversibility.

[b] Only C^{14}-labeled and unlabeled species present.

[c] Data of ref 2*c*.

[d] Significance doubtful.

[e] The insignificant contribution of the terminal C^{14} has been neglected.

The deuterium isotope effects (k_D/k_H) calculated from Table 5.1 are listed in Table 5.2. The data for runs 1, 5, 6, and 9 are plotted in Fig. 5.1, and the data for runs 3 and 13 are given in Fig. 5.2. These plots are typical and demonstrate the value of the differential method. Figure 5.2 illustrates that even the very small isotope effects reported in Table 5.1 can be significant and meaningful.

None of the conventional explanations[5-9] for previously observed secondary isotope effects will uniquely explain all the data. Therefore, further experiments are under way which, it is hoped, will help clarify the nature and origin of these small rate differences.

Nuclear Magnetic Resonance Studies: Conformation and the Deamination Reaction of *erythro*-2-Amino-1-phenylpropanol

B. M. Benjamin

It has been shown, through a series of investigations involving C^{14} labeling, resolutions, degradations and isotope dilution experiments, that the distribution of products of deamination of substituted ethanolamines is controlled by the conformations of the reacting molecules. For example, the model compound, (+)-*erythro*-1-amino-

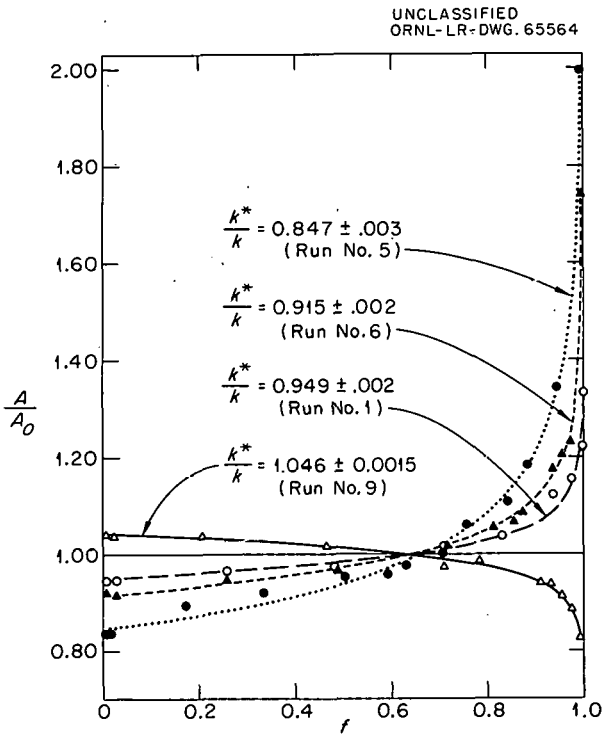

Fig. 5.1. Deuterium Isotope Effects for Runs 1, 5, 6, and 9.

[5] V. J. Shiner, *Tetrahedron* **5**, 243 (1959); V. J. Shiner *et al.*, *Ann. N. Y. Acad. Sci.* **84**, 583 (1960).

[6] E. S. Lewis, *Tetrahedron* **5**, 135 (1959).

[7] A. Streitwieser, Jr., *Ann. N. Y. Acad. Sci.* **84**, 576 (1960).

[8] E. A. Halevi *et al.*, *J. Chem. Soc.* 630 (1960); *ibid.*, 394, 1967, 1974 (1959); *Tetrahedron* **1**, 174 (1957).

[9] L. S. Bartell, *Tetrahedron Letters* **1960**, 13.

Table 5.2. Summary of k_D/k_H Isotope Effects in the Conversion of Ketones I–IV to Their 2,4-Dinitrophenylhydrazones

No.	Compound	k_D/k_H	Run No. from Table 5.1
1	$PhCOCD_3$	1.119 ±0.005	1, 5
2	$PhCOCD_3$	1.104 ±0.002	2, 6
3	$PhCOC(CH_3)(CD_3)_2$	1.046 ±0.0015	9
4	$PhCOCD_2CH_3$	1.124 ±0.005	10, 11, 12
5	$PhCOCH_2CD_3$	0.9952 ±0.0006	13

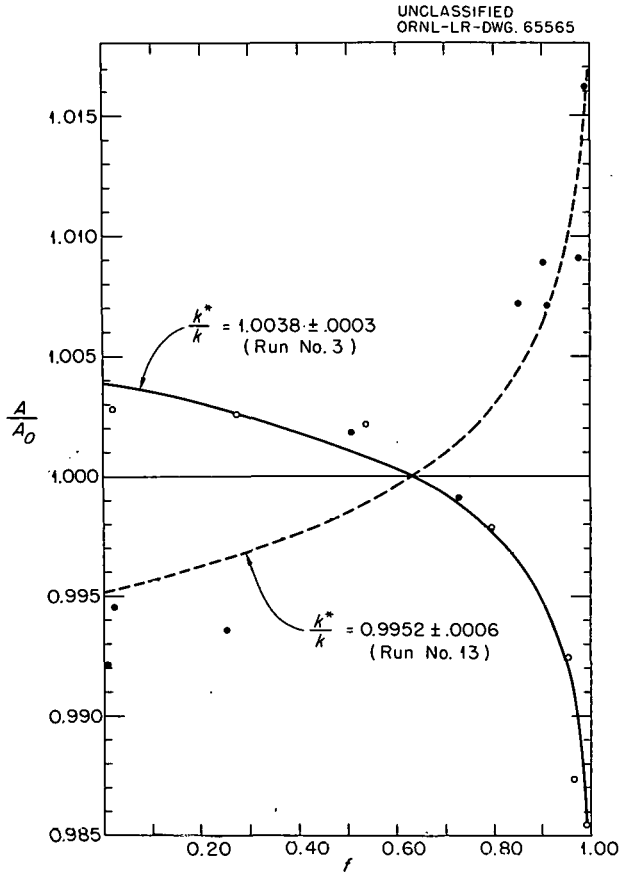

Fig. 5.2. Deuterium Isotope Effects for Runs 3 and 13.

1-phenyl-2-*p*-tolylpropanol-2, upon deamination, gave an 80% yield of ketonic product of which 75% had inverted and 25% had retained configuration. The data permit the approximate estimate of populations of rotational conformations, the preferred conformation (60 to 75%) having the large nonmigrating groups (phenyl and methyl) *trans*, and the hydroxyl and amino groups *gauche*, I:

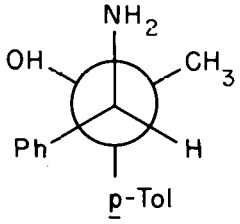

I

It is possible with certain compounds of the series to obtain an estimate of the conformational variety by analysis of their nuclear magnetic resonance (NMR) spectra.

The NMR spectrum[10] of *erythro*-2-amino-1-phenylpropanol hydrochloride (II) in deuterium oxide solution gave the following data: CH_3, doublet at 8.34 τ, J = 6.70 cps; N–C–H, eight components centered at 5.9 τ; O–C–H, doublet at 4.6 τ, J = 4.47 cps; rapidly exchanging $-NH_3^+$ and –OH at 4.9 τ; phenyl protons, one peak at 2.1 τ. The magnitude of the spin-spin coupling constant J between protons in $H-C_1-C_2-H$ systems is a function of the dihedral angle between the two C–H bonds, as shown theoretically and experimentally[11–13] for rigid cyclic molecules. The coupling constants for systems undergoing rotation is averaged over all conformations, and for systems in which rotation is restricted, J is a key to the equilibrium population of the rotational conformations.[14] The value of J for the two protons,

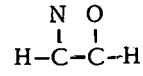

of II is 4.47 cps. Assuming from the data of Sheppard[12,15] for the *gauche* conformations II*a* and II*b* the coupling constant J = 1 to 3 cps, and for the *trans* conformation II, J_T = 11 to 13 cps, and, using the equation of Bothner-By,[14] $P_{IIc} = (J_{obs} - J_g)/(J_T - J_g)$, it was calculated that the population of conformation IIc was (25 ± 10)%:

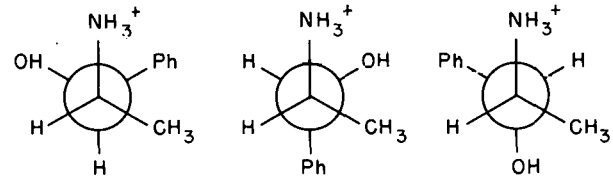

II*a* II*b* II*c*

[10]Kindly obtained by Varian Associates, Palo Alto, Calif., on an A-60 spectrometer.

[11]M. Karplus, *J. Chem. Phys.* **30**, 11 (1959).

[12]N. Sheppard and J. J. Turner, *Proc. Roy. Soc. (London)* **A252**, 506 (1959).

[13]H. Conroy, p 265 in *Advances in Organic Chemistry, Methods and Results*, Interscience, New York, 1960.

[14]A. A. Bothner-By and C. Naar-Colin, *J. Am. Chem. Soc.* **84**, 743 (1962) and references therein.

[15]C. N. Barnwell, N. Sheppard, and J. J. Turner, *Spectrochim. Acta* **16**, 794 (1960).

Since the large, medium, and small interactions are probably about the same for II*a* and II*b*, they should be present in equal quantities and should make equal contributions to the observed coupling constant.

Interpreting these results in terms of chemical behavior during the deamination reaction, the following results would be expected: the breaking of the carbon-nitrogen bond through nitrous acid deamination of molecules of II residing in conformation II*a* would result in hydrogen migration, and propiophenone would be formed. Conformation II*a* would afford hydratropic aldehyde through phenyl migration, whereas II*c* would give the ionic intermediate III, which would either undergo rotation through a 30° angle about the central carbon-carbon bond before phenyl migration or could give some glycolic material by interaction with solvent:

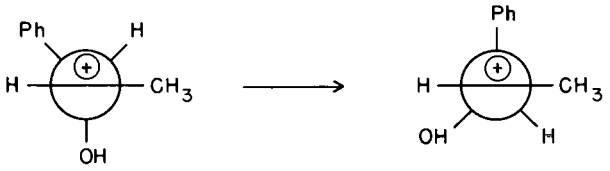

III IV

Thus, hydratropic aldehyde would be expected to be formed to the extent of about 62%, and if the starting amine II were resolved, the upper limit of aldehyde of inverted configuration would be about 74%.

Infrared analysis of the deamination product of II showed that the carbonyl fraction contained 56% of hydratropic aldehyde and that some glycolic material was present, thus confirming predictions from the NMR spectrum. The resolution of II has not yet been accomplished.

The Deamination Reaction: Rearrangement of (−)-*exo*-Norbornyl Amine

B. M. Benjamin C. J. Collins

In previous work on the deamination rearrangement[16] we demonstrated that no driving force for participation of the migrating group, *bridging*, occurred in 1,2-disubstituted ethanol amine systems. We have now used similar methods to investigate the deamination of a system, norbornyl amine, which has been reported[17] to rearrange through bridged ion intermediates and subsequently was used as the classic example of that mechanism. Accordingly, *endo*-5-norbornene-2-carboxylic acid was prepared by fractional crystallization of its cinchonidine salt, and it was resolved into the optically pure enantiomer, $[\alpha]_D^{25} = -144.5$.[18] This acid was converted to the methyl ester, which was then isomerized to a mixture of *exo*- and *endo*-stereoisomers by treating it with sodium methoxide in methanol. The resolved free *exo*-acid was recovered by separating a mixture of *endo*- and *exo*-iodolactone.[19] It was then catalytically reduced to *exo*-2-norbornanecarboxylic acid, $[\alpha]_D^{25} = -26.8$. Optically active *exo*-norbornyl amine (I) was obtained from the above saturated *exo*-acid by an adaptation of the Schmidt reaction. The rotation $[\alpha]_C^{25} = -18.1$ was the same in two separate preparations. Optical and chemical purities of the amine were demonstrated by the fact that it formed only one acetyl derivative, $[\alpha]_D^{25} = +12.3$.

Treatment of the optically pure amine in glacial acetic acid solution with sodium nitrite afforded, after appropriate workup of the reaction product, optically active *exo*-norbornyl acetate, $\alpha_D^{25} = 1.6210 \pm 0.0030$ (neat, 1 dm). Chemical purity of the acetate was established by its refractive index[20] ($N_D^{24} = 1.4562$) and infrared spectrum[20] and by the fact that it gave only one peak upon vapor-phase chromatography.

Since the maximum rotation of *exo*-norbornyl acetate is 12.65,[21] it follows that the deamination of (−)-*exo*-norbornyl amine produced *exo*-norbornyl acetate, which had retained 12.8% of its optical activity. Therefore the reaction took place with

[16] B. M. Benjamin, P. Wilder, Jr., and C. J. Collins, *J. Am. Chem. Soc.* **83**, 3654 (1961); B. M. Benjamin and C. J. Collins, *J. Am. Chem. Soc.* **83**, 3662 (1961); *Chem. Div. Ann. Progr. Rept. June 20, 1961*, ORNL-3176, p 42.

[17] J. D. Roberts, C. C. Lee, and W. H. Saunders, Jr., *J. Am. Chem. Soc.* **76**, 4501 (1954).

[18] J. A. Berson and D. A. Ben-Efraim, *J. Am. Chem. Soc.* **81**, 4094 (1959).

[19] C. D. Ver Nooy and C. S. Rondestvedt, *J. Am. Chem. Soc.* **77**, 3583 (1955).

[20] S. Winstein and D. Trifan, *J. Am. Chem. Soc.* **74**, 1147 (1952).

[21] J. A. Berson and S. Suzuki, *J. Am. Chem. Soc.* **81**, 4088 (1959).

43.6% inversion of configuration and 56.4% retention of configuration. This result is not compatible with the current hypothesis that the important intermediates in the rearrangement process are the norbornonium cation (II) and the nortricyclonium (III) cation because, when correctly drawn, these ions are seen to possess a plane of symmetry and thus would be expected to react equally at positions 1 and 2 in ion II or at positions 1 and 6 in ion III, thus producing a racemic product:

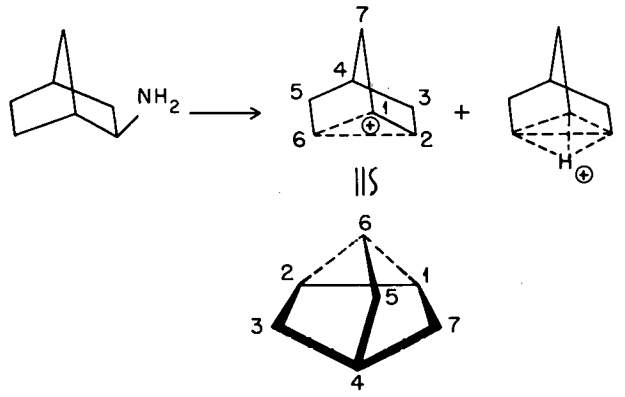

I II III

A more satisfactory interpretation of the mechanism is that deamination of I initially produces the classical carbonium ion IV, which reacts with solvent to give a product of retained configuration faster than it rearranges to ion V. Once formed, ion V can react with solvent to give inverted product or can be converted back to ion IV:

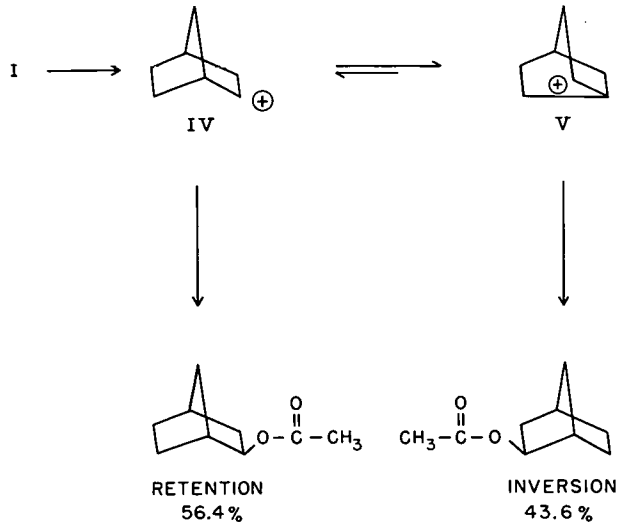

The *syn*- and *anti*-Isomers of *iso*-Butyrophenone-2,4-Dinitrophenylhydrazone

B. M. Benjamin A. C. Rutenberg

The problem of stereoisomerism about the C=N bond of ketone 2,4-dinitrophenylhydrazones was studied[22] by means of their proton nuclear magnetic resonance (NMR) spectra. The resulting data were interpreted in terms of restricted rotation about the C=N bond. Although individual *syn*- and *anti*-isomers were not available, assignments of nuclear magnetic resonance (NMR) signals to protons of a single isomer were made, based on certain assumptions. The 2,4-dinitrophenylhydrazone of methyl ethyl ketone is used as an example. This compound gives two resonance signals for each of the two different methyl groups and the methylene group, the larger signal of each pair being assigned to the *syn*-methyl isomer, which from steric considerations would be the favored configuration. Thus, the more intense α-methyl and β-methyl signals were shifted upfield, and the more intense α-methylene signal was shifted downfield. Therefore, it was reasoned that α-hydrogens *syn* to the anisotropic 2,4-dinitrophenyl group are shielded and that *syn* β-hydrogens are deshielded. Data obtained in this Laboratory does not confirm the generality of the above conclusions.

During work on the deuterium isotope effect problem,[23] it was found that between 0°C and room temperature *iso*-butyrophenone reacted with 2,4-dinitrophenyl hydrazine reagent[24] to give a yellow derivative, mp 162°C, and that at −5°C the same reactants gave an orange derivative, mp 152°. Three crystallizations from a chloroform-ethanol mixture did not change the melting points. An NMR study at 56.4 Mc of the two compounds dissolved in deuterochloroform revealed the following information. The yellow compound gave the expected spectrum for a pure individual stereoisomer of *iso*-butyrophenone-2,4-dinitrophenylhydrazone, whereas the spectrum of the orange compound was more striking. Pertinent signals

[22]G. J. Karabatsos, J. D. Graham, and F. M. Vane, *J. Am. Chem. Soc.* **84**, 753 (1962).

[23]V. F. Raaen, T. K. Dunham, and C. J. Collins, previous section of this report.

[24]R. L. Shriner and R. C. Fuson, p 171 in *Systematic Identification of Organic Compounds*, Wiley, New York, 1948.

for the yellow compound are the spin-coupled methyl doublet at 8.74 τ and the methene septet centered at 6.99 τ, the aromatic proton between the two nitro groups at 0.97 τ and the N–H proton at –0.97 τ. The orange compound gave two absorption regions with an intensity ratio of 2 to 1 for each of the above groups. The more intense signal of the pair had the same chemical shift as for the yellow compound, and each of the less intense signals was shifted downfield. The absorption spectrum of the other two protons on the nitro-substituted ring and the protons on the unsubstituted phenyl appeared unaffected under the available resolution. Therefore it seemed that the orange compound was actually a mixture of *syn*- and *anti*-isomers. Careful crystallization of the low-melting-point orange form afforded two kinds of crystals: yellow plates melting at 162°C and red prisms melting at 186–187.5°C. Furthermore, upon standing a month the chloroform solution of the orange compound turned yellow, and the downfield-shifted low-intensity signals disappeared. Chemical shifts (τ) and chemical-shift differences (δ) for the two stereoisomers are recorded in Table 5.3.

Table 5.3. Chemical Shifts of the *syn*- and *anti*-Isomers of Isobutyrophenone-2,4-dinitrophenyl Hydrazone in Deutero-Chloroform at 56.4 Mc

Group (1)	τ (ppm)		δ (ppm)
	Yellow Form	Red Form	
CH_3	8.74	8.56	0.18
CH	6.99	6.58	0.41
Ph–H	2.52	2.52	0
o–H	1.97	1.97	0
m_1–H	1.66	1.66	0
m_2–H	0.97	0.86	0.11
N–H	–0.97	–1.62	0.65

The present data do not allow assignment of configuration to either form. However, the chemical-shift difference for α and β hydrogens between the two different isomers is in the same direction. Equilibrium between the two isomeric forms due to restricted rotation about the C=N bond does not exist because one form is unstable and slowly isomerizes to the other. More data are presently being obtained from the pure, red stereoisomer and from other model compounds. The protons are defined by the following structural formula:

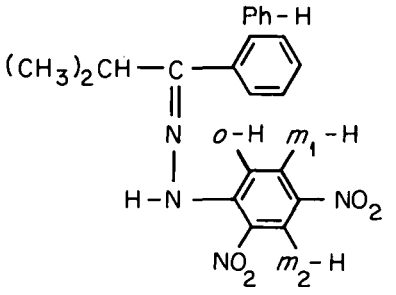

Thermally Induced Reactions of Tributyl Phosphate with Sodium Nitrate

W. H. Baldwin

Differential thermal analysis (DTA) techniques were used earlier for the qualitative study of the reaction between nitrates and tributyl phosphates.[25] Since that time it has been possible to study quantitative aspects of the reaction between tributyl phosphate (TBP) and solid sodium nitrate. The apparatus was calibrated by using the reported heats of fusion of lithium nitrate, sodium nitrate, and potassium nitrate. A significant advantage of the DTA method was found in the small quantity of reagents that are required, 50 to 100 mg of ester covered with 500 mg of (200-mesh) sodium nitrate. The temperature was raised uniformly (5°C/min) during the analysis.

The first observed reaction is an exothermic one that commences in the range of 210 to 230°C and reaches a maximum at 260°C. The heat of reaction was found to be 79 ± 5 cal per g of TBP (average of five runs).

The above reaction was quenched by the first endothermic reaction of sodium nitrate (maximum, 290°C), probably a phase change. After this the net effect was exothermic for a short time until it was quenched by the endothermic fusion of sodium nitrate.

[25] W. H. Baldwin, *Chem. Div. Ann. Progr. Rept. June 20, 1960*, ORNL-2983, p 43.

This complicated series of reactions may well be encountered in the process of waste calcination; however, significant differences exist between the above test and the conditions that obtain in the evaporation and calcination pot. Some of these differences are the escape of volatile reaction products under the above conditions of testing, visible amounts of charring that were not quantitatively estimated, and the flotation of the residue on the molten sodium nitrate that was thus carried outside the area of detection by the thermocouple.

Organic Thiophosphorus Compounds as Ligands

W. H. Baldwin C. E. Higgins

Handley and Dean[26] showed recently that neutral thiono phosphate esters are useful solvents for the extraction of silver and mercuric salts from aqueous solution. Subsequently, we prepared analogs of these thiono phosphate esters and tested certain relationships between structure and distribution coefficients. In the series of thiono phosphorus compounds, as in the series of analogous phosphoryl compounds (see Higgins, Baldwin, and Ruth[27] and Burger[28]), higher distribution coefficients were observed with electron-releasing groups attached to the phosphorus atom (see Tables 5.4 and 5.5).

Several solid adducts were isolated in pure form (see Table 5.6). The 1:1 adduct between tributyl phosphine sulfide and silver nitrate is associated in benzene solution, while the corresponding adduct with mercuric iodide is not associated. When tributyl phosphine sulfide (2 moles) was added to silver nitrate (1 mole) and when triphenyl phosphine sulfide was mixed with silver nitrate in a 1:1 ratio, viscous liquids were obtained that did not crystallize.

The strong interaction between neutral organic thiophosphorus compounds and salts of such metals as Ag(I) and Hg(II) permit the isolation of solid adducts and their use in solvent extraction. We have now extended this investigation to include the sulfur analogs of dibutyl phosphoric acid: dibutyl dithio phosphoric acid, $(BuO)_2PSSH$, and dibutyl thiophosphoric acid, $(BuO)_2PHOS$. Handley surveyed[29] the distribution of many elements between water and dialkyl dithiophosphoric acid. We are reporting a comparison of the properties of the three acids in the extraction of silver from aqueous silver nitrate, and the melting points and molecular weights of the complexes.

The selective action of the sulfur-containing acids on silver is evident from the data in Table 5.7. The oxygen acid $(BuO)_2POOH$ extracts very little silver from water; the distribution coefficient $E_a^o = 0.02$. However, with dibutyl thiophosphoric

[26] T. H. Handley and J. A. Dean, *Anal. Chem.* **32**, 1878 (1960).

[27] C. E. Higgins, W. H. Baldwin, and J. M. Ruth, ORNL-1338, (July 24, 1952) (declassified July 31, 1957).

[28] L. L. Burger, *J. Phys. Chem.* **62**, 590 (1958).

[29] T. H. Handley, private communication.

Table 5.4. Distribution of Silver Nitrate Between Organic and Aqueous Layers

Aqueous feed: 0.01 *M* $AgNO_3$, 4 μc Ag^{110}/millimole
Organic feed: 0.1 *M* compound in benzene

Extractant	Ag^+ in Organic Phase at Equilibrium (*M*/liter × 10^3)	Distribution Coefficient, E_a^o
$(C_4H_9)_3PS$	10	190
$(C_6H_5)_3PS$	2.6	0.35
$(C_4H_9O)_3PS$	0.14	0.014
$(C_6H_5O)_3PS$	0.01	0.001
$(C_4H_9)_3PO$	0.01	0.001

Table 5.5. Distribution of $Hg(NO_3)_2$ Between Aqueous and Organic Layers

Aqueous feed: 2 *M* HNO_3, 0.01 *M* $Hg(NO_3)_2$, 8 μc Hg^{203}/millimole

Organic feed: 0.1 *M* compound in benzene

Compound	Hg^{II} in Organic Phase at Equilibrium (*M*/liter × 10^3)	Distribution Coefficient, E_a^o
$(C_4H_9)_3PS$	3.8	Precipitation
$(C_4H_9O)_3PS$	4.7	0.9
$(C_6H_5O)_3PS$	0.02	0.002

Table 5.6. Analytical Data for Adducts Prepared

Adduct	Melting Point (°C)	Analytical Results			
		Percentage of Silver		Molecular Weight of Adduct	
		Found	Calculated	Found	Calculated
$Bu_3PS \cdot AgNO_3$	138–138.5	27.0[a] 26.9[c]	26.7	2800[b]	404
$Bu_3PS \cdot HgI_2$	75–75.5			695	698
$2\phi PS \cdot AgNO_3$	157	14.7[c]	14.2		

[a]Ionic analysis.
[b]Cryoscopically in benzene, 3% solution.
[c]Radiometric analysis.

acid a high distribution coefficient (1000) was observed. Dibutyl dithiophosphoric acid forms a benzene-soluble silver complex, but in the test reported in Table 5.7 with no supporting electrolyte in the aqueous phase, the separation of an insoluble phase limited the amount of silver in the benzene to 24% of the total.

The complex nature of the systems is reflected in the molecular weights recorded in Table 5.8. The acids $(BuO)_2POOH$ and $(BuO)_2PSOH$ are associated in benzene, presumably by hydrogen bonding through the oxygen atoms. The silver complex of $(BuO)_2PSSH$ was more highly associated than the complex of $(BuO)_2PSOH$. Here, the coordination bonding may be between silver and the sulfur atoms on the phosphorus.

Table 5.7. Distribution of Silver Between Water and Benzene Solutions of Organic Phosphorus Acids

Aqueous feed: 0.01 *M* $AgNO_4$, 2 μc Ag^{110}/millimole
Organic feed: 0.10 *M* acid in benzene

Acid	Distribution Coefficient, E_a^o
$(BuO)_2POOH$	0.02
$(BuO)_2PSOH$	1000
$(BuO)_2PSSH$	Precipitation (24% Ag^{110} in benzene phase)

Table 5.8. Analytical Results for Acids and Their Silver Complexes

	$(BuO)_2POOH$	$(BuO)_2PSOH$	$(BuO)_2PSSH$
Acid			
Molecular Weight[a]			
Found	421	382	224
Calculated	210	226	242
Silver Complex			
Melting Point, °C	196–207	119–124	167–168
Molecular Weight[a]			
Found		701	1360
Calculated		333	349

[a]Cryoscopically in benzene, 3% solution.

6. Chemistry of Aqueous Systems

The Solubility of Silver Sulfate in KNO_3-K_2SO_4, K_2SO_4-$MgSO_4$, and K_2SO_4-H_2SO_4 Mixtures

M. H. Lietzke R. W. Stoughton

In a series of papers[1] the solubility of Ag_2SO_4 in a variety of electrolyte solutions was investigated. It was shown that single-parameter semi-empirical expressions of the type

$$\ln S - \ln 4s_0^3 + \delta_T \left[\frac{\sqrt{I}}{1 + A\sqrt{I}} - \frac{\sqrt{I_0}}{1 + A\sqrt{I_0}} \right] \quad (1)$$

could be used to describe the variation of the solubility product of Ag_2SO_4 over a wide range of temperature and ionic strength. In Eq. (1) s_0 is the solubility of Ag_2SO_4 in pure water, δ_T is the appropriate Debye-Hückel slope, I the ionic strength of the solution, and A the adjustable parameter. In all cases best agreement between calculated and observed solubilities was obtained when each single parameter A, was assumed to be temperature independent and to be either ionic-strength independent or to decrease slowly with increasing ionic strength. The justification for using Eq. (1) without a linear term has been discussed previously.[1]

In the present work the treatment of the solubility of Ag_2SO_4 in single electrolyte systems was extended to the solubility in three electrolyte mixtures: (1) KNO_3-K_2SO_4, (2) K_2SO_4-$MgSO_4$, and (3) K_2SO_4-H_2SO_4. In each of the three systems the total ionic strength of the solubility medium was held constant at two different values, while the ratio of the two components was varied. Weight concentrations were used in reporting the data, and the Debye-Hückel limiting slope at any temperature was made density dependent by multiplying its value on the molal scale by the square root of the density of water at that temperature.

Experimental. – All solubility measurements were performed with the same techniques described previously[2] and were carried out in the temperature range 90 to 175°C.

Results and Discussion. – The values for the solubility of Ag_2SO_4 in each system as a function of temperature were fitted by the method of least squares to an equation

$$s = a_0 + a_1 t + a_2 t^2 . \quad (2)$$

The resulting equations were solved at 25°C intervals from 25 to 200 in the case of the KNO_3-K_2SO_4 system ($I_{KNO_3} + I_{K_2SO_4} = 1.0$), where data were obtained over the entire temperature range, and from 100 to 175°C in the other systems. The coefficients and the standard error of fit for Eq. (2) describing the solubility of Ag_2SO_4 in each system as a function of temperature are given in Table 6.1, while a typical set of solubility curves for one of the systems ($I_{KNO_3} + I_{K_2SO_4} = 1.0$) is shown in Fig. 6.1. The other families of curves were similar.

Since in previous work[1] it was demonstrated that temperature-independent values of the parameter A in Eq. (1) could be calculated such that the difference between observed and calculated solubilities be minimized for systems in which Ag_2SO_4 was dissolved in solutions of a simple electrolyte, it seemed of interest in the present work to calculate values of A for the mixtures studied to determine whether a simple combining relationship existed between the values of A in the simple systems and in the mixtures. In

[1] M. H. Lietzke and R. W. Stoughton, *J. Phys. Chem.* **63**, 1183, 1186, 1188, 1190, 1984 (1959); **64**, 133, 816 (1960).

[2] M. H. Lietzke and R. W. Stoughton, *J. Am. Chem. Soc.* **78**, 3023 (1956).

Table 6.1. Coefficients of Equation (2) for the Solubility of Ag_2SO_4 in the Electrolyte Mixtures Studied

I of the mixture	m_{KNO_3}	$m_{K_2SO_4}$	$a_0 \times 10^2$	$a_1 \times 10^4$	$a_2 \times 10^6$	σ_{fit}[a] $\times 10^3$
1.0	1.0	0	4.31016	6.41420	−1.57687	2.12
	0.7	0.1	3.47859	3.57152	−0.532662	1.37
	0.5	0.16	2.88124	3.12836	−0.284457	2.57
	0.28	0.24	1.90299	4.43650	−0.701309	1.00
	0	0.333	1.41304	5.47167	−0.875239	0.16
1.416	1.416	0	5.84143	4.86857	−0.697144	0.48
	0.3484	0.3564	−0.202929	7.32640	−1.45714	1.86
	0	0.472	1.59375	5.67500	−0.473332	0.22
	$m_{K_2SO_4}$	m_{MgSO_4}				
1.0	0.333	0	1.41304	5.47167	−0.875239	0.16
	0.25	0.0625	0.642984	5.86084	−1.32865	0.92
	0.167	0.125	0.00169903	6.99906	−1.86183	0.43
	0.0833	0.1875	1.42525	4.68734	−1.06849	1.09
	0	0.25	1.27142	5.00573	−1.24572	0.27
1.437	0.479	0	1.58357	5.71667	−0.470478	0.15
	0.2395	0.1796	−1.26804	7.94620	−1.49270	2.20
	0	0.3592	1.22750	5.38381	−1.16191	0.30
	$m_{H_2SO_4}$[b]	$m_{K_2SO_4}$[b]				
1.007	0.2507	0.2500	−0.883321	9.58466	−2.63613	1.39
2.000	0.5000	0.5000	−3.26708	13.0980	−3.06707	0.68

[a] Standard error of fit.

[b] Formal molality based on considering H_2SO_4 as a 1:1 electrolyte.

carrying out the calculations for the KNO_3-K_2SO_4 and K_2SO_4-$MgSO_4$ mixtures, values of ln S and $\sqrt{I}$ in Eq. (1) were computed at 25°C intervals for each system, using the smoothed values of the solubility of Ag_2SO_4 as obtained from Eq. (2) and the appropriate molalities of the components of the mixture. Then the value of A was determined in each case between 100 and 175°C by selecting the value which equated the right and left sides of Eq. (1). The A parameters so obtained for each system are given in Table 6.2. The values shown are the mean values calculated between 100 and 175°C.

Additional calculations were performed in which a linear term was added to Eq. (1), namely, BI. In these calculations A was set equal either to 1.0 or 1.5 and the value of B determined such that the right side of Eq. (1) augmented by the linear term was equal to the left side. The values of B so obtained showed a much greater dependence on temperature than did the values of A obtained without the linear term. Since the latter calculation (involving the BI term) offered no advantage over the former, no attempt was made to correlate the B values with temperature and ionic strength fractions.

The observed solubility of Ag_2SO_4 in each system as a function of temperature was compared with values calculated using the average A values given in Table 6.2. In all cases the agreement

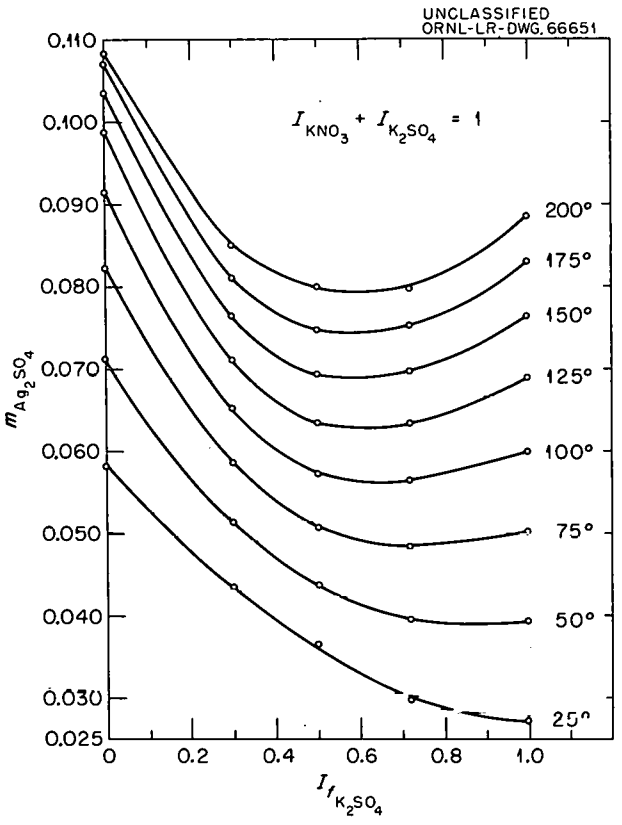

Fig. 6.1. The Solubility of Ag_2SO_4 in KNO_3-K_2SO_4 Mixtures Where $I_{KNO_3} + I_{K_2SO_4} = 1.0$.

was very good — within a few tenths of a percent in most cases and within 2% in the remainder. Hence the behavior of the A values in the electrolyte mixtures was very similar to the behavior of the A values in the individual components.

In the case of the solubility of Ag_2SO_4 in K_2SO_4-H_2SO_4 mixtures, the calculations were performed essentially as described previously[1] for the solubility of Ag_2SO_4 in H_2SO_4 solutions except that the ionic strength term included the concentration of K_2SO_4. The denominator parameter in the term correcting the bisulfate acid constant for the ionic strength of the solution was taken as 0.4, consistent with previous calculations.[1] At all temperatures from 100 to 175°C the observed and calculated solubilities of Ag_2SO_4 agreed to within 1%, with a mean A value for $I = 1.0$ of 0.922 and for $I = 2.0$ of 0.832.

An attempt was made to relate the A values shown in Table 6.2 for each system. In no system was it possible to relate the A value calculated for a mixture with the A values calculated for the corresponding pure systems by taking a linear combination of the latter values weighted according to the ionic strength fractions f_i of the appropriate electrolytes; that is,

$$A_{\text{mixture}} = A_1 f_1 + A_2 f_2 \qquad (3)$$

did not hold. However, in the KNO_3-K_2SO_4 systems ($I = 1.0$) the relationship

$$A_{\text{mixture}} = A_1 f_1 + A_2 f_2 + A_1^2 A_2^2 f_1 f_2 \qquad (4)$$

held very well. In the remaining systems the A value for the mixture lay between values computed from the A values of the simple systems by Eqs. (3) and (4).

Since a simple general combining relationship based on the A values could not be found, it seemed of interest to try a direct correlation of the solubility of Ag_2SO_4 in the electrolyte mixtures with the solubilities in the pure component solutions using Eq. (5):

$$s_M = s_1 f_1 + s_2 f_2 + s_{12} f_1 f_2 . \qquad (5)$$

However, the coefficient s_{12} was not constant but varied quadratically with either f_1 or f_2 and quadratically with temperature. Thus a direct correlation of the solubilities is neither simpler nor more complicated than a correlation through an activity coefficient function.

A Mathematical Model for the Solvent Extraction of Uranyl Nitrate and Nitric Acid

M. H. Lietzke R. W. Stoughton

A series of computer programs is being written in an attempt to calculate distribution ratios in successively more complicated solvent extraction equilibria. The general procedure involves setting up equilibrium expressions and determining the parameters by a generalized least-squares technique. The present report describes calculations on the distribution of $UO_2(NO_3)_2$ and HNO_3 between an aqueous phase and an organic phase consisting of tributyl phosphate (TBP) dissolved in an inert diluent (Amsco 125-90W). Since it is desired to keep the model simple, the assumed equilibria do not necessarily involve all species which may have been shown to exist in the solutions in question.

Table 6.2. *A* Parameters for Equation (1)

Total I	m_{KNO_3}	$m_{K_2SO_4}$	A	Standard Deviation from the Mean
1.0	1.0	0	0.991	0.004
	0.7	0.1	0.994	0.018
	0.5	0.16	0.956	0.030
	0.28	0.24	0.815	0.014
	0	0.333	0.656	0.002
1.416	1.416	0	0.997	0.012
	0.3484	0.3564	0.811	0.021
	0	0.472	0.630	0.000
	$m_{K_2SO_4}$	m_{MgSO_4}		
1.0	0.333	0	0.656	0.002
	0.25	0.0625	0.794	0.006
	0.167	0.125	0.834	0.006
	0.0833	0.1875	0.892	0.003
	0	0.25	0.940	0.006
1.437	0.479	0	0.634	0.000
	0.2395	0.1796	0.815	0.043
	0	0.3592	0.885	0.004
	$m_{K_2SO_4}$	$m_{H_2SO_4}$ [a]		
1.007	0.2500	0.2507	0.922	0.036
2.000	0.5000	0.5000	0.832	0.013

[a] Formal molality based on considering H_2SO_4 as a 1:1 electrolyte.

The $UO_2(NO_3)_2$-NH_4NO_3 System. – In considering the equilibration of the aqueous $UO_2(NO_3)_2$-NH_4NO_3 system with TBP-diluent the following equilibrium was assumed:

$$UO_2^{2+}_{aq} + 2NO_3^-_{aq} + 2TBP_{org} = UO_2(NO_3)_2 \cdot 2TBP_{org}\, Q_D \; ; \quad (1)$$

in this equation,

$$Q_D = \frac{[UO_2(NO_3)_2 \cdot 2TBP]_{org}}{[UO_2^{2+}]_{aq}[NO_3^-]^2_{aq}[TBP]^2_{org}} , \quad (2)$$

where

$[NO_3^-] = 2[UO_2^{2+}] + m_s$,

m_s = molarity of NH_4NO_3 ,

$[TBP] = T_0 - 2[UO_2(NO_3)_2 \cdot 2TBP]$,

T_0 = initial molarity of TBP .

The equation for conservation of total uranium with equal volumes in the two phases is

$$[UO_2^{2+}]_{aq} + [UO_2(NO_3)_2 \cdot 2TBP]_{org} = UTOT , \quad (3)$$

where UTOT is the sum of the initial concentrations in both phases. Hence Eqs. (2) and (3)

represent two equations in the two unknowns $[UO_2^{2+}]$ and $[UO_2(NO_3)_2 \cdot 2TBP]$ which may be solved for any particular value of Q_D. It was assumed that the ionic strength dependence of the logarithm of the distribution quotient can be expressed by

$$\ln Q_D = \ln K_D - \frac{6\mathring{A}\sqrt{I}}{1 + A\sqrt{I}} + BI , \qquad (4)$$

where K_D is the distribution constant, $\mathring{A}$ is the Debye-Hückel limiting slope for a singly charged ion, A and B are adjustable parameters, and I is the ionic strength of the solution, given by

$$I = m_s + 3[UO_2^{2+}] . \qquad (5)$$

Equation (4) was used without the Debye-Hückel term in all cases where a salting agent was present and the ionic strength was fairly high, and without the linear term in the absence of a salting agent. This procedure is consistent with theory since the Debye-Hückel (DH) term varies considerably with ionic strength at low electrolyte concentrations, where the linear term is relatively unimportant; at high values of ionic strength the linear term becomes much more important, while the DH term approaches a limiting value of $-6\mathring{A}/A$. Since it was desired to use a minimum number of parameters, only one of the two terms mentioned was allowed to have an adjustable value; hence Eq. (4) will be written in two alternative forms:

$$\ln Q_D = \ln K_D - \frac{6\mathring{A}\sqrt{I}}{1 + A\sqrt{I}} , \qquad (4a)$$

$$\ln Q_D = \ln K_D' + BI , \qquad (4b)$$

where $\ln K_D'$ may be considered to be approximately equal to the high concentration limit of Eq. (4a), that is, $\ln K_D' \cong \ln K_D - 6\mathring{A}/A$. Thus the overall problem involved the evaluation of $\ln K_D$ and A or $\ln K_D'$ and B by a nonlinear least-squares procedure, subject to the restrictions represented by Eqs. (2), (3), and (5).

The criterion adopted in solving the above set of equations was that

$$\sum_i (D_{obs} - D_{calc})_i^2$$

be a minimum, where the distribution coefficient D is defined as the ratio

$$[UO_2(NO_3)_2 \cdot 2TBP]_{org} / [UO_2^{2+}]_{aq}$$

and the summation is taken over all the data points. Accordingly a series expansion of D was made in terms of the partial derivatives with respect to the adjustable parameters, either K_D and A or K_D' and B, as

$$D_{obs} = D_{calc} + \frac{\partial D}{\partial \ln K_D} \Delta \ln K_D + \frac{\partial D}{\partial A} \Delta A , \qquad (6a)$$

$$D_{obs} = D_{calc} + \frac{\partial D}{\partial \ln K_D'} \Delta \ln K_D' + \frac{\partial D}{\partial B} \Delta B , \qquad (6b)$$

in which D_{calc} and the partial derivatives are computed for approximate values of the parameters. The increments $\Delta \ln K_D$ and ΔA or $\Delta \ln K_D'$ and ΔB then give approximate corrections to these parameters.

Calculations were performed on two different sets of data; the first set was taken from IDO-14501.[3] In Table 6.3 are shown the observed and calculated distribution ratios for $UO_2(NO_3)_2$ between aqueous NH_4NO_3 and TBP-diluent phases as well as the $\ln K_D'$ and linear term B as a function of TBP concentration.

Calculations were also performed on a set of data that included much higher concentrations of $UO_2(NO_3)_2$.[4] In Fig. 6.2 are shown the observed and calculated concentrations of uranium in the organic and aqueous phases for the extraction of $UO_2(NO_3)_2$ with 5.39% TBP in Amsco as a function of NH_4NO_3 concentration. The results for 10.3 and 20.1% TBP were equally good.

The values of $\ln K_D'$ computed by the method outlined above varied slightly with the concentration of salting agent, the concentration of uranium, and the concentration of TBP used. Hence all the individual values were grouped together and used to determine the coefficients of Eq. (7) by the method of least squares:

$$\ln K_D' = \ln K^0 + B_1 I_{NH_4NO_3} + B_2 I_{UO_2(NO_3)_{2(aq)}} + B_3 (\text{vol \% TBP}) . \qquad (7)$$

The coefficients of Eq. (7) describing the two sets of data are given in Table 6.4.

---

[3] R. A. Kent and K. L. Rohde, IDO-14501, Table 3 (July 1960).

[4] *Chem. Technol. Div., Chem. Develop. Sec B, Quarterly Progress Report, Oct.–Dec. 1961*, TM-177.

Table 6.3. Observed and Calculated Distribution Ratios D (Organic/Aqueous) for $UO_2(NO_3)_2$ Between Aqueous NH_4NO_3 and TBP-Diluent Phases

Vol % TBP	M NH_4NO_3	Initial M $UO_2(NO_3)_2$	$D(o/a)_{obs}$	$D(o/a)_{calc}$
		$\ln K_D' = 2.17$ $B = 0.111$		
5	0.68	0.0098	0.18	0.13
	1.37	0.0102	0.68	0.53
	2.00	0.0112	1.22	1.13
	2.74	0.0109	2.17	2.20
	3.42	0.0111	3.50	3.58
	4.70	0.0158	6.83	6.80
		$\ln K_D' = 2.22$ $B = 0.115$		
10	0.68	0.0107	0.68	0.54
	1.37	0.0102	1.98	2.21
	1.97	0.0270	4.85	4.08
	2.00	0.0099	4.88	4.97
	2.74	0.0106	9.54	9.96
	3.42	0.0108	16.2	16.6
	3.42	0.0114	17.1	16.5
		$\ln K_D' = 2.30$ $B = 0.0964$		
20	0.68	0.0101	2.58	2.27
	1.37	0.0141	12.95	9.38
	2.00	0.0134	28.1	21.2
	2.74	0.0105	44.7	43.3
	3.42	0.0094	60.8	72.5
	3.94	0.0273	97.4	90.7

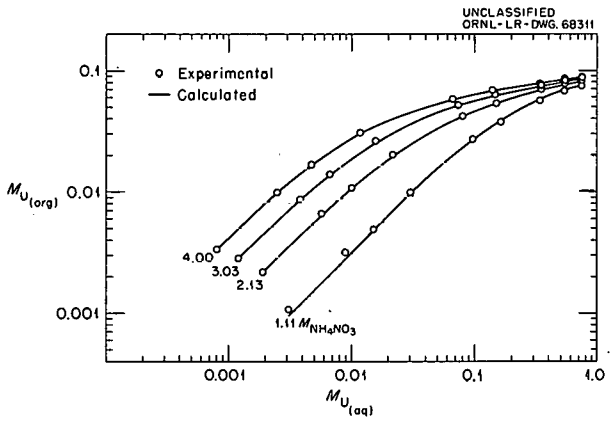

Fig. 6.2. Observed and Calculated Concentrations of Uranium in the Organic and Aqueous Phases for the Extraction of $UO_2(NO_3)_2$ with 5.39% TBP in Amsco.

Table 6.4. Coefficients of Equation (7)

	IDO Data[a]	ORNL Data[b]
$\ln K^0$	2.14	2.57
B_1	0.110	−0.116
B_2	−0.174	0.468
B_3	0.0083	−0.0440

[a] See ref 3.
[b] See ref 4.

The calculations so far described involved the use of a salting agent. In all cases the ionic strength of the aqueous phase was high, and no DH activity-coefficient term was used. However, the calculations converged equally well at lower concentrations of uranium in the absence of a salting agent and with a DH activity-coefficient term. In this case the parameters of the fit were ln K_D and A (as defined above), and the linear term was not used. In Table 6.5 is shown a comparison of D_{obs} (ref 5) and D_{calc} for the distribution of uranium between TBP-Amsco in the absence of a salting agent. The best agreement between observed and calculated distribution coefficients was obtained with A taken as 2.0 at both 5 and 10% TBP in Amsco. Also, if the limiting value for the DH term (−3.5) is added to ln K_D (about 5.55), a value of about 2.05 is obtained for ln K_D', which compares favorably with the values shown in Table 6.3.

The HNO_3 System. – In considering the equilibration of aqueous HNO_3 with TBP diluent the following equilibrium was assumed:

$$H^+_{aq} + NO_3^-{}_{aq} + TBP_{org} = HNO_3 \cdot TBP_{org} \; Q_{DN} \; ; \quad (8)$$

in this equation,

$$Q_{DN} = \frac{[HNO_3 \cdot TBP]_{org}}{[H^+]_{aq}\,[NO_3^-]_{aq}\,[TBP]_{org}} , \quad (9)$$

where

$$[H^+] = [NO_3^-] ,$$

$$[TBP] = T_0 - [HNO_3 \cdot TBP] ,$$

T_0 = initial molarity of TBP .

The equation for conservation of HNO_3 (on the assumption of equal volumes in the two phases) is

$$[H^+] + [HNO_3 \cdot TBP] = HNO , \quad (10)$$

where HNO is the sum of the original concentrations in both phases. Thus Eqs. (9) and (10) represent two equations in the two unknowns $[H^+]$ and $[HNO_3 \cdot TBP]$, which may be solved for any particular value of Q_{DN}. Again it was assumed that the ionic strength dependence of the logarithm of the distribution quotient can be expressed by

$$\ln Q_{DN} = \ln K_{DN} - \frac{2\delta\sqrt{I}}{1 + A\sqrt{I}} , \quad (11)$$

where K_{DN} is the distribution constant, δ and A have the same significance as before, and the

[5] *Chem. Technol. Div., Chem. Develop. Sec B, Monthly Progress Report, June–July 1960,* ORNL CF-60-7-76.

Table 6.5. Distribution of Uranium between TBP-Amsco and Water in the Absence of a Salting Agent

Vol % TBP	Concentration of Uranium feed (M)	A	D_{obs} [a]	D_{calc}	ln K_D
5	0.0417	2.0	0.012	0.012	5.5731
	0.0837		0.029	0.033	
	0.2058		0.089	0.087	
	0.2376		0.10	0.095	
10	0.0412	2.0	0.033	0.043	5.5292
	0.0824		0.091	0.11	
	0.1172		0.15	0.16	
	0.1566		0.20	0.20	
	0.2021		0.24	0.24	
	0.2381		0.26	0.26	
	0.2978		0.29	0.28	
	0.3475		0.31	0.28	

[a] See ref 5.

ionic strength of the aqueous solution is given by $[H^+]$. The DH term should correct for the variation in activity coefficient of the HNO_3 in the aqueous phase.

The calculation itself was carried out as described previously for the $UO_2(NO_3)_2$ system, and the results are summarized in Table 6.6. The value of 2.0 for the *A* parameter at the lower TBP concentrations does indeed correct (to a reasonably good approximation) for the variation in activity coefficient of the aqueous HNO_3 to nearly 1.0 *M*, as can be verified by comparing values of

Table 6.6. Distribution of HNO_3 Between TBP-Amsco and Water

Vol % TBP	HNO_3 Concentration (*M*)	*A*	D_{obs}	D_{calc}	ln K_{DN}	ln K_{DN} (ref a)
5	0.1991	2.0	0.0054	0.0055	−1.2682	−1.330
	0.4084		0.0085	0.0099		
	0.5989		0.0134	0.0134		
	0.8062		0.0167	0.0167		
	1.0035		0.0209	0.0194		
10	0.1990	2.0	0.0152	0.0151	−0.9322	−1.023
	0.4088		0.0271	0.0271		
	0.6004		0.0352	0.0362		
	0.8070		0.0426	0.0445		
	1.0042		0.0482	0.0510		
15	0.1001	1.0	0.0214	0.0184	−0.4464	−0.646
	0.1997		0.0291	0.0308		
	0.4090		0.0486	0.0502		
	0.6073		0.0654	0.0638		
	0.8216		0.0754	0.0750		
	1.0163		0.0812	0.0829		
30	0.4041	1.0	0.126	0.128	−0.1344	−0.342
	0.6042		0.169	0.161		
	0.8110		0.184	0.187		
	1.0140		0.203	0.205		
65	0.1004	0.8	0.131	0.133	0.1715	0.051
	0.2071		0.206	0.215		
	0.4135		0.332	0.320		
	0.5670		0.414	0.376		
	0.8005		0.459	0.439		
	0.9845		0.459	0.476		
	1.5305		0.502	0.543		
100	0.1002	0.5	0.253	0.261	0.5396	0.405
	0.2045		0.401	0.399		
	0.4080		0.588	0.566		
	0.6050		0.681	0.670		
	0.8160		0.786	0.748		
	1.0180		0.824	0.802		
	1.5480		0.850	0.884		
	1.9840		0.854	0.910		

[a] W. Davis, Jr., private communication.

the above term with those of known activity coefficients. At higher concentrations of TBP, however, the best agreement between observed and calculated distribution coefficients was obtained with smaller values of the A parameter. Since the A parameter as used should correct for ionic strength effects in the aqueous phase only, there is no obvious reason why it should vary with the percentage of TBP. If one considers the DH term merely as an empirical expression, it evidently does correct for effects in the nonaqueous phase as well. The values of ln K_{DH} do not vary linearly with TBP concentration throughout the entire range, but appear to be quadratic, at least at the higher percentages of TBP. However, if only the three lowest TBP concentrations are considered, then one can compute a linear coefficient, such as B_3 in Eq. (7), with a value of about 0.08.

Davis[6] treated the same HNO_3 data by correcting with literature values for the aqueous HNO_3 activity coefficients, assuming that the logarithm of the ratio of the activity coefficients of $HNO_3 \cdot TBP_{org}$ to TBP_{org} was a linear function of the concentration of HNO_3 in the organic phase and evaluating ln K_{DN} by extrapolating to zero HNO_3 concentration in that phase. His values are given in the last column of Table 6.6.

Distribution of Uranium Between HNO_3 Solutions and TBP-Amsco. – In describing the solvent extraction of uranium from HNO_3 solutions it is necessary to consider simultaneously the equilibrium quotients given by Eqs. (2) and (9) and observe that

$$[NO_3^-] = m_s + 2[UO_2^{2+}] + [H^+] ,$$

and

$$[TBP] = T_0 - 2[U\emptyset] - [HN\emptyset] ,$$

where

$U\emptyset$ = molarity of uranium in the organic phase,

$HN\emptyset$ = molarity of HNO_3 in the organic phase.

In these equations m_s and T_0 have the same significance as before. In addition to the two equilibrium quotients, Eq. (3) for conservation of total uranium and Eq. (10) for the conservation of HNO_3 are needed to permit the evaluation of the unknowns $[H^+]$, $[UO_2^{2+}]$, $[U\emptyset]$, and $[HN\emptyset]$. In practice the conservation equations were used to express $[U\emptyset]$ and $[HN\emptyset]$ in terms of $[H^+]$ and $[UO_2^{2+}]$; hence, it was necessary to solve only Eqs. (2) and (9) by the Newton-Raphson method.

In carrying out the calculation an attempt was first made to determine the four parameters ln K_{DH}, ln K_{DU}, B_1, and B_2 as defined in Eqs. (12a) and (12b):

$$\ln Q_{DU} = \ln K_{DU} + B_1 I , \qquad (12a)$$

$$\ln Q_{DH} = \ln K_{DH} + B_2 I , \qquad (12b)$$

where the K values represent distribution constants and

$$I = m_s + [H^+] + 3[UO_2^{2+}] . \qquad (13)$$

However, mathematical difficulties were encountered in the evaluation of $\partial D/\partial B_1$ and $\partial D/\partial B_2$ (undoubtedly because the data were not sufficiently precise to determine unique values of the B parameters) and hence only two parameters, the ln K values in Eqs. (12a) and (12b), were used.

In Table 6.7 is shown a comparison of observed[3] and calculated distribution coefficients for the $UO_2(NO_3)_2$-HNO_3 system at two different NH_4NO_3 and two different TBP concentrations. It is interesting to compare the values of ln K_D and ln K_{DN} (really ln Q_D and ln Q_{DN}, since no linear term was used) shown in Table 6.7 with the corresponding values given in Tables 6.3 and 6.6, where each was determined separately. In the case of 5% TBP, ln K_D' = 2.17, and B = 0.111 (Table 6.3). Hence ln Q_D = 2.61 in 3.94 M NH_4NO_3 and 2.95 in 6.89 M NH_4NO_3. These values are to be compared with 3.09 in Table 6.7. In the case of 10% TBP, values of 2.68 for ln Q_D' in 3.94 M NH_4NO_3 and 3.02 for ln Q_D' in 6.89 M NH_4NO_3 are to be compared with 2.98 as shown in Table 6.6. Similarly, average ln Q_{DN} values of −2.24 and −1.90 computed for 5 and 10% TBP from the parameters given in Table 6.6 are to be compared with the corresponding values of −2.16 and −2.24 in Table 6.7. Hence the parameters calculated for the combined $UO_2(NO_3)_2$-HNO_3 system are consistent with those obtained in each system separately.

Calculations were also performed on the $UO_2(NO_3)_2$-HNO_3-TBP system in the absence of a salting agent; the values of the parameters ln K_D (for uranium) and ln K_{DN} (for nitric acid)

[6] Wallace Davis, Jr., private communication (June 1962).

Table 6.7. Observed and Calculated Distribution Ratios D (Organic/Aqueous) for $UO_2(NO_3)_2$ Between Aqueous NH_4NO_3-HNO_3 and TBP-Diluent Phases

D_{obs}	D_{calc}	Concentration (M)			
		NH_4NO_3	HNO_3	H^+	UO_2^{2+}
		5 vol % TBP,			
		ln K_D (uranium) = 3.09,			
		ln K_{DN} (nitric acid) = −2.16			$\times 10^{-3}$
4.82	4.57	3.94	1.04	0.98	3.02
4.55	3.72	3.94	1.55	1.48	3.49
3.65	3.00	3.94	2.07	1.99	4.19
3.16	2.51	3.94	2.59	2.49	4.45
11.2	11.6	6.89	0.52	0.48	1.44
7.81	7.23	6.89	1.04	0.97	2.41
4.44	5.05	6.89	1.55	1.47	3.32
2.83	3.87	6.89	2.07	1.97	3.77
2.97	3.10	6.89	2.59	2.48	3.95
		10 vol % TBP,			
		ln K_D (uranium) = 2.98,			
		ln K_{DN} (nitric acid) = −2.24			$\times 10^{-4}$
22.6	24.3	3.94	0.517	0.46	7.35
22.1	22.0	3.94	1.04	0.93	4.85
21.1	16.9	3.94	1.55	1.41	9.14
19.7	13.5	3.94	2.07	1.90	12.4
15.2	11.3	3.94	2.59	2.40	13.1
35.2	38.1	6.89	1.04	0.90	4.00
33.0	28.4	6.89	1.55	1.37	3.83
17.0	19.1	6.89	2.07	1.87	8.90
7.5	16.1	6.89	2.59	2.36	5.92

are given in Table 6.8. In carrying out the calculations an attempt was first made to consider each acid concentration separately. However, except in the case of 0.5 M HNO_3 and 10% TBP, convergence difficulties were experienced unless all the data were considered simultaneously. Hence it was necessary with the 15% TBP system to calculate single values of ln K_D and ln K_{DN} determined by all the data; as expected, the values of D_{obs} and D_{calc} showed much greater discrepancies at 0.5 M HNO_3 than the values calculated separately for the 10% TBP system at the same acid concentration.

The values of ln Q_D for this system can also be calculated in two different ways: either by using the parameters in Table 6.3 or those in Table 6.4 along with an average ionic strength value (and the assumption that the Q values vary with ionic strength alone, i.e., are independent of the medium). A comparison of the values calculated in these two ways with those shown in Table 6.8 is given in Table 6.9.

Since the values calculated using the Table 6.5 parameters agree more closely with the observed values than do those calculated using the Table 6.3 parameters, it seems that the activity coefficients of $UO_2(NO_3)_2$ in HNO_3 media more closely resemble those in pure aqueous $UO_2(NO_3)_2$ solution than those in the presence of NH_4NO_3.

A comparison of the ln Q_{DN} values shows reasonably good agreement at 0.5 M HNO_3. In the higher-concentration regions all that can be

said is that the calculated values are qualitatively in the right direction. The parameters given in Table 6.6 were obtained in the concentration range 0 to 1 *M*; the poor agreement in the 2 to 4 *M* range in the mixed system indicates that a DH activity coefficient term is not sufficient and that a linear term is needed. Actually this is known to be the case; the activity coefficient of HNO_3 increases with ionic strength above about 1 *M*.

Hence a relatively simple mathematical model may be used to describe solvent extraction equilibria over wide ranges of concentration of material being extracted, of salting agent, and of extractant. In principle there is no reason why the model cannot be extended to much more elaborate systems. However, more precise data will be needed in order that the dependence of linear-activity-coefficient terms on the medium may be elucidated.

Table 6.8. Values of the Distribution Constants for the System $UO_2(NO_3)_2$-HNO_3-TBP-Diluent in the Absence of a Salting Agent

TBP (%)	M_{HNO_3}	ln K_D (uranium)	ln K_{DN} (nitric acid)
10	0.5	3.27	−1.94
	2.0–4.0	2.72	−3.48
15	0.5–4.0	2.47	−3.47

Hydrolysis of Metal Ions

R. M. Rush O. E. Esval[7]
J. S. Johnson D. F. Keeley[8]
K. A. Kraus

Hydrolysis of U(VI): EMF. – The study of the hydrolysis of U(VI) reported in the Chemistry Division Annual Report of last year has been continued. Since that time, emf measurements of the acidity of hydrolyzed uranyl chloride were completed and interpreted in the same manner as we previously dealt with the (literature) perchlorate data. This work was published[9] and will be only briefly outlined here. In perchlorate media, we had found that the predominant hydrolytic species seemed to be $(UO_2)_2(OH)_2^{2+}$ and $(UO_2)_3(OH)_5^{+}$; the frequently postulated UO_2OH^{+} was not present in major amounts, although we could not conclude that it was essentially absent under our conditions. In 1 *M* chloride, our acidity measurements indicate that an additional species $(UO_2)_3(OH)_4^{2+}$ (which also presumably includes some complexed chloride) is important. The question of UO_2OH^{+} is also unresolved here.

[7]ORINS predoctoral Fellow, University of North Carolina.

[8]ORINS summer research participant, 1961, University of Southwestern Louisiana.

[9]R. M. Rush, J. S. Johnson, and K. A. Kraus, *Inorg. Chem.* 1, 378 (1962).

Table 6.9. Comparison of Observed and Calculated Equilibrium Quotients (10% TBP)

M_{HNO_3}	ln Q_D (calculated)		ln Q_D (observed)
	Using Table 6.3 Parameters	Using Table 6.5 Parameters	
0.5	2.28	3.43	3.27
2.0–4.0	2.57	2.80	2.72
	ln Q_{DN} (calculated)		
	Using Table 6.6 Parameters		
0.5	−1.63		−1.94
2.0–4.0	−1.8		−3.5
0.5–4.0[a]	−1.9		−3.5

[a]15% TBP.

Hydrolysis of U(VI): Spectrophotometric Studies. – Absorption spectra of hydrolyzed uranyl chloride solutions (0.001 to 0.1 *M*) and of a few uranyl perchlorate solutions have been measured in the range 3600 to 5100 A. Typical extinction curves are shown in Fig. 6.3. It can be seen that optical absorption increases rapidly with hydroxyl number [average number of moles of hydroxide bound per mole of U(VI)] and that the peak shifts somewhat toward longer wavelengths. Chloride complexing of the unhydrolyzed uranyl and of at least one of the hydrolyzed species is suggested by the greater light absorption in chloride media than in perchlorate.

We correlated the spectra of the chloride solutions with the emf hydrolysis scheme involving $(UO_2)_2(OH)_2^{2+}$, $(UO_2)_3(OH)_4^{2+}$, and $(UO_2)_3(OH)_5^{+}$ by finding the values of the molar absorptivities of these species at each wavelength which give the best least-squares fit to the total absorption for all solutions (the molar absorptivity for the unhydrolyzed species was directly measured). Figure 6.4 shows the values thus obtained. With these absorptivities and the fractions of the various species computed from the formation

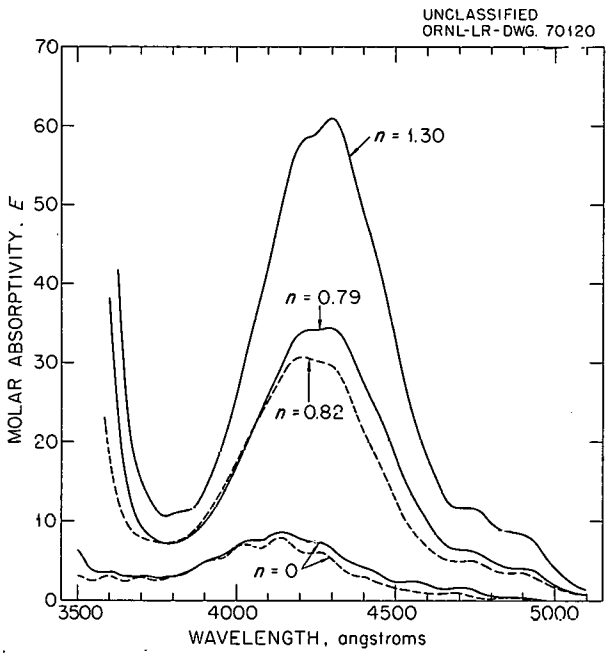

Fig. 6.3. Absorption Spectra of 0.010 *M* U(VI) Solutions in 1 *M* Total Chloride (Solid Curves) and 1 *M* Total Perchlorate (Broken Curves) at 25°C.

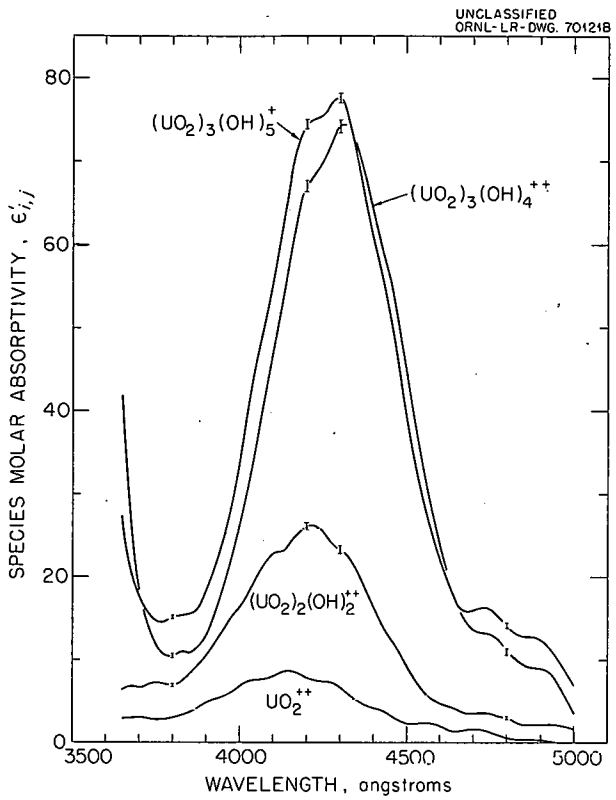

Fig. 6.4. Species Molar Absorptivities for U(VI) Species in 1 *M* Total Chloride. Equilibrium quotients used are $k_{2,2} = 6.7 \times 10^{-7}$, $k_{3,4} = 4.7 \times 10^{-13}$, and $k_{3,5} = 1.0 \times 10^{-17}$. Vertical lines indicate one standard error on each side of the value.

quotients of the above hydrolysis scheme, satisfactory agreement between observed and computed optical absorption was attained for all concentrations and hydroxyl numbers investigated.

Evaluation of Hydrolysis Constants with the Ultracentrifuge: Temperature Coefficients of Bi(III) Polymerization. – Normally in ultracentrifugation one interprets the equilibrium refractive index pattern in terms of molecular weights of the solute in question. The approximations in doing so can become serious with polydisperse inorganic polymeric systems. The equations customarily used for interpretation are strictly correct only for a constant charge/mass ratio and refractive index increment for all species; this condition is normally not fulfilled in polydisperse hydrolytic solutions. Consequently, although valuable information can frequently be obtained, it is difficult to interpret the apparent molecular weights in

terms of concentration quotients for the equilibria involved.

An alternative possibility is to adopt the approach used in structural studies: attempt to reproduce the observed equilibrium interference pattern by an assumed model. This is especially attractive when something is known concerning the major species present. Such a case is Bi(III) in perchlorate media, which is known from work here and elsewhere to form hexamers of hydroxyl number 2; that is, $[Bi(OH)_2]_6(ClO_4)_l^{(6-l)+}$, where l, the number of perchlorates complexed by the species, apparently is about 2. A $BiOH^{2+}$ species has also been suggested from emf measurements,[10] although in a similar study it was not found necessary for explanation of results.[11]

We attempted to test ultracentrifugation for evaluation of equilibrium quotients by centrifuging a number of solutions of different Bi(III) concentration and hydroxyl number; in addition, equilibrium was attained at three different temperatures for each solution, so that a temperature coefficient could be estimated. The method of estimating an equilibrium quotient is illustrated in Fig. 6.5, which is essentially an IBM 7090 plot of deviations between observed interference-fringe patterns as a function of radius and the pattern computed for different values of the formation quotient for the hexamer $K_{6,12}$. It was necessary to include a $BiOH^+$ species (formation quotient, $K_{1,1}$) in order to obtain reasonably consistent values of $K_{6,12}$ for the range of Bi(III) concentrations and hydroxyl numbers covered in the study. The present, quite preliminary, status is illustrated in Fig. 6.6, which gives the estimates of $K_{6,12}$ for all centrifugations, except for those in which less than 1% of total bismuth was present as hexamer; the values of $K_{1,1}$ listed in the figure must be considered only very rough estimates.

The value of $K_{6,12}$ at 25°C is about 8 times less than that given by Olin;[10] this is in the direction and of the approximate magnitude to be expected if the hexamer complexes two perchlorate ions, since Olin's measurements were in 3 *M* total perchlorate, and these were at approximately 1 *M*. The value also is not very different from that given by Tobias,[11] who worked in 1 *M* perchlorate, but exact comparison is not possible, since he did not include $BiOH^{2+}$. The room-temperature ΔH for hexamer formation (from $6Bi^{3+}$ and 12 waters) implied by these results is about 40 kcal/mole.

Hydrolysis of Pb(II). – A preliminary ultracentrifugation study of the hydrolytic polymerization of Pb(II) in perchlorate was carried out here several years ago. Since then, on the basis of an emf study, Olin[12] postulated that the major species were $Pb_4(OH)_4^{4+}$ and $Pb_6(OH)_8^{4+}$; he also listed as present in relatively minor amounts under his conditions, $PbOH^+$ and $Pb_3(OH)_4^{2+}$. Recently we completed a more extensive ultracentrifugation study. These results confirm in general our earlier study and are also consistent with Olin's conclusions. We also reexamined Olin's data by subjecting it to a least-squares analysis. The scheme he proposes gives a good fit to his results; the constants were refined only slightly. A poorer fit was obtained if either of the minor species were dropped.

Identification of Niobium Double Fluoride Species in HF Solutions by Raman Spectroscopy

O. L. Keller, Jr.

The identification of ionic species in concentrated electrolytes presents a difficult problem. Thermodynamic methods cannot be used in many cases because applicable activity coefficients are not available. Kinetic methods, such as conductance, are less widely applicable than thermodynamic methods. Direct identification of complex ions by molecular spectroscopy often requires a detailed theoretical treatment. If some of the characteristic frequencies of the ion are too weak to be seen, or if there is a mixture of complex ions, such a treatment is difficult. Identification of species in solution can be accomplished simply, however, if direct comparison can be made between spectra of the solutions and spectra of crystals of known composition and structure.

Niobium double-fluoride complexes found in 0% to 50% HF are identified in this investigation by comparing the Raman spectra of the solutions with Raman spectra of crystals of $CsNbF_6$, K_2NbF_7, and $K_2NbOF_5 \cdot H_2O$.

[10] A. Olin, *Acta Chem. Scand.* **11**, 1445 (1957).

[11] R. S. Tobias, *J. Am. Chem. Soc.* **82**, 1070 (1960).

[12] A. Olin, *Acta Chem. Scand.* **14**, 126 (1960).

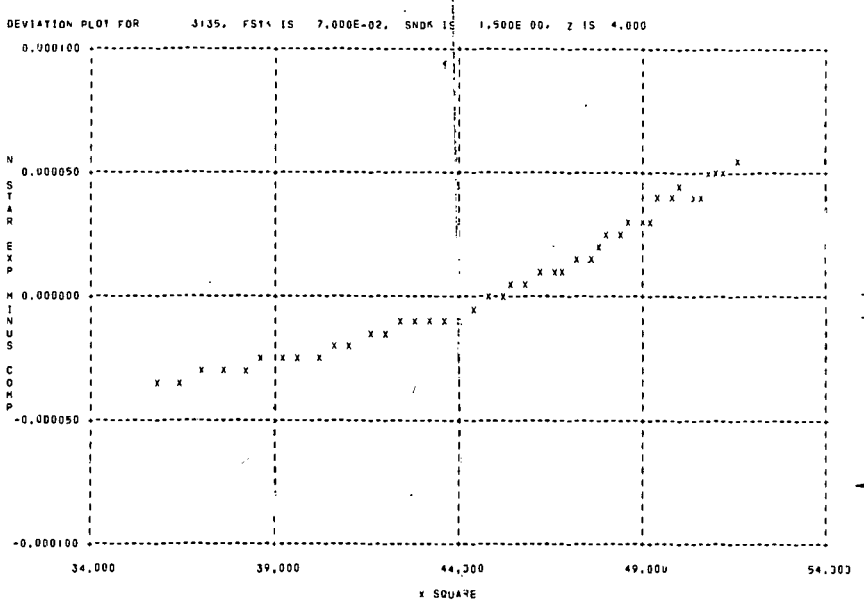

I 0.2 fringe

← $K_{6,12}$ = 1.5

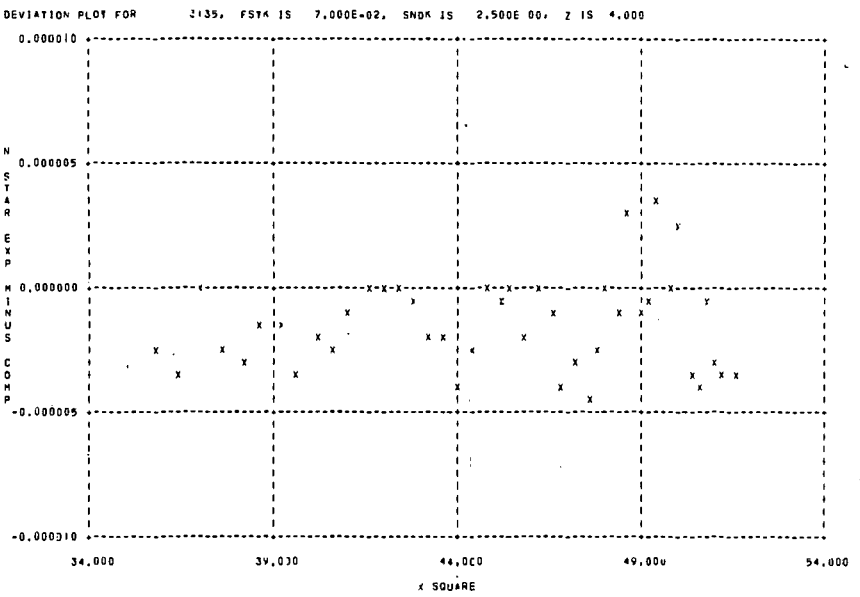

← 0.2 fringe equiv. to ca .023 in log $K_{6,12}$

← ca 0.1 mv acidity

← ca 0.1 mv, Bi electrode

← $K_{6,12}$ = 2.5

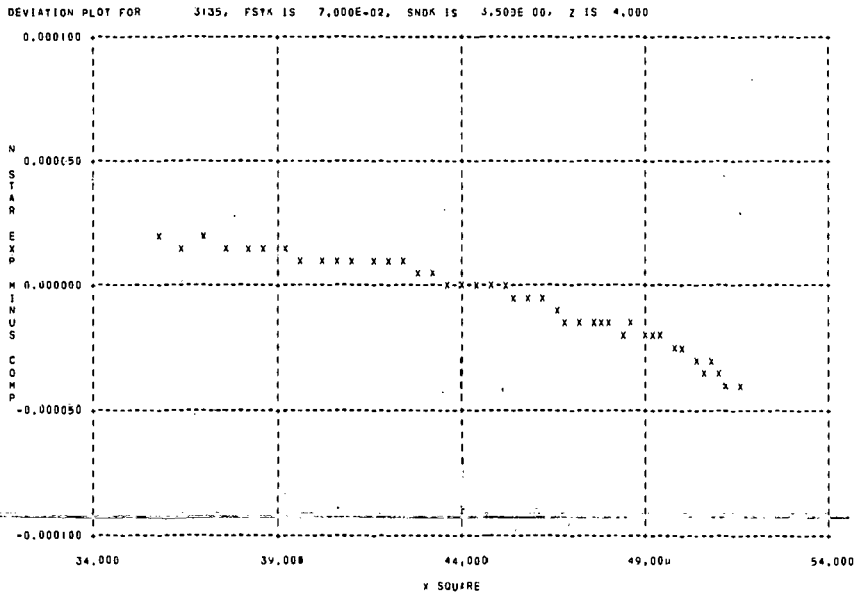

I 0.2 fringe

← $K_{6,12}$ = 3.5

X^2

Fig. 6.5. Evaluation of Equilibrium Constant, $K_{6,12} = \frac{([Bi(OH)_2{}^{6+}]_6)(H^+)^{12}}{(Bi^{3+})^6}$, by Ultracentrifugation. 0.1 *M* Bi(III), 1 *M* ($HClO_4$ + $NaClO_4$); hydroxyl number, about 0.78; rpm, 17,980; $K_{1,1} = \frac{(BiOH^{2+})(H^+)}{(Bi^{3+})} = 0.07$.

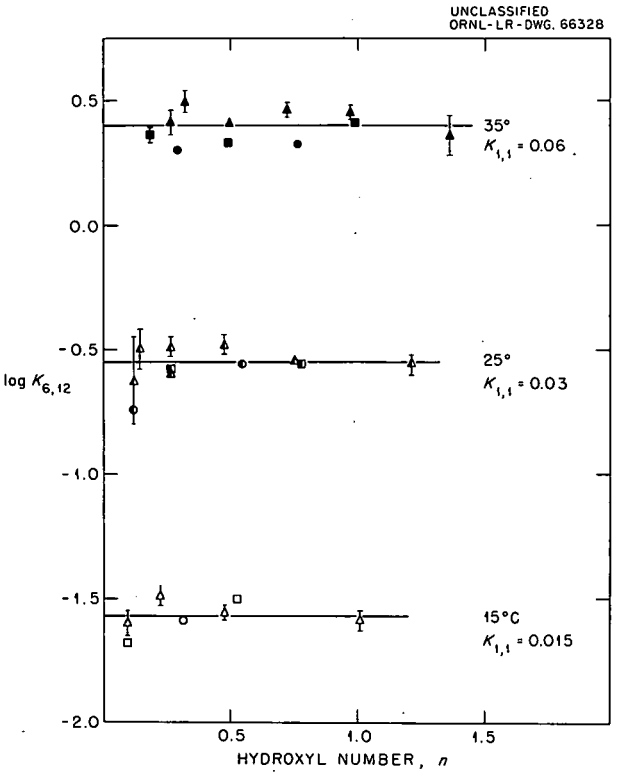

Fig. 6.6. Formation Constants for Bi(III) Hexamer from Ultracentrifugation. Range equivalent to about 0.2 fringe. Molarity of Bi(III): triangles, 0.02–0.04 *M*; squares, 0.04–0.075 *M*; circles, 0.075–0.105 *M*.

Infrared spectra of $K_2NbOF_5 \cdot H_2O$ crystals were also obtained to gain information on whether the $NbOF_5^{2-}$ or $Nb(OH)_2F_5^{2-}$ ion is present in the crystals and the solutions.

One of the author's principal interests is protactinium chemistry. This investigation was undertaken to develop a way to study protactinium ions in HF solutions.

For the HF solutions a Raman cell was made from Kel-F (Minnesota Mining and Manufacturing Company). The end window is sapphire. The wall of the tube was machined to a thickness of about 15 mils to make it more transparent. The dimensions of the cell are those of the Cary 19-mm cell.

The cells used for the Raman crystal spectra of K_2NbF_7 and $CsNbF_6$ are glass and have conical windows. These windows are better than flat ones for many crystals because more of the Raman scattered light leaves the cell to enter the monochromator and be detected.

The results of the Raman studies are given in Tables 6.10 and 6.11. Figures 6.7*a* and *b* and 6.8*a* and *b* allow direct comparison of the spectra of crystalline $CsNbF_6$ and $K_2NbOF_5 \cdot H_2O$ with typical solution spectra.

We assume for the moment that crystalline $CsNbF_6$ and $K_2NbOF_5 \cdot H_2O$ contain the NbF_6^- and $NbOF_5^{2-}$ ions respectively (see below). A comparison of the Raman lines characteristic of the crystals with the lines found for the solutions then shows that the $NbOF_5^{2-}$ ion is present in solutions containing up to about 35% HF and that NbF_6^- ion is present in solutions containing at least about 25% HF.

No lines characteristic of K_2NbF_7 (Table 6.10) appear in the solutions.

Table 6.10. Raman Spectra of Crystals

Compound	Raman Frequencies (Δ cm^{-1} from 4358 A)
$CsNbF_6$	280 (m)[a] [ν_5]
	562 (w) [ν_2]
	683 (s) [ν_1] (sharp)
K_2NbF_7	388 (m)
	630 (vs) (sharp)
	785 (w)
$K_2NbOF_5 \cdot H_2O$	295 (m)
	600 (vw)
	935 (m)

[a] m = medium; vw = very weak; w = weak; s = strong; vs = very strong.

Table 6.11. Raman Spectra of K_2NbF_7 in HF Solutions

First line of frequencies at each concentration due to $NbOF_5^{2-}$; second line due to NbF_6^-

Solvent	Raman Frequencies (Δ cm^{-1} from 4358 A Hg)	mg Nb/ml
H_2O[a]	290(m),[b] 595(w) , 920(s)	31.3
	——, ——— , ———	
1% HF	290(s), 595(w) , 920(s)	37.4
	——, ——— , ———	
10% HF	285(m), 596(w) , 925(s)	45.6
	——, ——— , ———	
20% HF	280(m), ——— , 939(m)	20.8
	——, ——— , ———	
25% HF	275(m), 600(vw), 935(m)	20.3
	——, ———, 683(w)	
30% HF	——, ———, 935(w)	21.6
	280(m), ———, 685(m)	
35% HF	——, ———, 935(vvw)	20.4
	275(m), ———, 686(m)	
40% HF	——, ———, ———	36.1
	275(m), ———, 685(vs)	
50% HF	——, ———, ———	56.9
	280(s), ———, 685(vs)	

[a] $K_2NbOF_5 \cdot H_2O$ was dissolved in H_2O.

[b] (m) = medium; (vvw) = very very weak; (vw) = very weak; (w) = weak; (s) = strong; (vs) = very strong.

The spectrum of crystalline $CsNbF_6$ fits the theoretical relationship given by Yost, Steffens, and Gross[13] for a regular octahedral structure such as that expected for NbF_6^-. The composition of the crystals (which was established by analysis), and the agreement of their Raman lines with what is theoretically expected for symmetry O_h, demonstrate that the NbF_6^- ion exists as such in the crystals and, by inference, in the solutions.

$K_2NbOF_5 \cdot H_2O$ could also be $K_2Nb(OH)_2F_5$. It is believed[14] that the octahedral $NbOF_5^{2-}$ ion is present because $K_2NbOF_5 \cdot H_2O$ is isomorphous with $K_2TiF_6 \cdot H_2O$.

The infrared spectrum was recorded for crystalline $K_2NbOF_5 \cdot H_2O$ (see below and Fig. 6.9). The Raman and the infrared spectrum, which both show a line at 935 cm^{-1}, are consistent with an octahedral $NbOF_5^{2-}$ ion but not with a pentagonal bipyramidal $Nb(OH)_2F_5^{2-}$ ion. This follows from group theory because point group C_{4v} allows coincidences between the infrared and Raman, whereas D_{5h} does not.

Compound	Infrared Absorption Frequency, cm^{-1}
$K_2NbOF_5 \cdot H_2O$	738, 932, 1083 ($NbOF_5^{2-}$)
	1626, 3572, 3643 (H_2O)

If $NbOF_5^{2-}$ ion is present, water of hydration must be present also. The line at 1626 cm^{-1} found in the infrared spectrum of $K_2NbOF_5 \cdot H_2O$ is in the region (1590 to 1630 cm^{-1})[15,16] expected for the H_2O bend, but it is at least 450 cm^{-1} too high for a heavy atom–OH bend.[17,18] Water of hydration is therefore present.

[13] D. M. Yost, C. C. Steffens, and S. T. Gross, *J. Chem. Phys.* **2**, 311 (1934).

[14] J. L. Hoard and W. J. Martin, *J. Am. Chem. Soc.* **63**, 11 (1941).

[15] P. J. Lucchesi and W. A. Glasson, *J. Am. Chem. Soc.* **78**, 1347 (1956).

[16] L. H. Jones, *J. Chem. Phys.* **22**, 217 (1954).

[17] D. F. Hornig and R. C. Plumb, *J. Chem. Phys.* **26**, 637 (1957).

[18] O. Glemser and E. Hartert, *Naturwissenschaften* **40**, 552 (1953).

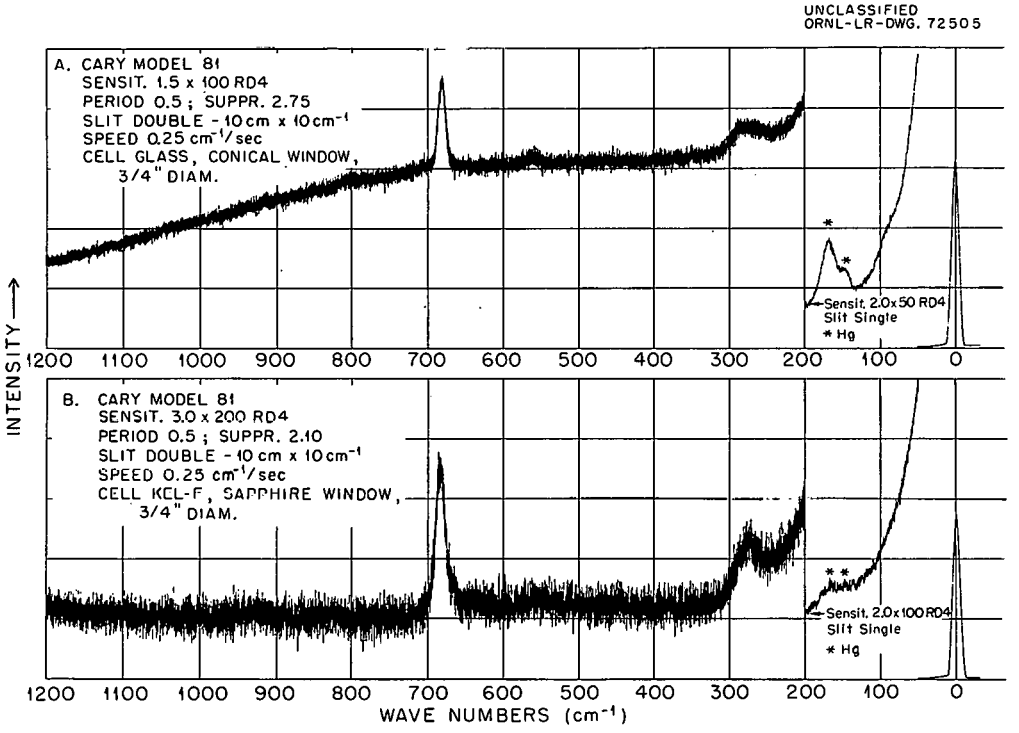

Fig. 6.7. (*a*) Raman Spectrum of Crystalline $CsNbF_6$; (*b*) Raman Spectrum of K_2NbF_7 in 40% HF Solution.

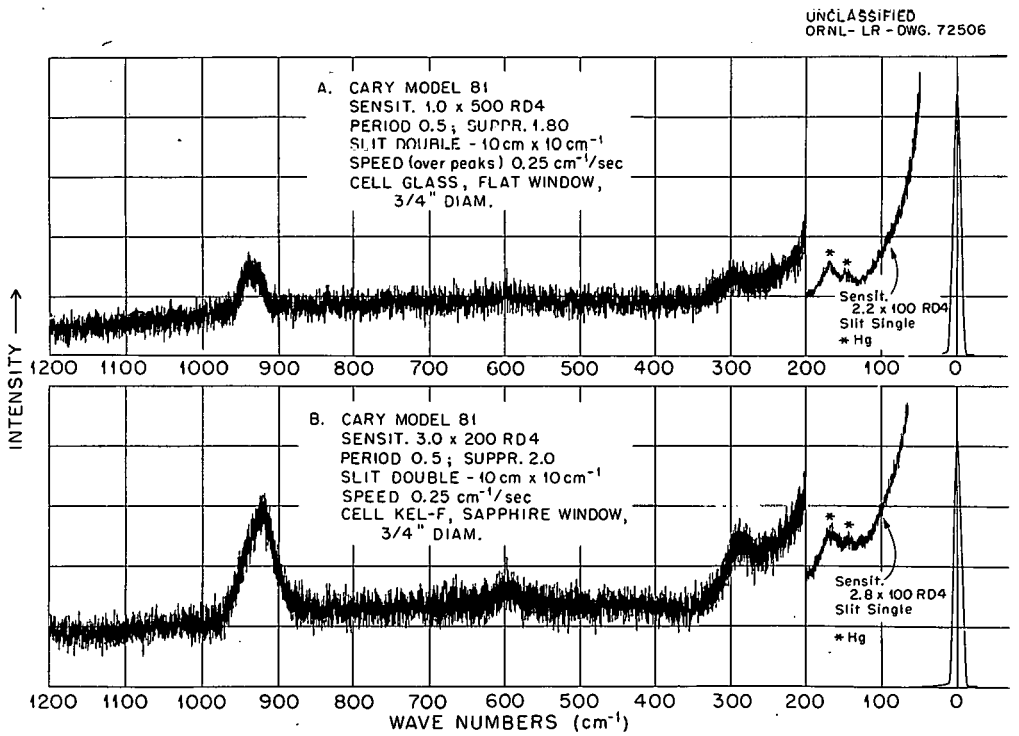

Fig. 6.8. (*a*) Raman Spectrum of Crystalline $K_2NbOF_5 \cdot H_2O$; (*b*) Raman Spectrum of K_2NbF_7 in 1% HF Solution.

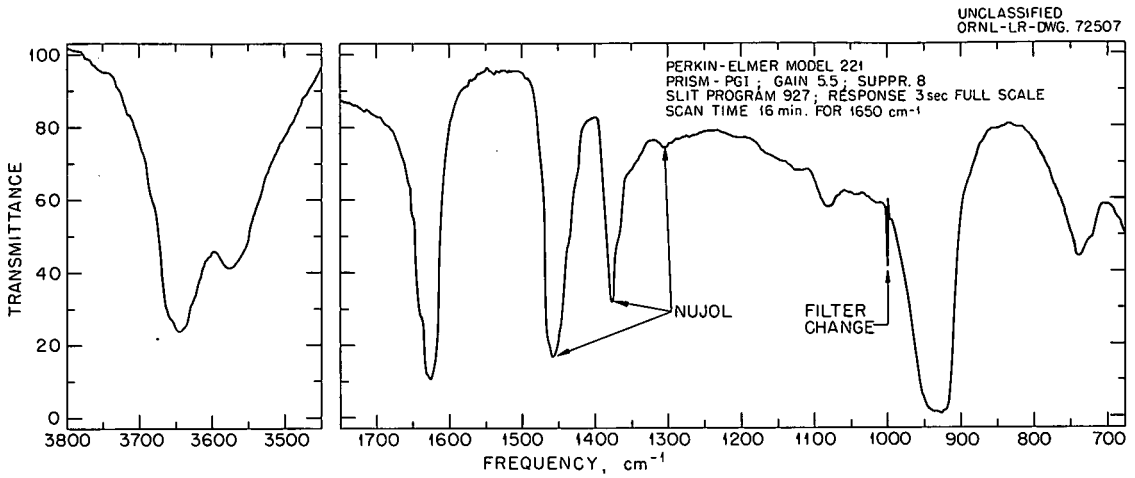

Fig. 6.9. Infrared Spectrum of Crystalline $K_2NbOF_5 \cdot H_2O$.

Analyses of all crystals and solutions were carried out by L. J. Brady and W. R. Laing of the ORNL Analytical Division.

CHEMISTRY OF HEAVY ELEMENTS: AQUEOUS SPECTROPHOTOMETRY AT ELEVATED TEMPERATURES AND PRESSURES

An Improved High-Temperature Aqueous Spectrophotometer Cell Assembly

W. C. Waggener A. J. Weinberger
R. W. Stoughton

A new spectrophotometer cell assembly, designed and constructed during the past 24 months, is being tested. Both the sample cell and the reference cell are designed to permit gas-liquid equilibration and have identical control systems for temperature and pressure over the ranges 0 to 280°C and 0 to 1000 psia respectively.[19] Maintaining both sample and reference cells at the same temperature cancels the effect of the large variations of the spectra of H_2O and D_2O with temperature which would otherwise obscure the spectral changes of the solute. This assembly, used with the standard Cary model 14 monochromator and detector, should make the spectral ranges, 0.7 to 1.2 μ for H_2O and 1.2 to 1.8 μ for D_2O solutions, accessible to the study of absorbing ions at elevated temperatures[20] for the first time. The new equipment incorporates a number of features and improvements, some of which are intended to offset the added complexity of simultaneous operation and control of two high-temperature-pressure cells.

The titanium absorption cells are practically identical with the revised cell described previously.[19] However, the heater-cooler in the form of a cylindrical annulus which surrounds each cell body is designed to (1) fit the limited space available in the reference cell compartment, (2) allow for simple removal and replacement of cells, and (3) provide rapid and uniform cell heating and cooling, primarily through radiative transfer. It is made with a cooling channel and a resistance-heater winding both embedded in pure copper. Several narrow embossed rings machined on the inner circumference of this heater-cooler annulus support the titanium cell body out of contact with the wall of the annulus. The facing surfaces are coated with a film of graphite for good radiative heat transfer. The above assembly in turn is "canned" in a gold-plated thermal radiation sheath and is cradle-mounted as in the previous assembly.[21]

Each of the two heater-cooler assemblies was test operated satisfactorily in vacuum from −70

[19] W. C. Waggener, A. J. Weinberger, and R. W. Stoughton, *Chem. Div. Ann. Progr. Rept. June 20, 1961*, ORNL-3176.

[20] W. C. Waggener, *Anal. Chem.* **30**, 1569 (1958).

[21] W. C. Waggener, *Rev. Sci. Instr.* **30**, 788–93 (1959).

to 300°C, with cell heating and cooling rates of 5–10°C/min. Liquid-nitrogen-cooled helium was used as the coolant.

The temperatures of the sample and reference cells are controlled above and below room temperature by modulation of heating and cooling supplies respectively. A Leeds and Northrup millivolt recorder with a stable millivolt suppression supply and a Leeds and Northrup duration-adjust type of controller is used for each cell. Experiments indicate that adequate (±0.1°C) control of cell temperature can be achieved by a thermocouple located in either cell or heater-cooler body.

An integrated piping arrangement involving sample and reference cells was worked out to allow necessary operations to be performed without disconnecting piping: (1) addition and withdrawal of samples; (2) metered additions of gases to cells at operating temperature; (3) cell washing and backwashing, using alternate additions of wash liquid and purge gas; and (4) drying by alternate gas purge and evacuation.

The cell windows and contents of either absorption cell may be examined visually for bubbles and turbidity by inserting a special borescope into one of the alignment sleeves installed in the phototube compartment. The visible beam of the spectrophotometer provides illumination of various colors and intensities.

Spectrophotometric Studies of the $DClO_4$-D_2O-H_2O System at Elevated Temperatures

W. C. Waggener A. J. Weinberger
R. W. Stoughton

The $DClO_4$-D_2O-H_2O system is a desirable solvent for high-temperature aqueous spectrophotometry of inorganic ions. The transparency of the ClO_4^- anion throughout the wavelength range of interest (0.2 to 1.8 μ) suggests it as an ideal reference medium. However, at elevated temperatures it is a powerful oxidizing agent, and the reduction products (HOCl, Cl_2, Cl_3^-) absorb in the spectral region below 0.5 μ.

Initially, samples of 0.01 *f* and 0.1 *f* (25°C) $DClO_4$ were examined by using a high-temperature-pressure absorption cell[19] in which the solutions were in contact with titanium, sapphire, gold, and Teflon. Reaction with the gold was indicated by the growth of a spectrum characteristic of the chloroaurate(III) species.[22] Decomposition rates of perchloric acid at 250°C estimated from the 0.31-μ band ($\epsilon_{max} \sim 4200$) were <20 ppm/hr and 25 ppm/hr for 0.01 and 0.1 *f* $DClO_4$ respectively.

After removal of the gold washers from the interior side of the window mounts, solutions of 0.01, 0.1, 0.5, and 1.0 *f* $DClO_4$ were examined for periods up to several days at temperatures up to 250°C. At these concentrations and in this environment, aqueous $DClO_4$ remained nonabsorbing in the wavelength range 0.33 to 1.8 μ. However, neither the titanium nor the sapphire is inert in this system. The 250°C studies were complicated by pitting of the synthetic sapphire windows. The onset and progress of pitting were manifested by a steadily rising base-line absorbance (0.001–0.002/hr) throughout the visible and near-infrared region while the cell was held at 250°C. Examination of the windows revealed hexagonal pyramidal pits (6 to 10 μ across and 0.8 to 1.1 μ deep, covering 15 to 40% of the surface). The amount of titanium and aluminum appearing in cell samples (determined by spectrographic analysis) increased with the time and temperature of exposure and was roughly proportional to the acid concentration. Estimated corrosion expressed in terms of mils $year^{-1}$ (unit formality)$^{-1}$ $DClO_4$ is given below.

	25°C	250°C
Titanium	0.005	0.08
Sapphire	0.001	340

Perhaps it is worth pointing out that these rates are certainly tolerable for experiments of a few hours duration.

In numerous previous experiments involving nitrate and sulfate media no pitting occurred, but the sapphire window surfaces were smoothly eroded.

[22] A. A. Vlcek and P. Beran, *Chem. Listy* **50**, 1306 (1956).

PHYSICAL CHEMISTRY OF ION EXCHANGERS

Absorption of Bromide Ion from Aqueous Chloride Solutions by Liquid Amine and Resin Anion Exchangers: Evidence for Bichloride Ion in Anion Exchangers

S. Lindenbaum G. E. Boyd

The absorption of microquantities of bromide ion from aqueous solutions of hydrochloric acid, lithium, sodium, potassium, and cesium chloride by tri-*n*-octyl amine solutions in toluene, and from hydrochloric acid by a strong-base anion exchanger was measured. The departure of the equilibrium distribution coefficients for the liquid ion exchanger from a "mass law" dependence on electrolyte concentration could be explained quantitatively by the nonideality of the aqueous phase. With the anion exchange resin, however, corrections for aqueous-phase nonideality and for deswelling were not sufficient to give conformity with the mass law; in addition, an important correction for the organic-phase nonideality was required. The magnitude of the organic-phase nonideality could be correlated with the invasion of this phase by electrolyte. When the invasion was small, or absent, as with the liquid exchanger, the nonideality was small and could be neglected.

An attractive explanation for the large nonideality associated with the invasion of anion exchangers, liquid and resinous, by hydrochloric acid would be the strong binding of HCl to the exchange site to form hydrogen dichloride ion, HCl_2^-. This species was observed recently, and its infrared spectrum was identified in crystalline tetramethyl ammonium hydrogen dichloride.[23] Strong absorption by the hydrogen dichloride ion was found at 1180 and 1565 cm^{-1}. To determine whether this ion was present in the liquid anion exchange system, infrared spectra were measured on solutions of tri-*n*-octyl amine hydrochloride in carbon tetrachloride or toluene that had been equilibrated with concentrated aqueous hydrochloric acid. Prominent absorption bands were observed in the 1180 cm^{-1} and 1565 cm^{-1} regions of the spectrum, supporting the view that the dichloride ion is found in these solutions.

[23]T. C. Waddington, *J. Chem. Soc.* 1708 (1958).

The decomposition pressure of tetramethyl ammonium hydrogen dichloride was reported recently by Chang and Westrum.[24] The vapor pressure was independent of composition for the system tetramethyl ammonium chloride–tetramethyl ammonium hydrogen dichloride, indicating that a second phase formed as HCl was added to the tetramethyl ammonium chloride. Our measurements[25] of the vapor pressure of HCl gas over a dry sample of Dowex 1 in the chloride form showed that HCl was strongly absorbed; however, the vapor pressure varied with the composition of the exchanger, indicating that the latter must be regarded as a single phase containing HCl_2^- ions.

Osmotic Coefficients of Quaternary Ammonium Halides

S. Lindenbaum

Osmotic coefficients of tetramethyl ammonium chloride and bromide, trimethyl benzyl ammonium chloride and bromide, and β-hydroxyethyl-dimethyl-benzyl ammonium chloride and bromide were measured by the isopiestic method. The trimethyl benzyl ammonium compounds are structurally analogous to Dowex 1, and the β-hydroxyethyl-dimethyl benzyl ammonium compounds are analogous to Dowex 2; hence, both serve as "model compounds" for these ion exchange resins. Osmotic coefficients for the pure salts and several mixtures are shown in Fig. 6.10. In each case the curve for the bromide salt lies lower than that for the corresponding chloride, indicating that the bromide ion is bound more tightly to the quaternary nitrogen. Strong-base anion exchange resins also exhibit a strong preference for bromide over chloride ions. The curves for the trimethyl benzyl ammonium salts and those for the β-hydroxy-ethyl-dimethyl-benzyl ammonium salts were found to lie much lower than those for the tetramethyl ammonium salts. Evidently, the presence of a benzyl group in a quaternary ammonium ion greatly enhances its anion binding ability.

[24]S. Chang and E. F. Westrum, *J. Chem. Phys.* **36**, 2571 (1962).

[25]The authors gratefully acknowledge the advice and help of R. H. Busey in making these measurements.

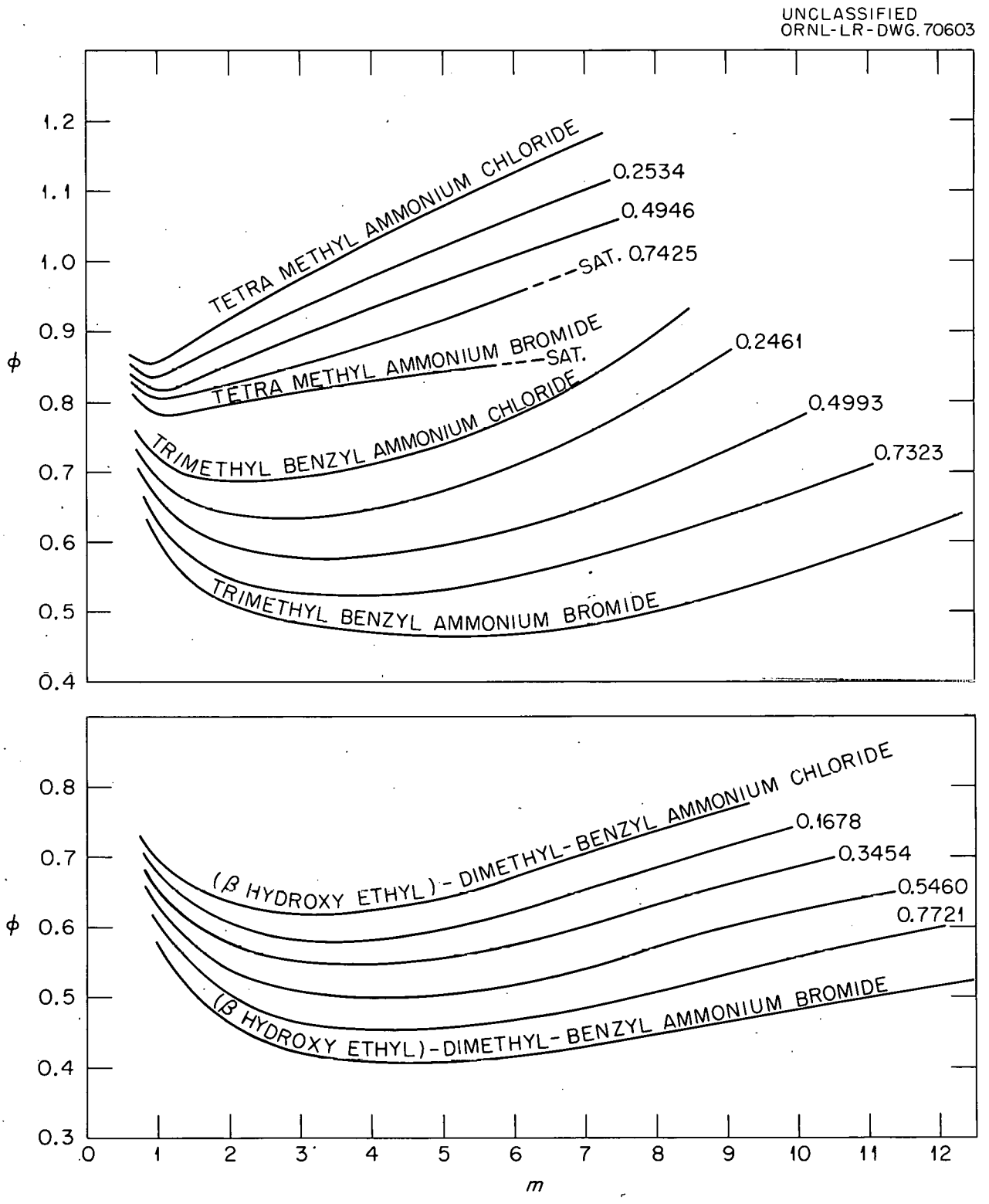

Fig. 6.10. Osmotic Coefficients of Some Quaternary Ammonium Halides. The curves for the mixtures are labeled with the fraction of bromide in each mixture.

Heat-of-Exchange Measurements with Linear Anion Exchangers

Fred Vaslow

An apparent Br/Cl selectivity coefficient and a standard heat of exchange were determined calorimetrically for Dowex 1 linear polymer at 8×10^{-4} weight normality. These results were obtained by measuring the heat effects on adding equivalent amounts of Cl^- ion to the Br^- polymer solution and the converse reaction of Br^- ion to the Cl^- polymer so that the final states are identical. The heat is the algebraic sum of the two reaction heats, and the apparent selectivity

$$K = Br^-_{pol} Cl^-_{sol} / Cl^-_{pol} Br^-_{sol}$$

is given by $(\Delta H_1/\Delta H_2)^2$. The values are $K = 1.9 \pm 0.6$ and $\Delta H^\circ = -630 \pm 50$ cal/equiv. It is clear that the polyelectrolyte does not approach ideality even at this low concentration. The differences in heats of dilution of the Cl^- and Br^- linear polymers for concentrations corresponding to Dowex 2 resins of 2 to 24% cross-linking ranged from -455 to -550 cal/equiv as compared with -1300 to -1730 cal/equiv for the heat of anion exchange with cross-linked anion exchangers. Addition of the linear polymer exchange heat to the dilution heats gives a reasonable agreement with the resin exchange heat. Some of the difference may be due to the fact that data for the Dowex 1 linear polymer only was available for comparison with results on Dowex 2.

Heat effects on adding low concentrations of like ions to the linear polymers were endothermal and very small, although on adding the like-ion polymer to a 1 *N* solution of NaCl or NaBr a net heat effect of $\Delta H = -440$ and -1000 cal/equiv resin was observed.

Heat of Solution and Dilution Measurements with the *p*-Ethylbenzene Sulfonates

Fred Vaslow G. E. Boyd

Apparent molal heat contents and heats of solution relative to about 0.001 *m* final solutions were measured for *p*-ethylbenzene sulfonic acid and its alkali-metal salts. The concentration dependence of the apparent molal heat contents (i.e., "integral heat of dilution") for these compounds is shown in Fig. 6.11. The integral heats of solution for the monohydrate of the sulfonic acid and for the lithium, sodium, potassium, and cesium salts were -4250, -1660, $+1780$, $+3305$, and $+5410$ cal/mole, respectively. The heat content curves are notable in that their initial slopes are larger than for any other common, 1:1, alkali-metal salt.

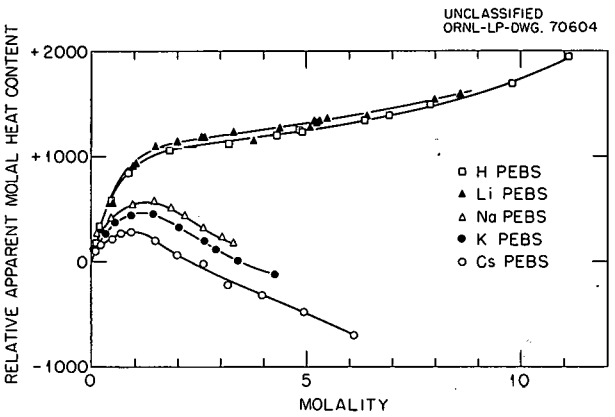

Fig. 6.11. Relative Apparent Molal Heat Contents of *p*-Ethylbenzene Sulfonate Solutions.

Comparisons of the apparent molal heat content differences, $\Delta\phi_L$, for four cationic salts of the *p*-ethylbenzene sulfonate with the calorimetrically estimated standard heats of ion exchange, ΔH°_{ex}, for several Dowex 50 cation exchangers are given in Table 6.12. The agreement of the heats for the exchange of Na^+ ion with Li^+, H^+, and Cs^+ ions is satisfactory. There is a significant discrepancy for the exchange of K^+ ion with sodium ion, however, and it is expected that a departure will be found even in the Na^+/Li^+, Na^+/H^+, and Cs^+/Na^+ exchanges when the heats of exchange for copolymers of less than 2% nominal DVB cross-linking are measured.

Extraction of Fe(III) from Aqueous Hydrochloric and Perchloric Acid Solutions by Liquid and Resinous Cation Exchangers

S. Lindenbaum G. E. Boyd

The phenomenon of ion exchange selectivity from concentrated aqueous electrolyte solutions

Table 6.12. Comparison of Heats of Exchange and Heats of Dilution Differences

Percentage of Cross-Linking of Resin	Na/H		Na/Li		K/Na		Cs/Na	
	$\Delta\phi_L$	ΔH°_{ex}	$\Delta\phi_L$	ΔH°_{ex}	$\Delta\phi_L$	ΔH°_{ex}	$\Delta\phi_L$	ΔH°_{ex}
2	−380	−460	−550	−650	−170	−290	−600	−560
4	−720	−860	−1070	−1080	−160	−410	−580	−620
8	−1030	−1180	−1520	−1460	−190	−550	−770	−770

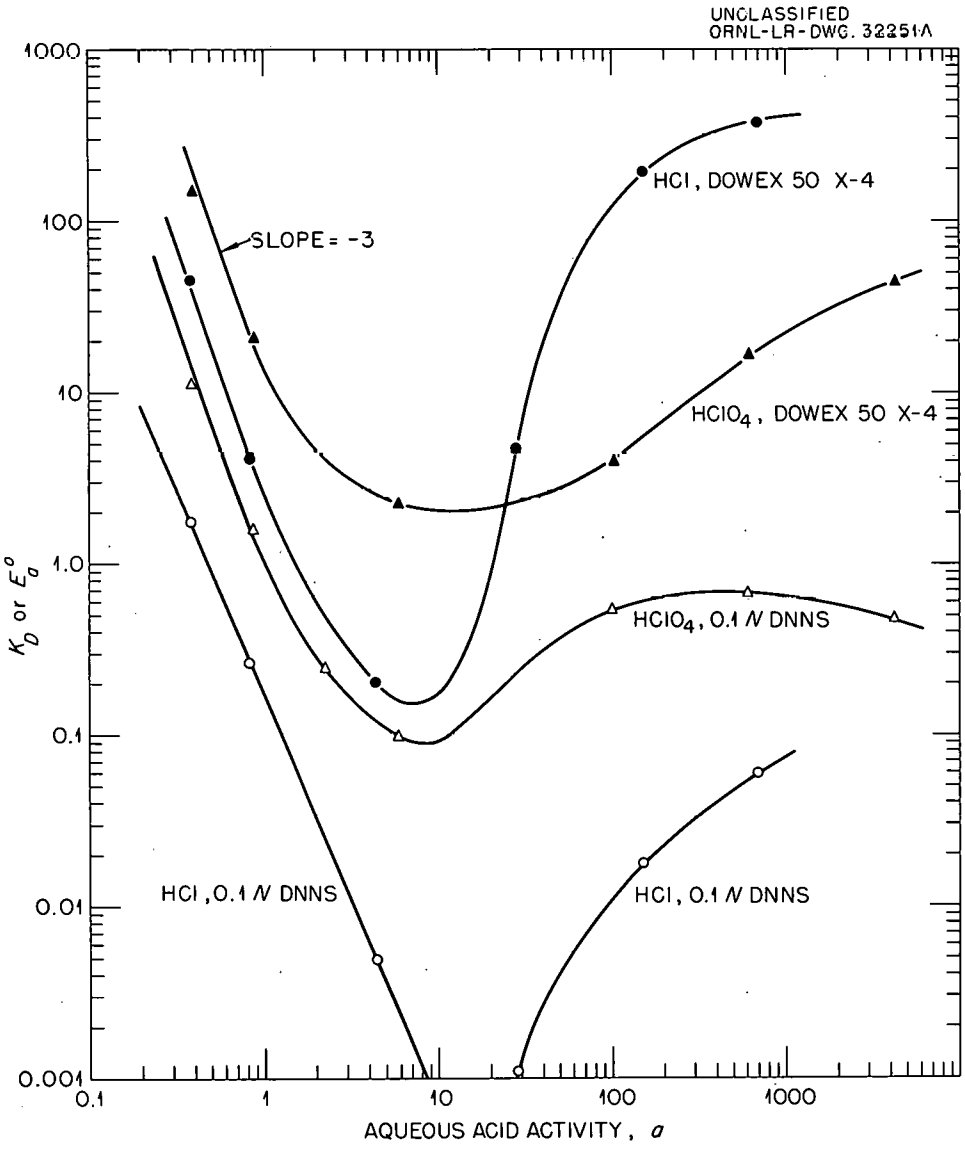

Fig. 6.12. Extraction of Fe^{59}(III) by 0.1 *N* DNNS in Benzene and Dowex 50 from Hydrochloric and Perchloric Acid Solutions.

has attracted an increased interest recently, although observations on the increased uptake of cations by strong acid cation exchangers from acid solutions were reported as early as 1950. In Fig. 6.12 are reported observations made some time ago[26] on the anomalous absorption of microquantities of Fe(III) ion from concentrated HCl and $HClO_4$ solutions by a liquid cation exchanger (dinonyl napthalene sulfonic acid, DNNS, dissolved in benzene) and by a lightly cross-linked polystyrene sulfonate cation exchanger (Dowex 50-X4). The unusual behavior found with the liquid and resinous exchanger was the marked increase in the extraction of Fe(III) above acid concentrations of 3 to 4 *M*. At lower concentrations the distribution coefficient decreased with increasing acid activity at a rate consistent with the hypothesis that an ion exchange reaction between H^+ and Fe^{3+} ions occurred. The effect with Dowex 50 shown in Fig. 6.12 was observed[27] previously with Fe(III) in hydrochloric acid solutions, using a methylene sulfonic acid cation exchanger. The phenomenon of increased uptake of cations by Dowex 50 from concentrated hydrochloric acid has been shown to be a general one.[28]

The data of Fig. 6.12 reveal that the effect with Fe(III) occurs from $HClO_4$ as well as from HCl solutions and with both a liquid and a resinous strong acid cation exchanger. The result with perchloric acid suggests that a change in the Fe(III) ionic species in the aqueous phase must occur, leading to an increased distribution coefficient at high concentrations. It is also possible with both acids that anion exchange groups were formed in the organic phase ($RSO_3H_2^+$), resulting in the larger uptake of iron (presumably as $FeCl_4^-$) from concentrated hydrochloric than from perchloric acid.

ION EXCHANGE STUDIES

Development of an Ion Exchange Separations Scheme

F. Nelson
J. H. Holloway[29]
J. A. Hauschild[29]
K. A. Kraus
D. C. Michelson

Systematic investigation of ion exchange properties of essentially all the metallic elements has continued with the objective of developing a general ion exchange separations scheme. Both anion and cation exchange methods have been explored. The media were mixtures of HCl, HNO_3, HF, $HClO_4$, and, in a few cases, H_2SO_4.

It is intended, on the basis of these studies, to divide the elements into logical ion exchange groups which can be separated from each other reasonably rapidly and with minimum overlap. Simultaneously, the studies are intended to supply the fundamental information for division of the groups into subgroups and for isolation of individual elements.

Most existing methods, for example, anion exchange techniques or low- and medium-ionic-strength cation exchange techniques, did not seem adequate for the main group development, particularly in the initial stages of the analysis where the number of elements could be exceedingly large. Use of concentrated perchloric acid with admixture of complexing acids appeared to offer, as mentioned in the previous annual report,[30] an important new set of conditions for the isolation of an initial group of elements. Accordingly, the cation exchange studies in concentrated $HClO_4$-HCl and $HClO_4$-HCl-HF solutions were extended to some 80 elements. About 25 were studied in $HClO_4$-HNO_3 and $HClO_4$-HNO_3-HF solutions. In addition, about 20 elements were studied with cation exchangers in HCl-HNO_3 solutions with and without added HF. The effect of temperature on adsorbability was investigated in the range 25 to 75°C for approximately 40 elements in a variety of media.

The elements adsorbed from concentrated $HClO_4$, containing moderate amounts of HCl and small amounts of HF, constitute one of the first groups which may be isolated in a general separations scheme. HF is added to ensure dissolution of the hydrolyzable elements principally of the 4th, 5th, and 6th groups. Even small amounts of HF,

---

[26] G. E. Boyd and S. Lindenbaum, 134th National Meeting, American Chemical Society, Chicago, Ill., Sept. 7–12, 1958.

[27] R. Djurfeldt and O. Samuelson, *Acta Chem. Scand.* **4**, 165 (1950).

[28] R. M. Diamond, *J. Am. Chem. Soc.* **77**, 2978 (1955).

[29] Present address, McClellan Air Force Base, California.

[30] *Chem. Div. Ann. Progr. Rept. June 20, 1961*, ORNL-3176, p 47.

in certain instances, drastically lowered adsorbabilities from concentrated $HClO_4$, and systematic investigations of a number of elements in $HClO_4$ solutions as a function of HF concentrations have been initiated.

The presence of HF in the initial medium limits the solubility of a number of elements, particularly alkaline earths and rare earths. Earlier studies of the solubility of lanthanum fluoride in HF-HCl solutions at high HCl concentrations implied that the solubility limitations would not be very serious. However, additional studies in concentrated $HClO_4$ solutions showed that in this medium lanthanum fluoride is several orders of magnitude less soluble and that, therefore, solubility might cause much more serious limitations than originally assumed.

In trying to establish a hypothetical set of conditions for the initial sample to which the group separations scheme is to apply, it was recognized that certain elements could be lost because of volatility. Further, other elements might be lost through volatilization during the repeated evaporations now deemed necessary during the prosecution of the scheme. Work has been initiated to establish which elements might be quantitatively removed by distillation and to determine how they might be collected. It is anticipated that certain volatilization techniques could be used to advantage to simplify the overall separations scheme.

The current status of the scheme itself may be summarized as follows: Six major ion exchange adsorption groups have been established in a preliminary manner. These groups involve anion and cation exchangers at high, medium, and low ionic strength. For several of these groups, detailed breakdown into subgroups and individual elements has been possible. Approximately a dozen ion exchange separations schemes, which are anticipated to play an important role in the overall scheme, have been established in detail and most of these have been written up. The group scheme has been applied successfully to fission product samples.

Cation Exchange Studies of Uranium at High Ionic Strength

T. Murase[31] F. Nelson
K. A. Kraus

Detailed investigations have been carried out on adsorption of U(VI) (as tracer U^{237}) by cation exchangers from $HClO_4$, HNO_3, HCl, and H_2SO_4 solutions and high ionic strength mixtures.

Adsorbabilities at 25°C by Dowex 50-X4 from the various acids over a wide ionic strength range are given in Fig. 6.13. In perchloric acid, adsorbability decreases with increasing *M* $HClO_4$ at low ionic strength in the usual manner. However, at high ionic strength, *D* passes through a minimum and then increases rapidly, reaching values larger than 10^4 for *M* $HClO_4$ >10. In the other media, the rise of *D* at high ionic strength is small or nonexistent. The divergence in adsorbabilities at high ionic strength between perchloric acid solutions and the other acids results, at least in part, from complexing of U(VI) by the other anions, the complexes apparently having relatively low adsorbability at high ionic strength.

Adsorbabilities of U(VI) in various acid mixtures ($HClO_4$-HCl, $HClO_4$-H_2SO_4, $HClO_4$-HNO_3) at constant 9 *M* acidity are shown in Fig. 6.14. While

[31]Guest scientist from Atomic Fuel Corporation, Tokyo, Japan.

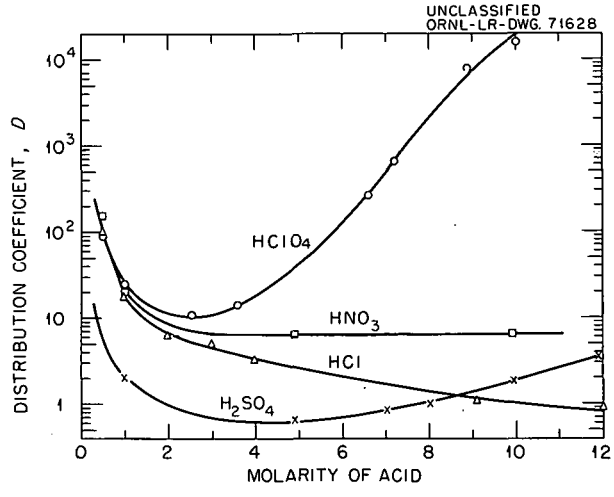

Fig. 6.13. Adsorption of U(VI) from Various Mineral Acids.

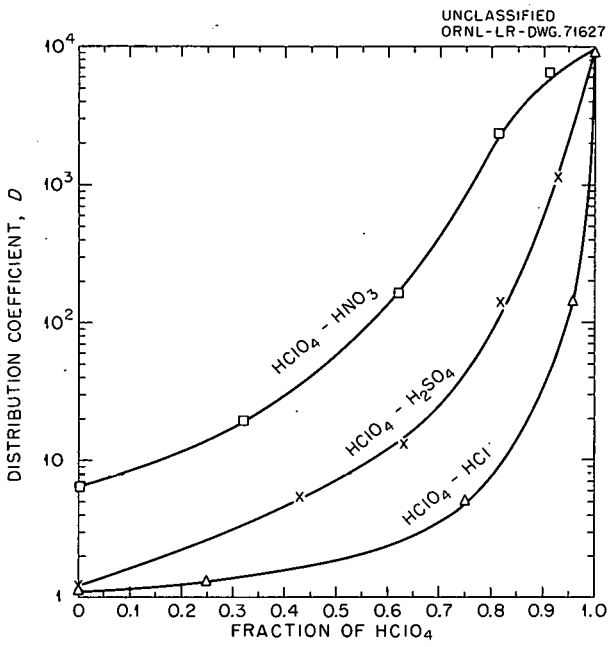

Fig. 6.14. Adsorption of U(VI) from 9 *M* Acid Mixtures (Dowex 50-X4, 25°C).

in all cases the distribution coefficients decrease with decreasing fraction F of $HClO_4$

$$\left(F_i = M_i / \sum_j M_j\right) ,$$

the effect is most pronounced with HCl where the distribution coefficient at

$$F_{HClO_4} = 0.95 \; (F_{HCl} = 0.05)$$

is almost two orders of magnitude lower than at $F_{HClO_4} = 1$. At this high ionic strength U(VI) thus appears to be strongly complexed by chloride ions in contrast to its behavior at low ionic strength where U(VI) is only slightly complexed by chloride ions.

The rapid variation of D of U(VI) with F_{HClO_4} in acid mixtures of high concentration can form the basis of a large number of separations. An interesting example of the use of high-ionic-strength electrolyte mixtures for cation exchange separations is shown in Fig. 6.15. This separation of Cs^+, Ba^{2+}, Sr^{2+}, U(VI), and rare earths is based on the strong adsorption of Sr^{2+}, rare earths, and U(VI) from concentrated $HClO_4$, the modest sensitivity of Sr^{2+} to nitric acid in $HClO_4$-HNO_3 mixtures, the sensitivity of U(VI) to HCl in $HClO_4$-HCl mixtures, and the relatively low sensitivity of the rare earths to admixtures of either HNO_3 or HCl. Elution of the rare earths is achieved in the absence of perchloric acid at moderate ionic strength, where their adsorbabilities go through a minimum.

Adsorption on Inorganic Materials

H. O. Phillips K. A. Kraus

Study of the methods of preparation and of the ion exchange behavior of various inorganic materials was continued. These studies included evaluation of rates of exchange, uptakes as a function of acidity, and selectivity. Special emphasis was placed on a search for new combinations which might show unusual properties.

A large number of vanadates were prepared in which an excess of vanadate was coprecipitated with Bi, Nb, Sn, Ta, Ti, and Th. All these materials showed cation exchange properties in acid solutions, with capacities for cesium of the order of 0.5 to 2 moles/kg. They showed moderate selectivity for cesium vs rubidium, with separation factors varying between 3 and 5. Distribution coefficients of the rare earths in 0.1 *M* HNO_3 varied considerably from compound to compound. Thus, the distribution coefficients for Ce^{3+} and Eu^{3+} were less than 1 for niobium vanadate and larger than 1000 for zirconium vanadate.

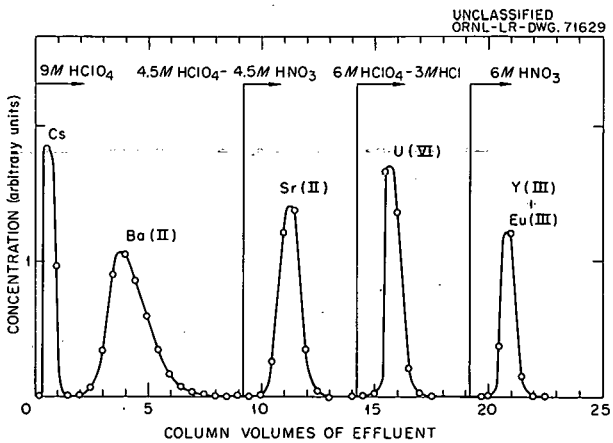

Fig. 6.15. Separation of Cs, Ba, Sr, U, Y, and Eu by Cation Exchange at High Ionic Strength. Column, 3 cm × 0.28 cm^2; Dowex 50-X4, −400 mesh; 50°C.

By far the most interesting compound investigated was, however, zirconium antimonate. This material was prepared by adding excess $SbCl_5$ in HCl solution to zirconium oxychloride solution and then adding ammonia to the mixture. After filtration, the material was washed and dried at 25°C. It had an Sb(V):Zr(IV) ratio of approximately 2 to 1 and a water content of approximately 27%. By using an antimonate containing Sb^{124} tracer, the material was found to be reasonably stable in ammonia, NaOH, HNO_3, HCl, and H_2SO_4, provided that the concentration of these reagents was less than 2 *M*. Uptake of Cs^+ near pH 3 was about 0.5 mole/kg, and uptake of Na^+ from 0.9 *M* NaOH was about 5 moles/kg.

In acid solutions, the antimonate showed high distribution coefficients for alkaline earths and rare earths. Thus the distribution coefficient for Sr^{2+} (Sr^{85}) in 1 *M* HNO_3 was larger than 10^4 and for Ce^{3+} larger than 10^3. These distribution coefficients from acid solutions for polyvalent ions are very much larger than those normally exhibited by hydrous oxide exchangers.

The selectivity of zirconium antimonate for the alkali metals in acid solutions, and particularly for Na^+, is unique and can lead to interesting separations, as shown in Fig. 6.16, a separation of K^+, Rb^+, and Na^+. Potassium can be removed with 2 *M* HNO_3; it is well separated from Rb^+ which can be removed with about 6 *M* HNO_3. The separation factor for these two elements is thus unusually large. Cesium ion, had it been present, would have eluted together with Rb^+ with little separation. Lithium ion, had it been present, would have eluted ahead of, and well separated from, K^+. Sodium is exceedingly strongly adsorbed from acid solutions and cannot be removed even with concentrated nitric acid. It may, however, readily be removed at lower acidity, for example, with 2 *M* NH_4NO_3.

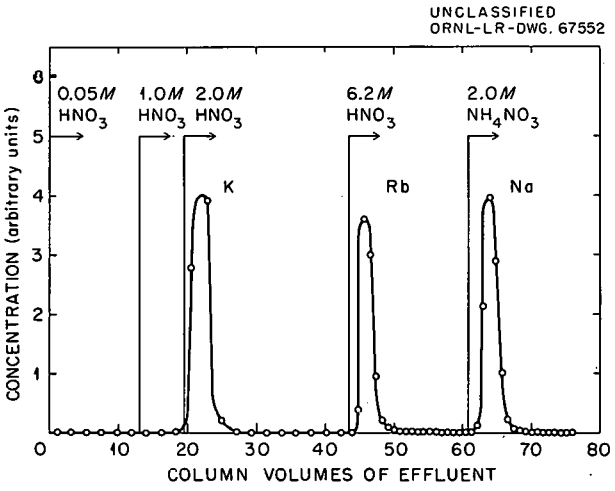

Fig. 6.16. Separation of Alkali Metals with Hydrous Zirconium Antimonate. Column, 2.6 cm × 0.19 cm^2; 80–170 mesh; drying temperature, 25°C.

7. Electrochemical Kinetics and Its Application to Corrosion

Ion Exchange at the Passive Film on Iron and Steel

G. H. Cartledge D. H. Spahrbier[1]

As reported previously,[2] the passive film on iron and steel was shown to possess the property of ion exchange. Specimens passivated in a dichromate solution and thoroughly rinsed retained a Cr(VI) species which was removable by exchange with sulfate or hydroxide ions, for example. By use of Cr^{51}, the kinetics of the exchange process is being investigated. The procedure involves immersion of a passivated and rinsed specimen in successive portions of the solution containing the ion to be exchanged. The activity extracted at the measured times is determined in a multichannel analyzer. In order to follow changes in the potential of the specimen during extraction and to control this potential at a fixed value, when desired, the apparatus shown in Fig. 7.1 was used in certain experiments.

The reliability of the procedure adopted and the freedom of the exchange process from complications due to diffusion were demonstrated by measuring the rate of exchange of aqueous $Cr_2^{52}O_7^{2-}$ ions with $Cr_2^{51}O_7^{2-}$ (or $Cr^{51}O_4^{2-}$) on the film. As seen in Fig. 7.2, the process followed accurately a first-order course with respect to the residual chromate on the surface, as would be expected. That the exchange involves essentially

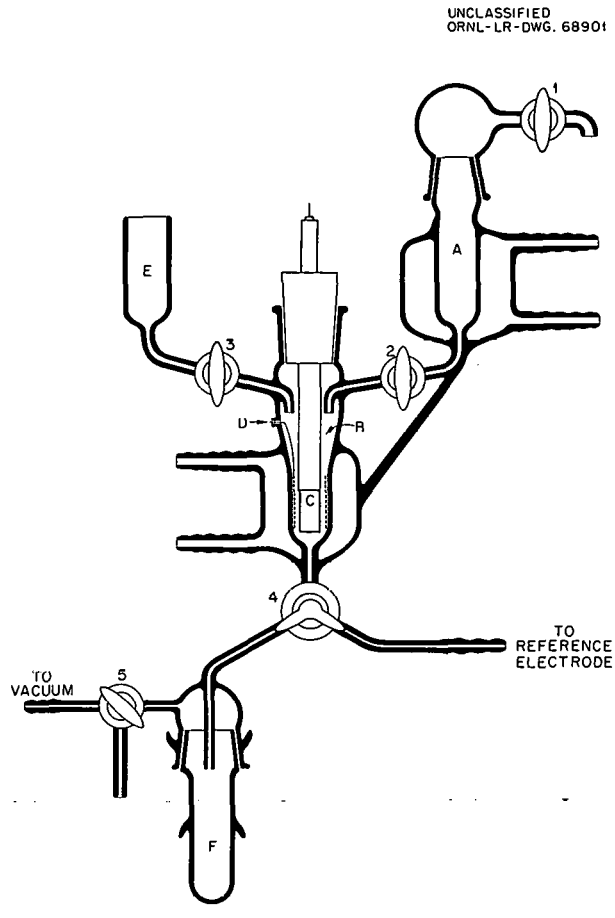

Fig. 7.1. Apparatus for Ion Exchange. A, water-jacketed reservoir; B, jacketed extraction cell; C, specimen, held by a Teflon support having an axial stainless steel rod for electrical connection; D, contact for platinum gauze counter electrode; E, reservoir for rinsing; F, holder for counting tubes.

[1]Present address: Frankfurt, Germany.

[2]D. H. Spahrbier and G. H. Cartledge, *Chem. Div. Ann. Progr. Rept. June 20, 1961*, ORNL-3176, p 60.

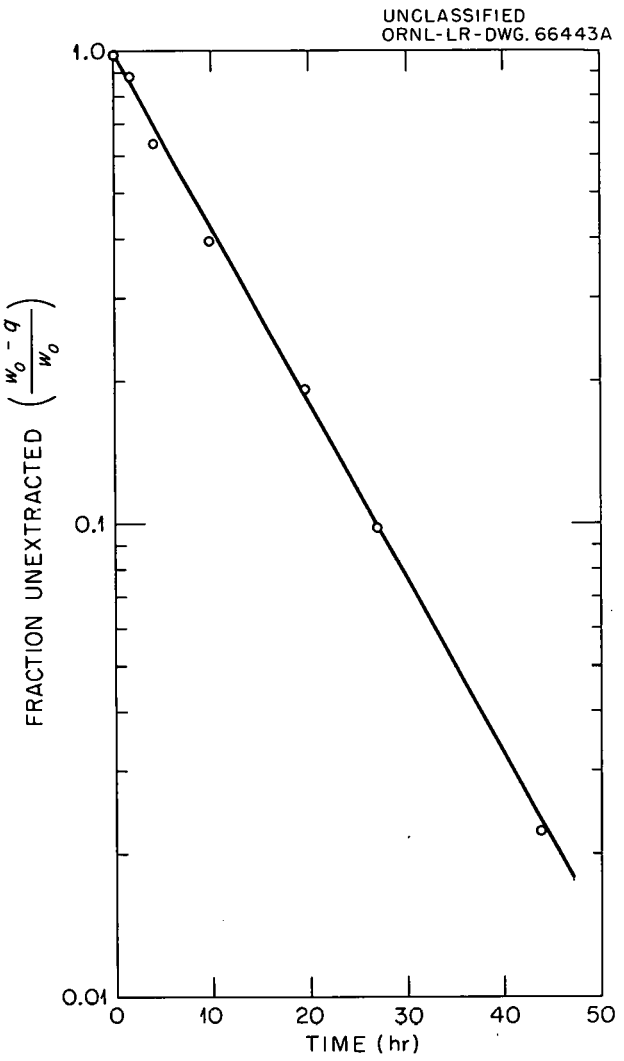

Fig. 7.2. First-Order Exchange of Cr^{51} on Surface by Aqueous $Cr_2^{52}O_7^{2-}$; w_0 is the Initial Exchangeable Chromate and q is the Amount Exchanged at Time t.

only surface ions, as distinguished from chromium within the film, was shown in two parallel experiments. In one, the specimen was exposed to $Cr_2^{51}O_7^{2-}$ only after initial passivation in $Cr_2^{52}O_7^{2-}$ and removal of the surface ions by the usual exchange procedure. The other specimen was passivated in $Cr_2^{51}O_7^{2-}$, extracted with sulfate, and again exposed to $Cr_2^{51}O_7^{2-}$. There was no significant difference in the rates of exchange at 40°C during the first 5 hr, at the end of which time the exchange from each specimen was roughly 80% complete, although Cr^{51} was present in the entire film in the second case.

Numerous measurements of the rate of exchange by $(NH_4)_2SO_4$ were made in both ammoniacal and weakly acidic solutions, extraction times being from 1 min to more than a week. Figure 7.3 shows the type of result uniformly obtained: the cumulative amount of chromium displaced per square centimeter quickly became almost linearly proportional to log t; this continued until the rate fell off as exhaustion of the film was approached. The initial decrease in rate was much greater than that for a first-order dependence on residual chromium on the surface.

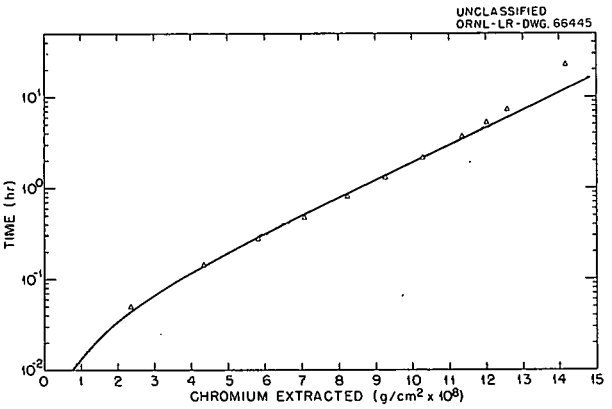

Fig. 7.3. Typical Exchange-Time Curve.

The log t relationship suggests an analogy to the Elovich equation for the rate of adsorption or desorption at a metallic surface, which is associated with a dependence of the heat of activation upon the coverage, θ. A rate equation was therefore developed from the Eyring absolute rate theory, under the assumption that the heat of activation increases linearly with the extent of exchange, q:

$$\Delta H_q^{\ddagger} = \Delta H_0^{\ddagger} + \frac{rq}{f}. \qquad (1)$$

In order that r may be referred to the surface area available for ion exchange, the factor f is introduced to represent the ratio of this area to the projected area. The factor r thus has the dimensions cal mole^{-1} cm^2 g^{-1} based on the available area, when q is in g of Cr per cm^2 (projected).

The rate equation then contains a linear depletion term, $w_0 - q$, where w_0 is the total exchangeable chromium, and an exponential term in q:

$$\frac{dq}{dt} = S_0'(w_0 - q) \exp\left(-\frac{rq}{fRT}\right), \qquad (2)$$

in which S_0' includes the usual kinetic factors, besides the constant concentration of the extracting ion (e.g., SO_4^{2-}), $\Delta H_0^{\ddagger}$, and $\Delta S^{\ddagger}$, variation of which is assumed to be of minor importance. So long as the exponential term is dominant, Eq. (2) can be integrated to give

$$q = 2.3\frac{fRT}{r}\log\left(\frac{rS_0}{fRT}\cdot t + 1\right)$$

$$= 2.3m \log\left(\frac{S_0}{m}\cdot t + 1\right), \qquad (3)$$

where S_0 is the initial rate, $S_0' w_0$ ($q = 0$). The curve in Fig. 7.3 is a least-squares fit of one set of data to Eq. (3) up to the point at which depletion is clearly being approached. All experiments conformed closely to this relationship.

A test of the complete Eq. (2) may be made by taking its logarithm after multiplication and division by w_0 and then plotting the logarithm of the rate vs q:

$$\log\frac{dq}{dt} = \log S_0 + \log\frac{w_0 - q}{w_0} - \frac{rq}{2.3\,fRT}. \qquad (4)$$

The rates are obtained as tangents to linear plots of q vs t. Curve III in Fig. 7.4 is such an experimental result. Since the rate measurements become less accurate as the process approaches completion, the extractions were never carried quite that far, but a value of w_0 was sought such that the combination of linear and exponential terms correctly represented the experimental curve. In Fig. 7.4, such an analysis of one experiment is shown. Curve I would be the rate if only the first-order term were involved; Curve II represents the exponential term alone, and the product of the two (divided by S_0, which appears in each of them) gives Curve III. It is clear that the initial predominance of the exponential curve over the linear one accounts for the applicability of the simplified

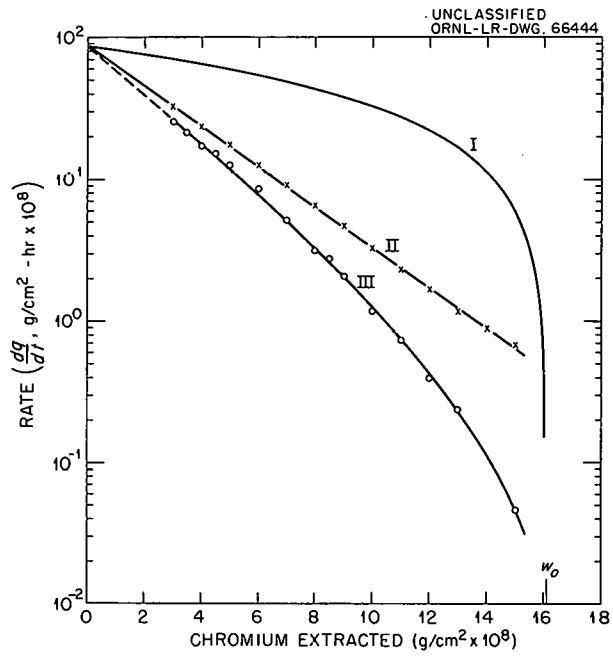

Fig. 7.4. Analysis of Experimental Rate-q Curve (III) into a First-Order Term (I) and a Term Exponential in q (II). The circles on III are taken from tangents to a linear plot of q vs t.

Eq. (3) over so extensive a range. From the slope of Curve II, the value of r/f for a particular specimen is obtainable.

From the analysis of 13 experiments at 40°C, in which the surface treatments were varied radically, the variation of r/f with surface treatment makes it possible to conclude that maximum initial coverage in the passivated specimens is about 2.26×10^{-8} g of Cr per cm^2 (true), or 65% of the value for close-packed tetrahedral chromate ions. The corresponding value of r indicates that the activation energy increases by 4300 cal $mole^{-1}$ during replacement of this monolayer. The results show a striking similarity to those for adsorption of gases on metals, where the effects can be understood in terms of changes in the energy levels of the substrate resulting from adsorption. It is believed that they are further evidence for similar electrical effects at the interface between film and solution. The significance of the results for passivation theory will be discussed in a

forthcoming paper. The experiments are being continued with other ions and with potentiostatic control of the potential at which exchange occurs.

The Role of Hydrogen Penetration into the Metal in the Electrochemistry of Iron

E. J. Kelly

In an earlier report, it was shown that the electrochemical polarization characteristics of iron, undergoing active corrosion in acid media, are strongly time dependent.[3] The rates of both the hydrogen-evolution reaction and the iron-dissolution reaction slowly increase or decrease with time to their new steady-state rates following a potentiostatic shift to more positive or more negative potentials, respectively. These findings made it possible to account for many of the apparent contradictions in the literature regarding the corrosion potential – pH relationship, Tafel slopes, $[OH^-]$ orders, and other diagnostic criteria in the reaction mechanisms of the iron-acid system – and afforded an explanation for the frequently cited phenomenon of electrochemical polarization hysteresis. On the basis of the evidence available at the time, it was suggested that the slow transient behavior might be attributed to hydrogen penetration into the iron. During the past year studies have been directed at verifying this conclusion. Two approaches to the problem have been followed, the first involving the analyses of numerous cathodic transient curves, and the second involving the effects produced on the electrode reaction rates when atomic hydrogen, generated on the opposite side of the iron membrane electrode, diffuses through the metal to the surface under observation.[4]

Analysis of Cathodic Transients. – The hydrogen evolution reaction on any metal in deoxygenated acid media may be described by the following set of partial reactions,

$$H^+ + e^- = H^\bullet_s \,, \qquad (1)$$

$$H^+ + H^\bullet_s + e^- = H_2 \,, \qquad (2)$$

$$2H^\bullet_s = H_2 \,, \qquad (3)$$

$$H^\bullet_s = H^\bullet_0 \,, \qquad (4)$$

$$H^\bullet_0 = H^\bullet_x \,, \qquad (5)$$

where $H^\bullet_s$, $H^\bullet_0$, and $H^\bullet_x$ represent atomic hydrogen on the electrode surface, at a point just within the metal, and at any point in the metal at a distance x (cm) from the electrode surface, respectively.[5] Electrochemists have tended to ignore reactions (4) and (5), which are those involved in the hydrogen penetration into the metal. While this may be justified in the case of a metal like mercury, such an *a priori* assumption cannot be made when dealing with metals in which hydrogen is known to be appreciably soluble, like iron, nickel, and platinum.[6] On the other hand, the experimental data, as well as theoretical considerations, indicate that, under the conditions prevailing in this study, the recombination reaction (3) on iron can be ignored.[7]

For the system of reactions given above, the net current density, i (amp/cm^2), is given by

$$-\frac{i}{F} = \bar{k}_1[H^+](\psi - \theta) - \bar{k}_{-1}\theta + \bar{k}_2[H^+]\theta - \bar{k}_{-2}\rho_{H_2}(\psi - \theta) \,, \qquad (6)$$

where the negative sign in front of i arises from a convention whereby a net cathodic current corresponds to a negative current. A line over a rate constant symbolizes its potential dependency. The fraction of the electrode surface available to the reaction system is represented by ψ, and the fraction of the surface covered by adsorbed atomic hydrogen is represented by θ. The other symbols in Eq. (6) have their customary significance, with F being the Faraday constant. The rate of change of θ with time is given by

$$\beta\frac{d\theta}{dt} = \bar{k}_1[H^+](\psi - \theta) - \bar{k}_{-1}\theta - \bar{k}_2[H^+]\theta + \bar{k}_{-2}\rho_{H_2}(\psi - \theta) - k_4\theta + k_{-4}[H^\bullet_0](\psi - \theta) \,, \qquad (7)$$

[3] E. J. Kelly, *Chem. Div. Ann. Progr. Rept. June 20, 1961*, ORNL-3176, p 65.

[4] A. N. Frumkin, *Zh. Fiz. Khim.* **31**, 1875 (1957).

[5] J. O'M. Bockris and H. Mauser, *Can. J. Chem.* **37**, 475 (1959).

[6] J. O'M. Bockris, *Chem. Rev.* **43**, 541 (1948).

[7] L. I. Khrishtalik, *Russ. J. Phys. Chem. (English Transl.)* **34**, 53 (1960).

in which β is a constant relating the coverage θ to the concentration of atomic hydrogen on the surface. The rate at which hydrogen penetrates into the metal may be either surface controlled, reaction (4), or controlled by diffusion within the bulk of the metal, reaction (5). In what follows, it will be assumed that the hydrogen penetration rate is surface controlled. This implies that the ratio of the diffusion coefficient of atomic hydrogen in iron to the length of the diffusion path is large compared to k_{-4}. In this case, $[H^{\bullet}_0]$ in Eq. (7) becomes $[H^{\bullet}_m]$, the concentration of atomic hydrogen in the interior of the metal. Furthermore, one can then write

$$\frac{V}{A} \cdot \frac{d[H^{\bullet}_m]}{dt} = k_4\theta - k_{-4}[H^{\bullet}_m](\psi - \theta) , \qquad (8)$$

where V (cm^3) and A (cm^2) represent the volume and the surface area, respectively, of the electrode.

In Fig. 7.5, the absolute value of the cathodic current is shown as a function of time for a typical cathodic transient. At time zero, the electrode potential was shifted potentiostatically to −0.850 v vs S.C.E., that is, to a new cathodic overvoltage of about −200 mv as compared with the original steady-state cathodic overvoltage of −100 mv. Accompanying the shift in potential, the cathodic current rises instantly to $|i_0| = 9.41 \times 10^{-5}$ amp as shown, and then slowly diminishes over the next 1800 min to the indicated steady-state current, $|i_{ss}| = 1.83 \times 10^{-5}$ amp. During this transient, the rate constants are independent of time, since the potential is fixed. If it is assumed that ψ is also independent of time during the slow transient, then it is evident from Eq. (6) that the change in the current with time must be ascribed to the time dependency of θ. In shifting the electrode potential to a more negative value, θ increases. However, due to the transfer of hydrogen into the metal, θ at any time t is less than in the steady state, and as θ slowly increases to its steady-state value the cathodic current simultaneously drops. If it is assumed that during the slow transient $d\theta/dt \cong 0$, but $d[H^{\bullet}_m]/dt \neq 0$, one can obtain θ as a function of $[H^{\bullet}_m]$ from Eq. (7) and thereby obtain a solution of Eq. (8) for $[H^{\bullet}_m]$ as a function of time. Relating $[H^{\bullet}_m]$ to the current through θ, one then obtains Eq. (9) for the current as a function of time:

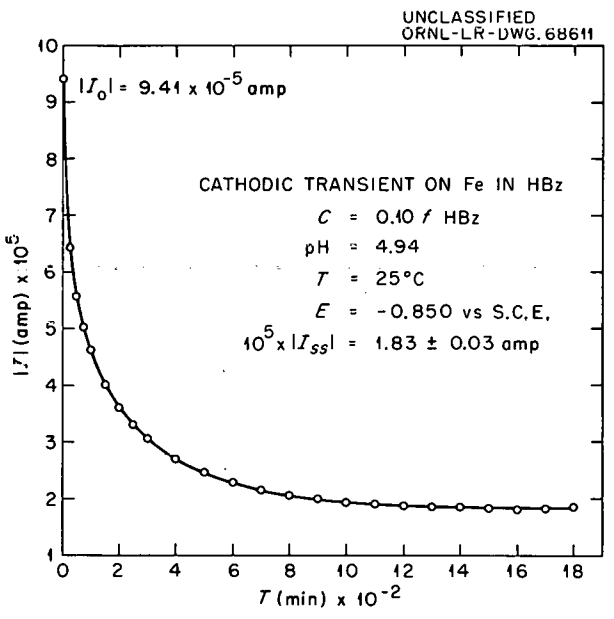

Fig. 7.5. Cathodic Current as a Function of Time for a Cathodic Transient on Iron in Benzoic Acid.

$$\log (i_{ss} - i_t) = Gt + H(i_t - i_0) + \log (i_{ss} - i_0) . \qquad (9)$$

In Eq. (9), i_0, i_t, and i_{ss} represent the currents at time zero, at any time t, and in the steady state, respectively, and G and H are constants for a given electrode potential. The variation with time of the second term on the right side of Eq. (9) becomes insignificant at long time and, as a result, Eq. (9) reduces to

$$\log (i_{ss} - i_t) = Gt + C' \qquad (10)$$

for long time. In Fig. 7.6, $\log (i_{ss} - i_t)$ is plotted against time and, as anticipated, the resulting curve becomes linear only after approximately 200 min. The constant G can be determined from the slope of the linear section of the curve. Equation (9) can be rearranged to give

$$\log (i_{ss} - i_t) - Gt = Hi_t + C'' . \qquad (11)$$

In Fig. 7.7, the left side of Eq. (11), evaluated by using the value of G obtained from Fig. 7.6, is plotted against the current over the initial portion of the transient – that portion where Eq. (10) is inadequate (Fig. 7.6). From the slope of

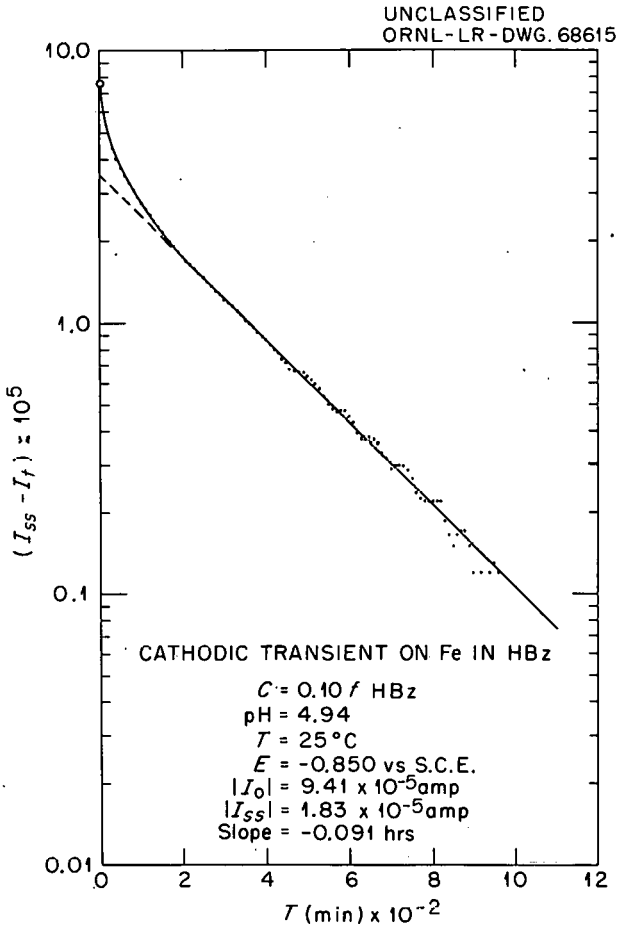

Fig. 7.6. Log $(i_{ss} - i_t)$ as a Function of Time for a Cathodic Transient on Iron in Benzoic Acid.

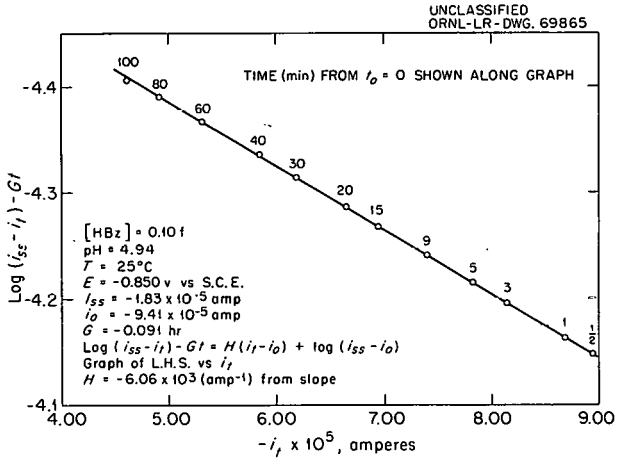

Fig. 7.7. Log $(i_{ss} - i_t) - Gt$ as a Function of $-i_t$ for a Cathodic Transient on Iron in Benzoic Acid.

the resulting straight line, H can be evaluated. With G and H determined, the entire current-time curve can be calculated by means of Eq. (9). The results for the first 100 min are given by the circles in Fig. 7.8. The experimental data are given by the curve which is essentially coincident with the circles. For comparison, the results calculated by means of Eq. (10) are shown by the lower curve. In summary, it has been shown that the experimental results can be interpreted [cf. Eq. (9)] on the basis of hydrogen penetration into the metal.

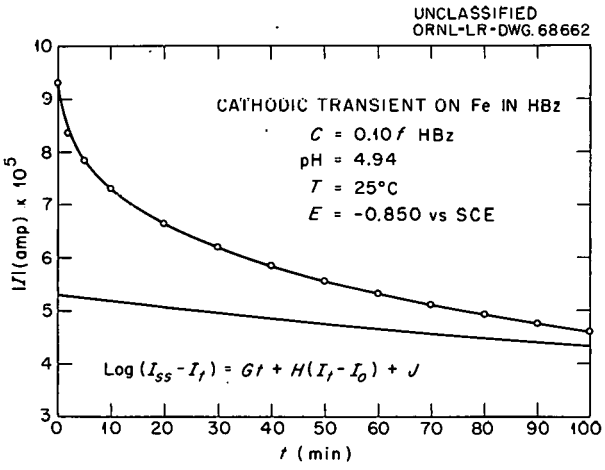

Fig. 7.8. Experimental and Calculated Curves of Current vs Time for a Cathodic Transient on Iron in Benzoic Acid.

Diffusion of Hydrogen Through an Iron Membrane. – On the basis of the model presented above, it can be shown that, at a fixed cathodic potential, the cathodic current density should decrease if θ increases. This hypothesis was tested directly by using an iron membrane electrode, rather than a cylindrical electrode as used in the previous studies. The iron membrane separated two complete electrochemical cells, the only contact between the two cells being via diffusion of atomic hydrogen through the membrane. One side of the membrane was set at a fixed cathodic potential until a steady state was attained. Then, hydrogen was cathodically generated on the opposite side of the membrane. The diffusion of the hydrogen to the side of the membrane under observation resulted in a decrease in the cathodic current at the fixed potential,

in accordance with the model. These preliminary observations suggest that a quantitative study of the behavior of an iron membrane electrode would add considerably to our knowledge of hydrogen penetration into iron, and its effects on the hydrogen-evolution and iron-dissolution reactions.

Electrochemistry of Zirconium

R. E. Meyer

Dissolution of Zirconium in HF. – Although it is well known that aqueous solutions of HF will dissolve zirconium at significant rates, the mechanism of this reaction is not clear. Using a tracer method of measuring dissolution rates, Smith and Hill[8] showed that the rate of dissolution of zirconium in various solutions containing HF was directly proportional to the concentration of undissociated HF and to no other species which contained fluorine, such as F^- or HF_2^-. Because they also found that the rate of dissolution depended on the stirring rate, they postulated that the reaction was limited by the rate of diffusion of undissociated HF to the metal surface. Since it is surprising that fluoride ion itself does not participate in the reaction, an investigation was undertaken to confirm this effect and to try to determine the electrochemical mechanism of dissolution.

Preliminary experiments showed that this reaction was at least partially under diffusion control as Smith and Hill had postulated, and that therefore the usual steady-state polarization methods of obtaining the dissolution rates and other kinetic constants could not be applied. Polarization measurements were therefore obtained by applying constant current pulses 50 to 100 msec in duration and recording the resulting potential variations with an oscilloscope. Potential traces were then extrapolated to zero time in order to obtain polarization data corresponding to the concentration gradients existing before the onset of polarization. Dissolution rates were then obtained either by extrapolation of the anodic or cathodic Tafel lines to the dissolution potential or by calculation from Eq. (1):[9]

$$i = \frac{\beta_a \beta_c (di_x/d\eta)_{\eta \to 0}}{(\beta_a + \beta_c)2.303} . \qquad (1)$$

Here, i is the dissolution rate, β_a and β_c are the anodic and cathodic Tafel slopes, respectively, i_x is the applied polarization current, and η is the overpotential. In comparison with tracer methods of measuring the rate, these electrochemical methods have the advantages of giving the instantaneous rate directly and of yielding additional kinetic data.

In order to compare rates of dissolution in different solutions, a cell was designed in which any of six Teflon cups could be quickly placed in position around the electrode assembly. Rates of dissolution in different solutions could therefore be compared before the electrode surface changed appreciably.

A typical determination of the dissolution rate and the Tafel slopes is shown in Fig. 7.9. The circled points represent external applied current. The true Tafel lines were calculated in the usual way from the relation that the external applied current at any one potential must equal the difference between the absolute values of the anodic and the cathodic current. The dissolution rate is determined by extrapolation of the linear sections of the plots of log current vs overpotential to zero overpotential.

Figure 7.10, a plot of log rate vs log concentration of undissociated HF, shows that the rates of dissolution are directly proportional to the HF concentration. By varying the pH, it was possible to vary the concentration of the fluoride ion. No relation was found between the rate of dissolution and the fluoride-ion concentration.

Weight-loss experiments, in which zirconium specimens were weighed before and after extended periods of dissolution, were also performed. During the dissolution period a large number of rate measurements were made using the method of Eq. (1), and the average rate was calculated. This average rate was then compared with the average rate determined by weight loss. Table 7.1 shows the results of these measurements. The table shows that the actual weight loss is greater than the weight loss calculated on the assumption that there are four equivalents per mole of zir-

[8] T. Smith and G. R. Hill, *J. Electrochem. Soc.* **105**, 117 (1958).

[9] For derivations and explanations of this equation see M. Stern and A. L. Geary, *J. Electrochem. Soc.* **104**, 56 (1957) and F. A. Posey, *Chem. Div. Ann. Progr. Rept. June 20, 1957*, ORNL-2386, p 110.

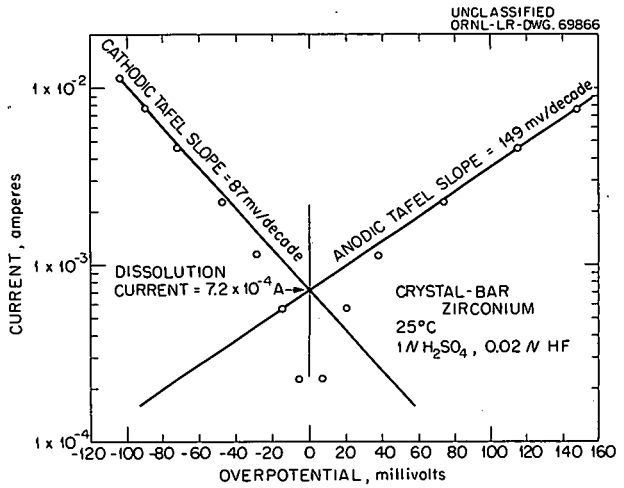

Fig. 7.9. Transient Current-Potential Relations on Zirconium Dissolving in Aqueous Solution Containing 0.02 *N* HF and 1 *N* H_2SO_4.

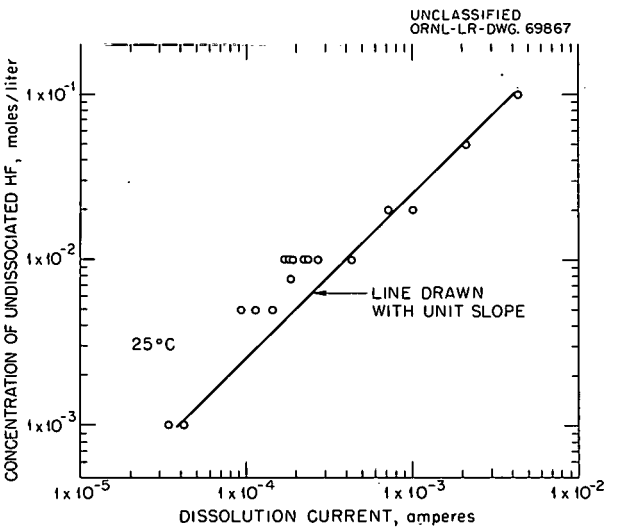

Fig. 7.10. Relation Between Dissolution Rate and Concentration of Undissociated HF in Aqueous HF-H_2SO_4 Solutions.

Table 7.1. Comparison of Weight-Loss and Electrochemical Methods of Measuring Dissolution Rates in Aqueous Solutions of HF and H_2SO_4

Run No.	Weight Loss (mg)	Average Rate of Dissolution (amp)	Duration of Run (sec)	Calculated Weight Loss (mg)	Effective Valence[a]
		$\times 10^{-4}$	$\times 10^{4}$		
1	7.0	8.4	2.52	5.0	2.86
2	5.9	7.43	2.61	4.6	3.12
3	7.1	10.2	2.52	6.1	3.42
4	7.6	9.0	2.52	5.4	2.83
5	3.4	3.3	2.52	2.0	2.32
6	7.5	8.1	2.59	5.0	2.65
7	7.5	8.45	2.70	5.4	2.88
				Av	2.87

[a] Average deviation from 3.0: 0.28.

conium, as one would expect from the normal valence of four. Agreement is obtained, as shown by the last column, if it is assumed that there are three equivalents per mole in the dissolving species. It should be noted that it is not uncommon for a metal to dissolve with an effective charge number less than the normal one. There are generally two ways in which this effect may be explained. Either the mechanism actually involves transfer of an ion of lower valence, with

immediate further oxidation in the solution, or the solvent tends to undercut the metal, removing "chunks" of metal which later dissolve without electrical contact with the bulk of the metal. The effective valence obtained if the latter effect ("chunk" effect) operates should vary with changing surface conditions, and experiments are being conducted to test this possibility.

Anodic Tafel slopes tended to increase with lower rates of dissolution. Further, oscillatory phenomena were noted during long-term anodic polarization. Both of these phenomena are characteristic of film-covered surfaces; therefore the possibility exists that the dissolution of zirconium proceeds through the continuous formation and dissolution of an oxide film. Further experimentation is planned to test this postulate.

The cathodic reaction during dissolution is the reduction of hydrogen ions. Measurements of the cathodic Tafel lines as a function of pH showed that the reaction is first-order with respect to hydrogen ion and that the Tafel slopes varied from 80 to 130 mv per decade; both observations are normal for hydrogen overvoltage on metals.

Studies on Passive Zirconium. – The investigation of the effects of films on reduction processes on film-covered electrodes is made difficult by the absence of reliable methods of measuring the thickness of thin films in the experimental cell. For this reason, the capacity of passive zirconium was investigated as a possible means of determining at least relative film thickness. Since there is no absolute way of determining film thickness under the desired conditions, it is possible only to compare various indirect methods. A series of experiments was therefore conducted to compare the thickness calculated from a fast-pulse method of measuring the capacity with the thickness calculated from the total charge passed in galvanostatic or potentiostatic experiments. Experiments performed so far indicate that, in the early stages of the formation of the film, there is good correspondence between thicknesses calculated by the two methods. In the later stages of film formation this relation is not valid. These experiments appear promising, and further work is planned.

Passivity and Transpassivity in Iron and Ferrous Alloys

F. A. Posey

The existence of a passive state on iron and ferrous alloys in contact with a solution is one of the most important characteristics of this metal and its alloys. On the other hand, no comprehensive treatment of kinetics of the passive state has been available to assist in understanding the diverse phenomena which have been observed on passive electrodes. In an effort to contribute to the solution of this classical problem in electrochemical kinetics, a model was developed on the bases of well-known laws of electrode processes and of certain concepts of semiconductor theory. Some aspects of the model are presented below and discussed in relation to experimental observations.

Comprehensive reviews are available[10-13] which discuss recent experimental findings on passive iron. According to the consensus of opinion, the passivity of iron in contact with an acid solution is due to the presence of a thin, pore-free oxide layer which forms at a definite electrode potential, known as the Flade potential.[14-15] Over a potential range of approximately 1 v positive to the Flade potential, the corrosion rate of iron is independent of the electrode potential,[16] ferric ions are produced in solution, and the logarithm of the corrosion rate varies directly with pH.[17] The passive layer is a good electronic but a poor ionic conductor.[18-19] At sufficiently

[10] K. F. Bonhoeffer, p 210 in *Soviet Electrochem., Proc. Conf. Electrochem. (English Translation) 4th, Moscow, 1956*, Consultants Bureau, New York, 1961.

[11] K. G. Weil, *Z. Elektrochem.* **62**, 638 (1958).

[12] L. Young, *Anodic Oxide Films*, p 227, Academic Press, New York, 1961.

[13] K. J. Vetter, *Elektrochemische Kinetik*, p 602, Springer-Verlag, Berlin, 1961.

[14] F. Flade, *Z. Physik. Chem. (Leipzig)* **76**, 513 (1911).

[15] U. F. Franck, *Z. Naturforsch.* **4a**, 378 (1949).

[16] U. F. Franck and K. Weil, *Z. Elektrochem.* **56**, 814 (1952).

[17] K. J. Vetter, *Z. Elektrochem.* **59**, 67 (1955).

[18] K. J. Vetter, *Z. Elektrochem.* **55**, 274 (1951).

[19] K. J. Vetter, *Z. Physik. Chem. (Leipzig)* **202**, 1 (1953).

high electrode potentials, corrosion current is no longer independent of, but increases exponentially with, potential; this is the region of transpassivity. At constant potential in the transpassive region, the logarithm of corrosion current varies linearly with pH, but in a direction opposite to the variation in the passive region.[20] The thickness of the oxide layer increases linearly with potential above the Flade potential, at least up to the transpassive region.[21-22] All applied anodic current in excess of the corrosion current in the passive region forms an equivalent amount of oxide; growth of the oxide is responsible for characteristic current-time transients observed when electrode potential is suddenly changed in potentiostatic experiments and for anodization under galvanostatic conditions.

The semiconducting nature of the transition-metal oxides is well established, and recent reviews[23-25] on semiconductor electrode kinetics suggest the need for application of semiconductor theory to the passive state on metals. The present treatment assumes the validity of certain kinetic laws for the transport of particles in a semiconducting lattice under the influence of an electric field. The transport equations and Poisson's equation are solved for a particular quasi-equilibrium situation to give the distributions of potential and concentration in the passive layer. Finally, with the aid of boundary conditions derived from assumed mechanisms and the formalism of electrochemical kinetics, expressions are developed for several properties of the passive and transpassive states.

Examination of transport equations[26-28] for the net flux of ions across a series of potential-energy barriers in the presence of an electric field shows that, for high fields, the flux of positive particles may be expressed by

$$v^+(x) = k^+ C^+(x) \exp\left[\frac{\alpha^+ z^+ \mathfrak{F}}{RT}(\delta x)\cdot E(x)\right], \qquad (1)$$

where $v^+(x)$ and $C^+(x)$ are the flux and (volume) concentration of positive ions, k^+ is a rate constant, z^+ is the particle charge, (δx) is the thickness of the barrier of symmetry factor α^+, $E(x)$ is the electric field, and $RT/\mathfrak{F} \equiv kT/e_0$ is the thermal volt equivalent. An analogous equation holds for the flux of negative ions. For the high-field case, there is no significant back reaction and, therefore, no important concentration gradient of positive ions (or, similarly, of negative ions). In order to obtain results consistent with experiment, the quasi-equilibrium assumption must be made that the distribution of electrons in the passive oxide lattice is essentially undisturbed by the electron flux due to reactions occurring at the oxide-solution interface. This approximation leads to the classical nondegenerate Boltzmann distribution

$$n(x) = n(0) \exp\left[-\frac{F}{RT}\Delta\phi(x)\right], \qquad (2)$$

where $\Delta\phi(x) \equiv \phi(0) - \phi(x)$ is the difference between the Galvani potential at the inner surface of the passive layer and the potential at the point x, and $n(x)$ is electron concentration.

The distribution of potential in the passive layer is calculated from Poisson's equation,

$$\nabla^2\phi(x) = -\frac{e_0}{\epsilon\epsilon_0}\left[C^+(x) - C^-(x) + p(x) - n(x)\right], \qquad (3)$$

together with Eq. (2) and certain assumptions. In Eq. (3), ϵ is the relative dielectric constant, ϵ_0 is the permittivity of free space in the rationalized *MKSA* system, and $C^+(x)$, $C^-(x)$, $p(x)$, and

[20] K. G. Weil and K. F. Bonhoeffer, *Z. Physik. Chem. (Frankfurt)* **4**, 175 (1955).

[21] K. J. Vetter, *Z. Elektrochem.* **58**, 230 (1954).

[22] K. J. Vetter, *Z. Elektrochem.* **62**, 642 (1958).

[23] M. Green, p 343 in *Modern Aspects of Electrochemistry*, vol 2, ed. by J. O'M. Bockris, Butterworths, London, 1959.

[24] J. F. Dewald, p 727 in *Semiconductors*, ed. by N. B. Hannay, ACS Monograph No. 140, Reinhold, New York, 1959.

[25] H. Gerischer, p 139 in *Advances in Electrochemistry and Electrochemical Engineering*, vol 1, ed. by P. Delahay, Interscience, New York, 1961.

[26] A. Guntherschulze and H. Betz, *Z. Physik.* **91**, 70 (1934); **92**, 367 (1934).

[27] E. J. W. Verwey, *Physica* **2**, 1059 (1935).

[28] N. Cabrera and N. F. Mott, *Rept. Progr. Phys.* **12**, 163 (1949).

$n(x)$ are concentrations of positive ions, negative ions, holes, and electrons, respectively. On the assumption of essentially complete electroneutrality with respect to lattice ions, so that $C^+(x) \cong C^-(x)$, and on restriction of the calculation to the region where $n(x) >> p(x)$, Eqs. (2) and (3) may be solved for the potential distribution of

$$\Delta\phi(x) = \frac{2RT}{F} \ln \left[\cosh(\xi x) + \sqrt{Q} \cdot \sinh(\xi x)\right] . \quad (4)$$

In Eq. (4), $\xi = (\beta/2)\sqrt{C}$, and $Q = (1 + C)/C$, where

$$\beta = \sqrt{2 \frac{n(0) e_0 F}{\epsilon\epsilon_0 RT}}$$

and

$$C = \left(\frac{E(0)\, F}{\beta RT}\right)^2 - 1 ,$$

while $E(0)$, the field at $x = 0$, follows from Gauss's law as $E(0) = \sigma_M/\epsilon\epsilon_0$, where σ_M is the surface charge density on the metal side of the metal-oxide interface. For the high-field approximation of interest here, and in particular for the case of large $E(0)/n(0)$, Eq. (4) reduces to the simple form

$$\Delta\phi(x) = E(0) \cdot x . \quad (5)$$

The potential changes linearly with distance in the passive layer, and electrons are distributed exponentially with distance in a field determined largely by the excess charges on the metal and solution sides of the interface.

In order to approximate the experimental behavior of the passive iron system, several additional relations must be postulated. It may be assumed that electron transfer between the metal and the oxide layer is fast, and that this electronic equilibrium poises the potential difference, $\Delta\phi_M$, of the interface between metal and oxide. The equilibrium condition is given by

$$n(0) = n(M) \exp\left(+\frac{\Delta\mu_e^0}{RT} - \frac{F}{RT}\Delta\phi_M\right), \quad (6)$$

where $n(M)$ is the electron concentration in the metal and $\Delta\mu_e^0$ is the difference in the standard chemical potential of electrons in the two phases.

In addition, a rapid exchange of oxygen species between oxide layer and solution poises the potential difference, $\Delta\phi_s$, between the passive film and the solution. The overall stiochiometry of this process is expressed by $OH^-(aq) = O^{2-}(\text{lattice}) + H^+(aq)$, and the equilibrium condition is given by

$$\exp\left(+\frac{F}{RT}\Delta\phi_s\right) = \left(\frac{k_0^-\, C^-(l)}{k_s^-\, C_{OH^-}}\right), \quad (7)$$

where k_0^- and k_s^- are rate constants for the forward and reverse steps of the process, $C^-(l)$ is the concentration of negative lattice ions at the outer interface (at $x = l$, where l is oxide-layer thickness), and $C_{OH^-} \equiv [OH^-]$ is hydroxide-ion concentration in solution. To account for the existence of the transpassive region, two parallel reaction paths for dissolution of metallic ions at the oxide-solution interface may be assumed; both depend on the potential difference $\Delta\phi_s$ (which is constant because it is poised by the oxygen-exchange equilibrium), but one depends on the concentration of holes, $p(l)$, at the surface of the layer. The overall flux of the dissolution process is given by

$$v_+ = k_s^+\, C^+(l) \exp\left(+\frac{\alpha_s^+ z_s^+ F}{RT}\Delta\phi_s\right) + k_p^+\, C^+(l)\, p(l) \exp\left(+\frac{\alpha_p^+ z_p^+ F}{RT}\Delta\phi_s\right), \quad (8)$$

where k_s^+ and k_p^+ are rate constants, and $C^+(l)$ is the concentration of lattice cations at $x = l$. The presence of a hole means that one of the chemical bonds in the lattice is weakened, and this increases the probability of the associated anodic reaction. In the event that a significant concentration, C_s, of reducible species is present in solution, the flux of electrons across the oxide-solution interface because of the cathodic reaction is given by

$$v_e = k_c\, C_s \cdot n(l) \exp\left(-\frac{\alpha_c z_c F}{RT}\Delta\phi_s\right) , \quad (9)$$

where k_c is the rate constant of the cathodic process.

The net flux across the entire interface is given by $v_N = v_+ - v_e$ (the difference in the fluxes of

anodic and cathodic processes), the overall interfacial potential difference, $\Delta\phi_T$, is given by $\Delta\phi_T = \Delta\phi_M + \Delta\phi(l) + \Delta\phi_s$, and $C^+(0) = C^+(l) = C^+$ and $C^-(0) = C^-(l) = C^-$ because of the absence of a concentration gradient of lattice ions in the high field. The preceding equations may be combined, using the well-known relation $n(x) \cdot p(x) = n_i^2$ for the product of hole and electron concentrations, to give

$$v_N = k_s^+ C^+ \left(\frac{k_0^- C^-}{k_s^- C_{OH^-}}\right)^{\alpha_s^+ z_s^+} + \left[\frac{k_p^+ C^+ n_i^2}{n(M)\exp\left(+\frac{\Delta\mu_e^0}{RT}\right)}\left(\frac{k_0^- C^-}{k_s^- C_{OH^-}}\right)^{(\alpha_p^+ z_p^+ - 1)}\right]\exp\left(+\frac{F}{RT}\Delta\phi_T\right)$$
$$- k_c C_s \left(\frac{k_0^- C^-}{k_s^- C_{OH^-}}\right)^{(1-\alpha_c z_c)} \left[n(M)\exp\left(+\frac{\Delta\mu_e^0}{RT}\right)\exp\left(-\frac{F}{RT}\Delta\phi_T\right)\right]. \quad (10)$$

The predictions of this expression coincide closely with experimental observations on passive iron. In the absence of a significant cathodic process, the net flux of current is essentially equal to the corrosion rate, which is given by the first two terms in Eq. (10). At low potentials, the second term is unimportant, and the corrosion rate is given by the potential-independent first term in the equation; this term corresponds to the corrosion rate in the passive region. The corrosion rate in the passive region increases with acidity according to the proper functional relationship, and the exponent $\alpha_s^+ z_s^+$ has a theoretical value which is close to that found experimentally.[17] At higher potentials, the second term in Eq. (10) begins to contribute significantly to the corrosion rate; this term represents the hole-catalyzed corrosion rate in the transpassive state. The exponent $\alpha_p^+ z_p^+ - 1$, for the reasonable assumption that $\alpha_p^+ z_p^+ \simeq \alpha_s^+ z_s^+$, is a negative quantity such that the corrosion rate decreases with acidity at constant potential in the transpassive region, as found experimentally.[20] Oxygen evolution also occurs on passive iron in the transpassive region,[16] and probably proceeds by a hole mechanism. In this case, Eq. (10) would contain an additional potential-dependent term corresponding to the anodic reaction of oxygen evolution.

The course of potentiostatic and galvanostatic transients on passive iron may be calculated from Eqs. (1) and (8) together with certain differential relations and conversion factors relating excess anodic current to the change in the oxide-layer thickness. The forms of calculated and experimental transients agree well. Eqs. (4) and (5) show that $\Delta\phi(l)$ approaches zero as the thickness of the passive layer approaches zero. If the Flade potential, $\Delta\phi_F$, represents the lower limit of existence of the oxide layer, the present quasi-equilibrium model predicts, on the basis of Eqs. (6) and (7), that the overall interfacial potential difference in this limit is given by Eq. (11). Because the corrosion reaction,

$$\Delta\phi_F \equiv \Delta\phi_T(l \to 0) = \frac{\Delta\mu_e^0}{F} + \frac{RT}{F}\ln\frac{n(M)\, k_0^- C^-}{n(0)\, k_s^- C_{OH^-}}, \quad (11)$$

still proceeds with the finite rate given by the first term of Eq. (10) even in the limit, this potential does not have thermodynamic significance with respect to stoichiometric reactions of iron and its oxides. Since $C_{OH^-} \equiv [OH^-] = K_w/[H^+]$, where K_w is the ionization constant of water, Eq. (11) predicts an RT/F dependence of the Flade potential on pH, as found experimentally.[15]

Because of the assumptions necessary to obtain expressions which reproduce the behavior of passive iron, the model presented above is restricted in applicability to passive systems generally. However, the method of approach is capable of extension to more sophisticated situations. Specific adsorption of anions and inhibitors undoubtedly changes energy levels of surface states at the oxide-solution interface, and these changes exert important effects on the distributions of particles and on reaction kinetics. Such effects are not included in the present model, and further studies will explore the consequences of including these and other factors in the theory.

The Differential Capacity of the Electrical Double Layer on Electrolytic Iron in Neutral and Acid Solutions

D. H. Spahrbier[29] F. A. Posey

The corrosion of iron in sulfuric acid solution is inhibited by the addition of halide ions.[30-33] The effectiveness of the inhibition increases in the sequence, $Cl^- < Br^- < I^-$. Studies on transient and steady-state polarization characteristics of iron in the presence of iodide ions, as well as direct measurements using radioactive tracers, have suggested that specific adsorption of the halide ion is involved in the mechanism of inhibition.[34-36] Since the structure of the electrical double layer is sensitive to specific adsorption of anions, measurements of the differential capacity of iron were made in order to provide additional information on the nature of the inhibition.

Electrolytic iron, deposited on platinum wires from concentrated $FeCl_2$ solution by a modification of the method of Brauer,[37] was used as the electrode material. Studies were carried out in solutions of the anions, Cl^-, Br^-, I^-, and SO_4^{2-}. Differential capacities were measured by use of a pulse technique. Rectangular current pulses 100 μsec in duration were obtained by use of a special circuit employing a fast potentiostat ("Wenking elektronischerpotentiostat") and a Tektronix pulse generator. The potential-time transient obtained on application of the current pulse was observed on a Tektronix type 536 oscilloscope and recorded photographically. Differential capacities were calculated from the experimental observations by use of

$$C_{diff} = \frac{j_{pulse}}{(dV/dt)_{t\to 0}}, \qquad (1)$$

where C_{diff} is differential capacity, j_{pulse} is the current density of the pulse, and $(dV/dt)_{t\to 0}$ is the initial slope of the potential-time transient.

Figure 7.11 shows the variation of electrode potential and differential capacity with time for unpolarized iron electrodes in acid solutions of the anions of interest. In part, increases of capacity with time are associated with increases in surface area because of corrosion, as shown by electron microscopic examination. In general, values of differential capacity decrease in the sequence, $H_2SO_4 > HCl > HBr > HI$; the inhibiting effect of the anions increases in the same sequence. Many hours, or even days, are required for the attainment of steady states.

The results in Fig. 7.12 show that the electrode potential and differential capacity of unpolarized iron are nearly independent of the identity of the anion in neutral solutions. Specific differences

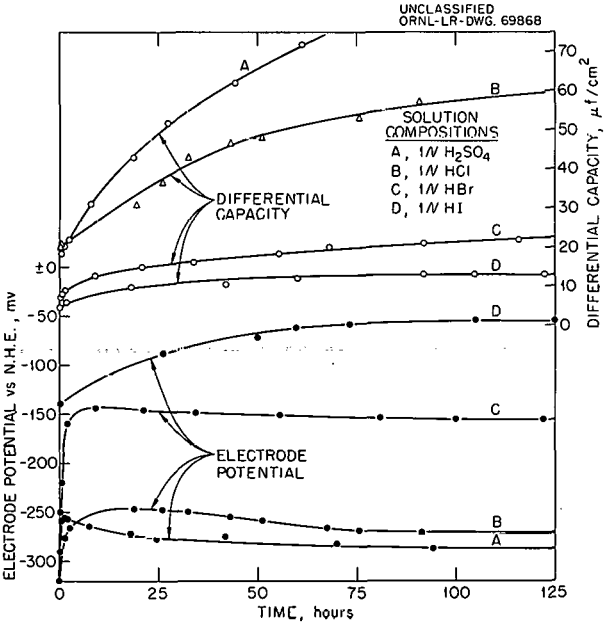

Fig. 7.11. Time Variation of Differential Capacity and Electrode Potential of Electrolytic Iron in Acidic Solutions; $T = 25^\circ C$; Helium Atmosphere.

[29] Present address: Frankfurt, Germany.

[30] G. Walpert, *Z. Physik. Chem.* **A151**, 219 (1930).

[31] M. Tzentnerohver and M. Straumanis, *Z. Physik. Chem. (Leipzig)* **A162**, 94 (1932).

[32] Z. A. Iofa and L. A. Medvedeva, *Dokl. Akad. Nauk SSSR* **69**, 213 (1949).

[33] Z. A. Iofa and G. B. Rozhdestvenskaya, *Dokl. Akad. Nauk SSSR* **91**, 1159 (1953).

[34] K. E. Heusler, *Chem. Div. Ann. Progr. Rept. June 20, 1959*, ORNL-2782, p 52.

[35] K. E. Heusler, *Chem. Div. Ann. Progr. Rept. June 20, 1960*, ORNL-2983, p 58.

[36] K. E. Heusler and G. H. Cartledge, *J. Electrochem. Soc.* **108**, 732 (1961).

[37] G. Brauer, *Handbuch der Präparativen Anorganischen Chemie*, p 1112, Ferdinand Enke Verlag, Stuttgart, 1959.

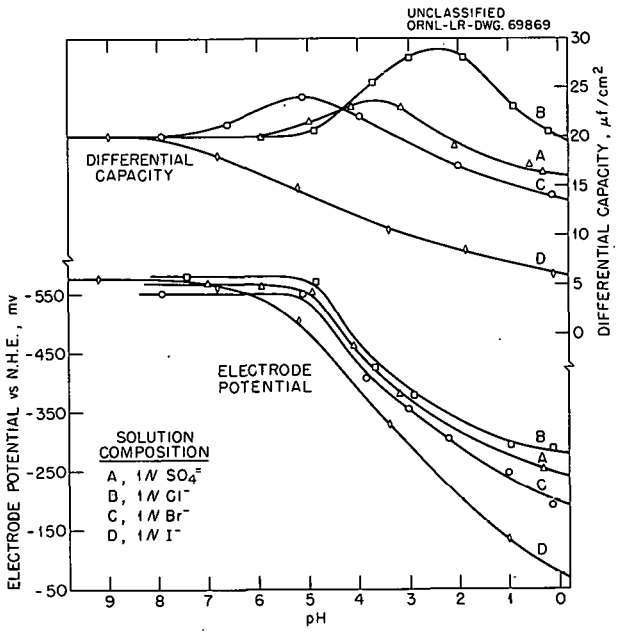

Fig. 7.12. Variation of Differential Capacity and Electrode Potential of Electrolytic Iron with Acidity as a Function of the Anion; T = 25°C; Helium Atmosphere.

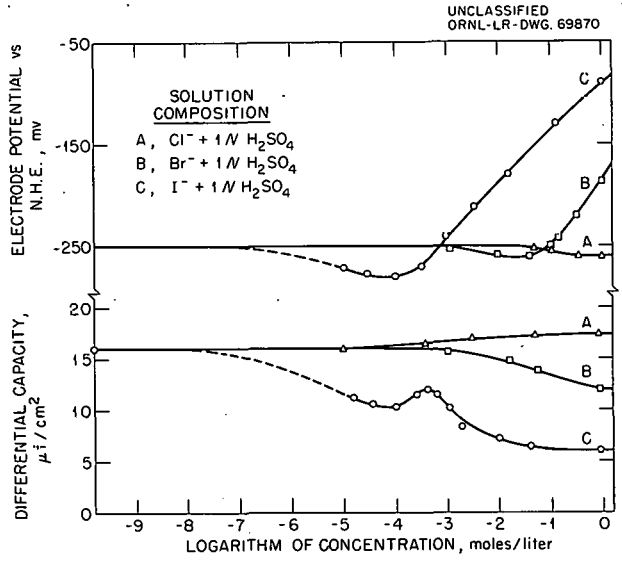

Fig. 7.13. Variation of Differential Capacity and Electrode Potential of Electrolytic Iron in 1 N H_2SO_4 with Halide-Ion Concentration; T = 25°C; Helium Atmosphere.

arise, however, when the solution is made more acidic. The variation of electrode potential with pH is similar for all the anions, while unique differences exist in the behavior of the capacity. At constant acidity (1 N H_2SO_4), the electrode potential and differential capacity of unpolarized iron change in characteristic fashion with halide ion concentration, as shown by the experimental results in Fig. 7.13. The electrode potential curves are quite similar for all three anions, but the behavior of the capacity depends markedly on the nature of the anion.

The effect of additions of iodide ion on the differential capacity of electrolytic iron in 1 N H_2SO_4 is shown in Fig. 7.14 as a function of electrode potential. In the absence of iodide ions, the corrosion rate is large, and the potential region accessible for measurements of capacity is limited by the current capacity of the apparatus; this

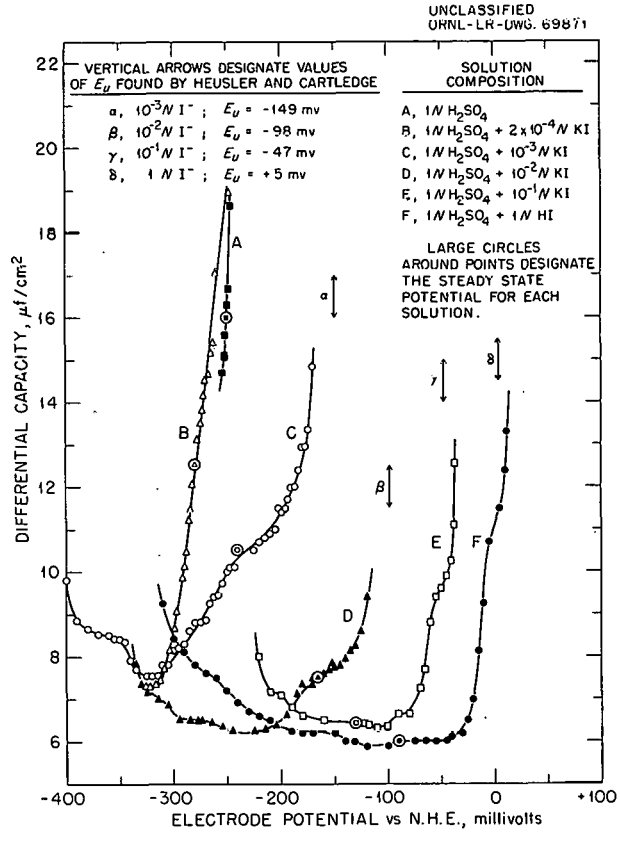

Fig. 7.14. Differential Capacity of Electrolytic Iron in 1 N H_2SO_4 as a Function of Electrode Potential and Iodide Ion Concentration; T = 25°C; Helium Atmosphere.

region increases considerably in the presence of iodide ions. At low iodide-ion concentrations, a sharp minimum of capacity is observed in the vicinity of −320 mv vs N. H. E.; this potential is approximately 50 mv positive to the potential of the electrocapillary maximum on iron in H_2SO_4.[38] For higher iodide concentrations, the width of the minimum increases, and the minimum capacity becomes lower. Low capacities of the order of magnitude observed here are associated with specific adsorption of anions, in this case I^-, as observed frequently in other systems.[39–41] Corresponding to each iodide-ion concentration, the capacity increases sharply on the anodic side of the minimum; this rise marks the beginning of a peak in capacity due to the desorption of iodide ions from the electrode surface. The vertical arrows in Fig. 7.14 show the positions of the "potential of unpolarizability" (E_u) observed by Heusler and Cartledge[36] in the anodic polarization curve of iron inhibited by iodide ions. These authors postulated that iodide ions, which are responsible for inhibition at potentials below E_u, are desorbed by an electrochemical corrosion mechanism at E_u. The present measurements confirm this interpretation; values of E_u correspond closely to the beginning of the desorption peaks.

---

[38] E. Ajasjan, *Dokl. Akad. Nauk SSSR* **100**, 473 (1955).

[39] D. C. Grahame, *Chem. Rev.* **41**, 441 (1947).

[40] A. Frumkin, Z. *Elektrochem.* **59**, 807 (1955).

[41] R. Parsons, p 1 in *Advances in Electrochemistry and Electrochemical Engineering*, vol 1, ed. by P. Delahay, Interscience, New York, 1961.

8. Nonaqueous Systems at High Temperature

Electrical Conductivity of Solutions of Metals in Their Molten Halides

H. R. Bronstein A. S. Dworkin
M. A. Bredig

The study of the electrical conductivity of metal solutions in molten salts continued to yield results that can be interpreted in terms of a variety of electronic and molecular structures.

Praseodymium in Praseodymium Trichloride.[1] – Figure 8.1 shows the behavior of Pr solutions to be, as expected from the phase diagram,[2] intermediate between that of La (or Ce) and Nd solutions, discussed previously.[3] The dissolution of La (or Ce) and of Nd in their trihalides may be represented by the two very different mechanisms, $La \rightarrow La^{3+} + 3e^-$ and $Nd + 2Nd^{3+} \rightarrow 3Nd^{2+}$, respectively. The mechanism in the case of Pr is likely to be a mixed one – in other words, to correspond to an equilibrium $Pr^{2+} \rightleftharpoons Pr^{3+} + e^-$ or to a stability of the Pr^{2+} ion intermediate between the unstable La^{2+} and the stable Nd^{2+}.

The specific conductivity of molten $PrCl_3$ between 800 and 860°C is given by the equation $\kappa = -1.189 + 0.75 \times 10^{-3} t$.

Rare-Earth Metals in Rare-Earth Triiodides.[4] – Figure 8.2 shows the specific conductivity in the systems La-LaI_3, Ce-CeI_3, Pr-PrI_3, and Nd-NdI_3. As in the chloride systems, Pr occupies an intermediate position but resembles somewhat more La and Ce than Nd. This is in agreement with the results of a study of the phase diagrams, in which the formation of a metallic solid PrI_2

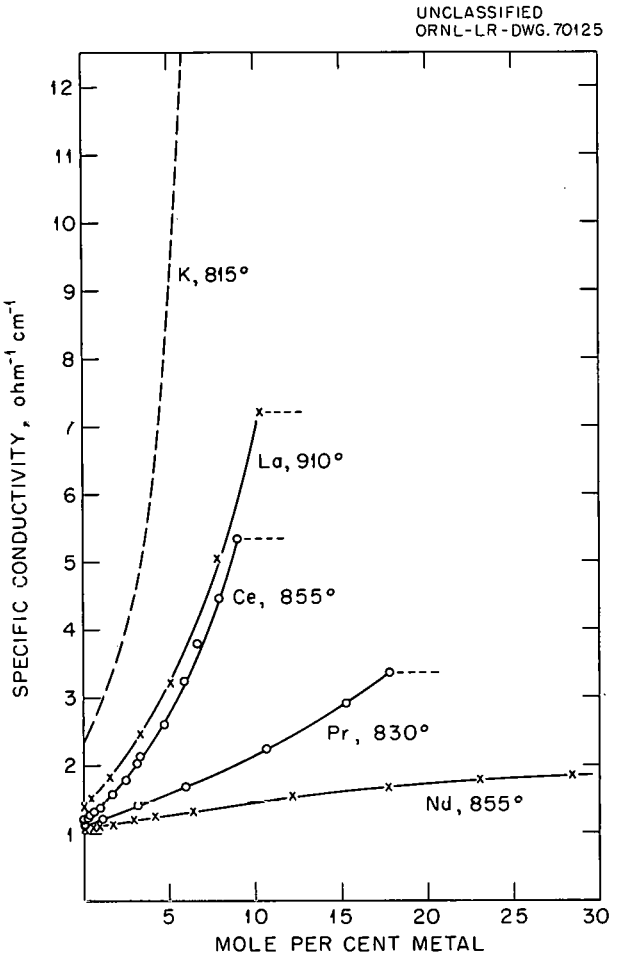

Fig. 8.1. Specific Conductivity of Solutions of Rare-Earth Metals in Their Molten Trichlorides, as Compared with K in KCl.

[1] Summary of paper by A. S. Dworkin, H. R. Bronstein, and M. A. Bredig, *J. Phys. Chem.* **66**, 1201 (1962).

[2] J. D. Corbett and associates, Ames Laboratory, private communication.

[3] A. S. Dworkin, H. R. Bronstein, and M. A. Bredig, *Discussions Faraday Soc.* **32**, 188 (1961).

[4] Work done at ORNL in cooperation with J. D. Corbett and R. Sallach of the Ames Laboratory.

similar to metallic LaI_2 and CeI_2, and distinct from nonmetallic NdI_2, has been established.[5]

If one considers that the equivalent volumes of the rare-earth metal solutions are not very different from that of K-KI, then Fig. 8.2 also implies that the equivalent conductance of the metal in the rare-earth systems is much smaller than in the K-KI system. This difference can be interpreted semiquantitatively if it is assumed that electronic conductance in metal–molten salts solutions is proportional not only to the concentration of mobile electrons but also to the concentration of the cations between which the electrons are being exchanged.[6] One equivalent of rare-earth metal–salt solution contains only one-third the number of cations that one equivalent of a solution of K in KI of equal metal concentration contains.

With the entropies of fusion discussed in another section of this chapter (see "The Heat of Fusion of Alkaline-Earth and Rare-Earth Metal Halides"), the melting-point depressions produced by small additions of rare-earth metals to the corresponding trihalides (taken from the M-MX_3 phase diagrams of Corbett and co-workers, Ames Laboratory) can be used to derive values of n in the formula

$$n = \frac{\Delta S_m}{RT_m} \cdot \frac{T_m - T}{N_{\text{solute}}},$$

representing the number of moles of foreign particles produced in the solution (molten trihalide) by one mole of the solute (metal). This number n was found to have the values 2.45 and 2.65 for the $LaCl_3$-La and $CeCl_3$-Ce systems, and 3.1 and 3.0 for the $PrCl_3$-Pr and $NdCl_3$-Nd systems. In the latter, $n \approx 3$ results from the dissolution reaction $1M + 2M^{3+} \rightarrow 3M^{2+}$. In the former two systems, the conductivity measurements indicate $1M \rightarrow M^{3+} + 3e^-$, also requiring $n = 3$. The deviation in n from 3, conceivably due to the formation of solid solutions of La and Ce metals in their trichlorides, needs further examination. In the iodide systems, n also approximates 3 at infinite dilution of the metal.

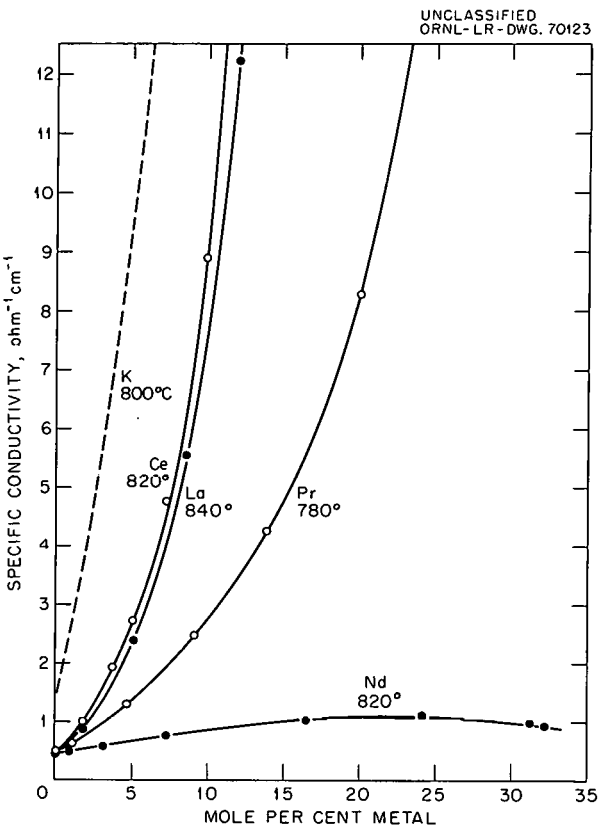

Fig. 8.2. Specific Conductivity of Solutions of Rare-Earth Metals in Their Molten Triiodides, as Compared with K in KI.

Electron Exchange in Molten Mixtures of Divalent and Trivalent Rare-Earth Halides. – A positive deviation from additivity in the conductance of mixtures of $NdCl_3$ with $NdCl_2$ had been tentatively interpreted[3] as reflecting an electronic contribution from an electron exchange between Nd^{2+} and Nd^{3+} ions (with a maximum in that contribution at 50 mole %) corresponding to proportionality of the deviation effect to the product of the concentrations of the two ions,

$$N_{Nd^{2+}} \times (1 - N_{Nd^{2+}}).$$

To further examine this effect and its interpretation, the system NdI_3-NdI_2 was studied, where greater polarizability of the iodide was expected to facilitate such an exchange. Indeed, the positive deviation was found to be enhanced to the extent of yielding a maximum in the curve of specific conductance vs composition. However,

[5] J. D. Corbett *et al.*, *Discussions Faraday Soc.* **32**, 79 (1962).

[6] M. A. Bredig, *Journal of Chemical Physics*, in press (July 1962).

a few cases of positive deviation in systems with assuredly merely ionic conductance are known ($MgCl_2$ with $CaCl_2$ or $BaCl_2$, and $CdCl_2$ with $PbCl_2$). Thus it seemed necessary to support the electronic explanation for NdX_3-NdX_2 by evidence showing that systems NdX_3-MX_2 containing an ion M in size similar to Nd^{2+}, such as Sr^{2+}, but incapable of supplying an electron to Nd^{3+} do *not* exhibit a positive deviation from additivity. Figure 8.3 demonstrates that this is indeed the case for the systems $NdCl_3$-$SrCl_2$ and NdI_3-SrI_2, and thus may be considered as at least indirect support for the assumption of a small electron-exchange contribution to the otherwise ionic conduction in the NdX_3-NdX_2 systems.

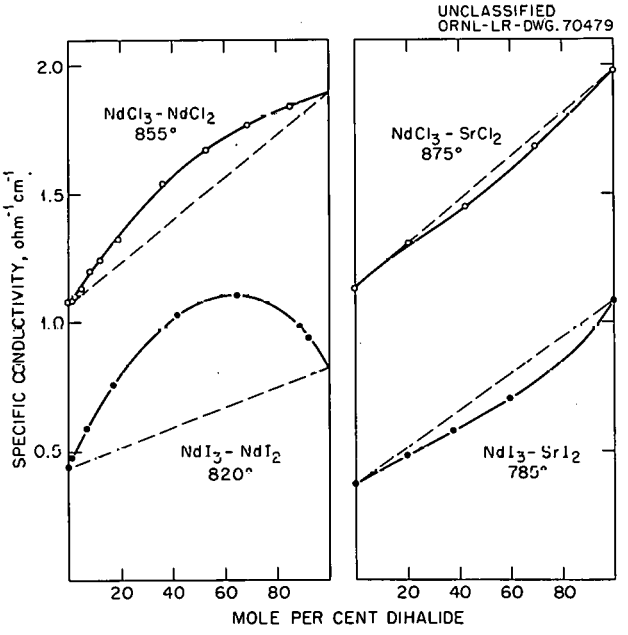

Fig. 8.3. Specific Conductivity in NdX_3-NdX_2 and NdX_3-SrX_2 Melts.

Alkaline-Earth Metals in Alkaline-Earth Dihalides. – The decreasing rate of increase in conductivity on addition of calcium metal to molten calcium chloride had been interpreted in terms of the increasing pairing of electrons with increasing metal concentration to form Ca_2^{2+} ions,[3] analogous to Na_2 molecules assumed previously in the Na-NaX systems. Similar observations are reported in Fig. 8.4 for the systems

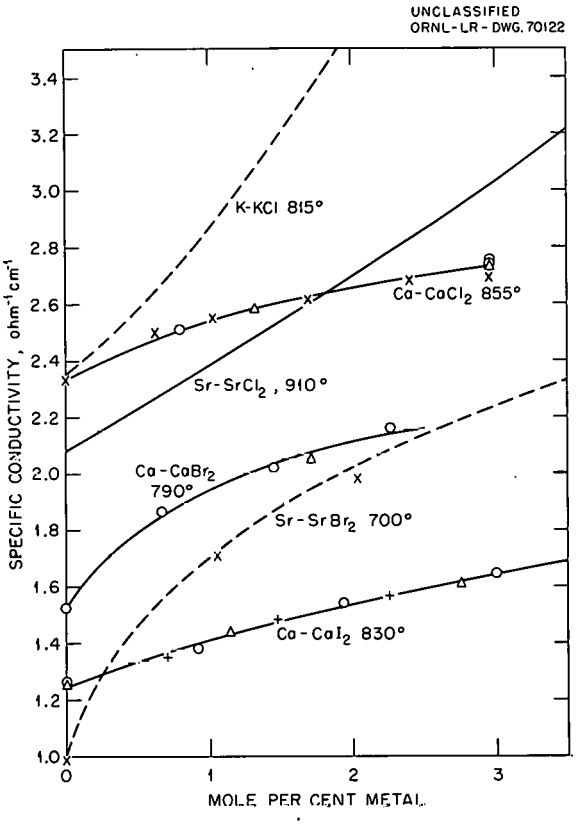

Fig. 8.4. Specific Conductivity of Solutions of Alkaline-Earth Metals in Their Molten Dihalides, as Compared with K in KCl.

Ca-$CaBr_2$, Ca-CaI_2, and Sr-$SrBr_2$. The much stronger curvature for the latter solutions at 700° compared with that for Sr-$SrCl_2$ at 910° may be due to the greater stability of Sr_2^{2+} ions at lower temperature. However, confirmation of these results may be required, because a slight instability that developed during the latest measurements needs further study.

The assumption of electron pairing with increasing metal concentration implies that at moderate concentrations the molecule ions do not contribute electronic conductance. It also implies that at infinite dilution or at low concentration the dissolved alkaline-earth metal is dissociated according to $M \rightarrow M^{2+} + 2e^-$, giving a cryoscopic $n = 2$. According to measurements, at both ORNL and the Imperial College, London,[7] of the depression of the melting point of $CaCl_2$ by Ca, in

[7] L. Staffansson, J. W. Tomlinson, and F. D. Richardson, personal communication (Ph.D. thesis).

conjunction with the calorimetric entropy of fusion of $CaCl_2$, n is indeed near 2. It was thought[3] to be also indicated by the liquidus data[7] in the case of $SrCl_2$-Sr, but an erroneous entropy of fusion of 7 eu was used for $SrCl_2$. To again reconcile the theory that $n = 2$, for $Sr \rightarrow Sr^{2+} + 2e^-$, with the new, calorimetrically measured, much lower entropy value of 3.39 eu, it seems necessary to connect the observed melting-point depression with the possible formation of solid solutions of Sr in $SrCl_2$. $SrCl_2$ possesses the CaF_2 type of crystal structure. Both CaF_2 and $SrCl_2$ have actually been reported[8] to dissolve large amounts of metal in solid solution at high temperatures. If confirmed, this would permit interpretation of the melting-point depressions of CaF_2 and $SrCl_2$ by low concentrations of metal in terms, also, of the ionization of the dissolved metal according to $M \rightarrow M^{2+} + 2e^-$, rather than in terms of M_2^{2+} molecule ions.[9]

Electrical Conductivity and Formation of Complex Ions in Cadmium-Potassium Chloride Melts

H. R. Bronstein M. A. Bredig

Electrical conductivity has been used among other properties as a criterion for the formation of complex ions in ionic melts. In $CdCl_2$-KCl mixtures, the formation of $CdCl_3^-$, $CdCl_4^{2-}$, and $CdCl_6^{4-}$ has been suggested. Tarasova,[10] in the temperature range 440 to 500°C, found a surprisingly sharp minimum in the specific conductance of $CdCl_2$-KCl mixtures at a mole ratio of 1KCl:1$CdCl_2$ (Fig. 8.5) and attributed it to the formation of $CdCl_3^-$ ions. Bloom and Heymann,[11] on the other hand, observed, at temperatures of 570°C and above, the decrease in specific conductivity with KCl concentration in this concentration region to continue to more than

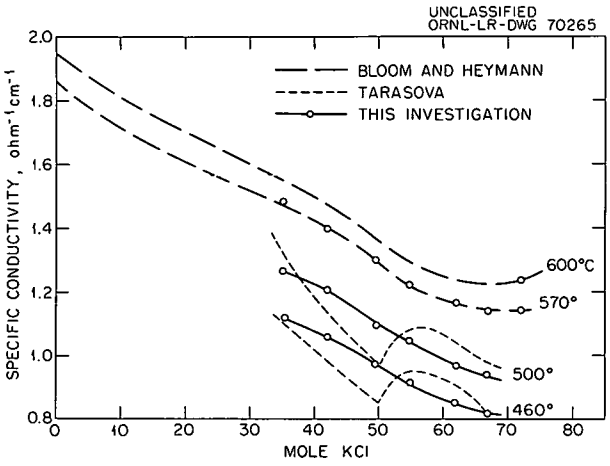

Fig. 8.5. Specific Conductivity of Molten $CdCl_2$-KCl Mixtures.

65 mole % KCl, with some indication that at lower temperature the decrease would continue to even slightly higher KCl concentration. These latter data, in conjunction with a new interpretation of Raman spectra, had been taken to suggest the formation of $CdCl_4^{2-}$ ions rather than $CdCl_3^-$ ions, which were thought to be unlikely also on theoretical grounds.[12,13]

In view of the discrepancy between the data of Bloom and Heymann and those of Tarasova – the latter being suspect for the very sharpness of the minimum – a series of measurements of the electrical conductivity of $CdCl_2$-KCl mixtures was carried out at 460, 500, and 570°C with an apparatus described elsewhere.[14] Figure 8.5 shows good agreement of these measurements with those of Bloom and Heymann, and no trace of a minimum at the mole ratio 1KCl:1$CdCl_2$. Rather, the decline in specific conductivity continues to the vicinity of the KCl concentration at which solid KCl precipitates, near 70 mole % KCl. The minimum in equivalent conductance calculated with densities from the literature[15] shifts with

[8] E. Mollwo, *Nachr. Akad. Wiss. Goettingen, Math.-Physik. Kl., IIa. Math.-Physik.-Chem. Abt.* **1934**(1) 79.

[9] P. S. Rogers, J. W. Tomlinson, and F. D. Richardson, p 909 in *Physical Chemistry of Process Metallurgy*, Interscience, New York, 1961.

[10] I. P. Tarasova, *Zh. Fiz. Khim.* **21**, 825 (1947), discussed in *Electrochemistry of Fused Salts*, by IU. K. Delimarskii and B. F. Markov, English translation, Sigma Press, Washington, D.C., 1961.

[11] H. Bloom and E. Heymann, *Proc. Roy. Soc. (London)* **A188**, 392 (1947).

[12] M. A. Bredig and E. R. Van Artsdalen, *J. Chem. Phys.* **24**, 478 (1956).

[13] M. A. Bredig, *Electrochim. Acta* **5**, 299 (1961).

[14] Capillary cell method, modified from that described by H. R. Bronstein and M. A. Bredig, *J. Am. Chem. Soc.* **80**, 2077 (1958).

[15] R. Lorenz and H. Adler, *Z. anorg. u. allgem. Chem.* **172**, 372 (1928).

the increasing temperature to mole ratios lower than 2KCl:1$CdCl_2$. This may be taken to reflect the increasing dissociation of the $CdCl_4^{2-}$ complex.

An analysis of measurements by Russian investigators[16,17] of the emf of the formation of CdX_2 in molten mixtures of $CdCl_2$ with KCl and of $CdBr_2$ with KBr showed the results of these measurements also to favor the assumption of CdX_4^{2-} complex ions.[18]

The Heat of Fusion of Alkaline-Earth and Rare-Earth Metal Halides

A. S. Dworkin M. A. Bredig

Heats of fusion of the alkaline-earth and rare-earth metal halides are of considerable interest in connection with the interpretation of the phase equilibria and electrical conductance measurements in metal-metal halide systems. Since very few calorimetrically measured values are available in the literature, the heats of fusion of some chlorides and iodides of lanthanum, cerium, praseodymium, and neodymium, as well as of all of the chlorides, bromides, and iodides of calcium, strontium, and barium, have been measured.

The copper-block drop calorimeter used for the measurements and the experimental procedure have been described in detail previously.[19]

The results are shown in Table 8.1. The entropy of fusion, ΔS_m, for $LaCl_3$, $PrCl_3$, and $NdCl_3$ is essentially constant and very similar to the ΔS_m for $CeCl_3$, 11.7 eu, reported by Walden and Smith.[20] The entropy of fusion of CeI_3 and PrI_3 is slightly higher than that of the chlorides, while NdI_3, distinguished above its transition temperature by a different crystal structure from CeI_3 and PrI_3, has an entropy lower than that for the other iodides by an amount approximately equal to the entropy of the transition taking place in the solid state approximately 200°C below the melting point.

Since the alkaline-earth metal halides possess a variety of crystal structures, they do not exhibit the simple regularities in ΔH_m and ΔS_m apparent in the alkali-metal halides.[19] However, $SrBr_2$ and $BaCl_2$, with transitions just below their melting points, and $SrCl_2$, which has a CaF_2 type of structure, have unusually low entropies of fusion. (Calcium fluoride also has an unusually low ΔS_m of 4.2 eu.[21] High-temperature x-ray studies to confirm that $SrBr_2$ and $BaCl_2$ also have the CaF_2 type of structure at their melting points, as suggested by the low entropies of fusion, will be initiated.)

Table 8.1 also shows considerably larger heat capacities for solid $SrCl_2$ and the high-temperature modifications of $SrBr_2$ and $BaCl_2$, which are also formed with a rather large heat of transition. This may support the assumption that the low entropies of fusion of these compounds are connected with relatively high entropies of the solids, probably due to considerable disorder in connection with the special geometry of the fluorite type of structure, in which lattice vacancies equal in size and number to the sites occupied by the cations occur.

Calcium iodide, with its layer-type structure, has a ΔS_m much higher than that of any of the other alkaline-earth halides reported here. It thus resembles the cadmium dihalides (excluding the fluoride) of similar layer-type crystal structure (ΔS_m = 7.5 to 9.5 eu).

The heat of fusion of only one of the compounds in Table 8.1 had been measured calorimetrically by other investigators. Moore's value of ΔH_m for $CaCl_2$ of 6.78 kcal[22] is in agreement with that reported here.

---

[16] M. F. Lantratov and T. N. Shevlyakova, *J. Appl. Chem. USSR (English Transl.)* **34**, 1017 (1961).

[17] M. F. Lantratov and A. F. Alabyshev, *J. Appl. Chem. USSR (English Transl.)* **26**, 353 (1953).

[18] M. A. Bredig, *Journal of Chemical Physics*, July 15, 1962 (in press).

[19] A. S. Dworkin and M. A. Bredig, *J. Phys. Chem.* **64**, 269 (1960).

[20] G. E. Walden and D. F. Smith, *U.S. Bur. Mines, Rept. Invest. No. 5859* (1961) (4 pp).

[21] B. F. Naylor, *J. Am. Chem. Soc.* **67**, 150 (1945).

[22] G. E. Moore, *J. Am. Chem. Soc.* **65**, 1700 (1943).

Table 8.1. Heat Capacity and Heat and Entropy of Fusion and Transition of Some Alkaline-Earth and Rare-Earth Metal Halides

Metal Halide	T_m (°K)	C_p Solid (cal mole^{-1} deg^{-1})	C_p Liquid (cal mole^{-1} deg^{-1})	$H_{T_m(\text{solid})} - H_{298}$ (kcal mole^{-1})	ΔH_m (kcal mole^{-1})	ΔS_m (eu mole^{-1})	T_{tr} (°K)	ΔH_{tr} (kcal mole^{-1})	ΔS_{tr} (eu mole^{-1})	Structure Type, 25°C
$LaCl_3$	1131	34.7 ± 2	37.7 ± 2	22.8	13.0	11.5				UCl_3
$PrCl_3$	1059	32.3 ± 2.5	32.0 ± 2.5	21.5	12.1	11.4				UCl_3
$NdCl_3$	1032	35.4 ± 2.5	35.0 ± 2.5	20.3	12.0	11.6				UCl_3
CeI_3	1033	36.5 ± 2	36.5 ± 2	20.8	12.4	12.0				$PuBr_3$ (?)
PrI_3	1011	31.3 ± 2	34.2 ± 2	19.5	12.7	12.6				$PuBr_3$ (?)
NdI_3	1060	α 27.6 ± 2	36.3 ± 2	24.3	9.7	9.2	847	3.4	4.0	$PuBr_3$ (?)
		β 30.4 ± 2								
$CaCl_2$	1045	23.6 ± 1.5	23.6 ± 1.5	14.3	6.78	6.49				SnO_2
$CaBr_2$	1015	23.0 ± 1.5	27.0 ± 2	14.0	6.95	6.85				SnO_2
CaI_2	1052	23.2 ± 1.0	24.7 ± 1.0	15.1	10.0	9.5				$Cd(OH)_2$
$SrCl_2$	1146	29.0 ± 2.5	28.6 ± 3	20.3	3.88	3.39				α-CaF_2
$SrBr_2$	930	α 20.9 ± 1	27.8 ± 1	15.6	2.50	2.70	918	2.90	3.16	$SrBr_2$
		β 27.5 ± 2.0								
SrI_2	811	22.9 ± 1.5	26.3 ± 1.5	10.4	4.70	5.80				SrI_2
$BaCl_2$	1233	α 23.1 ± 1.5	26.3 ± 2.5	23.5	3.90	3.17	1193	4.10	3.44	$PbCl_2$
		β 25.5 ± 2.5								
$BaBr_2$	1130	21.7 ± 1.5	25.6 ± 1.5	16.9	7.63	6.75				$PbCl_2$
BaI_2	984	21.8 ± 1.5	27.0 ± 2	13.9	6.34	6.44				$PbCl_2$

9. Chemical Physics

MICROWAVE AND RADIOFREQUENCY SPECTROSCOPY

Paramagnetic Resonance Equipment

Ralph Livingston R. W. Holmberg
Henry Zeldes

Practically all our equipment was altered, new equipment was purchased, and additional laboratory space was obtained. An 8-in. electromagnet was modified by placing it on a rotating base so that it will be more suitable for studying anisotropy effects in single crystals. A new 12-in. magnet with power supply was purchased and put into operation.

A new 9000-Mc spectrometer using a microwave bridge was assembled. This spectrometer includes automatic frequency control. A cavity and conversion kit was purchased from Varian Associates, and this spectrometer may now be operated as a 100-kc field-modulated instrument with greatly enhanced sensitivity. Flexibility was retained so that the spectrometer may easily be converted to other types more suitable for certain studies.

A simple spectrometer using a transmission cavity and operating at 23,000 Mc was built. The cavity is located inside a dewar and may be cooled with liquid nitrogen, with provision for pumping on the nitrogen in order to obtain a lower temperature. A tube connects from the cavity to outside the dewar so that samples may be easily changed. This tube connects from the top of the cylindrical cavity operating in the TE_{011} mode. The coupling irises are located on the sides of the cavity and wave-guide feed is used. The Q is high, and good sensitivity is obtained for this simple type of spectrometer.

Considerable progress was made in designing and building equipment for working with liquid helium. The design centers about a new microwave cavity, which is a reflection type operating at 9000 Mc. There will be provision for introducing and withdrawing samples while the cavity is at the low temperature. This means that there will be a vertical tube connecting from the top of the cavity to the outside of the dewar containing the cavity. The tube leaves very little remaining space on top of the cavity for making a connection to the microwave transmission line. Although there is enough space for a coaxial cable, earlier work showed a cable to be unsatisfactory for a reflection cavity because of severe reflections from the cable itself. Also, a variable and externally adjustable coupling to the cavity is desirable. A new design was electrically tested at room temperature and found to work very well. The cavity is a rectangular type fed from a wave-guide transmission line. Coupling with the electric vector is made from the broad side of the cavity, and a post with variable insertion is located at the iris ($\lambda/4$ from the end of the cavity) so that the coupling may be varied. Both TE_{101} and TE_{102} cavities have been tested. The latter have far higher Q's and are far superior even though the sample is located at the cavity wall, where maximum oscillating magnetic field is not found. The electrical tests were sufficiently gratifying to now warrant the construction of the final cavity.

This equipment was used to examine and reexamine a number of systems. For example, each of the three lines[1] from NO_2 in irradiated $NaNO_2$ is now found to be slightly split into quadruplets when the magnetic field is parallel to the b crystallographic axis. This splitting is almost certainly due to a neighboring ion of sodium ($I = 3/2$), which interacts most strongly with a p lobe from NO_2 just for this direction. Other studies are described in more detail in other sections of this report.

[1]Henry Zeldes and Ralph Livingston, *Chem. Div. Ann. Progr. Rept. June 20, 1961*, ORNL-3176, p 78.

A Paramagnetic Resonance Study of Irradiated Potassium Nitrate

Henry Zeldes Ralph Livingston

In the last annual report[2] the parameters of a spin Hamiltonian characterized by a *g*-tensor and a nitrogen hyperfine coupling tensor were reported for a paramagnetic species in gamma-irradiated KNO_3 at 77°K. This species was identified as NO_2, since the traces of the tensors agreed well with those for NO_2 studied previously[3] in gamma-irradiated $NaNO_2$. There were significant differences in the individual principal values for NO_2 in the two salts, which indicated that NO_2 in KNO_3 is experiencing motional effects at 77°K[4], and it was suggested that the motion is torsional oscillation of NO_2 with large amplitude. Since then, calculations were made for a model of torsional oscillation and for a model of rapid reorientation of NO_2 in a nitrate ion vacancy. The former model was rejected since the equilibrium position of NO_2 did not seem sensible. The model of rapid reorientation explains the findings very satisfactorily. It is assumed that NO_2 rapidly reorients between two mirror-related sites in an anion vacancy. Good agreement with the observed tensors was obtained by assuming that the principal values appropriate for stationary NO_2 are the values measured in irradiated $NaNO_2$ and that the atoms of NO_2 in KNO_3 occupy positions which are close to the corresponding atom positions for the nitrate ion. This interpretation has been prepared for publication.[4]

In previous work on KNO_3 it was found[4] that a good yield of NO_2 was formed upon gamma irradiation at 77°K if a small amount of KNO_2 was co-crystallized with the KNO_3. On the other hand, pure KNO_3 gave essentially no NO_2 upon irradiation at 77°K. However, a good yield of NO_2 was obtained from pure KNO_3 if it was first irradiated at 77°K and then warmed to room temperature and finally reirradiated at 77°K. These results suggest that NO_2^- is the precursor for NO_2 and are consistent with the well known fact that nitrite is a major product of the room-temperature irradiation of KNO_3. In order to explore this interpretation further, additional experiments were made.

A crystal of KNO_3 containing $KN^{15}O_2$ (95% N^{15}) was studied. An examination of the NO_2 spectrum formed after gamma irradiation at 77°K clearly showed that there was no isotopic exchange between NO_2^- and NO_3^- and that all observed NO_2 must have come from NO_2^-. Additional experiments consisted of showing that NO_2 could also be prepared from pure KNO_3 by carrying out the first irradiation at room temperature (where NO_2^- is known to be a product) followed by irradiation at 77°K. With new, more sensitive equipment a search was also made for NO_2 in pure KNO_3 after a single irradiation at 77°K. The amount of NO_2 formed was at least two orders of magnitude smaller than that produced in crystals containing KNO_2. These results are being submitted in greater detail for publication elsewhere.

A number of other features of the spectra formed in irradiated KNO_3 are being examined. In addition to NO_2 a variety of other species is present, and their relative abundances are found to vary with the nature of the sample, previous irradiation history, heat treatment, etc. A triplet of very sharp closely spaced lines has been observed which under some conditions may be made very intense. These lines might result from NO_3. Final measurements are being started.

A Paramagnetic Resonance Study of Irradiated Hydrogen Peroxide

Ralph Livingston R. W. Holmberg

Some years ago preliminary work was described[5] on irradiated single crystals of essentially 100% H_2O_2. Gamma irradiation at 77°K gave rise to a spectrum of very closely spaced lines, not completely resolved, which persisted even after warming to much above dry-ice temperature. A completely different spectrum was obtained by ultraviolet irradiation at low temperatures. This spectrum disappeared with first-order kinetics with a half-life of a little over an hour at 77°K

[2]Henry Zeldes, *Chem. Div. Ann. Progr. Rept. June 20, 1961*, ORNL-3176, p 77.

[3]Henry Zeldes and Ralph Livingston, *J. Chem. Phys.* **35**, 563 (1961).

[4]Henry Zeldes, *Proceedings of the First International Conference on Paramagnetic Resonance, Israel, July 16, 1962* (in press).

[5]Henry Zeldes, Ralph Livingston and R. W. Holmberg, *Chem. Div. Ann. Progr. Rept. June 20, 1957*, ORNL-2386, p 129.

and with an activation energy of 5 kcal/mole. Both spectra were anisotropic, but that formed by ultraviolet irradiation had larger overall separations and offered the greater possibility of being unraveled. It was pointed out that the species formed by ultraviolet irradiation might also be formed by gamma rays and might be observable if a gamma irradiation at a lower temperature or higher gamma intensity were used.

In the preliminary study the great multiplicity of lines was troublesome. Hydrogen peroxide is tetragonal, with four molecules in the unit cell. In general a paramagnetic species will give rise to eight lines or groups of lines which simplify to fewer lines for special orientations of the crystal in the magnetic field. Even for these special orientations the number of components in the spectra seemed excessive, and it appeared that "forbidden" transitions (environmental proton flips) and perhaps resolved dipolar interactions were present which would account for a large number of lines. To aid in unraveling the spectra it was decided to make measurements at 23,000 Mc as well as at 9000. These measurements are under way, and the present account is still preliminary.

The familiar ultraviolet-produced spectra have now been seen in a 9000-Mc spectrometer using 100-kc field modulation. After storage of photolyzed samples at 77°K the ultraviolet-produced species disappears, in keeping with early observations, but an entirely new spectrum appears which is quite distinct from that produced by ultraviolet and from that produced in the earlier work by gamma rays. If the sample is next warmed to dry-ice temperature, the new spectrum changes and appears to become the same as that formed by gamma rays. Thus three distinct types of spectra have now been seen, which suggests that three different species are formed but does not prove it since the same species in different environments could give rise to different spectra.

For two orientations of the ultraviolet-irradiated crystal a correspondence of the 9000 and 23,000 Mc spectra has been noted. This should help sort out those line spacings arising from hyperfine interactions.

Paramagnetic Resonance of Irradiated Chlorates

R. W. Holmberg

The irradiation of potassium and barium chlorates with gamma rays produces a large number of paramagnetic centers, some of which show hyperfine structure characteristic of chlorine nuclei. Attention was focused on one species found in $KClO_3$ which was tentatively identified as ClO_2. Measurements of the hyperfine splittings in two of the crystallographic planes of $KClO_3$ were made, and some observations were made in a third. The line separations are strongly anisotropic. In the *ac* plane near the *a* axis, the four Cl^{35} hyperfine lines are about equally spaced and reach their maximum separation of about 225 Mc. At directions normal to the *a* axis, the lines are no longer equally spaced; the hyperfine multiplet shows an overall spacing of about 120 Mc. In this region "forbidden" lines are also seen, and line intensities show pronounced anisotropy. This indicates the presence of a rather strong quadrupole interaction in addition to the magnetic hyperfine interaction.

The observed splittings are in good agreement with the magnetic hyperfine parameters deduced from microwave rotational spectra of ClO_2 (ref 6). Further, from the direction at which the maximum separation of hyperfine lines occurs, one can, with some assurance, speculate that the ClO_2 radical is trapped in a ClO_3^- vacancy in the crystal.

Because of the strong quadrupole interaction it is not possible to fit the data to explicit solutions of the spin Hamiltonian obtained from perturbation theory. A program was written for the IBM 7090 computer to solve the Hamiltonian numerically. Energy levels, transition energies, and relative transition probabilities are computed as a function of magnetic field strength and direction for assumed values of the magnetic and quadrupole hyperfine tensors. Transition energies are then compared with those obtained experimentally. Difficulties have arisen because of the large number of independent parameters that must be specified to

[6] R. F. Curl, Jr., *et al.*, *Phys. Rev.* **121**, 1119 (1961).

define the system. Even if the g tensor is assumed to be isotropic there are 11 independent parameters. If the simplifying assumption is made that the quadrupole and magnetic hyperfine tensors are parallel, this number is reduced to eight. Since these assumptions are in reasonable accord with the experimental data, they formed the basis of the initial computations. To date, however, a satisfactory fit to the data has not been obtained.

If $Ba(ClO_3)_2 \cdot H_2O$ is irradiated with gamma rays at 77°K and then warmed to room temperature, most of the paramagnetic centers formed at the low temperature disappear. A species containing a single chlorine atom grows in. Detailed measurements of this spectrum were made at room temperature. The hyperfine splittings are of similar magnitude and anisotropy to those ascribed to ClO_2 above, and intensity anisotropies and forbidden lines are also seen. It would appear that this species is also ClO_2, but this characterization is by no means definite.

NEUTRON AND X-RAY DIFFRACTION

A Neutron Diffraction Study of Chloral Hydrate

G. M. Brown H. A. Levy

Chloral hydrate, $CCl_3CH(OH)_2$, is an interesting subject for crystal-structure analysis because of the rarity of stable compounds having two hydroxyl groups attached to a single carbon atom. Spectroscopic study has confirmed the conclusion from chemical evidence that the chloral hydrate molecule contains single carbon-oxygen bonds – that is, that chemical reaction does occur when the hydrate is formed from chloral and water – but it has not supplied any reliable information about the hydrogen bonding that is probably important in stabilizing the compound. A crystal-structure analysis by neutron diffraction was undertaken in this laboratory to determine the details of the molecular structure and hydrogen bonding. The only previously reported structure analysis,[7] by x-ray methods, is clearly completely unreliable. Application of the neutron method is appropriate in this case because a major object is precise location of the hydrogen atoms, which cannot be done by x-ray methods.

Crystals of chloral hydrate are monoclinic, of space group $P2_1/c$, with a = 11.464, b = 5.985, c = 9.687 A, β = 120° 43′, and four molecules per unit cell. The parameters reported here were derived by the method of least squares from measurements of diffraction angles on the Oak Ridge three-dimensional automatic crystal orienter. They are believed to be reasonably accurate but are subject to check by x-ray methods.

Within the range of the neutron instrument (maximum 2θ = 111°) for the wavelength now employed (about 1.08 A) there are about 2150 nonequivalent reflections of chloral hydrate accessible to measurement. Each one of these was measured at least once; many were measured two or more times. Three crystal specimens of weight 29, 6, and 2 mg were used in an attempt to estimate and obviate the effects of extinction. The total number of reflections measured, including duplications, is about 4000. The number included in the structure-determining calculations so far is about 3600. The reflection intensities were corrected for absorption.

By the time our data had been obtained a set of approximate parameters for the carbon, oxygen, and chlorine atoms was made available to us from a new x-ray study in progress elsewhere.[8] These parameters were used to calculate structure factors whose signs were used with the observed structure factors as coefficients for a three-dimensional Fourier map. Reasonable locations for each of the three hydrogen atoms of the molecule were evident from the Fourier map, and least-squares refinement was started at once.

Five cycles of least-squares refinement were carried out, the last two of which included adjustment of individual anisotropic thermal parameters. The usual reliability index R on F^2 fell to 0.066 from an initial value of 0.40 when hydrogen contributions were first included. The value of the function

$$\sigma_1 = \left[\frac{\Sigma w(F_0^2 - F_c^2)^2}{n - p}\right]^{1/2},$$

where n is the number of observations, and, p, the number of parameters, is 1.28, compared with the

[7] S. Kondo and I. Nitta, *X-Rays, Japan* **6**, 53 (1950), cited in *Structure Reports* **13**, 448 (1950).

[8] I. Nitta, private communication.

value unity that should be reached on convergence of least-squares refinement when the errors are truly random and correctly estimated. The weighted *R* factor,

$$\left[\frac{\Sigma w(F_0^2 - F_c^2)^2}{\Sigma w F_0^2}\right]^{1/2},$$

has the value of 0.083. The largest standard deviation of an atomic coordinate is 0.0011 A for chlorine, 0.0015 A for oxygen, 0.0011 A for carbon, and 0.0031 A for hydrogen. The precision of the structure determination is clearly quite high.

The Cl_3C–and–$CH(OH)_2$ groups are in a staggered orientation about the C–C axis. Figure 9.1 shows the dihedral angles which specify the orientation of the various atoms about the C–C axis.

Bond lengths and angles are shown in Fig. 9.2, as calculated from the parameters before the last cycle of least squares. Bond lengths and angles from the final parameters have not yet been calculated, but they can be only trivially different from those reported. For the bond lengths involving hydrogen atoms these standard deviations are about 0.004 A; for the others, about 0.002 A. The standard deviations of the angles are probably from 0.1° to 0.2°. The bond lengths all appear normal, and differences in length among chemically equivalent but crystallographically nonequivalent bonds do not appear significant, with the exception of the difference between the two O–H bonds. This difference is probably a real effect arising from the different strengths of the two hydrogen bonds in which the two OH groups are involved (see below). Some of the differences among chemically equivalent angles are clearly significant and must be real effects resulting from the packing of the molecules.

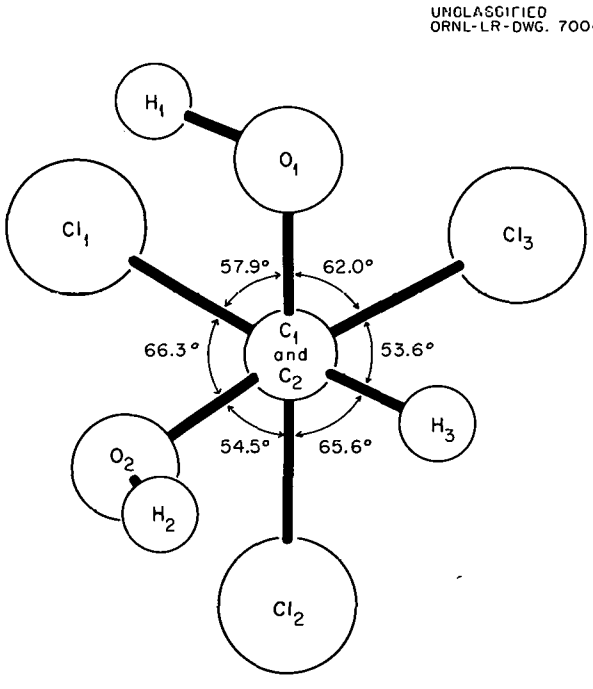

Fig. 9.1. View Along Carbon-Carbon Axis of Molecule Showing Orientation of Atom About That Axis.

Each oxygen atom is involved in two hydrogen bonds. Two O_2–$H_2 \ldots O_1$ bonds link two molecules about each of the symmetry centers at (0,0,0) and $(0, \frac{1}{2}, \frac{1}{2})$. Each molecule is also linked by two O_1–$H_1 \ldots O_2$ bonds to two neighbor molecules in a helical chain about one or the other of the screw axes at $(0,y,\frac{1}{4})$ and $(0,y,\frac{3}{4})$. This system of hydrogen bonding results in the formation of layers two molecules thick which are parallel to (100) and which are bounded on both sides by chlorine atoms. The arrangement of the molecules is made clear by reference to Figs. 9.3 and 9.4, of which the latter shows in perspective the structure of one of the layers, viewed at right angles to the layer. The easy cleavage parallel to (100) is consistent with the layer structure.

From the interatomic distances within the two types of hydrogen bond it appears that neither type is very strong. That the O_2–H_2 bond is slightly longer than the O_1–H_1 bond is consistent with the shorter overall length of the O_2–$H_2 \ldots O_1$ bond relative to the O_1–$H_1 \ldots O_2$ bond, even though the latter is more nearly straight.

The present study is apparently the first structure determination by neutron diffraction in which three-dimensional data has been used on the same large scale as is commonly employed in x-ray analysis. The results clearly show the practicability of such large-scale neutron diffraction problems and that the precision attainable is as high as in the x-ray method.

Neutron Diffraction Measurements from Alkali Halide Crystals

H. A. Levy W. R. Busing
P. A. Agron

Neutron diffraction measurements from single crystal specimens of a series of alkali halide crystals were undertaken for three reasons: (1) to

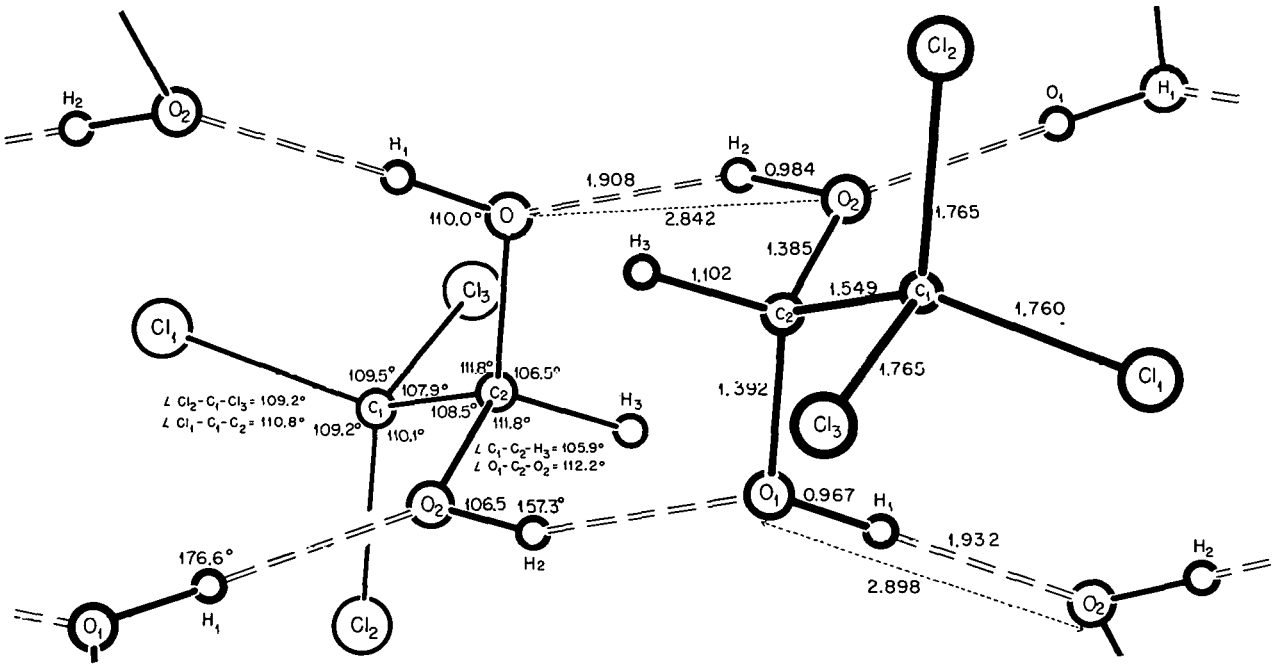

Fig. 9.2. Bond Length and Angles.

test the consistency and precision of intensity measurements with the Oak Ridge Automatic Neutron Diffractometer, (2) to obtain a consistent set of nuclear scattering amplitudes for the alkali metals and the halogens, and (3) to obtain precise values of the thermal-displacement parameters for these crystals. In this report, the results of measurements on KCl, NaCl, and RbCl are presented. Studies of other alkali halides are under way.

The measurements were all made with the Oak Ridge automatic instrument installed at the ORR. The sample crystals were at room temperature, 23 ± 2°C. Intensities were corrected for absorption and converted to squared structure factors in the usual way and were then analyzed by least squares to determine the scale factor for intensity, the ratio of the metal nuclear scattering amplitude to that of chlorine, and the thermal parameters of both ions.

Table 9.1 lists various measures of agreement between observed and computed squared structure factors for the three crystals. Table 9.2 lists the parameters resulting from refinement, along with their precision measures (standard error) resulting from the least-squares procedure. For these refinements, the chlorine scattering amplitude was given its presently accepted value, 0.98 fermi units; this procedure was adopted to avoid the need for establishing independently the absolute intensity scale, for which the available

Table 9.1. Measures of Agreement Between Observed and Computed Squared Structure Factors

	NaCl	KCl	RbCl
σ_1 [a]	0.99	0.86	0.88
R_1	0.019	0.026	0.023
R_2	0.029	0.036	0.046
Number of measurements	49	117	91
Number of nonequivalent reflections	32	38	45

[a] $\sigma_1 = [\Sigma w(F_0^2 - F_c^2)^2/(N_0 - N_p)]^{1/2}$

$R_1 = \Sigma|F_0^2 - F_c^2|/\Sigma F_0^2$

$R_2 = [\Sigma w(F_0^2 - F_c^2)^2/\Sigma w F_0^4]^{1/2}$

UNCLASSIFIED
ORNL-LR-DWG. 70092

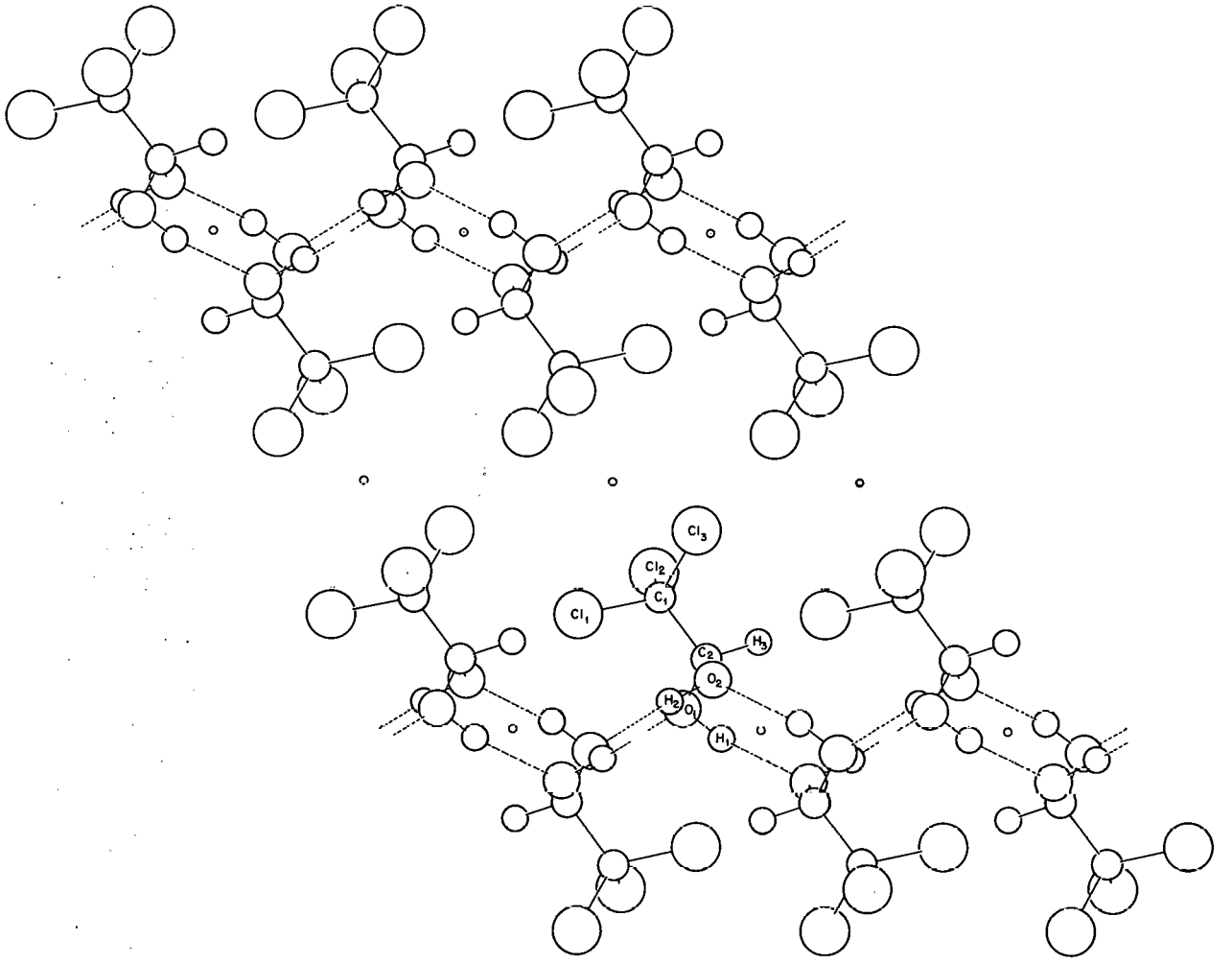

Fig. 9.3. Chloral Hydrate – *b*-Axis Projection.

Table 9.2. Nuclear Scattering Amplitudes and Thermal Parameters for NaCl, KCl, and RbCl

Parameter	NaCl	KCl	RbCl
f_M[a] (this study)	0.355 ±0.004[c]	0.370 ±0.003[c]	0.696 ±0.002[c]
f_M (previous measurements)	0.351 ±0.006[d]	0.35 ±0.01[d]	0.71 ±0.03[e] 0.69 ±0.03
B_M[b]	1.63 ±0.04	1.86 ±0.03	2.11 ±0.03
B_{Cl}[b]	1.42 ±0.01	1.90 ±0.01	2.24 ±0.02

[a] Metal scattering amplitude, relative to $f_{Cl} = 0.98$ (assumed).

[b] The isotropic temperature factor coefficient. The mean square thermal displacement is $B/8\pi^2$.

[c] The errors are least-squares standard errors and reflect precision of fit only.

[d] Reported in *Neutron Cross Sections*, BNL-325.

[e] Reported in *Chem. Div. Ann. Progr. Rept. June 20, 1961*, ORNL-3176, p 83.

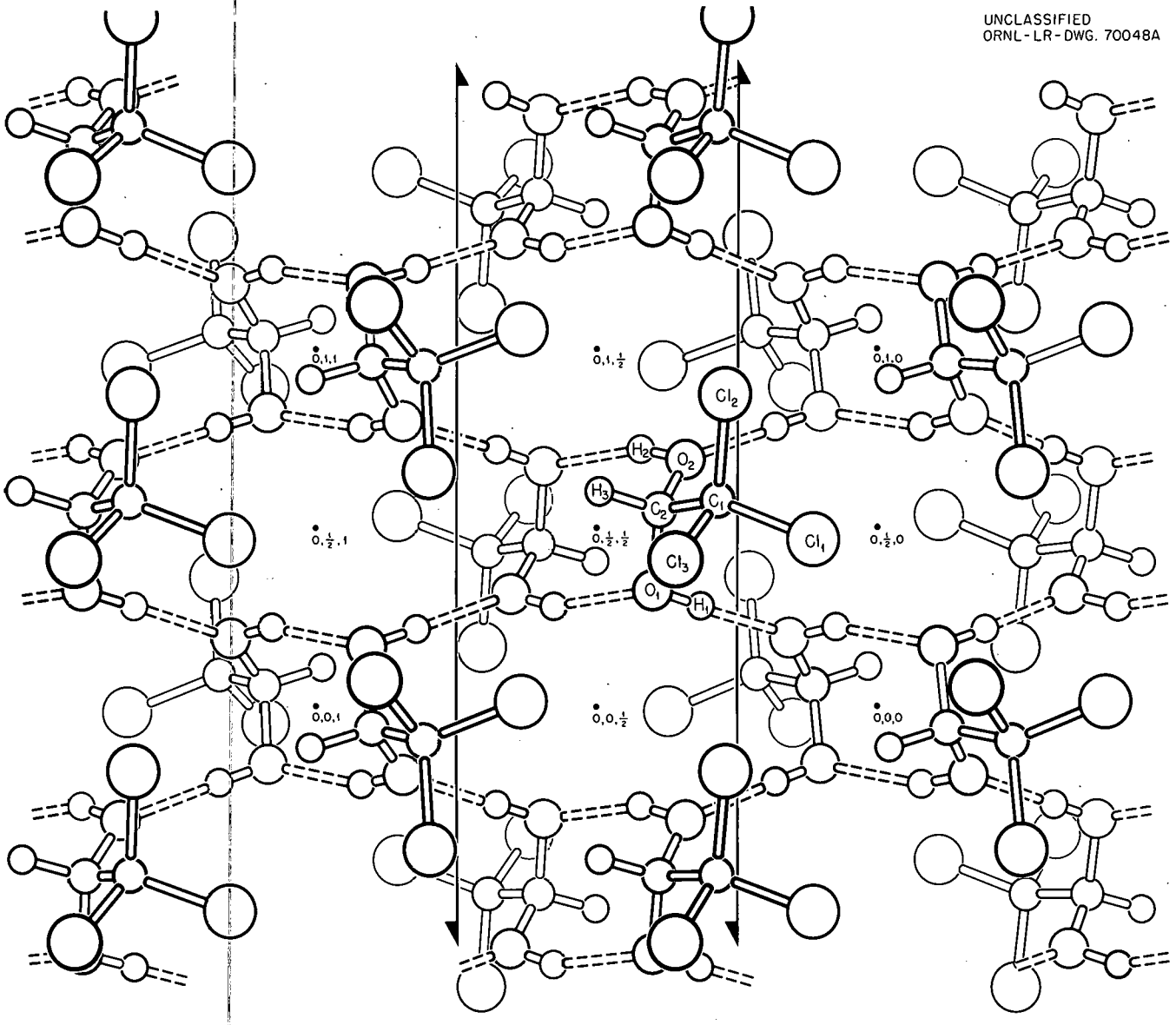

Fig. 9.4. Chloral Hydrate – View Perpendicular to (100), Showing Hydrogen Bonding in One Layer of the Crystal Structure.

accuracy is not as great as for relative measurements.

The resulting nuclear scattering amplitudes for Na, K, and Rb are of greater precision than were those previously available and are within the previous experimental uncertainties. The thermal parameters for a given crystal show the expected inverse variation with the mass of the atom, being greatest for sodium and least for rubidium. The near equality of the thermal parameters for K and Cl is in accord with their nearly equal masses. From one crystal to another, the thermal parameters increase directly as the unit cell dimension, probably reflecting the corresponding decrease in the binding energy of the crystal.

The agreement between observed and calculated squared structure factors is strikingly close, confirming the high consistency and precision of the measurements made by the automatic instrument.

X-Ray Diffraction Studies of Liquid Structure

M. D. Danford H. A. Levy
O. E. Esval[9]

Introduction. – Research for the past year centered around the development of methods for data analysis, including a least-squares program for parameter refinement. The FORTRAN general least-squares program, developed by W. R. Busing of this Laboratory, was adapted to the liquid-structure problem and is now an integral part of the data analysis procedure.

Work on structure in molten alkali halides has continued, but has not progressed sufficiently to warrant a report at this time. Data were obtained for three aqueous hydrolyzed uranyl chloride solutions and two uranyl perchlorate solutions, with statistical precision sufficient to define intensity-curve features to the largest scattering angles. Analysis of these data is proceeding. Work on the structure of water at room temperature and on an aqueous solution of hydrolyzed lead perchlorate is nearing completion, and preliminary results for these two cases are presented.

The Structure of Water. – The great number of reports on theoretical and experimental studies of the water structure have made a considerable contribution to a greater understanding of the liquid state,[10-17] although the basic conclusions, in many cases, have differed. This report presents preliminary results from an x-ray diffraction study of water at room temperature, undertaken in an attempt to consolidate results and remove conflicts from past studies.

The data were obtained using the x-ray diffractometer for liquids, described briefly in previous reports.

The observed diffracted intensity was interpreted in the usual way to yield the radial distribution function shown in Fig. 9.6. From this curve, the following conclusion may be drawn regarding the atomic arrangements in water.

The first peak at about 2.9 A is assignable with confidence to the nearest neighbor O–O interaction and corresponds to an average number of neighbors of about 4.5. A broad, rising, incompletely resolved feature shows a concentration of distances between 3 and 4.5 A, followed by a slightly more prominent maximum which indicates another group of neighbors at about 4.80 A.

Comparison of this distance spectrum with that of ice (four neighbors at 2.76 A and 12 at 4.50 A) suggests a close relation between the ice and water atomic arrangements and indeed led to a plausible model for describing the water arrangement. In this model the basic network arrangement of ice is maintained in a somewhat expanded form, conforming to the first radial distribution peaks at 2.9 and 4.8 A. The proper density then requires the addition of about one water molecule per four molecules in the network in a position to yield

[9] ORINS Pre-Doctoral Fellow, University of North Carolina.

[10] *Hydrogen Bonding*, p 1 (ed. by D. Hadzi), Pergamon, London, 1959; L. Pauling, *The Nature of the Chemical Bond* 3d ed., p 472, Cornell University Press, Ithaca, 1960.

[11] Sir John Lennard-Jones, and J. A. Pople, *Proc. Roy. Soc. (London)* **A205**, 155 (1951).

[12] E. Forslind, *Acta Polytech.* **3**, 115 (1952).

[13] J. D. Bernal and R. H. Fowler, *J. Chem. Phys.* **1**, 515 (1933).

[14] K. Grjotheim and J. Krogh-Moe, *Acta Chem. Scand.* **8**, 1195 (1954).

[15] J. Morgan and B. E. Warren, *J. Chem. Phys.* **6**, 666 (1938).

[16] H. S. Frank and W. Y. Wen, *Discussions Faraday Soc.* **24**, 133 (1957).

[17] C. Finbak and H. Viervoll, *Tidsskr. Kjemi, Bergvesen Met.* No. 5, 36 (1943).

distances intermediate between the first and second neighbors of ice; this "interstitial" molecule can be placed, in conformity with the radial distribution curve, within the cavities of the ice-like network.

The model was sufficiently successful in accounting for the radial-distribution curve features to warrant an attempt at refinement. For this purpose, in the interest of simplicity, the basic hexagonal symmetry of the ice structure was assumed, and the dimensions of the network were permitted to be altered anisotropically; that is, in the network there are two nearest O–O distances, one corresponding to three neighbors and the other to one. The interstitial molecule was restricted to positions of threefold symmetry within the cavity. The basic distance parameters of this model are thus the two O–O distances in the network and the shortest distance from the interstitial molecule to to the framework. The number of interstitial molecules was fixed to maintain proper density.

These basic parameters were refined by the method of least squares to give a fit to the observed reduced intensity function. All distances out to 10 A were included, properly related to the three basic parameters.

The result of this refinement is shown in Figs. 9.5 and 9.6, which compare observed and calculated reduced intensity functions and radial-distribution functions. Significant features of the refined model are the following:

1. Each network oxygen atom has one network neighbor at 2.77 A and three network neighbors at 2.95.

2. Each interstitial oxygen atom has three network neighbors at 2.96, 3.29, 3.43, and 3.90 A.

3. The ratio of network molecules to interstitial molecules, is 3.88, corresponding to filling 51.6% of the "cavities."

The success in fitting this model to the observed data is great enough to lend the model considerable credence. It may be mentioned that various models proposed by others, including those of Pauling[10] and Bernal,[13] were examined and were judged to be inconsistent with the observed radial-distribution function.

Correlation of the present results with other studies, including thermodynamic properties, is under way.

Hydrolyzed Lead Perchlorate Solution. – Ultracentrifugation of lead perchlorate solutions, with varying pH, discussed in another section of this report, indicated that polymeric species exist in solution. Specifically, at a ratio $(OH)^-/Pb$ equal to 0.93, the degree of polymerization is approximately 4, suggesting a species $[Pb(OH)]_4^{4+}$. To provide additional information concerning this species, an x-ray diffraction study of a solution approximately 5 *M* in Pb^{2+}, with about the same ratio $(OH)^-/Pb$, was undertaken.

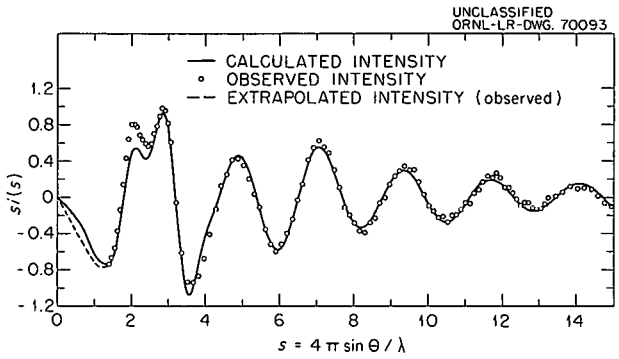

Fig. 9.5. Observed and Calculated Reduced Intensity Curves for H_2O. The smooth curve represents the calculated intensity from parameters of the model. Observed data points are designated by circles.

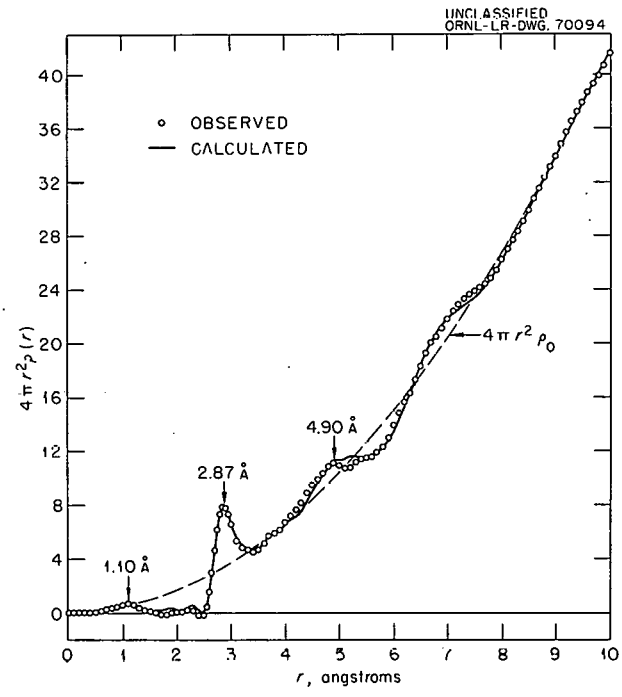

Fig. 9.6. Observed and Calculated Radial Distribution Functions for H_2O.

The radial-distribution function, Fig. 9.7, shows a prominent peak at about 3.83 A which is attributed to Pb–Pb interactions. The area of the peak, assuming that all other interactions in the neighborhood of this distance can be represented by a continuous distribution of distances, corresponds to about three lead neighbors per lead atom. The only other discernible feature of structural significance is the first peak at about 2.5 A, attributed to close Pb–O interactions. The area of the peak corresponds to about four oxygen atom neighbors per lead atom.

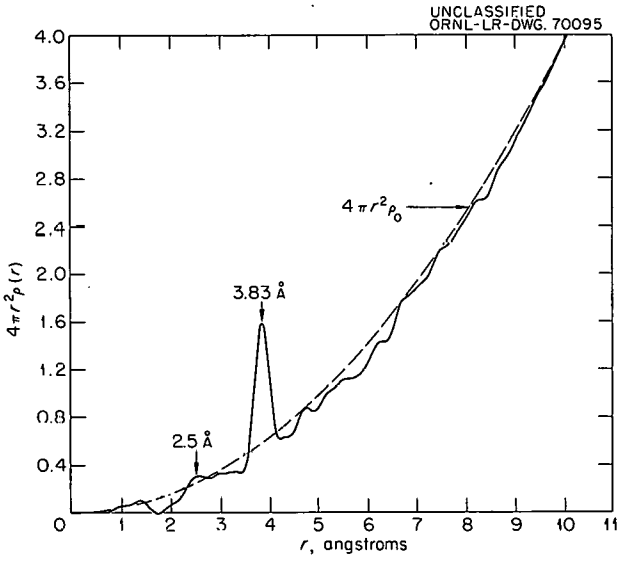

Fig. 9.7. Radial Distribution Function for Aqueous $Pb(OH)ClO_4$, Calculated from Observed Data.

The results are consistent with a model conforming to the symmetry of the point group T_d, having four lead atoms in a tetrahedral arrangement. A hydroxyl ion is assumed to be above the centers of each of the planes containing three lead atoms, along a line perpendicular to the planes as shown in Fig. 9.8, giving three $(OH)^-$ neighbors per lead atom.

A least-squares refinement of the parameters for this model, using the portion of the observed data with $s > 7$, gave a Pb–Pb distance of 3.828 ± 0.002 A and a Pb–O distance of 2.52 ± 0.02 A (the errors are the least squares standard deviations).

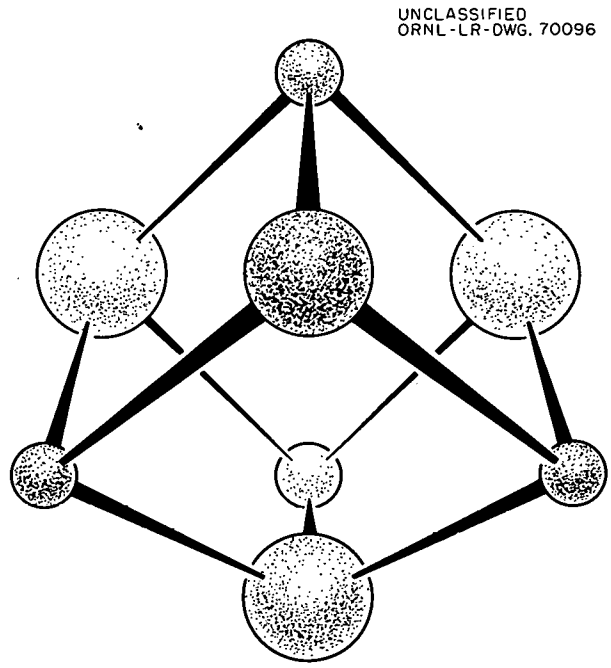

Fig. 9.8. Model for Polymeric Unit $[Pb(OH)]_4^{4+}$. Lead atoms are designated by small circles. Large circles represent assumed positions for oxygen atoms.

A Contour-Plotting Computer Program

H. A. Levy R. D. Ellison

A program has been prepared to plot contours of a two-dimensional density function using the California Computer Products model 570 magnetic-tape plotter. The code is written in FORTRAN, with all parts that apply specifically to this plotter contained in separate subroutines so as to facilitate conversion of the code for use with other plotters.

The function whose contours are to be plotted must have been previously evaluated at points on a grid. The user must supply this array and a subroutine to regulate its storage and conversion to proper form for use by this code. Other data to be supplied by the user are: (1) the direction of projection or, for a three-dimensional problem, the number of sections to be plotted; (2) the portions of the input array that are to be plotted; (3) the scale of the plot; (4) the angle between axes; (5) the unit of length as measured along each axis; and (6) the contour interval and the minimum and maximum contour levels to be plotted. The axes

may be interchanged to control the orientation of the plot on the page, and, if desired, a reference net may be plotted.

Contour points are located by inverse linear interpolation along the sides of triangles formed by passing three sets of parallel lines through the grid. The code finds all the contours passing through a pair of these triangles and scans the entire grid, using successive pairs of triangles rather than tracing a single contour its entire length before considering the next one.

Figure 9.9 shows one section of a Patterson (vector-density) function as plotted by this program. The data for this plot are the neutron diffraction intensities from a crystal of potassium hydrogen chloromaleate. The function was evaluated using the MIFR1 code written by W. G. Sly and D. P. Shoemaker (Accession No. 118, American Crystallographic Association Computer Program Listing); the array of values was put into form for use by the plotter program by the Patterson Superposition Program written by B. R. Penfold (Accession No. 167, American Crystallographic Association Computer Program Listing).

A Computer Program to Postulate Crystal Structures

W. R. Busing

An experimental computer program has been prepared which will postulate crystal structures when given the unit cell size, symmetry, and number of molecules per cell. The present program makes use of some chemical information by excluding structures with interatomic distances shorter than a specified radius sum. For ionic crystals it also calculates an approximate Coulomb energy for each structure. Future versions will make use of more detailed information on molecular geometry.

Two purposes are foreseen for a program of this type. One is to deduce new chemical knowledge by comparing crystal structures postulated on the

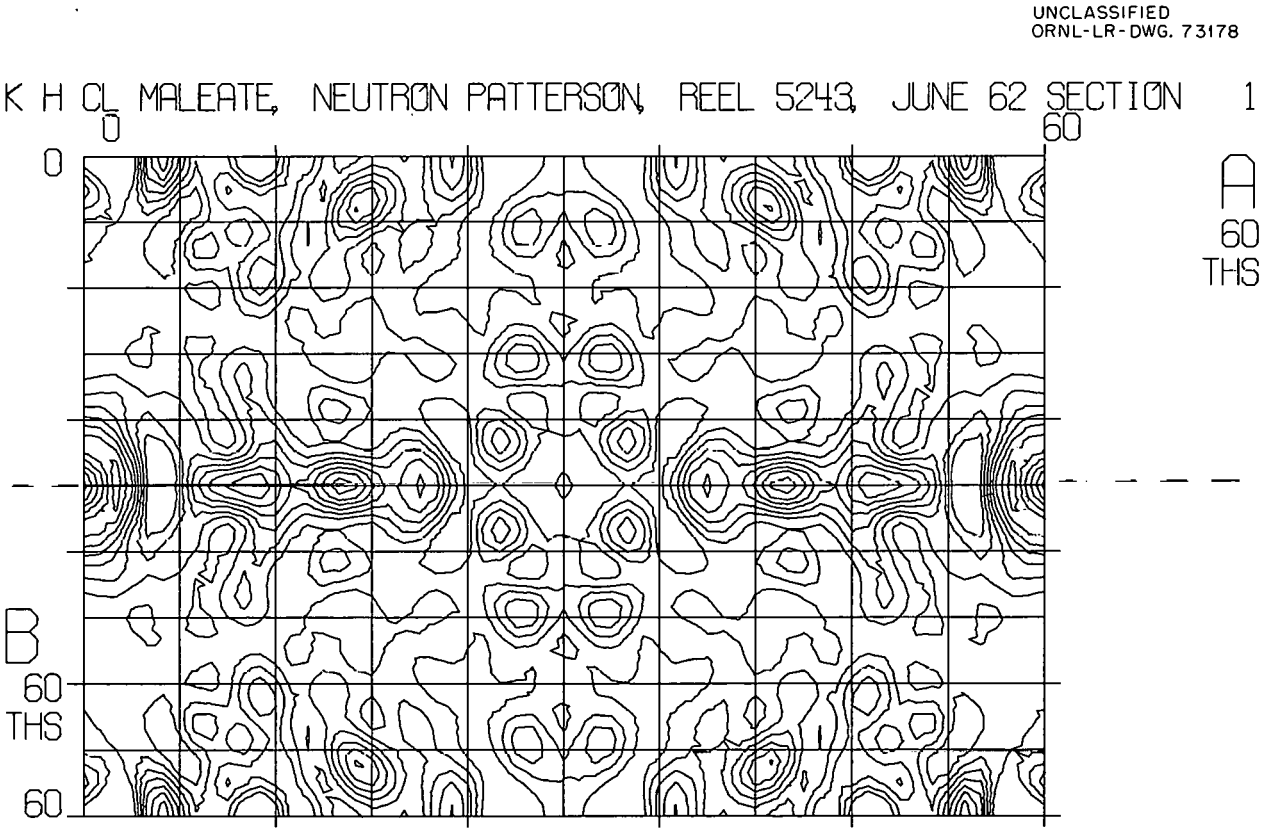

Fig. 9.9. Plot of One Section of a Patterson (Vector-Density) Function.

basis of preliminary information with those determined experimentally. The other is to serve as an aid to the solution of structures from x-ray or neutron diffraction data. For this purpose the program compares the structure factors calculated for each trial arrangement with those obtained from the observed diffraction intensities. The program has been used successfully in this way to obtain a trial structure for $LiCsF_2$ based on 13 observed x-ray intensities.[18]

Structures are generated by advancing the atoms across a grid of points in the basic asymmetric unit until all acceptable combinations of positions have been obtained. As each type of atom is placed, the symmetry-related atoms are generated in all the asymmetric units adjacent to the basic one. A position is rejected if it is too close either to a previously accepted atom or to a symmetry-related atom of its own type. Special positions are recognized by the coincidence of two or more equivalent locations, and the number of atoms occupying the site are computed. Any atoms of a given kind which are not needed to fill the site are treated as a new type of atom to be placed. Positions which require more than the available number of atoms are rejected.

The interval of the grid over which the atomic positions are scanned must be chosen so that the special positions of the space group are included, and the limits of the scan are selected to avoid duplication of symmetry-related points. Computing time is conserved by restricting the scan to the special positions when the number of atoms available is less than the number of general positions. The range of scan for the first type of atom is further reduced to prevent the generation of equivalent structures.

The time required on the IBM 7090 computer will be less than 20 min for many types of problems. Further work is in progress to improve the program and to extend its applications.

[18] J. H. Burns, *Reactor Chem. Div. Ann. Progr. Rept. Jan. 31, 1962*, ORNL-3262, p 17.

Computer Programs for Crystallography

D. J. Wehe[19] K. O. Martin[19]
W. R. Busing H. A. Levy

In the field of x-ray and neutron diffraction crystallography there are certain computational procedures which are used so universally that it would be very desirable to avoid duplicating the effort of programming them for a high-speed computer. This goal has been difficult to attain, however, because of the differences from time to time and from place to place in the kind of machine available and in the standard operating procedures used. For example, certain programs which were originally written for the Oracle were later reprogrammed for the IBM 704 computer. These were then revised once when the Oak Ridge operating system was adopted and again for use with the IBM 7090 computer. Crystallographers at other locations have made still other revisions to adapt these programs to the systems available to them.

Now, with new computing machines proposed for the Laboratory, we have attempted to expedite future changes by rewriting several programs in the universal language of FORTRAN and providing detailed reports or program descriptions. These programs include the calculation of absorption corrections for single crystal diffraction measurements,[20,21] a general least-squares program for fitting a set of observations with an arbitrary function,[22] a crystallographic structure factor least-squares refinement program,[23] and a program for evaluating interatomic distances, angles, and other functions of the least-squares parameters with their standard errors.[24] Work is also in prog-

[19] Mathematics Panel.

[20] W. R. Busing and H. A. Levy, *Acta Cryst.* **10**, 180 (1957).

[21] D. J. Wehe, W. R. Busing, and H. A. Levy, *OR ABS – A FORTRAN Program for Calculating Single Crystal Absorption Corrections*, ORNL TM-229 (1962).

[22] W. R. Busing and H. A. Levy, *OR GLS – A General FORTRAN Least Squares Program*, ORNL report (in preparation).

[23] W. R. Busing and H. A. Levy, *A Crystallographic Least Squares Refinement Program for the IBM-704*, ORNL CF-59-4-37 (April 1959).

[24] W. R. Busing and H. A. Levy, *A Crystallographic Function and Error Program for the IBM-704*, ORNL CF-59-12-3 (Dec. 9, 1959).

ress on revised programs to control the ORNL automatic three-dimensional neutron diffractometer and to process the data produced by this instrument.

CALORIMETRY

Low-Temperature Heat Capacity of Potassium Hexabromorhenate(IV)

R. B. Bevan, Jr. R. A. Gilbert
R. H. Busey

The need to confirm the anomalous heat capacity of K_2ReBr_6 observed[25] above 200°K has prompted further measurements on this compound. Unusual thermal behavior was not unexpected, however, since the similar compound, K_2ReCl_6, has a very extraordinary low-temperature heat capacity.[26] The procedure for verifying the results was the same as employed in the K_2ReCl_6 measurements, namely, measurement of the heat capacity of a sample of K_2ReBr_6 prepared by a different procedure. A bromide analysis is not a sensitive method for determining the purity with respect to a hydrolysis-product impurity. For example, the presence of 1 mole % $K_2Re(OH)Br_5$ would lower the bromide content only 0.1% of the theoretical value.

Preliminary measurements were made on a sample prepared by recrystallization of the original sample of K_2ReBr_6 from constant boiling aqueous HBr (48%). Results in the anomalous region (200 to 300°K) differed significantly from the results on the first sample. The measurements on this sample were discontinued.

A third sample was prepared[27] by HBr reduction[28] of $KReO_4$ in the presence of an equivalent amount of KBr. The solution was kept under 1 atm pressure of HBr during the reduction and crystallization of the product in order to minimize hydrolysis. The bromide analyses gave (64.33 ± 0.06)% vs 64.46% theoretical bromide content.

The heat capacity of this third sample is lower than the first by 0.5% at 40°K, 1.2% at 100°K, and 2.0% at 200°K. In the region of the antiferromagnetic transition (13 to 18°K), the temperature of the heat capacity maximum is approximately 14.8 vs 15.1°K for the first sample. In the anomalous region above 200°K, the heat capacity of the third sample has a single, broad maximum at 258°K instead of two maxima at 225 and 246°K observed on the first sample. The heat contents from 200 to 290°K of the two samples, however, agree to 0.1%.

The poor agreement between the two samples places a large uncertainty upon the entropy calculated from the data. With the data at present available, it is not possible to decide which sample most closely represents pure K_2ReBr_6, if it exists. The revised entropy of K_2ReBr_6 at 298.16°K is 108.0 ± 1.5 cal deg^{-1} $mole^{-1}$.

Molar Enthalpies of Mixing in the Molten LiF-KF System

R. A. Gilbert

Preliminary data reported elsewhere[29] showed that molar enthalpies of mixing in the liquid LiF-KF system are obtainable, as a function of the composition, by means of the Bunsen ice calorimeter. The study of this system at 875°C is now complete, and the results are given in Table 9.3 and shown graphically in Fig. 9.10

The value reported for the 50-50 mixture (−1213 cal/mole) confirms the estimate by Aukrust *et al.*,[30] that the maximum enthalphy of mixing in this system should be about 1.2 kcal.

The system exhibits energetic asymmetry as is shown by the following limiting heats of solution:

$$\text{for KF in LiF, } -\left(\frac{\partial \Delta H^m}{\partial X}\right)_{X \to 1} = -4945 \text{ cal/mole;}$$

$$\text{for LiF in KF, } \left(\frac{\partial \Delta H^m}{\partial X}\right)_{X \to 0} = -3886 \text{ cal/mole .}$$

[25] R. B. Bevan, Jr., and R. H. Busey, *Chem. Div. Ann. Progr. Rept. June 20, 1960*, ORNL-2983, p 71.

[26] R. H. Busey, H. H. Dearman, and R. B. Bevan, Jr., *J. Phys. Chem.* **66**, 82 (1962).

[27] By D. E. LaValle of the Analytical Chemistry Division.

[28] $CrBr_2$ was used as reducing agent for the first sample.

[29] R. A. Gilbert, *Reactor Chem. Div. Ann. Progr. Rept. Jan. 31, 1962*, ORNL-3262, p 41.

[30] E. Aukrust *et al.*, *Ann. N.Y. Acad. Sci.* **79**, 830 (1960).

Table 9.3. Heat-of-Mixing Data for the System LiF-KF

X_{LiF}, Mole Fraction of LiF	Total Moles	Calories Obtained	Calories Possible	Difference	ΔH^M (cal/mole)	$\frac{\Delta H^M}{X(1-X)}$ (cal/mole)
0.101	0.1833	3331	3399	− 68	− 371	−4090
0.193	0.1921	3470	3551	−131	− 682	−4371
0.301	0.2077	3616	3813	−197	− 948	−4502
0.385	0.2280	3937	4187	−250	−1096	−4624
0.503	0.2407	4082	4374	−292	−1213	−4852
0.593	0.2600	4404	4705	−301	−1158	−4805
0.747	0.3340	5682	5993	−311	− 931	−4942
0.900	0.3441	5970	6125	−155	− 450	−4987

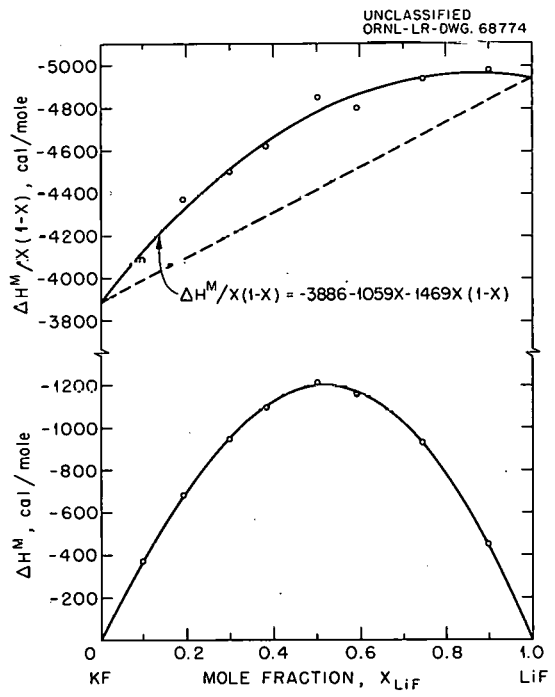

Fig. 9.10. Molar Integral Heats of Mixing (ΔH^M) in Mixtures of LiF-KF at 875°C.

The relative partial molal heat contents of the components can be calculated from the equation shown in Fig. 9.10 and are

$$\bar{L}_{LiF} = -X^2_{LiF}\,(1358 + 7994X_{LiF} - 4407X^2_{LiF}),$$

$$\bar{L}_{KF} = -X^2_{KF}\,(4535 + 3758X_{KF} - 4407X^2_{KF}).$$

MASS SPECTROMETRY

A Mass Spectrometric Investigation of the Decomposition of Ammonia

C. E. Melton

The radiolytic and catalytic decomposition of ammonia were investigated with our high pressure (up to 1 mm in the ionization chamber) research mass spectrometer.

In the radiolytic study, NH_3 was irradiated with 90-ev electrons over the pressure range of 0.001 to 1 mm, and charged transient species, both positive and negative, were observed by employing the techniques previously developed at this Laboratory.[31] The NH_4^+ was by far the most abundant species observed in the radiolysis at 0.1 mm pressure and accounted for over 80% of the total ionization (Table 9.4). The rate constant and cross section for NH_4^+ production by the reaction given in Table 9.4 were determined, using the estimates and approximations previously noted.[32]

In the negative ion spectrum, transient species of mass greater than the parent (mass 17) are negligible, as shown by Table 9.5. It is also noted in Table 9.5 that the positive ions are about 10^4 times more abundant than the negative

[31] C. E. Melton, *J. Chem. Phys.* **33**, 647 (1960).

[32] C. E. Melton, "Ion-Molecule Reactions," in *Mass Spectrometry of Organic Ions*, ed. by F. W. McLafferty, Academic Press, New York, 1962.

Table 9.4. Transient Species Observed in the Radiolysis of Ammonia at 0.1 mm Pressure

m/e	Positive Ion	Percent Abundance	Probable Reaction	k in 10^{-9} cc molecule^{-1} sec^{-1}	$\sigma(10^{-16}$ cm$^2)$
14	N	0.1	$N_3H \rightsquigarrow N^+ + 3H$		
15	NH	0.4	$NH_3 \rightsquigarrow NH^+ + 2H$		
16	NH_2	4.3	$NH_3 \rightsquigarrow NH_2^+ + H$		
17	NH_3	12.7	$NH_3 \rightsquigarrow NH_3^+$		
18	NH_4	82.2	$NH_3^+ + NH_3 \longrightarrow NH_4^+ + NH_2$	1.5	44
29	N_2H	0.03	$N^+ + NH_3 \longrightarrow N_2H^+ + 2H$ (?)		
30	N_2H_2	0.01	$NH^+ + NH_3 \longrightarrow N_2H_2^+ + 2H$ (?)		
31	N_2H_3	0.02	$NH^+ + NH_3 \longrightarrow N_2H_3^+ + H$ (?)		
32	N_2H_4	0.08	$NH_2^+ + NH_3 \longrightarrow N_2H_4 + H$	0.004	0.1
33	N_2H_5	0.02	$NH_2^+ + NH_3 \longrightarrow N_2H_5^+$	0.001	0.03
35	N_2H_7	0.10			

Table 9.5. Transient Species Observed in the Radiolysis of Ammonia at 1.2 mm Pressure

m/e	Negative Ion	Percent Abundance[a]	Probable Reaction
15	NH	0.24	$NH_3 \rightsquigarrow NH^- + 2H$
16	NH_2	45.90	$NH_3 \rightsquigarrow NH_2^- + H$
17	NH_3	51.91	$NH_3 \rightsquigarrow NH_3^{-*}$; $NH_3^{-*} + NH_3 \longrightarrow NH_3^- + NH_3$
28	N_2	0.04	$NH_3 + NH_3 \longrightarrow N_2^- + 6(H)$ (?)
31	N_2H_3	0.51	$NH_3^- + NH_3 \longrightarrow N_2H_3^- + 3H$
33	N_2H_5	0.21	$NH_2^- + NH_3 \longrightarrow N_2H_5^-$
34	$(NH_3)_2$	0.90	$NH_3^- + NH_3 \longrightarrow (NH_3)_2^-$
42	N_3	0.04	$N_2H_3^- + NH_3 \longrightarrow N_3^- + 6(H)$ (?)
43	N_3H	0.06	$N_2H_3^- + NH_3 \longrightarrow N_3H^- + 5(H)$ (?)
44	N_3H_2	0.12	$(NH_3)_2^- + NH_3 \longrightarrow N_3H_2^- + 7(H)$ (?)
49	N_3H_8	0.01	$(NH_3)_2^- + NH_3 \longrightarrow N_3H_8^- + 2(H)$
51	$(NH_3)_3$	0.01	$(NH_3)_2^- + NH_3 \longrightarrow (NH_3)_3^-$

[a] $\dfrac{NH_2^-}{NH_2^+} = \dfrac{1}{8000}$

ions, for the conditions utilized in this experiment. It is clear therefore, that the principal charged intermediate in the radiolytic decomposition of NH_3 is the NH_4^+ ion.

In the catalytic decomposition of NH_3, the NH_4^+ ion was also the most abundant transient species observed (Table 9.6). These results were obtained by using a platinum catalyst[33] in the ionization chamber of the mass spectrometer. The transient radicals were ionized by electrons for detection in the mass spectrometer, but the ions evolving from the hot catalyst were observed directly[34]. By utilizing mixtures of H_2:NH_3 and D_2:NH_3 we were able to ascertain that NH_4^+ is produced by a reaction between NH_3 and H_2 which is formed from the decomposition of NH_3. The rate of NH_4^+ formation is dependent upon the first power of the H_2 pressure rather than $(H_2)^{1/2}$, which suggests that NH_3 reacts with H_2 molecules rather than H atoms adsorbed on the surface.

The production of NH_4^+ by catalysis has an important bearing on our radiolytic study. We were unable to determine conclusively the fate of the NH_4^+ in the radiolytic study because of possible interference from such things as products formed by ion-molecule reactions. However, in the catalytic study, NH_4^+ was the only positive ion produced by the catalyst, thus giving us only a single ion beam to investigate. (We have already shown that the reactions of ions in ion-molecule reactions do not depend upon the source of the ion.[35]) Therefore, by adding N_2, H_2, or NH_3 to the system, any other ions observed would have been produced by a reaction between NH_4^+ and the neutral molecules added. Since no other positive ions were observed even at pressures in the ionization chamber as high as 1 mm of the reactant gases, we conclude that NH_4^+ does not undergo subsequent ion-molecule reactions with N_2, H_2, or NH_3. This illustrates how catalytic investigations can be utilized to supplement radiolysis studies.

The activation energy for the catalyzed decomposition of NH_3 was also investigated. This was done by using two different methods. Method 1 consisted in determining the activation energy for several different temperature ranges (e.g., 300 to 310, 320 to 330°C, etc.). Ordinarily the observed activation energy is independent of temperature, but in our flow system the concentration of NH_3 remains essentially constant, whereas the concentration of the product H_2 is a function of temperature. Since the reaction is retarded by H_2 (see Fig. 9.11), the measured activation energy varies with the concentration of H_2 and therefore temperature. Ten different determinations, utilizing this method and taking the extrapolated value as the "true" activation energy, gave a value of 44 kcal in the pressure range of from 5 to 15 μ. The value estimated utilizing this method is known to be low by the amount of the heat of adsorption of NH_3 on platinum.

Method 2 consisted in determining the activation energy over a very small temperature range, utilizing a $20H_2$:$80NH_3$ starting mixture in the reaction chamber. By starting with an excess of H_2 and producing less than 1% of NH_3 decomposition, the retarding by H_2 can be considered as constant. This method gives a value of 53 kcal for the activation energy, but the value is high by the amount of the heat of adsorption of H_2 on platinum. The true value of the activation energy therefore lies between 44 and 53 kcal. Literature data cover the broader interval from 40 to 140 kcal.[36]

Table 9.6. Concentration of Species Observed in the Catalytic Decomposition[a] of NH_3 over Platinum at 0.1 mm Pressure and 1200°C

Species	Concentration of N_2[b] (ppm)
$\cdot N$	1
$\cdot NH$	6
$\cdot NH_2$	130
NH_2^-	0.01
NH_4^+	140

[a] 10% NH_3 decomposition.

[b] May be in error by one or more orders of magnitude.

[33] C. E. Melton, *J. Chem. Phys.* **35**, 1751 (1961).

[34] C. E. Melton, *J. Am. Chem. Soc.* **84**, 1491 (1962).

[35] C. E. Melton, to be published in *Journal of Chemical Physics* (Aug. 1, 1962).

[36] K. J. Laidler, "Kinetic Laws in Surface Catalysis," in *Catalysis*, ed. by P. H. Emmett, Reinhold, Baltimore, 1954.

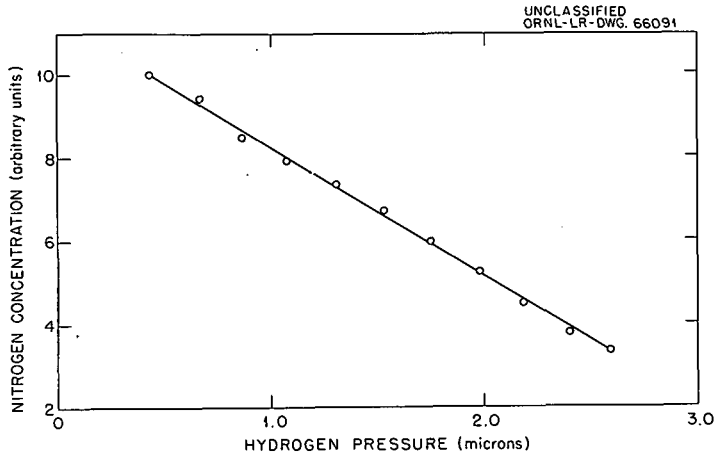

Fig. 9.11. Concentration of N_2 as a Function of H_2 Pressure in the Decomposition of NH_3 on Pt at 400°C and 10 Microns NH_3 Pressure.

Two-Stage Mass Spectrometer

Russell Baldock L. E. Idom

The two-stage mass spectrometer has been developed into a highly sensitive and reliable instrument for the accurate determination of isotopic abundance ratios and is being used continuously in support of the neutron cross-section measurement program of the Chemistry Division. Many measurements of an exploratory nature have been made in order to establish the quality and purity of the starting materials and to monitor chemical procedures for possible introduction of contaminants following irradiation.

Considerable effort has been made to ensure that the microgram or less of material used for the mass spectrometer analysis is in no way contaminated by impurities in the components of the ion-source oven. Tantalum ribbon baked for approximately 8 hr at 2500°C in a high vacuum has been satisfactorily used as an oven material in order to compile a series of measurements of the isotopic abundance ratios which were required in the neutron cross section of Ce^{140}. Tantalum ribbon, pretreated in the same manner, was also satisfactorily used to complete a series of isotopic abundance measurements required for the measurement of the neutron cross section of Sm^{150}. Rhenium ribbon baked for approximately 8 hr at 2000°C in a high vacuum has been entirely satisfactory as oven material to vaporize bismuth for analysis in the mass spectrometer.

Electron Shake-Off and Molecular Fragmentation as the Result of Nuclear Decay[37]

T. A. Carlson

A specially designed mass spectrometer has been used to measure the relative abundances of the ions formed following the decay of a radioactive gas. Much of the work was recently presented in the Physics Division Annual Progress Report, ORNL-3268, under the following titles:

1. "Recoil Energy and Charge Spectra for the Na^{23} Ions Formed from the β^- Decay of Ne^{23}," T. A. Carlson.
2. "Electron Shake-Off Following the β^- Decay of A^{41}," T. A. Carlson.
3. "Fragment and Charge Spectra of the Ions Formed Following Radioactive Decay of $C_2H_5I^{131}$ and CH_3I^{130}," T. A. Carlson and R. M. White.

Besides the above studies, a paper on the decomposition of $(CH_3Xe^{131})^+$ following the nuclear decay of CH_3I^{131} was published in the *Journal of Chemical Physics*. Completed, but not yet reported, is the investigation of CH_3I^{125} and $C_2H_5I^{125}$, in which the role of internal conversion was evaluated. Calculations were also made of the extent of electron shake-off due to recoil energy following

[37] In collaboration with the Physics Division.

the decay of He^6, by use of the sudden approximation; agreement with experimental results was found to be satisfactory.

MOLECULAR BEAM STUDIES

Reaction of D with H_2

S. Datz G. E. Moore E. H. Taylor

Crossed molecular beam techniques were used to study the reaction $D + H_2 = HD + H$. A schematic diagram of the apparatus is shown in Fig. 9.12. The deuterium atomic beam was formed by thermal dissociation in a tungsten furnace heated to 2800°K. The beam was modulated by a 1080-cycle mechanical chopper and collimated. The molecular beam of H_2 was formed by effusion through "crinkly foil" slits[38] at 77°K. The collision region was surrounded by a pumped liquid-helium-cooled trap which acted as a pump for the hydrogen gas. The detector was a 135° magnetic sector mass spectrometer that could be rotated about the scattering center. The use of beam modulation and phase sensitive detection[39]

[38] J. R. Zacharias and R. D. Haun, *MIT Research Laboratory of Electronics,* Rept. NP-5427 (October 1954).

[39] W. L. Fite and R. T. Brackman, *Phys. Rev.* **112**, 1141 (1958).

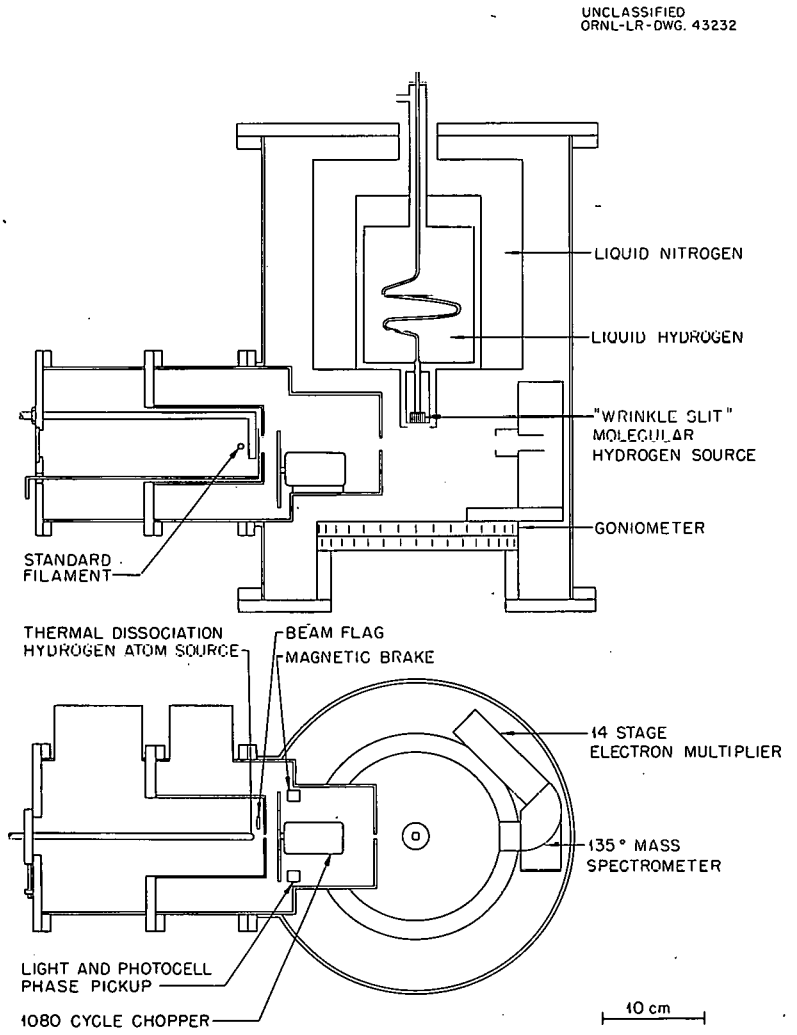

Fig. 9.12. Molecular Beam Apparatus.

permitted the observation of signals in the presence of the very high background levels (signal/background ratio = 10^{-4}) from ambient gas of the same mass. In addition, the choice of 1080 cycles for the modulating frequency permitted the observation of phase shifts resulting from time-of-flight changes.

A calculation of the angular distribution of centroid density was carried out for the two Maxwellian beams[40] for D at 2800 and H_2 at 100°K, with the assumption of an activation energy of 7.5 kcal (see Fig. 9.13). This distribution differs slightly from the centroid flux distribution calculation outlined in ref 40 and was used because the detection in this case (electron bombardment) is density sensitive rather than flux sensitive (as with surface ionization). The change in the calculation is accomplished by dividing the distribution functions [Eqs. (18) and (22) in ref 40] by the velocity of the center of mass in the laboratory system.

The angular distribution of reaction products in the laboratory system will depend upon the momentum imparted to the product fragment in the center-of-mass (c.m.) system upon breakup of the reaction complex. The magnitude of the momentum kick in the c.m. system is a function of the initial relative energy and the energy released in the reaction. The directions of the additional momentum vectors in the c.m. system will be anisotropic if the collision efficiency is different for different molecular orientations and if the lifetime of the complex is short compared to a rotation period.

The heat of reaction in this case is 0.8 kcal. Therefore, if it is assumed that the scattering in the c.m. system is isotropic and that there is no internal excitation of the HD product molecule, the maximum displacement of the product from its centroid vector will be about 60° [compare Eqs. (33–37) of ref 40].

The results of the experiment are shown in Fig. 9.13. Signals from HD were observed from about −20 to +35°. Unfortunately, in spite of all attempts of removal, an HD impurity of about 1% was present in the modulated D atom beam. The elastic scattering of this impurity in the main beam (width about 1°) prevented measurement of the HD reaction product in the angular region from −12 to +12°. However, it is believed that the HD signals outside of this region are sufficiently reliable (i.e., free of elastic scattering contribution) to be recorded here. One reason for this belief is the result of a

[40] Sheldon Datz, D. R. Herschbach, and E. H. Taylor, *J. Chem. Phys.* **35**, 1549 (1961).

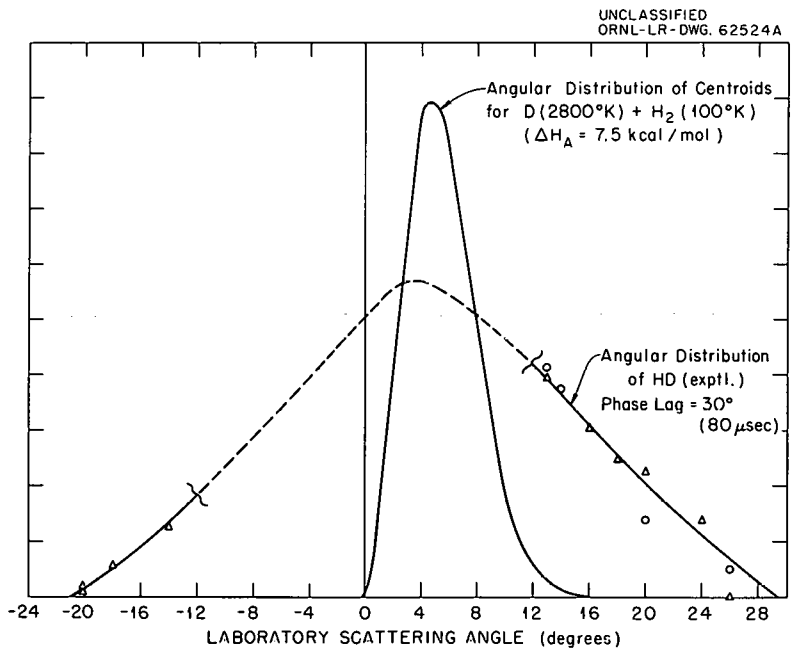

Fig. 9.13. Angular Distributions.

scattering experiment using helium in the cross beam, in which no HD signal was observable above 10° in scattering angle.

The observed distribution of product molecules is too narrow and displaced too little (10°) from that calculated for the centroids for the assumption of no internal excitation to be realistic. Excitation of vibration is certainly not to be expected for collision involving 6 to 8 kcal/mole (activation energy about 6 kcal/mole) since the first excited vibrational level is about 10 kcal/mole above the zero point level. This leaves an impasse, since the impact parameter necessary for the absorption of so much energy in rotation is preposterously large.

Interactions of Gases and Surfaces

S. Datz G. E. Moore E. H. Taylor

If a solid is placed at the scattering center of the system described above (and the cross beam eliminated), interactions between gases (as molecular or atomic beams) and surfaces can be studied. This technique has been used to study the interactions (adsorption and energy transfer) between polished polycrystalline platinum surfaces and helium, molecular and atomic deuterium, and argon. These experiments were preliminary to catalytic investigations now under way. A summary of the gas-surface interactions follows[41].

The angular distributions of He, D_2, and Ar scattered from platinum depend strongly upon the temperature of the platinum surface: The distributions from a high-temperature surface (greater than about 150 to 200°C) are surprisingly specular, whereas those from a surface at lower temperature are diffuse (illustrated for D_2 in Fig. 9.14). Specular reflection requires an atomically smooth reflecting surface as well as an absence of appreciable residence of the projectile on the surface. Microscopic and diffraction studies of the platinum foil after the experiments showed large, nearly parallel, single crystals, characterized by a surprising smoothness, which apparently met the first requirement for specular reflection. At the higher surface temperatures, then, the gas molecules in the beam must not have resided on the surface for appreciable times. The transition from specular reflection at high surface temperature to diffuse reflection at lower temperatures is probably associated with the adsorption of a gaseous contaminant (not hydrogen, but probably oxygen) at the lower temperature.

Variations in the displacement of the reflected distributions from high-temperature platinum with respect to the true specular angle, as the temperature of the beam, its composition, and the angle of incidence were varied, suggest some gas-surface interaction even under these conditions. This interaction seems most likely to be a partial exchange of energy without appreciable adsorption. Indeed, an appreciable increase in the velocity of argon atoms was detected when a room temperature beam was reflected (specularly) from a high-temperature platinum surface.

Reactions of Alkali Metals

R. E. Minturn S. Datz E. H. Taylor

A number of surface-ionization gages of different configurations were tested for the detection of atomic and molecular beams. New filament materials were studied, including a filament made by depositing and decomposing tungsten carbonyl on a very thin platinum strip. A high-purity tungsten wire drawn from single crystal tungsten by the Linde Company was superior as a filament material to any previously encountered. The problem of devising a differential detector that does not give rise to spurious effects because of scattering of beam molecules from its own members was attacked and solved.

A fast-response, surface-ionization detector utilizing an electron multiplier in order to amplify very weak signals was devised and constructed. It is to be utilized with a phase-sensitive electronic network in the study of energy distributions of product molecules.

A multidisk mechanical velocity selector was completed and installed, and it and its associated electronics were given preliminary trial runs.

Preliminary scattering experiments with rubidium and hydrogen bromide were made, and the reaction between potassium and hydrogen bromide was reexamined more closely.

---

[41] For details see Sheldon Datz, G. E. Moore, and E. H. Taylor, "The Reflection of Modulated Helium and Deuterium Molecular Beams from Platinum Surfaces," *Proceedings of the Third International Symposium on Rarefied Gas Dynamics, Paris, France, June 25–29,* 1962.

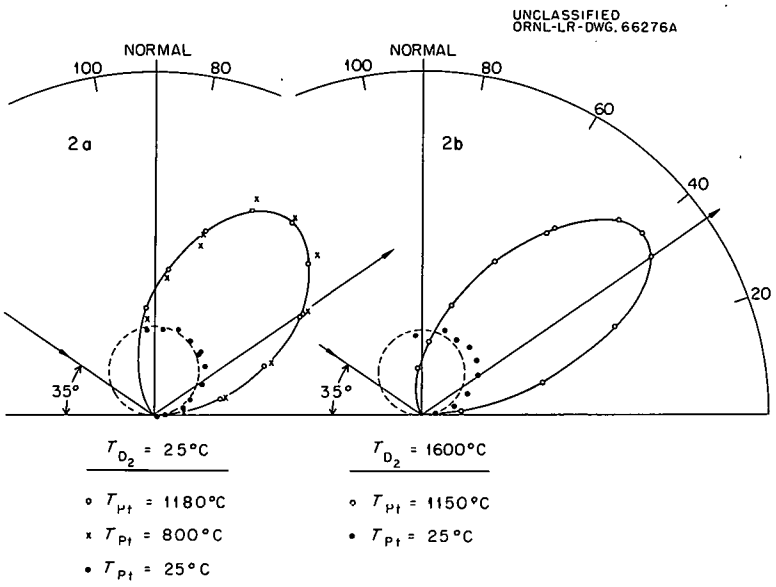

Fig. 9.14. Angular Distributions of Deuterium Reflected from Platinum.

Publications

NUCLEAR CHEMISTRY

A. C. Wahl, R. L. Ferguson, D. R. Nethaway, D. E. Troutner, and K. Wolfsberg, "Nuclear-Charge Distribution in Low-Energy Fission," *Phys. Rev.* **126**, 1112–27 (1962).

R. L. Ferguson and G. D. O'Kelley, "A Survey and Evaluation of U^{233} Fission Yield Data," ORNL CF-62-3-71 (Mar. 29, 1962).

G. D. O'Kelley, *Radiochemical Techniques – Detection and Measurement of Nuclear Radiation*, NAS-NS 3105, National Academy of Sciences–National Research Council, Washington, D.C., 1962.

G. D. O'Kelley, "Scintillation Spectrometry of Charged Particles," *Methods of Experimental Physics* (ed. by L. C. L. Yuan and C. S. Wu), vol 5A, pp 411–36, Academic Press, New York, 1961.

G. D. O'Kelley, "Gamma-Ray Scintillation Spectrometry," *ibid.*, pp 616–41.

R. W. Stoughton, Joseph Halperin, R. E. Druschel, F. J. Johnston, P. M. Lantz, J. H. Oliver, and G. W. Parker, "Measurements of Thermal Cross-Sections and Resonance Integrals Using Pile Neutrons and Activation Techniques," reprinted from *Pile Neutron Research in Physics*, International Atomic Energy Agency, Vienna, 1962.

CHEMICAL SEPARATION OF ISOTOPES

G. M. Begun and L. Landau, "Mass Spectra and Metastable Transitions in Isotopic Nitrous Oxides," *J. Chem. Phys.* **35**, 547–51 (1961).

G. M. Begun and L. Landau, "Metastable Transitions in N_2O^+," *J. Chem. Phys.* **36**, 1083–84 (1962).

J. S. Drury, "Application of Chemical Exchange Methods to Isotopic Separations," chap. 4 in *Progr. Nucl. Energy, Ser. IV* **4**, 308–48 (1961).

D. A. Lee, "Enrichment of Lithium Isotopes by Ion Exchange Chromatography. Influence of Exchange Functional Group on Separation Factor," *J. Chem. Eng. Data* **6**, 565 (1961).

A. A. Palko, J. S. Drury, and W. E. Bull, "Separation of Boron Isotopes. V. The Phenol-BF_3 System," *J. Chem. Phys.* **35**, 103–5 (1961).

G. M. Begun, W. H. Fletcher, and A. A. Palko, "Infrared and Raman Spectra of the Boron-Trifluoride-Dimethyl Ether Complex," *Spectrochim. Acta* **18**, 655–65 (1962).

RADIATION CHEMISTRY

C. J. Hochanadel and J. A. Ghormley, "Effect of Temperature on the Decomposition of Water by Gamma Rays," *Radiation Res.* **16**, 653–60 (1962).

C. J. Hochanadel, "Evidence for Thermal Spikes in the Alpha-Particle Radiolysis of Nitrate Crystals," *Radiation Res.* **16**, 286–302 (1962).

C. J. Hochanadel, "A Simple Device for Determining Slopes Using the Glass Rod Method," *J. Chem. Educ.* **39**, 299 (1962).

H. A. Mahlman, "The OH Yield in the Co-60 γ Radiolysis of HNO_3," *J. Chem. Phys.* **35**, 936 (1961).

J. W. Boyle and H. A. Mahlman, "Iron(III) Molar Extinction Coefficients in Light and Heavy Water Solutions," *Radiation Res.* **16**, 416 (1962).

J. W. Boyle, "Radiation Chemistry of Aqueous Sulfuric Acid Solutions," *Radiation Res.* **16**, 565 (1962).

A. R. Jones, "Radiolysis by Transferred Energy of Compounds Dispersed in Alkali Halide Matrices," *J. Chem. Phys.* **35**(2), 751–52 (1961).

A. R. Jones and R. L. Durfee, "The Radiolysis of Nitrate Ions Dispersed in a Potassium Bromide Matrix," *Radiation Res.* **15**(4), 546–52 (1961).

H. W. Kohn, "Deuterium Exchange Initiated on Silica Gel by Co^{60} Irradiation," *J. Phys. Chem.* **66**, 1017 (1962).

H. W. Kohn, "Surface Carbonium Ions Produced by Irradiating Silica Gel," *J. Phys. Chem.* **66**, 1185 (1962).

H. W. Kohn and E. H. Taylor, "The Effect of Ionizing Radiation on the Surface Properties of Silica Gel," *Actes Congres Intern. Catalyse, 2e, Paris, 1960* **2**, 1461 (1961).

E. H. Taylor, "Irradiation Effects on Catalysts," *Nucleonics* **20**(1), 53 (1962).

P. S. Rudolph, "The Irradiation of Glasses," *Fusion* **9**(1), 9 (1962).

P. S. Rudolph, S. C. Lind, and C. E. Melton, "Ionic Complexes of Xe and C_2H_2 Produced by the Radiolysis of These Gases," *J. Chem. Phys.* **36**, 1031 (1962).

P. S. Rudolph, "Induced Discharge in a Piece of Lead-Cerium Glass," cover picture, *Science* **135**(3505) (1962).

G. E. Boyd, E. W. Graham, and Q. V. Larson, "Recoil Reactions with High Intensity Slow Neutron Sources. IV. The Radiolysis of Crystalline Alkali Metal Bromates with γ-Rays," *J. Phys. Chem.* **66**, 300 (1962).

ORGANIC CHEMISTRY

Harold Kwart, R. W. Spayd, and C. J. Collins, "Evidence for Nitrogen Migration in the Benzilic Acid Rearrangement of Alloxan and Derivatives," *J. Am. Chem. Soc.* **83**, 2579 (1961).

B. M. Benjamin, Pelham Wilder, Jr., and C. J. Collins, "Molecular Rearrangements. XVII. The Deaminations of D- and L-*erythro*-1-Amino-1,2-diphenylpropanol-2 and of D-2-Amino-1,1-diphenylpropane," *J. Am. Chem. Soc.* **83**, 3654 (1961).

B. M. Benjamin and C. J. Collins, "Molecular Rearrangements. XVIII. The Deamination of *erythro*- and *threo*-1-Amino-1-phenyl-2-*p*-tolyl-2-propanol," *J. Am. Chem. Soc.* **83**, 3662 (1961).

C. J. Collins, Joan B. Christie, and V. F. Raaen, "Molecular Rearrangements. XIX. The Thermal Decomposition of N-Acetyl-N-nitroso-1,2,2-triphenylethylamine," *J. Am. Chem. Soc.* **83**, 4267 (1961).

CHEMISTRY OF AQUEOUS SYSTEMS

R. W. Stoughton, A. J. Fry, and J. E. Barney II, "A Study of Thorium-Iodate Complexing in Aqueous Solutions," *J. Inorg. Nucl. Chem.* **19**, 286–97 (1961).

M. H. Lietzke and R. W. Stoughton, "The Calculation of Activity Coefficients from Osmotic Coefficient Data," *J. Phys. Chem.* **66,** 508 (1962); ORNL CF-61-7-38.

M. H. Lietzke, R. W. Stoughton, and T. F. Young, "The Bisulfate Acid Constant from 25 to 225° as Computed from Solubility Data," *J. Phys. Chem.* **65,** 2247 (1961).

M. H. Lietzke and R. W. Stoughton, "The Thermodynamic Investigation of Aqueous Electrolytes to 275°C," *J. Chem. Educ.* **39,** 230 (1962).

M. H. Lietzke, *A Generalized Least Squares Program for the IBM 7090 Computer,* ORNL-3259 (Mar. 21, 1962).

R. M. Rush and G. Scatchard, "Molal Volumes and Refractive Index Increments of $BaCl_2$-HCl Solutions. Mixture Rules," *J. Phys. Chem.* **65,** 2240 (1961).

R. M. Rush, J. S. Johnson, and K. A. Kraus, "Hydrolysis of U(VI): Ultracentrifugation and Acidity Measurements in Chloride Solutions," *Inorg. Chem.* **1,** 378 (1962).

G. E. Boyd and F. Vaslow, "Heats of Solution and Derived Thermodynamic Properties of Alkali-Metal Bromates," *J. Chem. Engr. Data* **7,** 237 (1962).

H. O. Phillips and K. A. Kraus, "Adsorption of Inorganic Materials. IV. Cation Exchange Properties of Zirconium Antimonate," *J. Am. Chem. Soc.* **84,** 2267 (1962).

ELECTROCHEMICAL KINETICS AND ITS APPLICATION TO CORROSION

G. H. Cartledge, "The Comparative Roles of Oxygen and Inhibitors in the Passivation of Iron. III. The Chromate Ion," *J. Phys. Chem.* **65,** 1009 (1961).

G. H. Cartledge, "The Comparative Roles of Oxygen and Inhibitors in the Passivation of Iron. IV. Osmium (VIII) Oxide," *J. Phys. Chem.* **65,** 1361 (1961).

NONAQUEOUS SYSTEMS AT HIGH TEMPERATURE

H. R. Bronstein and M. A. Bredig, "The Electrical Conductivity of Solutions of Metals in Their Molten Halides. II. Sodium–Sodium Iodide, Potassium–Potassium Iodide, and Potassium–Potassium Fluoride," *J. Phys. Chem.* **65,** 1220 (1961).

H. R. Bronstein, A. S. Dworkin, and M. A. Bredig, "The Electrical Conductivity of Solutions of Metals in Their Molten Halides. III. Cerium–Cerium Trichloride," *J. Phys. Chem.* **66,** 44 (1962).

A. S. Dworkin, H. R. Bronstein, and M. A. Bredig, "Ionic Melts as Solvents for Electronic Conductors," *Discussions Faraday Soc.* **32,** 188 (1962).

A. S. Dworkin, H. R. Bronstein, and M. A. Bredig, "Miscibility of Metals with Salts. VI. Lithium–Lithium Halide Systems," *J. Phys. Chem.* **66,** 572 (1962).

A. S. Dworkin, H. R. Bronstein, and M. A. Bredig, "The Electrical Conductivity of Solutions of Metals in Their Molten Halides. V. Praseodymium–Praseodymium Trichloride," *J. Phys. Chem.* **66,** 1201 (1962).

M. A. Bredig, "The Constitution of Cadmium–Potassium Chloride Melts," *Electrochim. Acta* **5,** 299 (1961).

M. A. Bredig, "Notes on X-Ray Studies of Calcium Carbide," *Z. Anorg. Allgem. Chem.* **310,** 338 (1961).

CHEMICAL PHYSICS

Henry Zeldes and Ralph Livingston, "A Paramagnetic Species in Irradiated $NaNO_2$," *J. Chem. Phys.* **35,** 563 (1961).

Ralph Livingston, "Nuclear Quadrupole Resonance," chap. 4.3, *Methods of Experimental Physics*, vol 3, Academic Press, New York, 1962.

P. H. Emmett, Ralph Livingston, Henry Zeldes, and R. J. Kokes, "Formation of Hydrogen Atoms in Irradiated Catalysts," *J. Phys. Chem.* **66**, 921 (1962).

R. D. Ellison, H. A. Levy, and S. W. Peterson, "Cell Parameters and Space Group of Potassium, Rubidium, and Cesium Acid Chloromaleates," *Acta Cryst.* **14**, 1204–5 (1961).

H. G. Smith, "Use of Polaroid Film in Neutron and X-ray Diffraction," *Rev. Sci. Instr.* **33**, 128 (1962).

M. Zocchi, W. R. Busing, R. D. Ellison, and H. A. Levy, "An X-Ray Study of Hydrazine Hydrate, $N_2H_4 \cdot H_2O$," *Acta Cryst.* **15**, 803 (1962).

R. H. Busey and E. Sonder, "Magnetic Susceptibility of Potassium Hexachlororhenate(IV) and Potassium Hexabromorhenate(IV) from 5° to 300°K," *J. Chem. Phys.* **36**(1), 93–97 (1962).

R. H. Busey, H. H. Dearman, and R. B. Bevan, Jr., "The Heat Capacity of Potassium Hexachlororhenate(IV) from 7 to 320°K. Anomalies near 12, 76, 103, and 111°K. Entropy and Free Energy Functions. Solubility and Heat of Solution of K_2ReCl_6. Entropy of the Hexachlororhenate Ion," *J. Phys. Chem.* **66**, 82 (1962).

C. E. Melton, "Studies of Transient Species Formed During Catalytic Reactions of $CO_2 + D_2$ and of 1-Butene," *J. Chem. Phys.* **35**, 1751 (1961).

P. S. Rudolph, S. C. Lind, and C. E. Melton, "Ionic Complexes of Xe and C_2H_2 Produced by the Radiolysis of these Gases," *J. Chem. Phys.* **36**, 1031 (1962).

C. E. Melton, "Observation of NH_4^+ in the Decomposition of Ammonia on Platinum," *J. Am. Chem. Soc.* **84**, 1491 (1962).

S. Datz, D. R. Herschbach, and E. H. Taylor, "Collision Mechanics in Crossed Maxwellian Molecular Beams," *J. Chem. Phys.* **35**(5), 1549 (1961).

T. A. Carlson, A. H. Snell, Frances Pleasonton, and C. H. Johnson, "Electron Shake-Off Following Beta Decay," pp 155–60 in Proceedings of the International Atomic Energy Agency Symposium, *Chemical Effects of Nuclear Transformations, Prague, 1960*, vol 1, 1961.

A. H. Snell, Frances Pleasonton, and T. A. Carlson, "Techniques of Radioactive Recoil Spectrometry and Charge Spectrometry; The Atomic Consequences of Internal Conversion and Electron Capture," pp 147–54 in Proceedings of the International Atomic Energy Agency Symposium, *Chemical Effects of Nuclear Transformations, Prague, 1960*, vol 1, 1961.

T. A. Carlson and R. M. White, "Decomposition of $(CH_3Xe^{131})^+$ Following the Nuclear Decay of CH_3I^{131}," *J. Chem. Phys.* **36**, 2883–87 (1962).

Papers Presented at Scientific and Technical Meetings

NUCLEAR CHEMISTRY

R. L. Robinson,* N. R. Johnson, and E. Eichler, "Decay of Cs^{132}," American Physical Society, Washington, D.C., April 1962 [*Bull. Am. Phys. Soc.* [2]**7**, 352 (1962)].

N. R. Johnson, "Nuclear Spectroscopy Studies of Some Short-Lived Nuclides," Massachusetts Institute of Technology, Cambridge, Massachusetts, December 6, 1961.

N. R. Johnson, "Studies of Nuclear Level Schemes in the Medium-Weight Region," Massachusetts Institute of Technology, Cambridge, Massachusetts, December 7, 1961.

N. R. Johnson, "Uses of Radioactivity in Chemistry – Principles and Techniques," (1) Virginia Union University, Richmond, Virginia, December 5, 1961, (2) Tennessee Agricultural and Industrial State University, Nashville, Tennessee, February 9, 1962, (3) Jacksonville University, Jacksonville, Florida, May 1, 1962.

N. R. Johnson, "Nuclear Properties of Medium-Weight Nuclei," Florida State University, Tallahassee, Florida, April 27, 1962.

G. D. O'Kelley, "Special Topics in Scintillation Counting," ORINS Radioisotopes Training School, Oak Ridge, Tennessee, August 4, September 22, 1961; January 19, March 16, and May 11, 1962.

C. D. Goodman,* G. D. O'Kelley, and D. A. Bromley, "A 20,000-Channel Pulse-Height Analyzer with a Two-Coordinate Address," Symposium on Nuclear Instruments, Atomic Energy Research Establishment (AERE), Harwell, Berkshire, England; proceedings to be published by Academic Press, New York.

R. L. Ferguson,* D. E. Troutner, and G. D. O'Kelley, "Studies of the Mass-99 Fission-Product Chain," American Physical Society, Southeastern Section, Florida State University, April 5–7, 1962.

N. B. Gove* and G. D. O'Kelley, "Decay of Pm^{150}," American Physical Society, Washington, D.C., April 23–26, 1962 [*Bull Am. Phys. Soc.* [2]**7**, 352 (1962)].

R. J. Silva* and E. Eichler, "Level Structure of Ge^{71}, Ge^{73}, Ge^{75} and Ge^{77} from the (d,p) Reaction," American Physical Society Meeting, Washington, D.C., April 23–26, 1962 [*Bull. Am. Phys. Soc.* [2]**7**, 315 (1962)].

P. M. Lantz, "Thermal Neutron-Capture Cross Section and Resonance Capture Integral of Ce^{144}," American Nuclear Society, Boston, Massachusetts, June 18–21, 1962.

RADIATION CHEMISTRY

E. H. Taylor, "The Use of Ionizing Radiation in the Study of Catalysis," Chicago Catalysis Club, Chicago, Illinois, December 11, 1962.

---

*Speaker.

C. J. Hochanadel, "Photolysis of Dilute Hydrogen Peroxide Solution in the Presence of Dissolved Hydrogen and Oxygen. Evidence Relating to the Nature of the Hydroxyl Radical and Hydrogen Atom Produced in the Radiolysis of Water," Radiation Research Society, Colorado Springs, Colorado, May 20–23, 1962.

J. W. Boyle, "Radiation Chemistry," ORINS Industrial Radioisotopes Training Course, Oak Ridge, Tennessee, October 12, 1961, February 8, 1962, and April 4, 1962.

J. W. Boyle, "Some Recent Studies in Radiation Chemistry of Aqueous Solutions," Analytical Group of East Tennessee Section of the American Chemical Society, Oak Ridge, Tennessee, March 27, 1962.

J. W. Boyle, "Radiation Chemistry of Aqueous Sulfuric Acid Solutions," Radiation Research Society, Colorado Springs, Colorado, May 20–23, 1962.

J. W. Boyle, "Radiation Chemistry of Aqueous Sulfuric Acid Solutions," Michigan State University Section of the American Chemical Society, East Lansing, Michigan, May 24, 1962.

H. A. Mahlman, "Radiation Chemistry," ORINS Industrial Radioisotopes Training Course, Oak Ridge, Tennessee, August 22, and June 1961.

P. S. Rudolph, "The Irradiation of Glasses," American Scientific Glassblowers Society, Oak Ridge, Tennessee, September 2, 1961.

P. S. Rudolph, "Radiation Chemistry," ORINS Advanced Radioisotopes and Research Course, Oak Ridge, Tennessee, May 31, 1962.

ORGANIC CHEMISTRY

C. J. Collins, "The Deamination Reaction," (1) Clemson College, Clemson, South Carolina, October 24, 1961, (2) University of Georgia, Athens, Georgia, November 6, 1961.

C. J. Collins, "Some Secondary Isotope Effects of Deuterium in Carbon-14," University of Georgia, Athens, Georgia, November 7, 1961.

C. J. Collins, "Some Small Isotope Effects," University of Delaware, Newark, Delaware, April 17, 1962.

C. J. Collins, "Recent Experiments in the Deamination Reaction," University of Delaware, Newark, Delaware, April 18, 1962.

W. H. Baldwin, "Natural Radiocarbon Dating," Beta Kappa Chi Scientific Honorary Society, South Carolina State College, Orangeburg, South Carolina, December 1961.

CHEMISTRY OF AQUEOUS SYSTEMS

R. W. Stoughton, "Aqueous Electrolyte Solutions to 250°C," Chemistry Department of the University of Wisconsin, Madison, Wisconsin, January 31, 1962.

R. W. Stoughton, "Aqueous Electrolyte Solutions to 250°C: Species and Thermodynamic Properties," Minnesota Section of the American Chemical Society, St. Paul, Minnesota, February 1, 1962.

M. H. Lietzke and R. W. Stoughton,* "Some Thermodynamic Studies in Aqueous Solutions to 275°C," 141st National Meeting of the American Chemical Society, Washington, D.C., March 20–29, 1962.

M. H. Lietzke, "The Thermodynamic Investigation of Electrolyte Solutions to 275°C," 140th National Meeting of the American Chemical Society, Chicago, Illinois, September 3–8, 1961.

*Speaker.

M. H. Lietzke, "Thermodynamic Calculations on a High Speed Computer," (1) Midsouth Meeting of the Association for Computing Machinery, Oak Ridge, Tennessee, November 10, 1961, (2) University of Southwestern Louisiana, Lafayette, Louisiana, November 17, 1961.

M. H. Lietzke, "High Temperature Solution Thermodynamics," University of Georgia, Athens, Georgia, May 18, 1962.

M. H. Lietzke, "Mathematical Techniques for Correlating Thermodynamic Properties of Inorganic Compounds in Aqueous Solutions," Vanderbilt University, Nashville, Tennessee, May 8, 1962.

M. H. Lietzke, "A Mathematical Model for the Solvent Extraction of Uranyl Nitrate and Nitric Acid," Vanderbilt University, Nashville, Tennessee, May 8, 1962.

M. H. Lietzke, "The Impact of High Speed Computing on Chemistry," Fisk University, Nashville, Tennessee, July 24, 1961.

W. C. Waggener,* A. J. Weinberger, and R. W. Stoughton, "Spectrophotometry of Aqueous Homogeneous Reactor Fuel Components at Elevated Temperatures and Pressures," 2d Conference on Nuclear Reactor Chemistry, Gatlinburg, Tennessee, October 10, 1961.

R. M. Rush,* K. A. Kraus, and J. S. Johnson, "Ultracentrifugation Studies of Uranyl Hydrolysis," 140th National Meeting of the American Chemical Society, Chicago, Illinois, September 3–8, 1961.

D. F. Keeley, J. S. Johnson,* and K. A. Kraus, "Investigation of Inorganic Hydrolytic Polymerization with the Ultracentrifuge," 141st National Meeting of the American Chemical Society, Washington, D.C., March 20–29, 1962.

J. S. Johnson, R. M. Rush, K. A. Kraus, and E. W. Anacker,* "Equilibrium Ultracentrifugation and Light Scattering of Sodium Lauryl Sulfate and Dodecyltrimethylammonium Bromide Solutions," 141st National Meeting of the American Chemical Society, Washington, D.C., March 20–29, 1962.

J. S. Johnson,* R. M. Rush, and K. A. Kraus, "Activity Coefficients of Two and Three Component Systems with the Ultracentrifuge," 141st National Meeting of the American Chemical Society, Washington, D.C., March 20–29, 1961.

G. E. Boyd, "The Analogy Between Aqueous Electrolyte Solutions and Ion-Exchange Resins," ACS Kendall Award Symposium, 141st National Meeting of the American Chemical Society, Washington, D.C., March 20–29, 1962.

Fred Vaslow, "Calorimetric Measurements of the Heats of Ion Exchange and Related Reactions," 16th Annual Calorimetry Conference, Ottawa, Canada, August 17, 1961.

F. Nelson, "Study of Inorganic Complexes by Ion Exchange Tracer Techniques," Southwest-Southeast Regional American Chemical Society Meeting, New Orleans, Louisiana, December 7–9, 1961.

K. A. Kraus, "Ion Exchange in Inorganic Separations," 15th Annual Louisiana State University Symposium on Modern Methods of Analytical Chemistry, Baton Rouge, Louisiana, January 29–February 1, 1962.

ELECTROCHEMICAL KINETICS AND ITS APPLICATION TO CORROSION

G. H. Cartledge, "Recent Studies of the Action of Inorganic Inhibitors," Symposium on Recent Advances in Theoretical Corrosion, Kansas City, Missouri, March 1962.

E. J. Kelly, "Transient Polarization Characteristics of Iron in Benzoic Acid Solution," Electrochemical Society Meeting, Los Angeles, California, May 1962.

R. E. Meyer, "Reduction of Oxygen on Passive Zirconium," Electrochemical Society Meeting, Los Angeles, California, May 1962.

*Speaker.

F. A. Posey, "Effect of Adsorbed Anions on Reduction Processes on Passive Stainless Steel," Electrochemical Society Meeting, Los Angeles, California, May 1962.

NONAQUEOUS SYSTEMS AT HIGH TEMPERATURE

P. A. Agron, "X-Ray and Neutron Diffraction Studies of Molten Salts," Research Center, Union Carbide Nuclear Company, Tuxedo, New York, October 30, 1961.

M. A. Bredig, A. S. Dworkin,* and H. R. Bronstein, "Electrical Conductivities in a Variety of Metal–Molten Halide Systems," Gordon Research Conference on Fused Salts, Meriden, New Hampshire, August 31, 1961.

A. S. Dworkin, H. R. Bronstein,* and M. A. Bredig, "The Electrical Conductivity of Solutions of Metals in Their Molten Halides," 18th International Congress of Pure and Applied Chemistry, Montreal, Canada, August 8, 1961.

A. S. Dworkin, H. R. Bronstein, and M. A. Bredig,* "Ionic Melts as Solvents for Electronic Conductors," Discussion of the Faraday Society on Structure and Properties of Ionic Melts, Liverpool, England, September 7, 1961.

M. A. Bredig,"Metal–Molten Salt Solutions," Institutes of Inorganic Chemistry and Silicate Science," The Technical University of Norway, Trondheim, Norway, September 11, 1961.

M. A. Bredig, "Research on Metal Solutions in Molten Salts at the Oak Ridge National Laboratory," Chemical Physics Colloquium, Imperial College of the University of London, England, October 12, 1961.

M. A. Bredig, "Solutions of Metals in Molten Salts," Joint Meeting of Philadelphia Section American Chemical Society Groups, Physical and Inorganic Group, April 12, 1962.

M. A. Bredig, "Metal Solutions in Molten Salts," Seminar, Chemistry Department, University of Tennessee, Knoxville, April 26, 1962.

CHEMICAL PHYSICS

Ralph Livingston, "Electron Spin Resonance," Sigma Xi Lecture, Wake Forest College, Winston-Salem, North Carolina, October 18, 1962.

G. M. Begun, "Techniques of Raman Spectroscopy," ORINS Traveling Lecture, Division of Natural Sciences, Tuskegee Institute, Tuskegee, Alabama, November 30, 1961.

G. M. Brown* and H. A. Levy, "A Neutron-Diffraction Study of Chloral Hydrate," American Crystallographic Association Annual Meeting, Villanova, Pennsylvania, June 18–22, 1962.

W. R. Busing* and H. A. Levy, "Experience with the Oak Ridge Automatic Three-Dimensional Neutron Diffractometer," American Crystallographic Association Annual Meeting, Boulder, Colorado, July 31–August 4, 1961.

W. R. Busing,* M. Zocchi, and H. A. Levy, "A Single Crystal Neutron Diffraction Study of Hydrazine," American Crystallographic Association Annual Meeting, Boulder, Colorado, July 31–August 4, 1961.

W. R. Busing, "A Computer Program to Postulate Crystal Structures," American Crystallographic Association Annual Meeting, Villanova, Pennsylvania, June 18–22, 1962.

H. G. Smith, S. W. Peterson, and H. A. Levy,* "Neutron Diffraction Study of $Li_2SO_4 \cdot H_2O$," American Crystallographic Association Annual Meeting, Boulder, Colorado, July 31–August 4, 1961.

*Speaker.

H. A. Levy, "Recent Neutron Diffraction Studies," ORINS Traveling Lecture, University of North Carolina, Chapel Hill, North Carolina, March 9, 1962.

H. A. Levy, "X-Ray and Neutron Diffraction Studies of Molten Salts," Gordon Research Conference on Molten Salts, Meriden, New Hampshire, September 1961.

S. Datz,* G. E. Moore, and E. H. Taylor, "The Reflection of Modulated Helium and Deuterium Molecular Beams from Platinum Surfaces," 3d International Symposium on Rarefied Gas Dynamics, Paris, France, June 26–29, 1962.

S. Datz, "Crossed-Beam Experiments on Chemical Reactions," American Physical Society Meeting, Baltimore, Maryland, March 26, 28, 1962.

C. R. Baldock, "Some Unique Applications of Negative Ion Mass Spectra," ASTM Committee E-14 on Mass Spectrometry, New Orleans, Louisiana, June 3–8, 1962.

C. R. Baldock, "Mass Spectrometry," Health Physics Society, Chicago, Illinois, June 10–14, 1962.

C. E. Melton, "The Study of Chemical Reactions with a Mass Spectrometer," The Graduate School, Vanderbilt University, Nashville, Tennessee, November 2, 1961.

C. E. Melton, "Ionization and Excitation in the Mass Spectrometer," The Graduate School, University of Notre Dame, Notre Dame, Indiana, April 13, 1962.

T. A. Carlson, "Recoil and Charge Spectra Following the β^- Decay of Ne^{23}," American Physical Society Meeting, New York, January 1962 [*Bull. Am. Phys. Soc.* **7**, 33 (1962)].

T. A. Carlson and R. M. White,* "Decomposition of $(CH_3Xe^{130})^+$ Following the Beta Decay of CH_3I^{130}," American Chemical Society Meeting, Washington, D.C., March 1962 [*Abstracts of Papers, 141st American Chemical Society Meeting,* p 5R, 1962].

J. F. Riley, "Modern Concepts of Chemistry," Knox County In-Service Education Workshop, Knoxville, Tennessee, August 22, 1961.

J. F. Riley, "Teaching Methods of Modern Chemistry," Knox County In-Service Education Workshop, Knoxville, Tennessee, August 23, 1961.

J. F. Riley, "The Chemical Bond Approach," Knox County In-Service Education Workshop, Knoxville, Tennessee, August 24, 1961.

---

*Speaker.

ORNL-3320
UC-4 – Chemistry
TID-4500 (17th ed., Rev.)

INTERNAL DISTRIBUTION

1. C. E. Larson
2. Biology Library
3–5. Central Research Library
6. Laboratory Shift Supervisor
7. Reactor Division Library
8–9. ORNL – Y-12 Technical Library Document Reference Section
10–48. Laboratory Records Department
49. Laboratory Records, ORNL R.C.
50. A. M. Weinberg
51. J. P. Murray (K-25)
52. R. G. Jordan (Y-12)
53. J. A. Swartout
54–68. E. H. Taylor
69. E. D. Shipley
70. S. C. Lind
71. M. L. Nelson
72. W. H. Jordan
73. F. L. Culler
74. A. H. Snell
75. A. Hollaender
76. M. T. Kelley
77. W. D. Manly
78. K. Z. Morgan
79. T. A. Lincoln
80. A. S. Householder
81. M. H. Lietzke
82. F. A. Posey
83. H. E. Seagren
84. J. A. Lane
85. G. E. Boyd
86–93. M. A. Bredig
94. R. W. Stoughton
95. R. B. Briggs
96. G. W. Parker
97. C. J. Borkowski
98. G. H. Jenks
99. K. A. Kraus
100. H. A. Levy
101. R. S. Livingston
102. T. E. Willmarth
103. C. H. Secoy
104. C. J. Hochanadel
105. W. H. Baldwin
106. A. R. Brosi
107. R. N. Lyon
108. S. A. Reynolds
109. P. F. Thomason
110. E. G. Bohlmann
111. C. D. Susano
112. R. Livingston
113. G. H. Cartledge
114. B. H. Ketelle
115. E. Lamb
116. R. W. Johnson
117. J. R. McNally, Jr.
118. G. D. O'Kelley
119. M. J. Skinner
120. D. S. Billington
121. H. G. MacPherson
122. J. L. Gabbard
123. R. H. Busey
124. J. J. Pinajian
125. J. Halperin
126. C. R. Baldock
127. F. F. Blankenship
128. C. J. Collins
129. J. S. Drury
130. W. R. Grimes
131. J. S. Johnson
132. W. L. Marshall
133. H. F. McDuffie
134. S. Datz
135. G. M. Watson
136. R. E. Thoma
137. D. R. Cuneo
138. P. S. Rudolph
139. G. Scatchard (consultant)
140. D. F. Hornig (consultant)
141. Isadore Perlman (consultant)
142. T. H. Davies (consultant)
143. J. D. Roberts (consultant)

EXTERNAL DISTRIBUTION

144. H. Miller, Office of Isotope Development, AEC, Washington
145. R. W. McNamee, Union Carbide Corporation, New York
146. R. H. Schuler, Radiation Research Laboratories, Mellon Institute, 4400 Fifth Ave., Pittsburgh 13, Pa.
147. Division of Research and Development, AEC, Washington
148. Division of Research and Development, AEC, ORO
149. Boeing Airplane Company
150. Union Carbide and Carbon Chemicals Company (South Charleston)
151. North American Aviation, Inc.

152–743. Given distribution as shown in TID-4500 (17th ed., Rev.) under Chemistry category (75 copies – OTS)